



Contracts for field projects
and supporting research on . . .

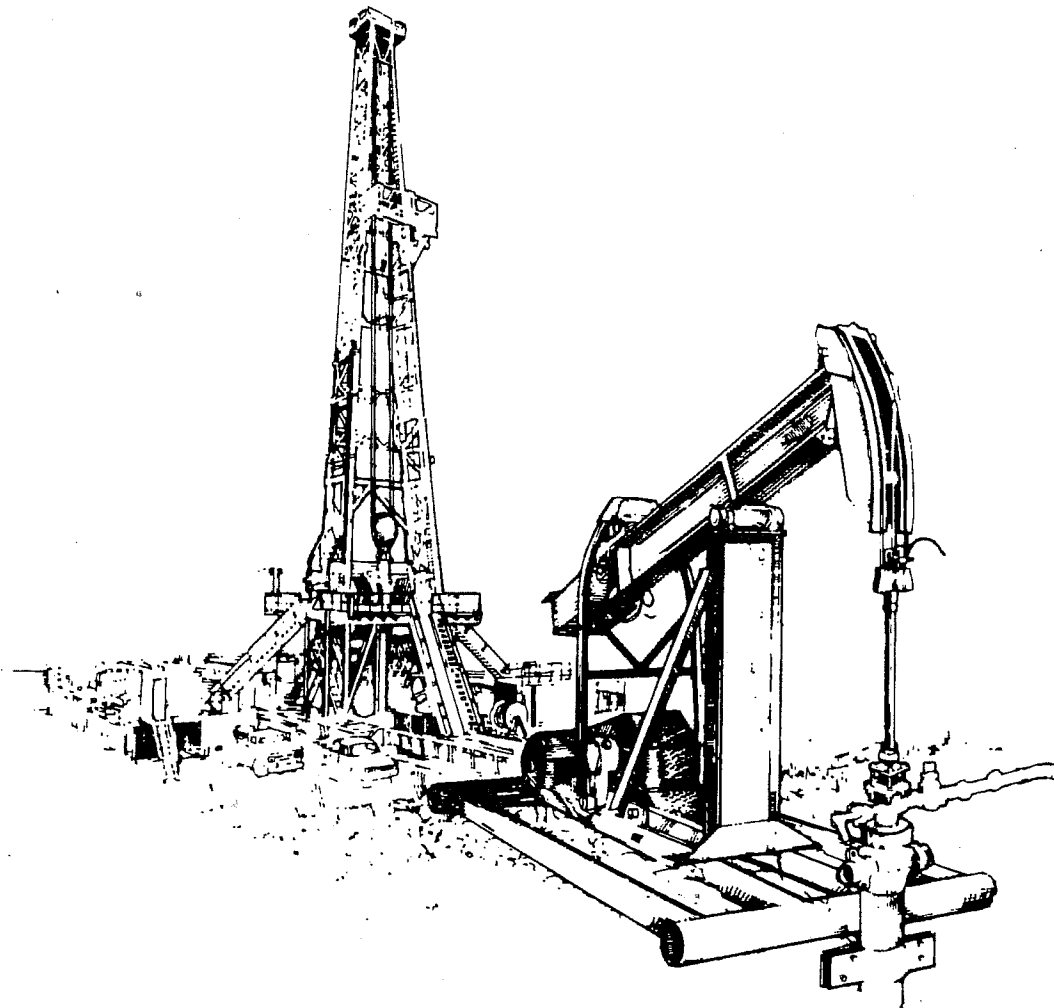
80

Enhanced Oil Recovery

Reporting Period July–September 1994

DOE/BC-94/4
(DE95000155)
PROGRESS REVIEW

Quarter Ending September 30, 1994



United States Department of Energy

Office of Gas and Petroleum Technology
and Bartlesville Project Office

DISCLAIMER

This report was prepared as an account of work sponsored by an agency of the United States Government. Neither the United States Government nor any agency thereof, nor any of their employees, makes any warranty, express or implied, or assumes any legal liability or responsibility for the accuracy, completeness, or usefulness of any information, apparatus, product, or process disclosed, or represents that its use would not infringe privately owned rights. Reference herein to any specific commercial product, process, or service by trade name, trademark, manufacturer, or otherwise does not necessarily constitute or imply its endorsement, recommendation, or favoring by the United States Government or any agency thereof. The views and opinions of authors expressed herein do not necessarily state or reflect those of the United States Government or any agency thereof.

Available to DOE and DOE contractors from the Office of Scientific and Technical Information, P.O. Box 62, Oak Ridge, Tennessee 37831; prices available from (423) 576-8401.

Available to the public from the U.S. Department of Commerce, Technology Administration, National Technical Information Service, Springfield, Virginia 22161; prices available from (703) 487-4650.

U.S. Department of Energy
Washington, D.C. 20545

PATRICIA GODLEY
Assistant Secretary for Fossil Energy
Room 4G-084 Forrestal Building
Telephone Number 202-586-4695

REGINAL SPILLER
*Deputy Assistant Secretary for Gas
and Petroleum Technologies*

SANDRA WAISLEY
*Director for Oil and Gas Exploration
and Production*

Bartlesville Project Office
P.O. Box 1398
Bartlesville, Oklahoma 74005
Telephone No. 918-337-4401

THOMAS C. WESSON
Director

R. M. RAY
Deputy Director

BETTY J. FELBER
*Manager for
Technology Development*

HERBERT A. TIEDEMANN
*Contact for
Technology Transfer*

DOE/BC--94/4
(DE95000155)

Distribution Category UC-122

PROGRESS REVIEW NO. 80

CONTRACTS FOR FIELD PROJECTS AND SUPPORTING RESEARCH ON ENHANCED OIL RECOVERY

Date Published - November 1995

UNITED STATES DEPARTMENT OF ENERGY

INDEX

COMPANIES AND INSTITUTIONS

	Page		Page
Amoco Production Company		Michigan Technological University	
West Hackberry Tertiary Project	83	Recovery of Bypassed Oil in the Dundee Formation Using Horizontal Drilling	117
Colorado School of Mines		Visual Display of Reservoir Parameters Affecting Enhanced Oil Recovery	144
Interdisciplinary Study of Reservoir Compartments	53	New Mexico Institute of Mining and Technology	
Columbia University		Improved Efficiency of Miscible CO ₂ Floods and Enhanced Prospects for CO ₂ Flooding in Heterogeneous Reservoirs	26
Dynamic Enhanced Recovery Technologies	113	Integration of Advanced Geoscience and Engineering Techniques To Quantify Interwell Heterogeneity	46
Surfactant Loss Control in Chemical Flooding: Spectroscopic and Calorimetric Study of Adsorption and Precipitation on Reservoir Minerals	7	Oklahoma Geological Survey	
Diversified Operating Corporation		Continued Support of the Natural Resources Information System for the State of Oklahoma	77
Advanced Secondary Recovery Demonstration for the Sooner Unit	104	Identification and Evaluation of Fluvial-Dominated Deltaic (Class I Oil) Reservoirs in Oklahoma	139
Hughes Eastern Corporation		Oxy USA, Inc.	
The Use of Indigenous Microbes To Selectively Plug the More Porous Zones To Increase Oil Recovery During Waterflooding	81	Application of Reservoir Characterization and Advanced Technology To Improve Recovery and Economics in a Lower Quality Shallow Shelf Carbonate Reservoir	136
Illinois Institute of Technology		Reservoir Engineering Research Institute	
Surfactant-Enhanced Alkaline Flooding for Light Oil Recovery	3	Research Program on Fractured Petroleum Reservoirs	68
Laguna Petroleum Corporation		Stanford University	
An Integrated Study of the Grayburg/San Andres Reservoir, Foster and South Cowden Fields, Ector County, Texas	141	Productivity and Injectivity of Horizontal Wells	15
Lawrence Berkeley Laboratory		Surtek, Inc.	
Lawrence Berkeley Laboratory/Industry Heterogeneous Reservoir Performance Definition Project	57	Detailed Evaluation of the West Kiehl Alkaline-Surfactant-Polymer Field Project and Its Application to Mature Minnelusa Waterfloods	19
Lawrence Livermore National Laboratory		Investigation of Oil Recovery Improvement by Coupling an Interfacial Tension Agent and a Mobility Control Agent in Light Oil Reservoirs	12
Oil Field Characterization and Process Monitoring Using Electromagnetic Methods	35	Texaco Exploration and Production, Inc.	
Lomax Exploration Company		CO ₂ Huff 'n' Puff Process in a Light Oil Shallow Shelf Carbonate Reservoir	114
Green River Formation Waterflood Demonstration Project, Uinta Basin, Utah	86	Postwaterflood CO ₂ Miscible Flood in Light Oil, Fluvial-Dominated Deltaic Reservoir	89
Luff Exploration Company		University of Alaska	
Improved Recovery Demonstration for Williston Basin Carbonates	126	Study of Hydrocarbon Miscible Solvent Slug Injection Process for Improved Recovery of Heavy Oil from Schrader Bluff Pool, Milne Point Unit, Alaska	31
Maurer Engineering, Inc.			
Horizontal Oil Well Applications and Oil Recovery Assessment	23		

University of Kansas

Improved Oil Recovery in Fluvial-Dominated Deltaic Reservoirs of Kansas—Near Term	92
Improving Reservoir Conformance Using Gelled Polymer Systems	1

University of Oklahoma

Gypsy Field Project in Reservoir Characterization	48
---	----

University of Texas

Geoscience/Engineering Characterization of the Interwell Environment in Carbonate Reservoirs Based on Outcrop Analogs, Permian Basin, West Texas and New Mexico	39
--	----

University of Tulsa

Integrated Approach Toward the Application of Horizontal Wells To Improve Waterflooding Performance	94
---	----

Utah Geological Survey

Geological and Petrophysical Characterization of the Ferron Sandstone for Three-Dimensional Simulation of a Fluvial-Deltaic Reservoir	40
Increased Oil Production and Reserves from Improved Completion Techniques in the Bluebell Field, Uinta Basin, Utah	111

CONTENTS BY EOR PROCESS

Chemical Flooding—Supporting Research	1
Gas Displacement—Supporting Research	15
Thermal Recovery—Supporting Research	31
Geoscience Technology	39
Resource Assessment Technology	77
Microbial Technology	81
Reservoir Class Field Demonstrations	83

**DOE Technical Project Officers for
Enhanced Oil Recovery**

DIRECTORY

Name	Phone number	Name of contractor
U. S. Department of Energy Gas and Petroleum Technology Oil and Gas Exploration and Production 3E-028/FORS Washington, D.C. 20585		
Bartlesville Project Office P. O. Box 1398 Bartlesville, Oklahoma 74005		
Edith Allison	918-337-4390	Columbia University Diversified Operating Corporation Lomax Exploration Company Utah Geological Survey
Jerry Casteel	918-337-4412	Columbia University Illinois Institute of Technology New Mexico Institute of Mining and Technology Surtek, Inc. Texaco Exploration and Production, Inc. University of Kansas
Robert Lemmon	918-337-4405	Colorado School of Mines Lawrence Berkeley Laboratory Michigan Technological University New Mexico Institute of Mining and Technology Reservoir Engineering Research Institute University of Oklahoma University of Texas Utah Geological Survey
Rhonda Lindsey	918-337-4407	Hughes Eastern Corporation Oklahoma Geological Survey University of Kansas University of Tulsa
Chandra Nautiyal	918-337-4409	Laguna Petroleum Corporation Luff Exploration Company Michigan Technological University Oxy USA, Inc. Texaco Exploration and Production, Inc.
R. Michael Ray	918-337-4403	Oklahoma Geological Survey
Thomas Reid	918-337-4233	Lawrence Livermore National Laboratory Maurer Engineering, Inc. Stanford University Surtek, Inc. University of Alaska
Metairie Site Office 900 Commerce Road, East New Orleans, Louisiana 70123		
Gene Pauling	504-734-4131	Amoco Production Company

CHEMICAL FLOODING— SUPPORTING RESEARCH

IMPROVING RESERVOIR CONFORMANCE USING GELLED POLYMER SYSTEMS

Contract No. DE-AC22-92BC14881

**University of Kansas
Center for Research
Lawrence, Kans.**

**Contract Date: Sept. 25, 1992
Anticipated Completion: Sept. 24, 1995
Government Award: \$707,123**

**Principal Investigators:
Don W. Green
G. Paul Willhite**

**Project Manager:
Jerry Casteel
Bartlesville Project Office**

Reporting Period: July 1–Sept. 30, 1994

Objectives

The general objectives of this research are to identify and develop gelled polymer systems with potential to improve

reservoir conformance of fluid displacement processes, determine the performance of these systems in bulk and in porous media, and develop methods to predict the capability of these systems to recover oil from petroleum reservoirs.

This work focuses on three types of gel systems: (1) an aqueous polysaccharide (KUSP1) system that gels as a function of pH, (2) the chromium(III)–polyacrylamide system, and (3) the aluminum citrate–polyacrylamide system. Laboratory research is directed at the fundamental understanding of the physics and chemistry of the gelation process in bulk form and in porous media. This knowledge will be used to develop conceptual and mathematical models of the gelation process. Mathematical models will then be extended to predict the performance of gelled polymer treatments in oil reservoirs.

Summary of Technical Progress

Physical and Chemical Characterization of Gel Systems

An alternate method for gelling KUSP1 is being investigated. This method involves the addition of *o*-boric acid to an alkaline solution of KUSP1. The gel times are regulated from a few hours to several days by altering the concentration of boric acid and/or the pH of the gel solution. The nature of the gels formed with the use of boric acid is different from that of the gels formed by reducing the pH of an

alkaline KUSP1 solution. Boric acid gels are transparent and appear much more resilient than the gels formed without boric acid, which are white and tend to shatter. KUSP1 solutions without boric acid form gels at a pH of 10.8, whereas solutions with boric acid form gels instantly at pH values around 8 to 9, depending on the concentration of boric acid. The different nature of the two gels is attributed to different gelation mechanisms. It is speculated that the borate cross-links the polymer molecules to form gels such as those found in gel systems used for hydraulic fracturing.

Concentrations studied for the KUSP1–boric acid system were 1.0% KUSP1, 0.1 to 0.5M boric acid, and pH values between 9 and 13. Typical results are shown in Table 1, where the gel time is given as a function of pH. Experiments showed that varying the boric acid concentration between 0.2 and 0.5M had a significant effect on the gel time. The KUSP1–boric acid gel system is being studied further.

Work is continuing on determining the size of polymer–gel aggregates for the polyacrylamide–aluminum(III) gel system. One step in this procedure is the determination of polymer concentrations. Two methods for determining polymer concentrations have proven unsatisfactory for the selected polymer, HiVis 350. For the size–exclusion chromatography (SEC)–ultraviolet (UV) adsorption method, the polymer plugs the SEC columns. For the bleach–turbidity method, problems developed as a result of interactions between the reagents and the aluminum citrate. A third method, Hyamine 1622–turbidity, is being examined.

TABLE 1

Gel Time as a Function of the pH*

pH	Gel time
9.6	6 h
10.0	4 d
10.1	5 d
10.2	6 d

*1.0% KUSP1 and 0.5M o-Boric Acid (25 °C).

Mechanisms of In Situ Gelation

Work continued on the in situ gelation of the KUSP1–ester gel system. Gelation of this system is triggered by a reduction in pH caused by the slow reaction of *m*-ethyl phthalate ester with water. Runs were conducted in which the gel system was injected through foot-long sandpacks and a foot-long Berea core. A shut-in period followed injection to allow for gelation. Brine was then injected to determine the reduction in permeability produced by the treatment. As shown in Table 2, the treatments significantly reduced the permeability. Pressure

drops measured across 2-in. long sections of porous media showed that the permeability reduction was uniform along the length. The difference in permeability reductions between the two sandpacks was attributed to improvements in the production and filterability of the KUSP1 polymer stock solution.

The stability of the permeability–reduction treatments is being assessed by continuously injecting brine under a constant head and measuring the flow rate. Preliminary results show that the gel is quite stable; for example, over 100 pore volumes of brine were flowed through sandpack No. 1 over 50 d without a change in permeability. Future runs include testing the performance of the KUSP1–ester system in carbonate plugs cut from reservoir core material.

In situ gelation experiments in sandpacks with the use of the polyacrylamide–aluminum(III) gel system were initiated. At the entrance and exit sections of the sandpack, high pressure drops, which were caused by gel formation at the screens that were used to secure the sand within the pack, were measured. Work is in progress to eliminate this problem.

TABLE 2

Permeability Reductions Using KUSP1–Ester Gelant

	Pre-treatment permeability (k_i), mD	Post-treatment permeability (k_f), mD	Permeability reductions factor (k_f/k_i)
Sandpack No. 1	8700	34	260
Sandpack No. 2	9400	2.0	4700
Berea No. 1	160	0.54	290

Mathematical Modeling of Gel Systems

A two-dimensional numerical model for the in situ gelation of cross-linking polymer solutions is being developed. The proposed model is an extension of the work by Todd et al.,¹ which incorporates the kinetics of the cross-linking reaction, formation of polymer aggregates, and the effect of deep filtration of polymer aggregates on the permeability of the porous medium. Two-dimensional fluid flow in layered reservoirs is being investigated. A fully implicit, finite-difference scheme is used for solving the governing partial differential equations.

Reference

1. B. J. Todd, G. P. Willhite, and D. W. Green, *A Mathematical Model of In-Situ Gelation of Polyacrylamide by a Redox Process*, paper SPE/DOE 20215 presented at the 7th SPE/DOE Enhanced Oil Recovery Symposium, Tulsa, Okla., April 22–25, 1990.

SURFACTANT-ENHANCED ALKALINE FLOODING FOR LIGHT OIL RECOVERY

Contract No. DE-AC22-92BC14883

**Illinois Institute of Technology
Chicago, Ill.**

**Contract Date: Sept. 21, 1992
Anticipated Completion: Sept. 20, 1995
Government Award: \$150,000
(Current year)**

**Principal Investigator:
Darsh T. Wasan**

**Project Manager:
Jerry Casteel
Bartlesville Project Office**

Reporting Period: July 1–Sept. 30, 1994

Objective

The overall objective of this project is to develop a cost-effective method for formulating a successful surfactant-enhanced alkaline flood by appropriately choosing mixed alkalis that form inexpensive buffers to obtain the desired pH (between 8.5 and 12.0) for ultimate spontaneous emulsification and ultralow tension. In addition, the novel concept of pH gradient design to optimize floodwater conditions will be tested.

Summary of Technical Progress

The recovery efficiency of crude oil from porous rock by displacement with water or chemical solution is dependent on both the nature of the rock and the chemical constituents. The wettability of a porous medium governs the distribution of fluids in the pores and therefore has considerable influence on the conditions under which the oil is recovered.

A new experimental technique has been developed and used to determine the three-phase contact angle and to study the three-phase contact angle kinetics with the use of common and differential interferometry. For most systems studied, the contact angle increases with time until the crude oil droplet separates from the silica surface. The addition of surfactant causes the kinetics of separation to be slower. With smaller drops the three-phase contact angle reaches its equilibrium value faster. Water was also observed to penetrate between the crude oil and silica surface to form a water film, which helps the crude oil to separate from the silica surface.

Fluid–Solid Interfaces: Optical Imaging by Differential and Common Interferometry

Long Beach crude oil/solid surface (silica) interactions were studied both in the presence of air and in the presence of water with low and high concentrations of electrolyte and with and without surfactant (Petrostep B-105) versus pH with the use of common and differential interferometry. Both types of interference techniques were used to study the three-phase contact angle kinetics versus time when an alkali solution approaches the surface of crude oil and solid silica surfaces. Generally, the three-phase contact angle kinetics depend on the tangential balance between the three interfacial tensions: solid/oil ($\sigma_{s/o}$), solid/water ($\sigma_{s/w}$), and oil/water ($\sigma_{o/w}$). If $\sigma_{s/w} - \sigma_{s/o} < \sigma_{o/w}$, the oil drop will separate from the solid, and a water film between solid and oil will form. When $\sigma_{s/w} - \sigma_{s/o} > \sigma_{o/w}$, the oil will spread on the solid. The equilibrium value of the three-phase contact angle is given by Young's equation: $\sigma_{s/o} = \sigma_{s/w} + \sigma_{o/w} \cos \theta$. In the case of liquid spreading phenomenon on the solid surface, a liquid film with thickness h is an equilibrium with droplet with capillary pressure P_σ and with a contact angle film–drop meniscus $-\theta$. The relation between contact angle film thickness and capillary pressure is given by the equation

$$\sigma_{o/w} \cos \theta = \sigma_{o/w} + P_\sigma h + \int_\infty^h \Pi(h) dh$$

where $\Pi(h)$ is the isotherm of disjoining pressure of wetting film. This macroscopic approach for the equilibrium film–meniscus was first developed by Frumkin–Derjaguin^{1,2} and was subsequently used by Landau and Lifshitz.³

The drop size is also important for the three-phase contact angle kinetics. The drop excess pressure is given by the Laplace equation: $P_\sigma = 2\sigma_{o/w}/R_d$, where R_d is drop radius. The drop excess pressure affects the contact angle kinetics, and the smallest droplets on the solid surface will reach their equilibrium value of the three-phase contact angle faster than the larger droplets. Moreover, in the presence of hysteresis (typical for $\theta > 20^\circ$), the large drops may never reach their equilibrium contact angle.

Contact Angle Kinetics at Low Concentration of Na⁺

The three-phase contact angle kinetics of preequilibrated Long Beach crude oil with alkali solution ($\text{Na}^+ = 0.085 \text{ mol/L}$ at $\text{pH} = 10.01$) are shown in Fig. 1, and the contact angle kinetics are shown in Table 1. The interferometric microphotograph clearly depicts the contact angle kinetics. Part a of Fig. 1 shows a microphotograph taken in common interferometry of an oil drop on the silica surface in the presence of air with size $500 \mu\text{m}$. The drop has an irregular shape, which indicates the contact angle hysteresis. The circular interference patterns in the microphotograph (part a of Fig. 1) were

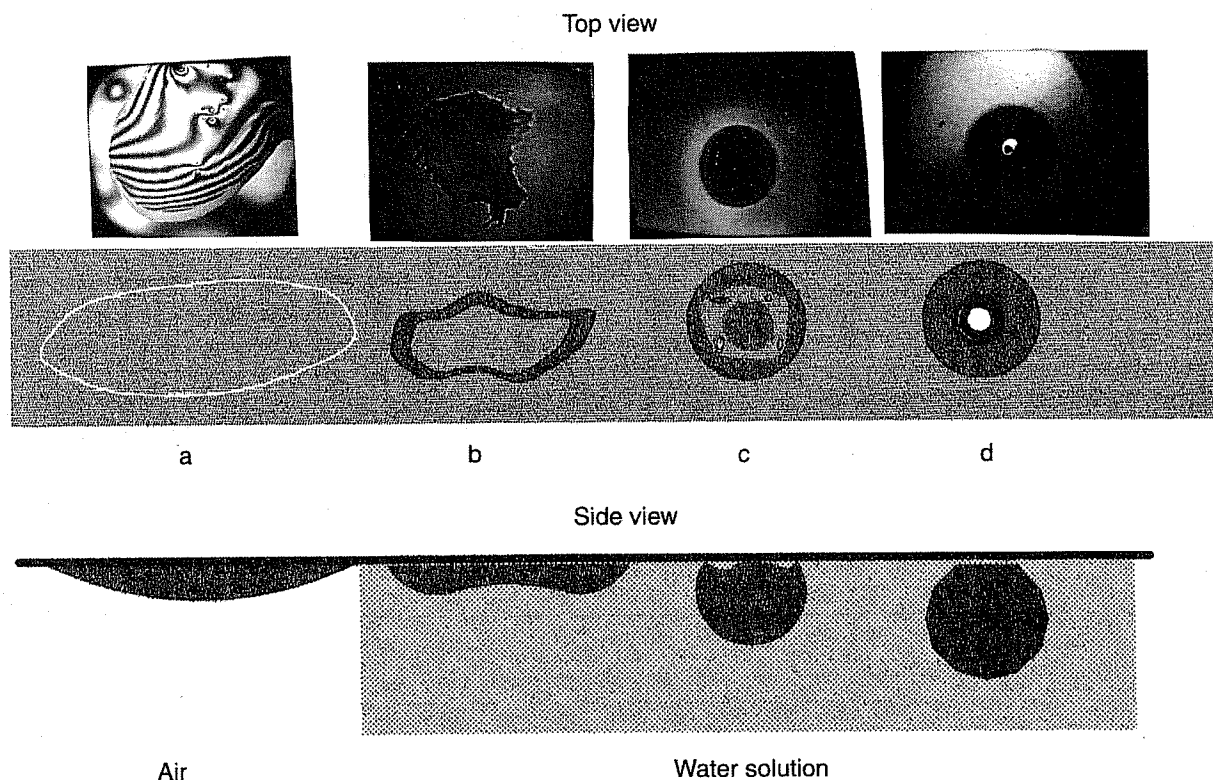


Fig. 1 Long Beach crude oil silica surface interactions vs. time. (a) Oil on solid surface in the presence of air. (b) Oil in the presence of water solution ($\text{Na}^+ = 0.085 \text{ mol/L}$ at $\text{pH} = 10.01$ after 1/2 h). (c) After 1 to 2 h, oil begins to separate from solid. (d) After 3 to 4 h, drop is separated from the solid with water film.

TABLE 1
Drop Size from 400 to 700 μm

	Drop size, μm			
	400	500	600	700
Sample, $\text{Na}^+ = 0.085 \text{ mol/L}$, $\text{pH} = 10.01$				
Time, h	0	0.5	1-2	3-4
Contact angle, $^\circ$	5-10	15-40	110-140	175
Sample, $\text{Na}^+ = 1.0 \text{ mol/L}$, $\text{pH} = 10.03$, 0.1 wt % Petrostep B-105				
Time, h	0	1-2	8-10	
Contact angle, $^\circ$	5-10	20-40	70-120	
Sample, $\text{Na}^+ = 1.0 \text{ mol/L}$, $\text{pH} = 10.20$				
Time, h	0	0.5	4-5	18-20
Contact angle, $^\circ$	5-10	1-3	0.1-0.5	0-0.1
Sample, $\text{Na}^+ = 0.085 \text{ mol/L}$, $\text{pH} = 10.01$, 0.1 wt % Petrostep B-105				
Time, h	0	1-2	5-6	10-14
Contact angle, $^\circ$	5-10	10-30	110-150	170

used to estimate the value of the contact angle (Table 1). Immediately after adding the water solution to the system, the three-phase contact angle begins to shrink irregularly (part b of Fig. 1), and the contact angle increases its value to 15 to 40 $^\circ$.

After 1 to 2 h, the oil drop has a spherical shape (part c of Fig. 1) with a macroscopic contact angle from 110 to 140 $^\circ$. Part c of Fig. 1 shows a formation of a speckled bright band inside the dark oil area. The specks show the formation of small water lenses between the oil and solid surface. From a microscopic point of view, two contact lines have been established: the first is between the oil drop, solid surface, and water film (outer line), and the second is between the oil drop, solid surface, and water film (inner line). After several hours, the oil drop is separated from the solid by the water film (part d of Fig. 1).

Contact Angle Kinetics at Low Concentration of Na^+ and in the Presence of Surfactant B-105

The three-phase contact angle kinetics of preequilibrated Long Beach crude oil with water solution ($\text{Na}^+ = 0.085 \text{ mol/L}$ and 0.1 wt % B-105 at $\text{pH} = 10.03$) were also studied. Figure 2 shows interferometric microphotographs depicting the kinetics and hysteresis of the contact angle. The contact angle kinetics are shown in Table 1. Part a of Fig. 2 shows a microphotograph taken in usual interferometry of an oil drop on silica surface in the presence of air. The drop size is about 700 μm . The small dark spots inside the oil drop are small air bubbles trapped inside the oil. The drop three-phase contact line has an irregular shape, which indicates the contact angle hysteresis. The circular interference patterns in the microphotograph (part a of Fig. 2)

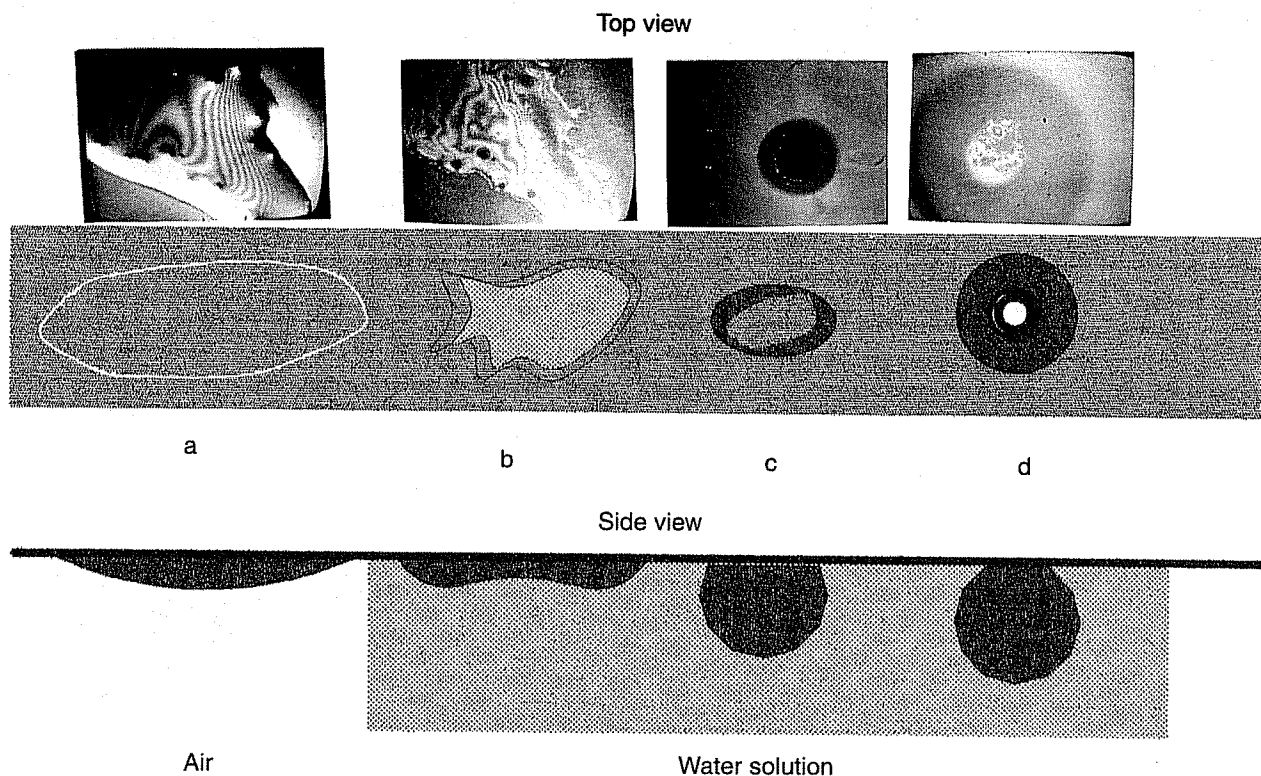


Fig. 2 Long Beach crude oil silica surface interactions vs. time. (a) Oil on solid surface in the presence of air. (b) Oil on solid surface in the presence of water solution ($\text{Na}^+ = 0.085 \text{ mol/L}$, 0.1 wt % B-105, and $\text{pH} = 10.03$) after 1 to 2 h. (c) After 5 to 6 h, oil begins to separate from solid. (d) After 10 to 14 h, some of the smaller oil drops are separated from the solid with water film.

have been used to estimate the value of the contact angle and its hysteresis (see the data in Table 1). After adding water solution ($\text{Na}^+ = 0.085 \text{ mol/L}$ and 0.1 wt % B-105 at $\text{pH} = 10.03$) to the system, the three-phase contact line begins to shrink irregularly (part b of Fig. 1), and the contact angle slowly increases its value to 10 to 30° . Compared with the previous case without surfactant, the contact angle kinetics are much slower, and even after several hours (part c of Fig. 2), the drop has an irregular shape. In the previous case, for that period of time the oil drop has been separated from the solid surface. In this case the drop is separated from the solid (part d of Fig. 2) after 10 to 14 h. As shown in the microphotograph in part d of Fig. 2, the water film separating oil drop from solid surface is much thinner (compare the intensity of the central bright spot of part d of Fig. 1 and part d of Fig. 2).

Contact Angle Kinetics at High Concentration of Na^+ Without Surfactant

So that the effect of electrolyte on the three-phase contact angle kinetics could be studied, the Long Beach crude oil was preequilibrated with water solution ($\text{Na}^+ = 1.0 \text{ mol/L}$ and $\text{pH} = 10.20$). Figure 3 shows interferometric microphotographs depicting the contact line kinetics, and Table 1 shows the contact angle kinetics. Part a of Fig. 3 shows a microphotograph taken in usual interferometry of an oil drop on a silica surface in the presence of air. The drop size is about $600 \mu\text{m}$.

After the addition of water solution ($\text{Na}^+ = 1.0 \text{ mol/L}$ and $\text{pH} = 10.20$) to the system, the three-phase contact line begins to spread, and an oil film is formed on the solid surface (part b and c of Fig. 3). The value of the contact angle decreases. The distance between the interference patterns versus time increases (compare parts b and c of Fig. 3), which shows that the contact angle between film and oil drop decreases, and almost all the oil spreads on the solid. The oil film thickness is about 100 to 200 nm (part d of Fig. 3), and the values of macroscopic contact angle versus time are shown in Table 1.

Contact Angle Kinetics at High Concentration of Na^+ with Surfactant

The three-phase contact angle kinetics of preequilibrated Long Beach crude oil with water solution ($\text{Na}^+ = 1.0 \text{ mol/L}$ with 0.1 wt % B-105 at $\text{pH} = 10.03$) are shown in Fig. 4. The macroscopic contact angle kinetics are shown in Table 1. The interferometric microphotograph in part a of Fig. 4 shows an oil drop on the solid silica surface in the presence of air. The macroscopic contact angle is from 5 to 10° as in the previous case. In the presence of alkali solution ($\text{Na}^+ = 1.0 \text{ mol/L}$ with 0.1 wt % B-105), the three-phase contact line was observed to begin to shrink irregularly (part b of Fig. 4), and the contact angle increases its value after 1 to 2 h to 20 to 40° . After 8 to 10 h, the oil splits into smaller drops (part c of Fig. 4).

Summary

The experimental observations show that the concentrations of electrolyte and surfactant are important factors affecting the macroscopic contact angle kinetics and oil-drop separation from the solid surface. The concentration of electrolyte and surfactant also affect the interfacial tension ($\sigma_{s/w}$ and $\sigma_{o/w}$). The surface charge density of a porous silica at pH = 10 is known to increase with an increase in the electrolyte concentration, and from that the interfacial tension ($\sigma_{s/w}$) decreases ($\sigma_{o/w}$ also decreases with increase in electrolyte concentration). Because of this, a spreading of the oil phase on the solid surface can be expected and, indeed, in the presence of high electrolyte concentration, oil spreading on the solid surface was observed (Fig. 3 and Table 1). It is known that, in the presence of surfactant, the interfacial tension of oil/water is reduced, and surfactant may also reduce the surface energy (interfacial tension) of solid/water. For the prediction of the effect of surfactant on the contact angle, it is also important to know the orientation of surfactant molecules on solid and oil/water surface. Because of the negative surface charge on the solid surface, the surfactant molecule orientation on the solid surface may be with the carbon chain on the solid surface. The orientation of surfactant molecules on the water/oil interface is well-known; the surfactant polar part is in the water. If the surfactant molecular orientation described above is assumed, the prediction can be made that, in the presence of surfactant, the contact angle of an oil drop will increase; however, the three-phase contact angle kinetics also depend on the drop size. With a smaller drop, the drop excess pressure is higher, and the three-phase contact angle reaches its equilibrium value faster.

References

1. A. Frumkin, *Acta Physicochim.*, 363:9 (1938).
2. B. Derjaguin, *Acta Physicochim.*, 181:12 (1940).
3. L. D. Landau and E. M. Lifshiz, *Statistical Physics, Nauka, Moscow*, p. 127 (1964) (in Russian).

SURFACTANT LOSS CONTROL IN CHEMICAL FLOODING: SPECTROSCOPIC AND CALORIMETRIC STUDY OF ADSORPTION AND PRECIPITATION ON RESERVOIR MINERALS

Contract No. DE-AC22-92BC14884

**Columbia University
New York, N.Y.**

**Contract Date: Sept. 30, 1992
Anticipated Completion: Sept. 29, 1995
Government Award: \$602,232**

**Principal Investigator:
P. Somasundaran**

**Project Manager:
Jerry Casteel
Bartlesville Project Office**

Reporting Period: July 1–Sept. 30, 1994

Objective

The objective of this research is to elucidate the mechanisms underlying adsorption and surface precipitation of flooding surfactants on reservoir minerals. The effect of surfactant structure, surfactant combinations, and other inorganic and polymeric species will also be determined. Solids of relevant mineralogy and a multipronged approach consisting of microspectroscopy and nanospectroscopy, microcalorimetry, electrokinetics, surface tension, and wettability will be used to achieve the goals. The results of this study should help in controlling surfactant loss in chemical flooding and also in developing optimum structures and conditions for efficient chemical flooding processes.

Summary of Technical Progress

Interactions between surfactants and solids can be understood completely by studying desorption and adsorption. During this report period desorption of tetradecyl trimethyl ammonium chloride (TTAC) and pentadecyl ethoxylated nonyl phenol (NP-15) mixtures from the alumina–water interface was studied. It was found that in TTAC-rich mixtures the desorption of the two surfactants from the interface was controlled by the TTAC and was similar to the desorption of TTAC alone. At high concentrations the adsorption of the mixtures was reversible. At low concentrations, however, the desorption of TTAC showed some positive

hysteresis. Because the adsorption of NP-15 was dependent upon the presence of TTAC, polyethoxylated nonyl phenol (NP-15) also, like TTAC, showed some positive desorption hysteresis. In contrast, the desorption of both of these surfactants from a 1:1 TTAC:NP-15 mixture showed some negative hysteresis. It was clear that the desorption behavior of the components in the mixture system studied here can be controlled by adjusting the ratio of the two surfactants. With an increase of NP-15 in the mixtures, the desorption of surfactants becomes easier.

In an attempt to understand adsorption and desorption behavior of mixed surfactant systems, a regular solution theory was used to model the interactions between TTAC and polyethoxylated nonyl phenol alcohol with fifteen ethylene oxide groups (NP-15). The interaction parameter β and the monomer concentrations were calculated for different mixtures.

Desorption of Surfactant Mixtures from Alumina–Water Interface

Desorption of different mixtures of an ionic surfactant TTAC and a nonionic surfactant NP-15 was studied. The desorption tests consisted of conditioning of supernatants of slurries from adsorption tests for 15 h with the desired amounts of diluents adjusted for pH and ionic strength. This procedure was repeated several times, depending on the concentration. Results obtained for the desorption of a 4:1 TTAC:NP-15 mixture are shown in Figs. 1 and 2. Note that the desorption of TTAC from a 4:1 mixture (Fig. 1) is similar to that of TTAC alone. At high concentrations the adsorption of TTAC is reversible, but at low concentrations the desorption shows some positive hysteresis (i.e., at same residual concentrations, the adsorption density is higher after desorption than that after adsorption). This may be due to the hysteresis involved in the decomposition of the hemimicelles from the interface. Interestingly, the fully grown hemimicelles come off the surface easily upon dilution, whereas the incipient ones do not. Similar isotherms for the desorption of NP-15 are shown in Fig. 2. As reported earlier, the adsorption of NP-15 on alumina requires the TTAC to adsorb first and act as an anchor. It is reasonable to expect the desorption behavior of the NP-15 to be controlled by the desorption of TTAC. At high concentrations the adsorption density of TTAC does not change much upon dilution; neither does the NP-15 desorb from the interface under these conditions. In cases where TTAC desorbs from the interface, however, desorption of NP-15 is significant, and S-shape desorption isotherms are obtained. The desorption of NP-15 is facilitated in this case by the desorption of TTAC. For dilutions from high concentrations, the desorption of NP-15 shows some positive hysteresis (similar to the positive hysteresis of TTAC), but only when the residual concentration becomes low as a result of dilution.

The desorption isotherms for a 1:1 TTAC:NP-15 mixture are shown in Figs. 3 and 4. As shown in the figures, at this ratio both TTAC and NP-15 desorb significantly, and the desorption isotherms show negative hysteresis (i.e., the surfactants adsorbed at the interface are less during desorption than that during adsorption at the same residual concentration).

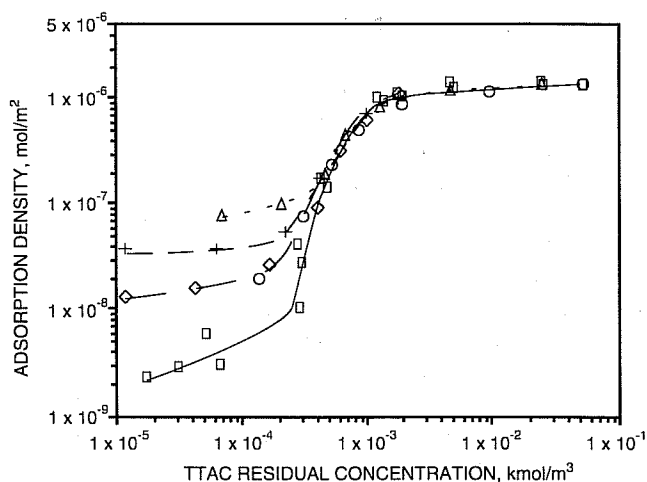


Fig. 1 Desorption of tetradecyl trimethyl ammonium chloride (TTAC) from alumina on dilution from different residual concentrations (C_r). TTAC:NP-15 = 4:1. \square , ADS. ISO. \circ , $C_r = 0.0524$. Δ , $C_r = 0.0251$. \diamond , $C_r = 0.0018$. $+$, $C_r = 0.000433$.

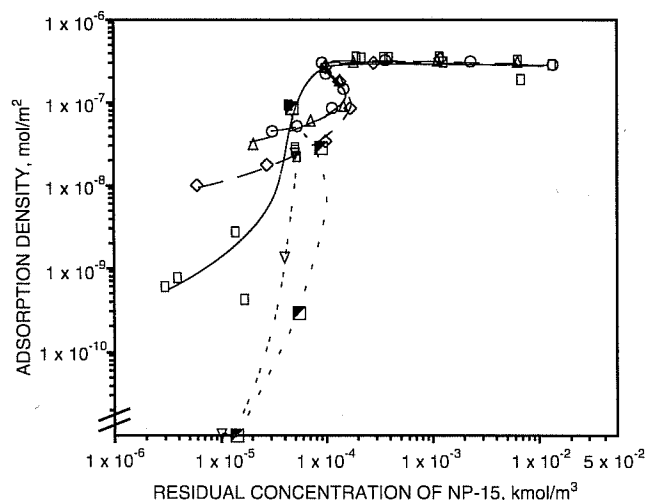


Fig. 2 Desorption of pentadecyl ethoxylated nonyl phenol (NP-15) from alumina on dilution from different residual concentrations (C_r). TTAC:NP-15 = 4:1. \square , ADS. ISO. \circ , $C_r = 0.0131$. Δ , $C_r = 0.00637$. \diamond , $C_r = 0.0012$. \blacksquare , $C_r = 0.000046$. ∇ , $C_r = 0.000052$.

As the NP-15 content of the mixture increases, the positively charged heads of the TTAC will be partially shielded from each other by the co-adsorbed nonionic NP-15 molecules. This will decrease the electrostatic interaction between the cationic TTAC molecules and the negatively charged alumina surface and thus facilitate desorption.

The desorption isotherms of a 1:4 TTAC:NP-15 mixture system are shown in Figs. 5 and 6. At this ratio the adsorption of TTAC is very low. Nevertheless, the desorption of TTAC in this system still shows some negative hysteresis. The desorption of NP-15 shows some positive hysteresis. The mechanisms of desorption in this mixed system are evidently complex and merit further investigation.

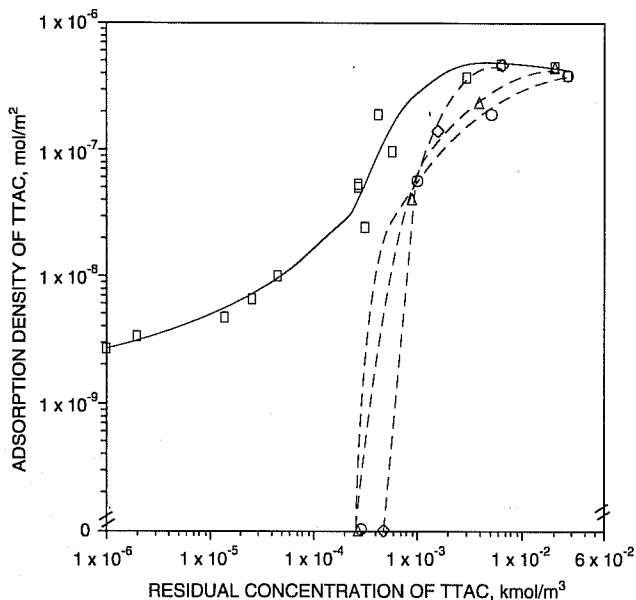


Fig. 3 Desorption of tetradecyl trimethyl ammonium chloride (TTAC) from alumina-water interface on dilution from different residual concentrations (C_r). TTAC:NP-15 = 1:1. \square , ADS. ISO. \circ , $C_r = 0.0271$. Δ , $C_r = 0.02$. \diamond , $C_r = 0.00624$.

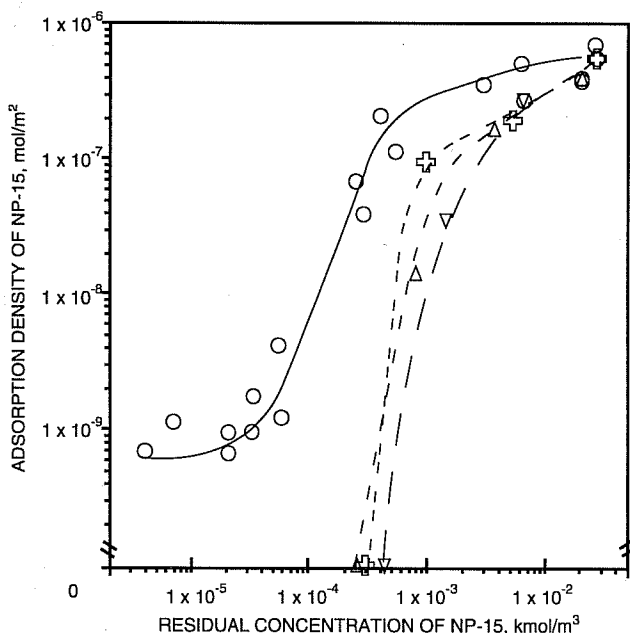


Fig. 4 Desorption of pentadecyl ethoxylated nonyl phenol (NP-15) from alumina on dilution from different residual concentrations (C_r). TTAC:NP-15 = 1:1. \circ , ADS. ISO. \oplus , $C_r = 0.027$. Δ , $C_r = 0.02$. ∇ , $C_r = 0.00624$.

From these results, it is evident that the desorption behavior of this mixed system depends on the ratio of surfactants in the mixture. With an increase of NP-15 in the mixture, the desorption of TTAC becomes easy. The desorption of both surfactants shows significant negative hysteresis at a ratio of 1:1. Further study is needed to understand the precise relationship

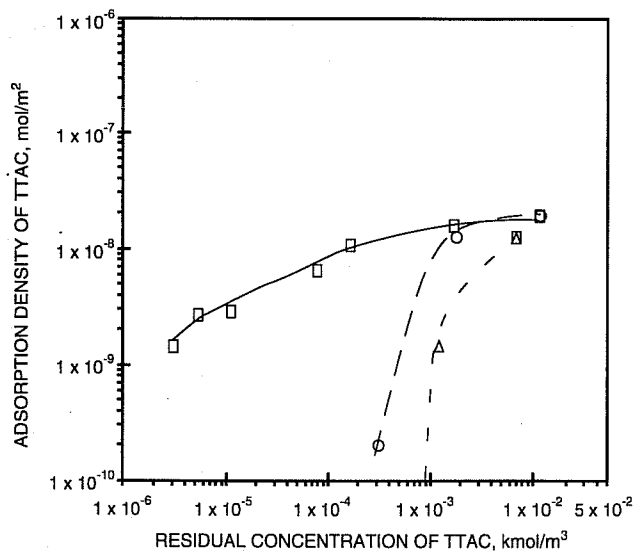


Fig. 5 Desorption of tetradecyl trimethyl ammonium chloride (TTAC) from alumina on dilution from different residual concentrations (C_r). TTAC:NP-15 = 1:4. \square , ADS. ISO. \circ , $C_r = 0.0114$. Δ , $C_r = 0.00683$.

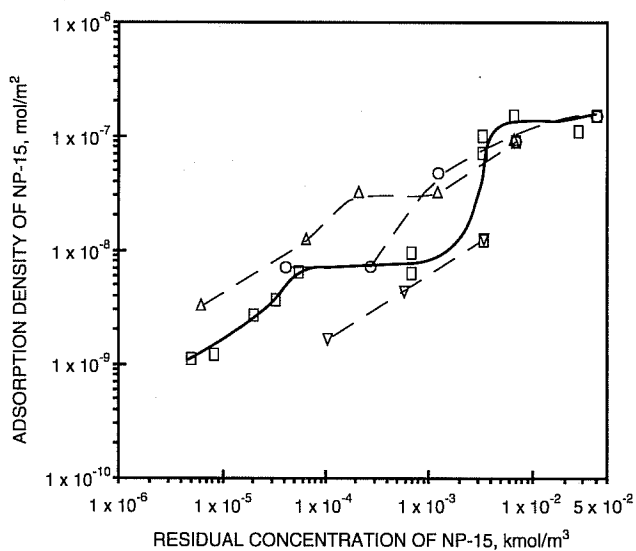


Fig. 6 Desorption of pentadecyl ethoxylated nonyl phenol (NP-15) from alumina on dilution from different residual concentrations (C_r). TTAC:NP-15 = 1:4. \square , ADS. ISO. \circ , $C_r = 0.041$. Δ , $C_r = 0.0067$. ∇ , $C_r = 0.0034$.

among desorption behavior, structure of the adsorbed layers, mixed micelles, and changes in monomer concentration ratio during desorption.

Solution Behavior of Surfactant Mixtures

On the basis of the pseudophase separation model, Rubingh¹ and Holland² have used the regular solution theory to treat mixed surfactant systems. For surfactant mixing, changes in the charged state of mixed micelles containing

ionic surfactants (ionic–ionic, ionic–nonionic, and cationic–anionic mixed micelles) can be included in the activity coefficients in the micelles. These activity coefficients f_i for binary mixtures can be expressed by the following equations:

$$f_1 = \exp [\beta \cdot (1 - x)^2] \quad (1)$$

$$f_2 = \exp (\beta \cdot x^2) \quad (2)$$

where x is the mole fraction of surfactant 1 in mixed micelles. β , which is a measure of the deviation of the mixture from ideality and which is related to the molecular interactions between surfactants 1 and 2 in the surface phase, is defined as follows:

$$\beta = \left[\frac{N_A (w_{11} + w_{22} - 2w_{12})}{RT} \right] \quad (3)$$

where w_{11} and w_{22} are the energies of interaction between similar kinds of surfactant molecules in the pure micelles; w_{12} is the interaction energy between different kinds of molecules in the mixed micelles; and N_A is the Avogadro number. The interaction parameter β can be evaluated as an experimental parameter from critical micelle concentration (CMC) values and used to interpret subsequent experiments. The following equations permit solution for β in terms of C_1 , C_2 , and C^* :

$$\left[\frac{x^2 \ln (C^* \alpha / C_1 x)}{(1 - x)^2 \ln [C^* (1 - \alpha) / C_2 (1 - x)]} \right] = 1 \quad (4)$$

$$\beta = \left[\frac{\ln (C^* \alpha / C_1 x)}{(1 - x)^2} \right] \quad (5)$$

where x = mole fraction of surfactant 1 in the mixed micelle

α = mole fraction of surfactant 1 in the total mixed solute

C^* = CMC of the mixture

C_1 and C_2 = CMCs of the individual surfactants 1 and 2, respectively

If the CMC of a binary mixed surfactant, C^* , is measured as a function of the mole fraction in bulk, α , and C_1 , C_2 , then x and C^* can be determined by means of Eqs. 4 and 5. The monomer concentrations of mixture can be calculated with the use of the following equations:

$$C_1^m = \left[\frac{-(C - \Delta) + [(C - \Delta)^2 + 4\alpha C \Delta]^{1/2}}{2 \cdot (f_2 C_2 / f_1 C_1 - 1)} \right] \quad (6)$$

where $\Delta = f_2 C_2 - f_1 C_1$

$$C_2^m = \left(1 - \frac{C_1^m}{f_1 C_1} \right) \cdot f_2 C_2 \quad (7)$$

Although regular solution theory has been criticized, it has provided a tractable way to describe the behavior of mixed surfactant aggregates. Some of the calculated results of x and C^* are shown in Table 1.

Critical micelle concentrations of the mixtures determined by surface-tension measurements are plotted in Fig. 7 as a function of NP-15 composition. Regular solution theory has been used to fit these data. The interaction parameter β for this system was found to be between -1.5 and -1.2 . A considerable number of binary mixed micellar systems have been studied with the use of regular solution theory.

Generally, the strength of interaction in mixed systems with cationic surfactants increases in the order of cationic–cationic, cationic–zwitterionic, cationic–nonionic, and cationic–anionic. For cationic–anionic systems, the value of the interaction parameter β can be about -25 ; for cationic–nonionic, -4.6 to -1.0 ; for cationic–cationic, about -0.2 to 0 . In addition to the nature of the components in the mixture, the interaction parameter is affected by the structure of the surfactants and the ionic strength of the mixed system. The interaction parameter observed for the TTAC:NP-15 system is small. This indicates that the interaction between TTAC and NP-15 is $0.03M$ sodium chloride (NaCl) solution is not very strong.

For a better understanding of the adsorption–desorption mechanisms, the monomer concentrations of different mixtures in this system were calculated with the use of regular solution theory with an interaction parameter of -1.5 . The results are shown in Figs. 8 and 9. A comparison of these monomer concentrations with the adsorption isotherms shows that the adsorption of NP-15 does not depend on its monomer concentration in the mixtures; for example, the adsorption of NP-15 in a 4:1 TTAC:NP-15 mixture is the most significant in all these mixtures, but its monomer concentrations are the lowest. This result is in agreement with the fact that the

TABLE 1
Calculated Results of x and C^* by Regular Solution Theory

α	$\beta = -1.5$		$\beta = -1.0$	
	x	$C^*(10^{-4}M)$	x	$C^*(10^{-4}M)$
0.05	0.4374	5.33	0.4271	6.03
0.10	0.5439	3.90	0.5512	4.42
0.125	0.5795	3.49	0.5925	3.93
0.20	0.6567	2.69	0.6808	3.01
0.25	0.6974	2.37	0.7232	2.63
0.30	0.7267	2.12	0.7580	2.34
0.40	0.7793	1.78	0.8135	1.92
0.50	0.8229	1.54	0.8571	1.65
0.60	0.8613	1.37	0.8932	1.44
0.70	0.8968	1.24	0.9244	1.29
0.80	0.9308	1.13	0.9520	1.16
0.90	0.9647	1.05	0.9770	1.06
0.95	0.9821	1.01	0.9887	1.02
0.99	0.9964	0.99	0.9978	0.99

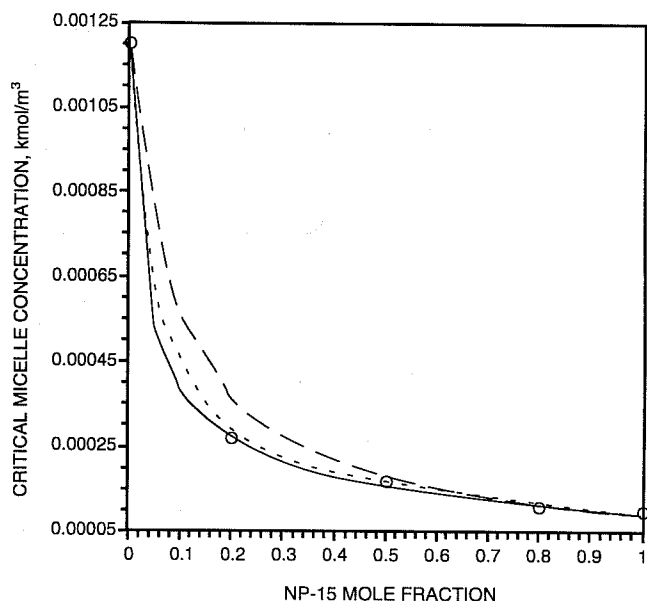


Fig. 7 Measured critical micelle concentration (CMC) and theoretical CMC calculated from ideal mixing and regular mixing for mixtures of tetradecyl trimethyl ammonium chloride (TTAC) and pentadecyl ethoxylated nonyl phenol (NP-15). \circ , experimental data. —, $\beta = -1.5$. - · - ·, $\beta = -1.0$. — — —, ideal mixing.

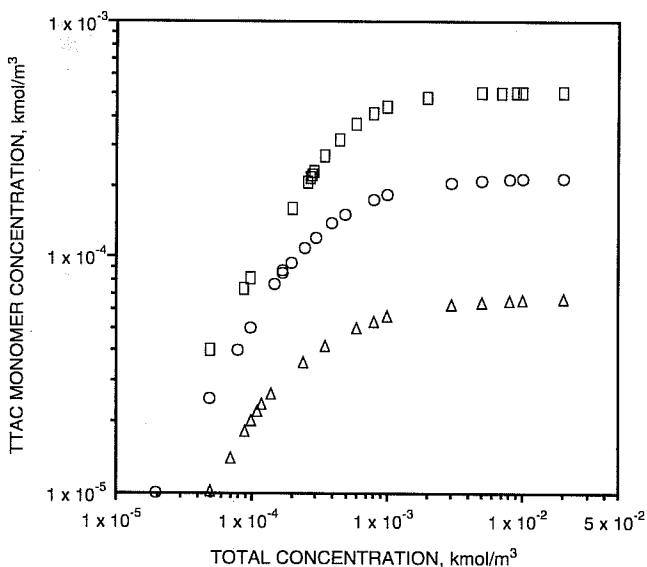


Fig. 8 Monomer concentrations of tetradecyl trimethyl ammonium chloride (TTAC) in different TTAC:NP-15 mixtures calculated from regular mixing theory with interaction parameter $\beta = -1.5$. \square , TTAC:NP-15 4:1. \circ , TTAC:NP-15 1:1. Δ , TTAC:NP-15 1:4.

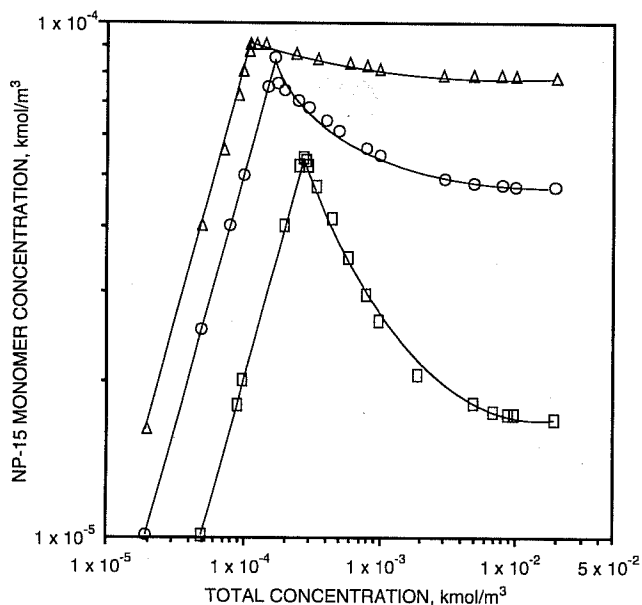


Fig. 9 Monomer concentrations of pentadecyl ethoxylated nonyl phenol (NP-15) in different tetradecyl trimethyl ammonium chloride (TTAC):NP-15 mixtures calculated from regular mixing theory with interaction parameter $\beta = -1.5$. \square , TTAC:NP-15 4:1. \circ , TTAC:NP-15 1:1. Δ , TTAC:NP-15 1:4.

adsorption of NP-15 depends on the pre-adsorbed TTAC acting as anchors. For the adsorption of TTAC, the adsorbed amount corresponds to the monomer concentrations in the mixtures. The higher the monomer concentration, the higher the adsorption density. Because these monomer concentrations are the concentrations calculated before adsorption, it is not directly related to changes in the monomer composition on adsorption and during desorption. It is therefore necessary to determine the variation of the monomer concentration of each component during the adsorption and desorption directly by some suitable experimental methods.

References

1. D. N. Rubingh, Mixed Micelle Solutions, in *Solution Chemistry of Surfactants*, K. L. Mittal (Ed.), Vol. 1, p. 337, Plenum Press, New York, 1979.
2. P. M. Holland and D. N. Rubingh, Nonideal Multicomponent Mixed Micelle Model, *J. Phys. Chem.*, 87: 1984 (1983).

INVESTIGATION OF OIL RECOVERY IMPROVEMENT BY COUPLING AN INTERFACIAL TENSION AGENT AND A MOBILITY CONTROL AGENT IN LIGHT OIL RESERVOIRS

Contract No. DE-AC22-92BC14886

Surtek, Inc.
Golden, Colo.

Contract Date: Sept. 28, 1992
Anticipated Completion: Sept. 30, 1995
Government Award: \$219,925
(Current year)

Principal Investigator:
Malcolm J. Pitts

Project Manager:
Jerry Casteel
Bartlesville Project Office

Reporting Period: July 1–Sept. 30, 1994

Objectives

Two major areas concerning the coinjection of an interfacial tension (IFT) reduction agent(s) and a mobility control agent into petroleum reservoirs will be studied. First, the mechanisms of interaction of an alkaline agent, a surfactant, and a polymer on a fluid–fluid and a fluid–rock basis will be defined, and then the improvement of the economics of the combined technology will be studied. The effect of injected fluid composition on incremental oil recovery is examined. Polymer concentration and alkali and surfactant design were studied. The effect on incremental oil recovery of injecting the alkaline–surfactant–polymer (ASP) solution either without a prior waterflood or after a waterflood is reported.

Summary of Technical Progress

Solutions were dissolved in 1000 mg/L sodium chloride (NaCl); 1000 mg/L NaCl was used to saturate the core and as the displacing fluid when water was injected. The crude oil used was from the Adena field, Morgan Co., Col., a fluvial–deltaic reservoir. Crude oil is a 42°API gravity crude oil with a dead oil viscosity of 3.8 cP at 72 °F and 1.3 cP at the 180 °F reservoir temperature. All studies were performed at 150 °F. Dead crude oil viscosity was 1.4 cP at evaluation temperature.

A previous series of relative permeability evaluations indicated that, when alkali and surfactant were added to the injected water, the mobility ratio increased.¹ When sodium carbonate (NaCO₃) and Petrostep B-100 are added to the

injection water, the previous relative permeability determinations indicate that the mobility ratio increases to 3.86 from 0.56.

So that the effect on oil recovery of changing the injected solution viscosity and, therefore, the mobility ratio could be defined, a series of radial corefloods with the use of Berea sandstone were performed in which different concentrations of polyacrylamide polymer were added to an alkaline–surfactant solution. Each core was waterflooded to an average residual oil saturation of 0.315 pore volume (PV). An injection of 0.300 PV of 1.0 wt % Na₂CO₃ plus 0.2 wt % Petrostep B-100 plus varying concentrations of Flopaam 3330S was followed by an injection of 0.300 PV of polymer at the ASP solution concentration. A water flush of 1.5 PV followed chemical injection. The incremental oil as a function of initial oil saturation is plotted against polymer concentration in Fig. 1. Incremental oil produced reaches an asymptote as the concentration of polymer increases. For the rock–oil–ASP solution studied, the ASP viscosity was approximately half the viscosity value required to achieve a mobility ratio of 1 on the basis of Brookfield viscometer measurements. The polymer drive solution calculated mobility ratio is about 1.

Figure 2 demonstrates that a previous waterflood does not alter the total oil recovery of an ASP solution. An identical procedure was listed for the previous series of corefloods except the 0.300 PV of 1.0 wt % Na₂CO₃ plus 0.2 wt % Petrostep B-100 plus 500 mg/L Flopaam 3330S was injected without a waterflood. Radial Berea sandstone corefloods were performed.

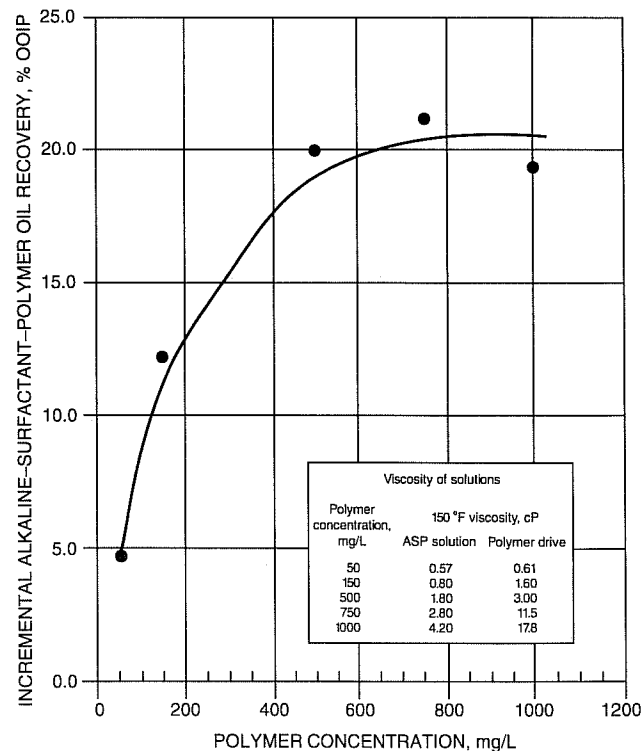


Fig. 1 Effect of polymer concentration on alkaline–surfactant–polymer oil recovery. OOIP, original oil in place.

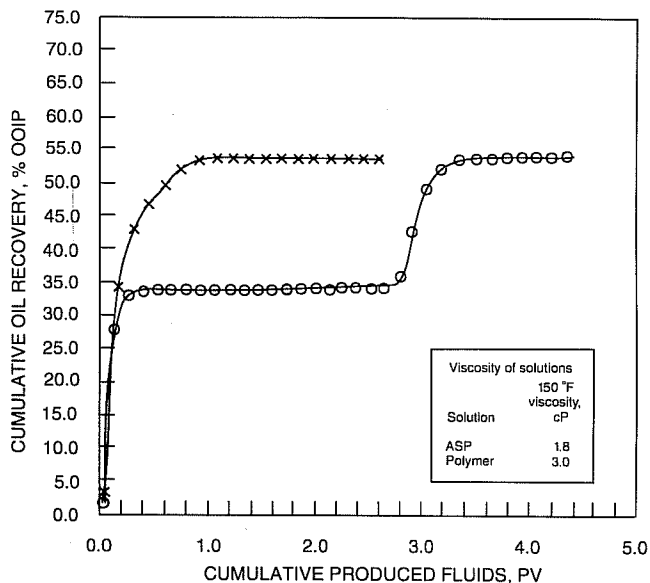


Fig. 2 Cumulative oil recovery vs. cumulative produced fluids of an alkaline-surfactant-polymer solution. Injected solution = 1.0 wt % Na_2CO_3 + 0.2 wt % Petrostep B-100 + 500 mg/L Flopaam 3330S. \circ , with a prior waterflood. \times , without a prior waterflood. OOIP, original oil in place.

Different ASP solutions with identical IFT values were injected into Berea sandstone radial corefloods after a waterflood following the same injection procedure outlined for the previously discussed corefloods. Figure 3 shows results of the corefloods. Even though all the solutions had ultralow IFT values, incremental oil varied from essentially 0 to 20% original oil in place.

The effect of rock composition on oil recovery will be evaluated next. Variations of the injection sequence on economics of the oil recovery process will be investigated after rock composition.

Reference

1. M. J. Pitts, *Investigation of Oil Recovery Improvement by Coupling an Interfacial Tension Agent and a Mobility Control Agent in Light Oil Reservoirs*, Quarterly Report, June 1994.

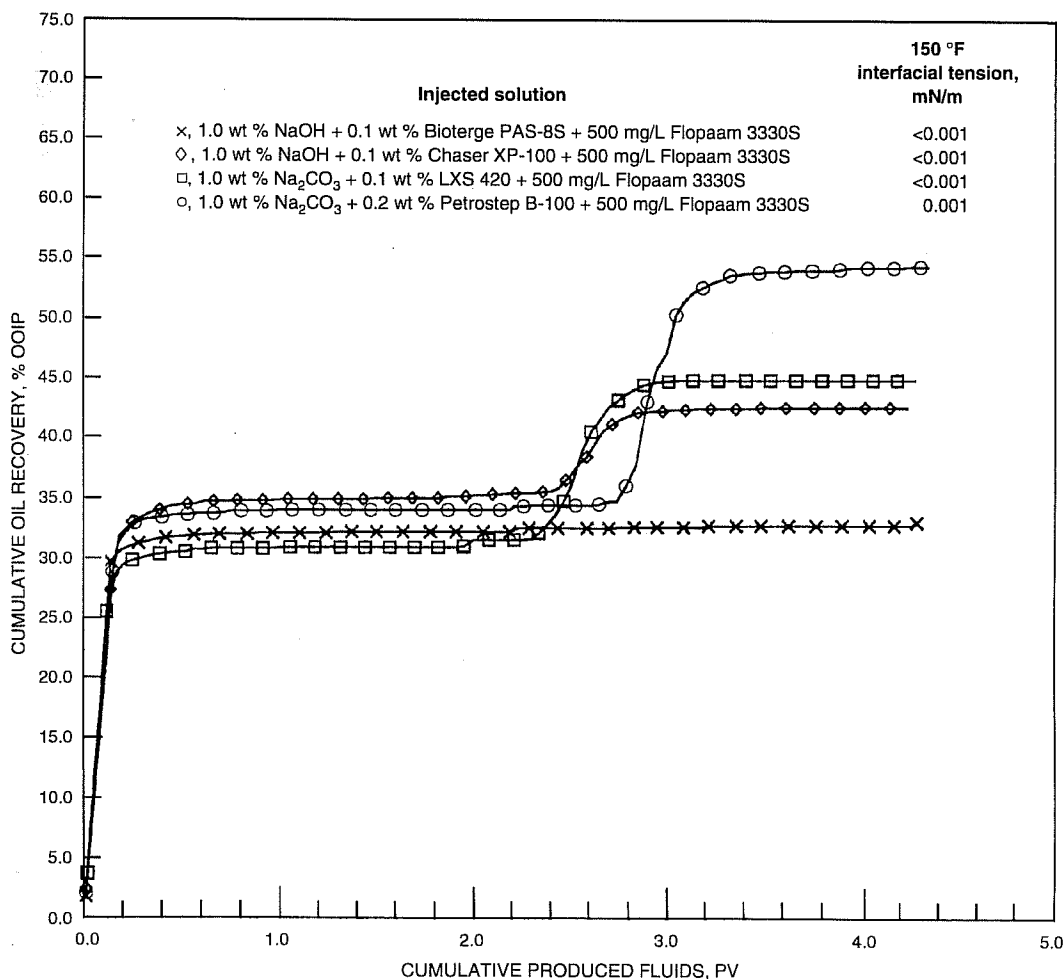


Fig. 3 Cumulative oil recovery vs. cumulative produced fluids of different chemical solutions with ultralow interfacial tension values. Waterflood cumulative oil recovery = 1.0. OOIP, original oil in place.

GAS DISPLACEMENT— SUPPORTING RESEARCH

PRODUCTIVITY AND INJECTIVITY OF HORIZONTAL WELLS

Contract No. DE-FG22-93BC14862

**Stanford University
Stanford, Calif.**

**Contract Date: Mar. 10, 1993
Anticipated Completion: Mar. 10, 1998
Government Award: \$359,000
(Current year)**

Principal Investigators:

**F. John Fayers
Khalid Aziz
Thomas A. Hewett**

Project Manager:

**Thomas Reid
Bartlesville Project Office**

Reporting Period: July 1–Sept. 30, 1994

Objectives

The project objectives include the following:

- *Modeling horizontal wells*—Establish detailed three-dimensional (3-D) methods of calculation that will successfully

predict horizontal well performance under a range of reservoir and flow conditions, review both commercial simulators and simple inflow performance relationships used by the industry, investigate the sensitivity of various parameters on the performance of horizontal wells, and develop modeling techniques and computer codes based on generalized 3-D flexible gridding techniques that can be incorporated into reservoir simulators.

- *Reservoir characterization*—Investigate reservoir heterogeneity descriptions of interest to applications of horizontal wells, develop averaging techniques in 3-D that will adequately compute the effective single-phase and two-phase directional permeabilities within the variable gridding characteristics of the model developed in task 1, and perform sensitivity studies of the averaging technique to uncertainties in the heterogeneity distribution.

- *Experimental planning and interpretation*—Critically review technical literature on two-phase flow in pipes and the correlation of these results in terms of their relevance to horizontal wells; perform sensitivity studies to choose parameter spaces of interest for some typical field conditions using the advice of oil companies; plan key experiments to investigate sensitivity to parameter variation, including inflow distribution, completion variations, void fractions, etc.; perform data analysis, including flow pattern distribution, scaling, dependence on perforation intervals, confidence levels, etc.; and revise two-phase pressure drop in horizontal wells and incorporate this capability in the analytic solutions for critical rates task.

Summary of Technical Progress

The sensitivity study on the effects of wellbore friction, inflow, skin, etc., on the productivity of a horizontal well is complete. Work on developing models for scale-up and coarse-grid pseudo functions for horizontal wells in heterogeneous reservoirs continued. A new method based on the calculation of dissipation energy and the reassignment of streamlines seems promising when applied to a single-phase example problem. The Marathon Oil Co. experimental data have been compiled in the form of Excel worksheets. Work on setting up a large computer database for two-phase flow measurements is proceeding. About 20,000 measurement points have been included in the database so far, and the Marathon data will also be added. The second review meeting of the Horizontal Well Industrial Affiliates Program was held on September 22–23, 1994, at Stanford. In addition to the project presentations, a number of member presentations were made.

The major activity in the current reporting period has been the analyses of the data of the experiments being conducted at the Marathon Oil Co. About 30 experiments were conducted, and all the data have been compiled and analyzed. Samples of the results of the analyses are presented.

Analyses of Experiments at Marathon Oil Co.

Figure 1 shows a simple sketch of the Marathon Wellbore Model. The wellbore is essentially a transparent acrylic pipe with an average inside diameter of 6.2 in. Variations in the diameter of the wellbore have been measured by mechanical and ultrasonic techniques. The layout consists of 20 ft of blank acrylic, followed by 20 ft of smooth perforations, followed by 15 ft of sharp perforations. Liquid or gas inflow can be supplied by the connected manifold to the next 40 ft of smooth-edged

perforations. The remaining 5 ft of the model is a blank section of acrylic casing.

Four types of experiments were performed in the wellbore model: single-phase flow of water or oil in the core flow with no inflow, single-phase flow of water or oil in the core flow plus inflow of water or oil through perforations, two-phase flow of oil and nitrogen in the core flow with no inflow through perforations, and single-phase flow of water or oil in the core flow with inflow of air or nitrogen through perforations. The oil flow rate was varied between 100 and 410 gal/min [3429 to 14057 stock tank barrels (STB)/d] in the experiments, whereas the nitrogen gas flow rate was supplied at the fixed maximum rate of about 0.45 MMscfd. Differential pressure drops per 10 ft were measured along the wellbore by two methods. In the first method, liquid manometers were used, and in the second method, the differential pressure drops were recorded electronically with Rosemount pressure transmitters, which have a relative accuracy of $\pm 0.2\%$. The Rosemount data were recorded about every 0.25 sec, and the experiments were run long enough so that steady conditions were achieved.

Single-Phase Flow Experiments

The single-phase core flow experiments were performed to characterize the wellbore model in terms of roughness and also to have a base-case experiment. Figure 2 shows data and calculated results for a sample of single-phase experiments with an oil rate of 408 gal/min. Both Rosemount and manometer measurements are shown, which are in close agreement. Two values of roughness, namely, $e = 8 \times 10^{-5}$ and $e = 2.5 \times 10^{-4}$ ft, were used for the calculations. The variations of the diameter of the wellbore were taken into account in the computations. Both values of roughness give reasonable match with the data, but the higher value of $e = 2.5 \times 10^{-4}$ ft provides the best overall fit to the seven data points and thus is the preferred choice for the

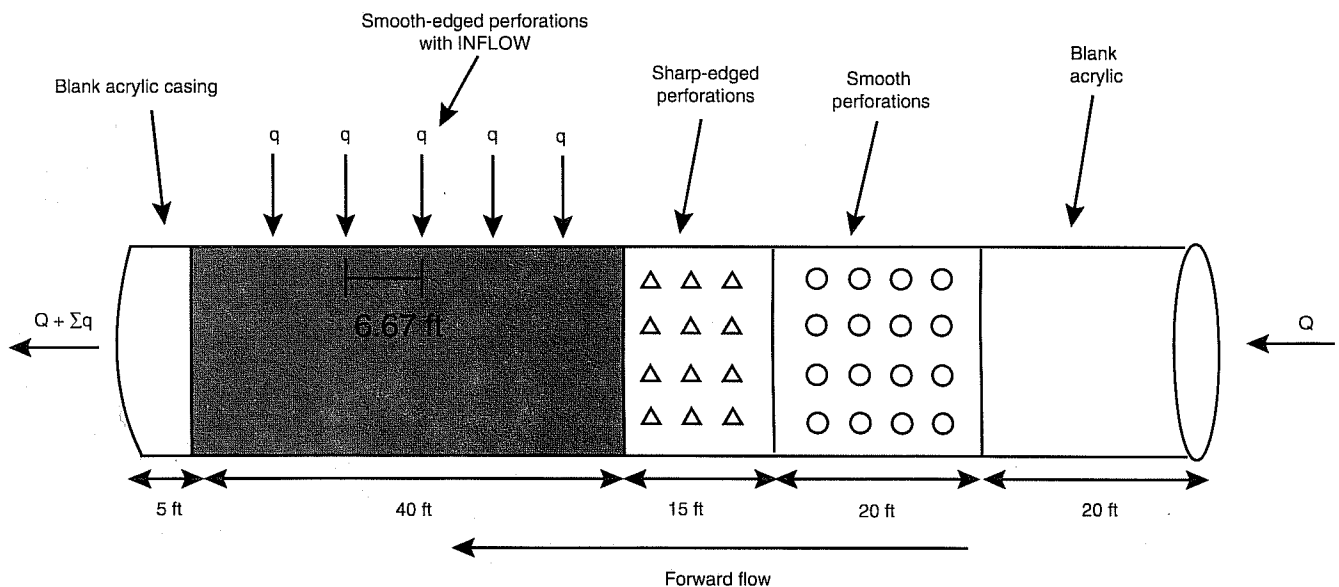


Fig. 1 Layout of the Marathon Wellbore Model.

roughness of the wellbore model. There is no apparent effect of different types of perforations on pressure drops when there is no inflow through them.

The effect of flow through perforations was studied in the second type of experiment, where 408 gal/min of oil flowed in the core but an additional 85 gal/min of oil also entered radially through perforations. The influx was uniformly distributed over the inflow length of 40 ft along the wellbore (Fig. 1). Figure 3 shows the data and the calculations. Computations with the base roughness of 2.5×10^{-4} nearly match the pressure drop data in the entrance section of the wellbore, but they underestimate the values in the inflow section. Conversely, calculated results based on $e = 0.001$ ft show a closer match with the data. A higher roughness in this experiment indicates that radial inflow of oil in a single-phase flow experiment increases the effective roughness of the wellbore.

Two-Phase Flow Experiments

The two-phase flow experiments involved two-phase core flows along the entire length of the wellbore with no inflow through the perforations. A sample of these experiments is

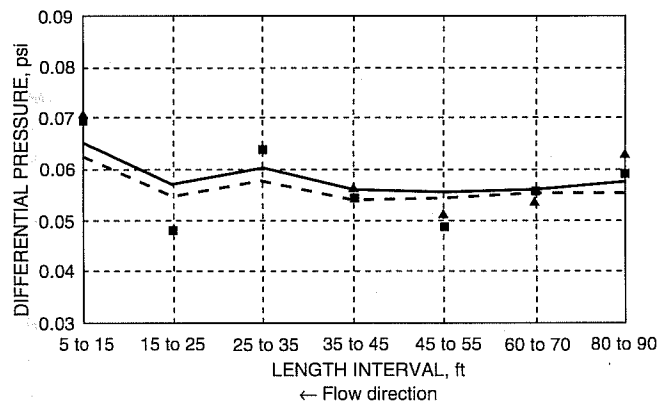


Fig. 2 Data and calculated results for a single-phase oil flow experiment with no inflow. Oil (408 gal/min) core flow with no inflow (oil viscosity = 9.17 cP). ■, Rosemount data. ▲, manometer data. —, calculated $e = 8 \times 10^{-5}$ ft. — —, calculated, $e = 0.00025$ ft.

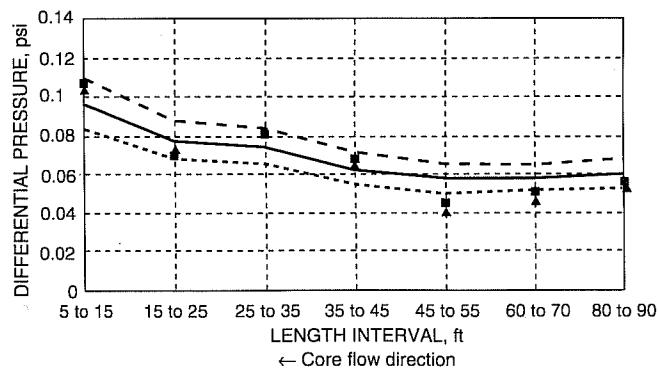


Fig. 3 Data and calculated results for a single-phase oil flow experiment with inflow. Oil (408 gal/min) core flow with oil (85 gal/min) inflow. ■, Rosemount data. ▲, manometer data. - - -, calculated, $e = 0.00025$ ft. —, calculated, $e = 0.001$ ft. - · -, calculated, $e = 0.002$ ft.

shown in Fig. 4 for an oil rate of 403 gal/min and a gas rate of 0.441 MMscfd, where pressure drops larger than those in the single-phase experiments are observed. The two data points at the 80- to 90- and 60- to 70-ft locations show much smaller pressure drops, which are due to the entrance effects. Calculations were performed with the Aziz, Spencer & Associates Inc. (ASA) Software¹ using the Beggs and Brill model,² the Dukler et al. model,³ and the newly developed Stanford Mechanistic model, all with the base roughness value of $e = 2.5 \times 10^{-4}$. The Stanford Mechanistic model is under development and testing, hence the present model predictions should be regarded as preliminary. Figure 4, however, indicates good agreement between all three models for this experiment. Figure 5 displays the results for the same type of experiment but with lower oil rate of 306 gal/min (gas rate of 0.466 MMscfd is almost the same as in the experiment in Fig. 4). For this case, the Stanford Mechanistic model predicted differently and is only in agreement with the two data points with high pressure drops.

In these experiments, two-phase flow was established only along the inflow section of the wellbore by supplying gas radially through perforations. Figure 6 shows the data and the

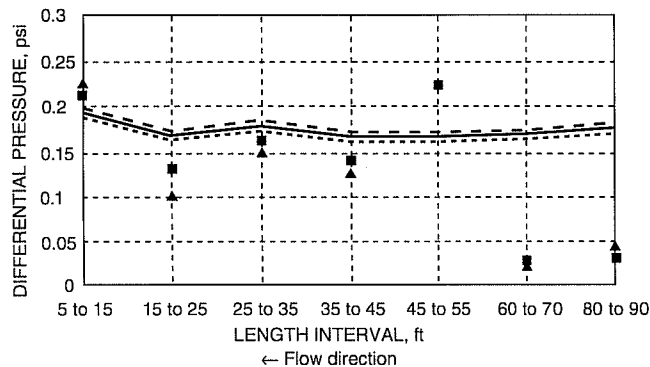


Fig. 4 Data and calculated results for a two-phase flow core experiment. Oil (403 gal/min) and N₂ (0.441 MMscfd) in core flow. ■, Rosemount data. ▲, manometer data. - - -, Beggs and Brill, $e = 0.00025$ ft. - · -, Dukler et al., $e = 0.00025$ ft. —, Stanford Mechanistic, $e = 0.00025$ ft.

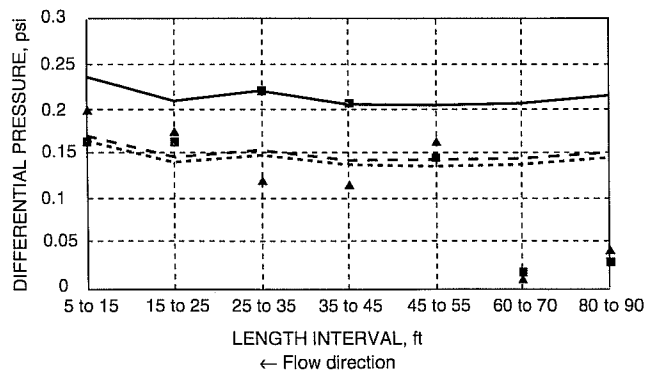


Fig. 5 Data and calculated results for a two-phase flow core experiment. Oil (306 gal/min) and N₂ (0.466 MMscfd) in core flow. ■, Rosemount data. ▲, manometer data. - - -, Beggs and Brill, $e = 0.00025$ ft. - · -, Dukler et al., $e = 0.00025$ ft. —, Stanford Mechanistic, $e = 0.00025$ ft.

calculated predictions with an oil rate of 408 gal/min and a gas rate of 0.425 MMscfd. It is clear that predictions with the base roughness value of $e = 2.5 \times 10^{-4}$ ft underestimate the data in the two-phase region. The results with the higher $e = 0.002$ ft show better agreement with the two-phase data, as depicted in Fig. 7. The results in Figs. 6 and 7 demonstrate that radial influx of gas through perforations increases the pressure drop in comparison with uniform two-phase core flow, and therefore a higher effective roughness is required to model the experiments.

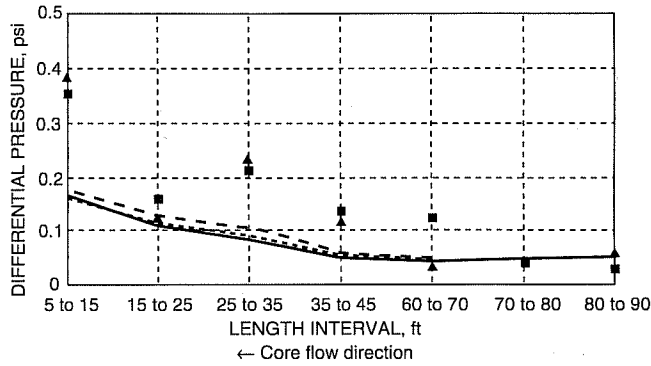


Fig. 6 Data and calculated results for a two-phase flow experiment with inflow of gas with $e = 0.00025$ ft. Oil (408 gal/min) core flow with N₂ (0.425 MMscfd) inflow. ■, Rosemount data. ▲, manometer data. --, Beggs and Brill, $e = 0.00025$ ft. - - -, Dukler et al., $e = 0.00025$ ft. —, Stanford Mechanistic, $e = 0.00025$ ft.

In addition to the pressure-drop measurements, liquid holdups (in situ liquid volume fractions) were measured by a capacitance holdup meter stationed downstream at the 12-ft mark of the wellbore. The effect of the inflow of gas on liquid holdup is shown in Fig. 8 and compared with the equivalent core flow case with oil rates of about 200 gal/min and gas rates of about 0.44 MMscfd. The cyclic jumps observed in Fig. 8 are the result of liquid slugs rapidly passing by the meter. The data clearly show that radial influx of gas increases the liquid holdup.

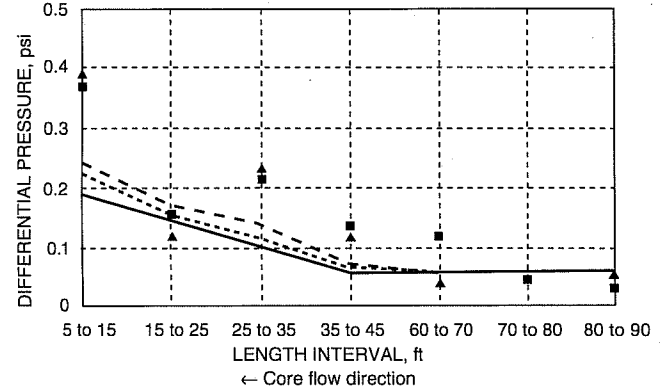


Fig. 7 Data and calculated results for a two-phase flow experiment with inflow of gas with $e = 0.002$ ft. Oil (408 gal/min) core flow with N₂ (0.425 MMscfd) inflow. ■, Rosemount data. ▲, manometer data. --, Beggs and Brill, $e = 0.002$ ft. - - -, Dukler et al., $e = 0.002$ ft. —, Stanford Mechanistic, $e = 0.002$ ft.

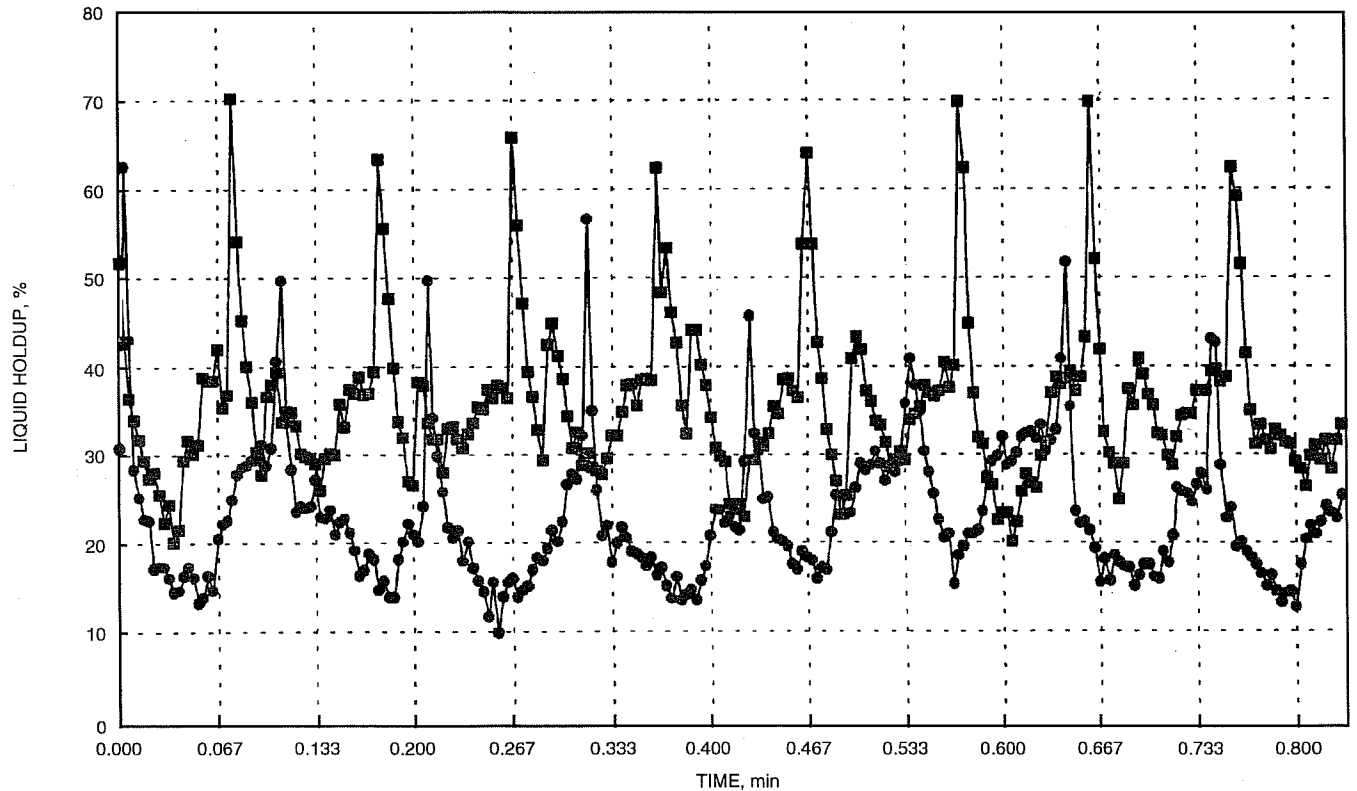


Fig. 8 Comparison of liquid holdup with inflow and no inflow of gas. Oil (200 gal/min) and N₂ (0.440 MMscfd). —●—, no inflow. —■—, with inflow of nitrogen.

References

1. *ASA Multiphase Flow Software Systems User Guide*, Aziz, Spencer & Associates Inc., 1993.
2. H. D. Beggs and J. P. Brill, A Study of Two Phase Flow in Inclined Pipes, *J. Pet. Technol.*, 25: 607-617 (May 1973).
3. A. E. Dukler, M. Wicks, and R. G. Cleveland, Frictional Pressure Drop in Two-Phase Flow: An Approach Through Similarity Analysis, *A.I.Ch.E. J.*, 10: 44-51 (January 1964).

DETAILED EVALUATION OF THE WEST KIEHL ALKALINE-SURFACTANT-POLYMER FIELD PROJECT AND ITS APPLICATION TO MATURE MINNELUSA WATERFLOODS

Contract No. DE-AC22-93BC14860

**Surtek, Inc.
Golden, Colo.**

**Contract Date: Jan. 7, 1993
Anticipated Completion: Sept. 30, 1994
Government Award for FY93: \$165,148
(Current year)**

**Principal Investigator:
Malcolm J. Pitts**

**Project Manager:
Thomas Reid
Bartlesville Project Office**

Reporting Period: July 1-Sept. 30, 1994

Objectives

The objectives of this research are to (1) quantify the incremental oil produced from the West Kiehl alkaline-surfactant-polymer (ASP) project by classical engineering and numerical simulation techniques, (2) quantify the effect of chemical slug volume on incremental oil in the two swept areas of the field, (3) determine the economics of the application of the ASP technology, (4) forecast the results of injecting an ASP solution to mature waterfloods and polymer floods, and (5) provide the basis for independent operators to book additional oil reserves by using the ASP technology.

Summary of Technical Progress

The numerical simulation of the waterflood, polymer flood, alkaline-surfactant flood, and ASP flood predictions from the

West Kiehl, Simpson Ranch, and Prairie Creek South fields has been performed.

Fields Selected for Numerical Simulation

A geological study of 72 Minnelusa fields surrounding the West Kiehl is complete. Of the 72 fields, 35 were studied in detail, and from these 35 fields, Prairie Creek South and Simpson Ranch were selected for numerical simulation as representative of Minnelusa waterfloods and polymer floods, respectively. Prairie Creek South and Simpson Ranch were selected because their geology and reservoir size were similar to West Kiehl, both floods are more mature than the West Kiehl, and both reservoirs have a single injection well.

The West Kiehl, Prairie Creek South, and Simpson Ranch reservoir characteristics used in the numerical simulation are listed in Table 1. The average formation characteristics are from the history matches. These Minnelusa reservoirs were modeled with the use of the GCOMP reservoir simulator. The GCOMP reservoir simulator provides black-oil, compositional, pseudo-miscible, and chemical matching and forecasting capabilities.

West Kiehl Simulation Predictions

The West Kiehl field ASP flood^{1,2} was history matched through December 1993. A 12 × 33 grid with three layers was used in the West Kiehl numerical simulation. The chemical option of the simulator was calibrated by matching laboratory corefloods.

Figure 1 shows the cumulative oil, cumulative water, and oil cut of the ASP history match with the field production data. The ASP forecast extends to October 2002. Figure 1 also depicts the prediction for a waterflood, mobility control polymer flood, and an alkaline-surfactant flood. The volume of alkaline-surfactant solution injected was equal to the volume of ASP solution in the ASP forecast. The volume of mobility controlled fluid injected into the polymer flood was equal to the volume of mobility controlled fluid injected into the ASP forecast. The projected oil recoveries for each forecast are listed in Table 2.

Figure 2 depicts the volume of incremental oil as a function of ASP solution injected. For each prediction, the volume of mobility controlled solution injected was the same with the mobility control polymer flood being the 0 volume alkaline-surfactant case. Extending polymer drive behind the ASP solution increases the incremental oil recovery at the West Kiehl. An additional 1.25 and 2.75 yr of polymer drive injection resulted in an increase of the incremental oil at well Nos. 32-36, 42-36, and 25-15. Additional incremental oil recovery was 42,000 and 61,000 bbl, respectively.

Two classical reservoir engineering techniques to estimate the amount of oil that the West Kiehl field will ultimately produce consisted of extrapolating a water-cut vs. cumulative-oil plot and a log barrels of oil per day vs. cumulative oil plot. The water-cut extrapolation estimates the ultimate oil recovery to be 943,000 bbl, and a log monthly oil rate extrapolation estimates the ultimate oil recovery to be 1,052,000 bbl.

TABLE 1

West Kiehl, Prairie Creek South, and Simpson Ranch
Reservoir Characteristics

	West Kiehl	Prairie Creek South	Simpson Ranch
Field characteristics			
Producing sand	B	B	B
Depth, ft	6630	6975	7885
Temperature, °F	134	138	165
Initial reservoir pressure, psi	2225	2580	3050
Field pore volume, MMbbl	3.10	2.65	3.69
Field initial oil saturation, MMbbl	2.17	2.00	2.28
Unit pore volume, MMbbl	1.37		
Kottabra pore volume, MMbbl	0.65		
Formation characteristics			
Average permeability, mD	457	336	597
Average porosity, %	18.3	17.4	19.4
Thickness, ft	15.1	22.0	20.3
Average initial water saturation, %	22.5	23.1	35.0
Field characteristics			
Crude oil API gravity, degree	24	20	21
Crude oil viscosity at reservoir conditions, cP	17.0	18.3	15.7
Oil formation volume factor	1.030	1.030	1.050
Water viscosity at reservoir conditions, cP	0.56	0.56	0.42

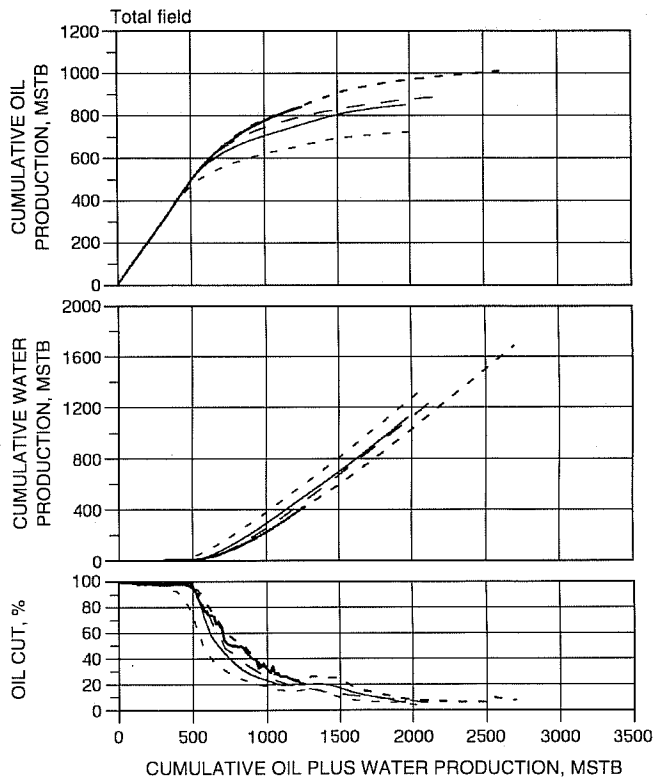


Fig. 1 West Kiehl cumulative oil, cumulative water, and oil cut vs. cumulative oil plus water. ---, waterflood forecast. -.-, alkaline-surfactant-polymer forecast. —, alkaline-surfactant forecast. — — —, actual alkaline-surfactant-polymer. - · - ·, polymer flood forecast.

Prairie Creek South Predictions

The Prairie Creek South field waterflood was history matched through 1993. The numerical simulation consisted of a 9 × 13 grid with three layers. Relative permeability data were identical to the West Kiehl data. The initial oil saturation was 65% pore volume (PV), which was consistent with log calculations. Figure 3 depicts the cumulative oil, cumulative water, and oil cut for the waterflood history match with the field production data.

An ASP flood and a polymer flood were forecasted with the chemical option parameters being identical to those of the West Kiehl forecast. Figure 3 shows the waterflood, polymer flood, and ASP flood forecasts. Incremental oil recoveries observed with the chemical floods are listed in Table 3. Estimated ultimate oil recoveries for the Prairie Creek South waterflood with water-cut and oil-rate-per-month extrapolation methods are 765,000 and 815,000 bbl, respectively.

Simpson Ranch Predictions

The Simpson Ranch polymer flood³ was history matched through 1993. The numerical simulation consisted of a 9 × 12 grid with five layers. Relative permeability data were identical to the West Kiehl data. The initial oil saturation was 75.9% PV, which was consistent with log calculations. Figure 4 depicts the cumulative oil, cumulative water, and oil cut for the polymer flood history match with the field production data.

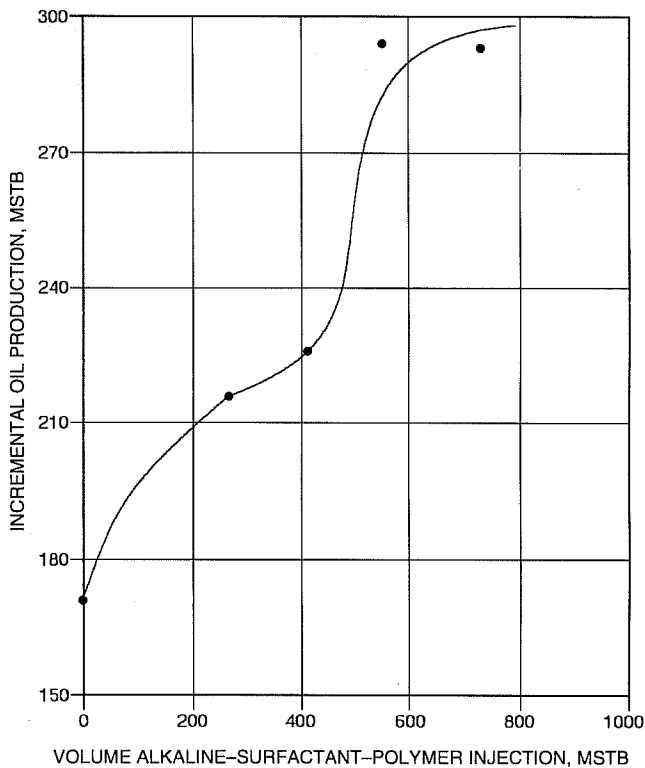


Fig. 2 West Kiehl incremental oil recovery by alkaline-surfactant-polymer vs. volume of alkaline-surfactant-polymer injection.

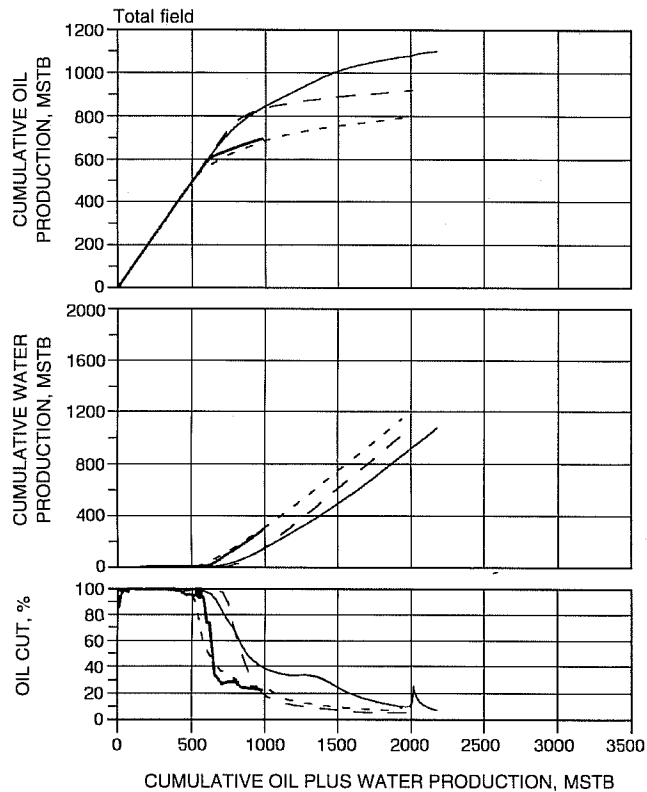


Fig. 3 Prairie Creek South cumulative oil, cumulative water, and oil cut vs. cumulative oil plus water. ---, waterflood forecast. —, actual waterflood. —·—, alkaline-surfactant-polymer forecast. - - - , polymer flood forecast.

TABLE 2
West Kiehl Numerical Simulation Predicted Oil and Water

Flooding process	Cumulative oil,* MSTB	Cumulative water,* MSTB	Incremental oil,* MSTB	Project ending date
Waterflood	726	1332		April 1998
Mobility control polymer	897	1304	171	December 2001
Alkaline-surfactant	850	1119	124	July 1997
Alkaline-surfactant-polymer	1017	1683	294	October 2002

*MSTB, thousand stock tank barrels.

TABLE 3
Prairie Creek South Numerical Simulation Predicted Oil and Water

Flooding process	Cumulative oil,* MSTB	Cumulative water,* MSTB	Incremental oil,* MSTB	Project ending date
Waterflood	790	1144		July 1999
Mobility control polymer	919	1090	129	September 2005
Alkaline-surfactant-polymer	1100	1075	310	October 2003

*MSTB, thousand stock tank barrels.

An ASP flood and a polymer flood were forecasted with the chemical option parameters being identical to those of the

West Kiehl forecast. Figure 4 shows the waterflood, polymer flood, and ASP flood forecasts. Incremental oil observed with

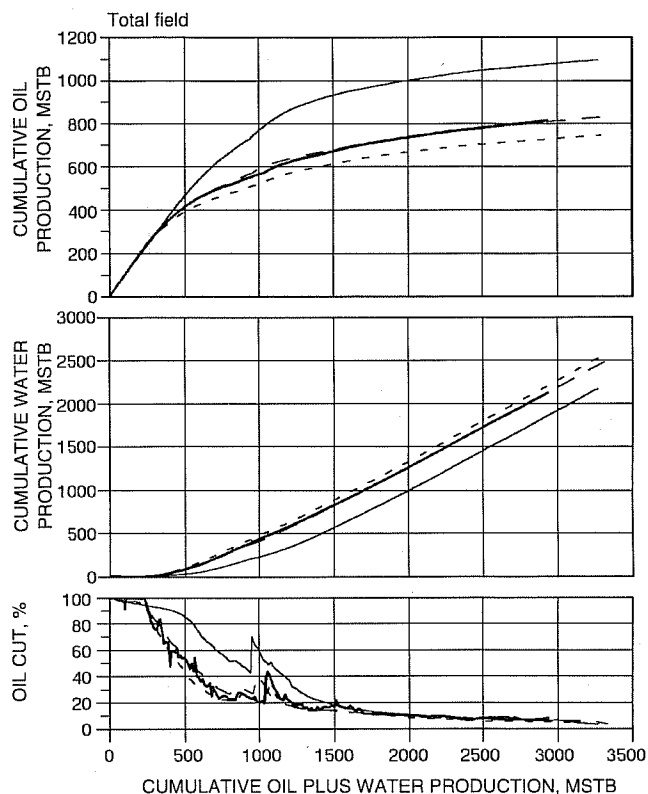


Fig. 4 Simpson Ranch cumulative oil, cumulative water, and oil cut vs. cumulative oil plus water. —, polymer flood forecast. —, actual polymer flood. —, alkaline-surfactant-polymer forecast. - - -, water-flood forecast.

the chemical floods is listed in Table 4. Estimated ultimate oil recoveries using water-cut and oil-per-month extrapolation methods for the Simpson Ranch polymer flood are 867,000 and 920,000 bbl, respectively.

Application to Waterflooded Minnelusa Fields

Numerical simulation was used to determine the amount of incremental oil an ASP project will recover in mature Minnelusa reservoirs. An ASP flood after a waterflood was numerically simulated for West Kiehl, Prairie Creek South, and Simpson Ranch. Conditions for each reservoir were identical to the previous numerical simulations except the initial oil saturation. Each of the waterfloods had reached the 12 bpd economic limit before ASP injection. The volume of ASP solution injected was proportional on a PV basis to that injected in the West Kiehl project. Table 5 indicates the incremental oil produced by an ASP flood implemented after a waterflood.

West Kiehl incremental oil recovery as the result of ASP injection after waterflood increased by 20,000 bbl. The change in incremental oil production is due to an increase in incremental oil at Kottabra 25-15 of 37,000 bbl (349,000 vs. 312,000 bbl) and a decrease in oil production at the State 32-36 and State 42-36 wells of 9,000 bbl (600,000 bbl vs. 609,000 bbl). The incremental oil production change is due to the Kottabra 25-15 well being on production for the entire

TABLE 4

Simpson Ranch Numerical Simulation Predicted Oil and Water

Flooding process	Cumulative oil,* MSTB	Cumulative water,* MSTB	Incremental oil,* MSTB	Project ending date
Waterflood	745	2544		March 1996
Mobility control polymer	831	2505	86	April 1996
Alkaline-surfactant-polymer	1095	2175	350	June 2003

*MSTB, thousand stock tank barrels.

TABLE 5

Mature Minnelusa Alkaline-Surfactant-Polymer After Waterflood Numerical Simulation Predicted Oil and Water

Flooding process	Cumulative oil,* MSTB	Cumulative water,* MSTB	Incremental oil,* MSTB	Additional project years
West Kiehl				
Waterflood	726	1332		0
Alkaline-surfactant-polymer	1047	4465	321	19.25
Prairie Creek South				
Waterflood	790	1144		0
Alkaline-surfactant-polymer	1062	2739	272	10.25
Simpson Ranch				
Waterflood	745	2544		0
Alkaline-surfactant-polymer	1068	5647	323	15.5

*MSTB, thousand stock tank barrels.

ASP injection period. In the actual flood, the Kottabra 25-15 was on production for only 6 months of ASP injection. Simpson Ranch and Prairie Creek South show a decrease in oil recovery of 23,000 and 38,000 bbl, respectively, compared with the injection of the ASP solution in a secondary mode.

Economic Evaluation

At the West Kiehl, from 1985 to 1990, \$376,119 was spent for chemicals and \$81,986 was spent for a laboratory feasibility study and incremental facilities cost. Incremental oil production of 291,000 bbl of oil predicted from the numerical simulation for ASP injection in a secondary mode gives an incremental cost per barrel of oil of \$1.57.

The 1994 costs for chemicals delivered to the Minnelusa area are polyacrylamide polymer, \$1.35/lb; Petrostep B-100, \$0.95/active lb; and sodium carbonate (Na_2CO_3), \$0.065/lb. Incremental facilities cost is estimated to be \$100,000, and laboratory feasibility cost and numerical simulation cost are estimated to be \$125,000. If these costs are applied to the ASP incremental oil recovery from the West Kiehl, Prairie Creek South, and Simpson Ranch, the incremental cost per barrel of oil is approximately \$3.00.

Estimated Ultimate Recovery Potential

Numerical simulation forecasts of ASP flooding suggest that the incremental oil produced from the combination of West Kiehl, Simpson Ranch, and Prairie Creek South was 906,000 bbl after waterflood and 951,000 bbl in a secondary mode from approximately 10,000,000 bbl of pore space. The Minnelusa trend has approximately 120 reservoirs with an estimated total pore space of 1.4 billion bbl. If the oil recovery efficiency of the West Kiehl is applied to all these fields, the incremental oil recovery potential is 130 million bbl of oil.

References

1. S. R. Clark, M. J. Pitts, and S. M. Smith, Design and Application of an Alkaline-Surfactant-Polymer Recovery System to the West Kiehl Field, *SPE Advanced Technology Series*, 1(1): 172-179 (April 1993).
2. J. J. Meyers, M. J. Pitts, and K. Wyatt, *Alkaline-Surfactant-Polymer Flood of the West Kiehl, Minnelusa Unit*, paper SPE/DOE 24144 presented at the Eighth SPE/DOE Enhanced Oil Recovery Symposium, Tulsa, Okla., April 21-24, 1992.
3. J. C. Mack and M. L. Duvall, *Performance and Economics of Minnelusa Polymer Floods*, paper SPE 12929 presented at the 1984 Rocky Mountain Regional Society of Petroleum Engineers Meeting, Casper, Wyo., May 20-23, 1984.

HORIZONTAL OIL WELL APPLICATIONS AND OIL RECOVERY ASSESSMENT

Contract No. DE-AC22-92BC14861

Maurer Engineering, Inc.
Houston, Tex.

Contract Date: June 3, 1993
Anticipated Completion: June 2, 1994
Government Award: \$124,119

Principal Investigator:
William J. McDonald

Project Manager:
Thomas Reid
Bartlesville Project Office

Reporting Period: July 1-Sept. 30, 1994

Objective

Thousands of horizontal wells are being drilled each year in the United States and around the world. Horizontal wells have increased oil and gas production rates 3 to 8 times those of vertical wells in many areas and have converted non-economic oil reserves to economic reserves. However, the use of horizontal technology in various formation types and applications has not always yielded anticipated success.

The primary objective of this project is to examine factors affecting technical and economic successes of horizontal well applications. The goals of the project will be accomplished through six tasks designed to evaluate the technical and economic successes of horizontal drilling, highlight current limitations, and outline technical needs to overcome these limitations. Data describing experiences of the operators throughout the domestic oil and gas industry will be gathered and organized. Maurer Engineering, Inc. (MEI) databases containing detailed horizontal case histories will also be used. All these data will be categorized and analyzed to assess the status of horizontal well technology and to estimate the impact of horizontal wells on present and future domestic oil recovery and reserves.

Summary of Technical Progress

Information Base on Horizontal Wells

A database was constructed from well data describing domestic horizontal wells. Three principal formations are the focus of the majority of this activity: the Austin Chalk in Texas, the Bakken Shale in North Dakota, and the Niobrara in Colorado and Wyoming. Results from these fields are well-known, and a large volume of published results is available. Because of the objective of the present study, analyses focused on formations other than these three fractured carbonates. On the basis of domestic well data, more than 670 horizontal wells (14% of the total) have been completed in other formations. About 180 operators drilled these other

wells in over 110 formations. Questionnaires covering more than 60% of these wells were returned.

Specialized Database for Horizontal Well Forecasting

A database for the data describing formations drilled horizontally was constructed in dBASE IV. Ninety-five questionnaires were received for the United States, with 23 formations described by two or more operators. The final industry response for the United States and Canada is summarized in Table 1.

TABLE 1
Horizontal Well Survey Responses

	Horizontal wells (as of 1/94)	Reservoirs with horizontal wells	Survey responses	Response rate
United States	4620	114	58	51%
Canada	1786	220	88	40%

Economic and Technical Trend Analysis

Multiple analyses have been performed on the database. Overview analyses were designed to determine the types and frequencies of the various applications of horizontal technology. The three most common applications for horizontal projects in the United States include intersecting fractures (listed for 53% of formations), delaying coning (33%), and favorable economics (35%).

Operators were asked whether their horizontal applications in each field were technical and/or economic successes. Of 57 responses, 54 were technically successful, which represents an overall 95% success rate. Economic success has not been so widespread as technical success. Of 56 responding formations, 28 were economic successes (50%) and 24 were economically successful (43%). An additional 4 formations (7%) had mixed economic results (i.e., multiple operators in a particular field reported both successful and unsuccessful projects). Carbonate applications have been slightly more technically successful clastic: 100% vs. 91%. Conversely, clastics were reported more economically successful than carbonates: 59% vs. 45%, respectively.

Production and cost ratios (Table 2) were used as an additional gage of success. These ratios compare the performance of a typical horizontal well with that of a typical vertical well. The benefit index compares production improvement with cost increment. Carbonates have been, on average, more economic than clastics. According to these results, the average horizontal application produces at a rate 3.2 times as great as a vertical well and costs twice as much. Thus the economics of horizontal development have been favorable for the average domestic application.

TABLE 2

Production and Cost Ratios for Horizontal Projects

Lithology	Production ratio	Cost ratio	Benefit index
Clastics	2.8	2.2	1.27
Carbonates	3.9	1.8	2.17
All formations	3.2	2.0	1.60

Horizontal Well Application Forecast

Another key parameter in the project data is the estimated increase in reserves as a result of implementing horizontal technology. Horizontal wells are expected to increase recoverable reserves through, for example, accessing oil not economically recoverable with vertical wells or delaying the onset of water coning.

Proven United States oil reserves amount to about 27 billion bbl according to the Tertiary Oil Recovery Information System. This volume represents 5% of the total domestic original oil in place (OOIP) of 513 billion bbl. Increases in reserves for individual reservoirs following horizontal development ranged from 0 to 300% (Fig. 1). The overall average increase is 8.7%. Extrapolated to the total United States reserves base, this represents an additional 12.3 billion bbl of reserves as the result of the widespread and appropriate application of horizontal technology. In terms of incremental recovery, this volume of oil corresponds to an additional 0.5% of OOIP.

Reserves increases for United States formations are summarized by lithology in Table 3. The average reserves increase for clastic formations is slightly less than that for carbonates.

Reserves increases by major application are shown in Table 4. For intersecting fracture applications, carbonate formations yielded a larger average increase than clastics. The opposite trend is true for coning applications.

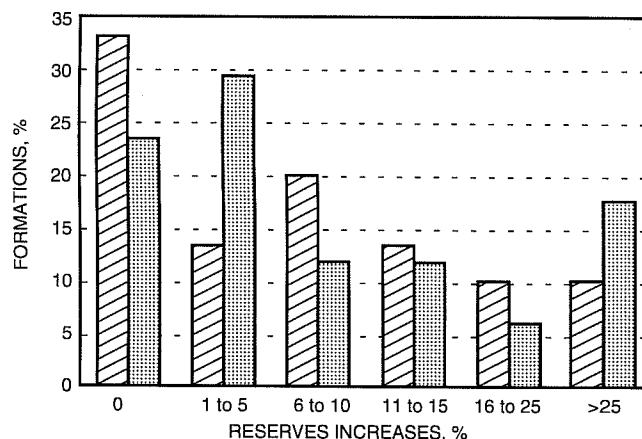


Fig. 1 Reserves increases for U.S. formations. ▨, clastics. ▩, carbonates.

TABLE 3
Reserves Increases

Lithology	Increase in reserves	
	%	BBO*
Clastics	8.4	1.5
Carbonates	9.2	0.7
Unknown	—	0.1
All formations	8.7	2.3

*BBO, billion barrels of oil.

TABLE 4
Reserves Increases by Application

Application	Increase in reserves, %		
	Clastics	Carbonates	All formations
Fractures	6.9	10.6	9.0
Coning	10.2	6.5	9.2

A forecast of the number of horizontal wells to be drilled over the next decade is shown in Fig. 2. This forecast was developed on the basis of the National Petroleum Council's model of the domestic resource base and future oil and gas consumption patterns. Two cases were utilized (assumed flat oil price and increasing price) and combined with the horizontal drilling share of the total drilling market. The average annual growth rate from 1994 to 2004 for this forecast is about 10% per year for a flat oil price scenario and 15% per year for an increasing oil price scenario.

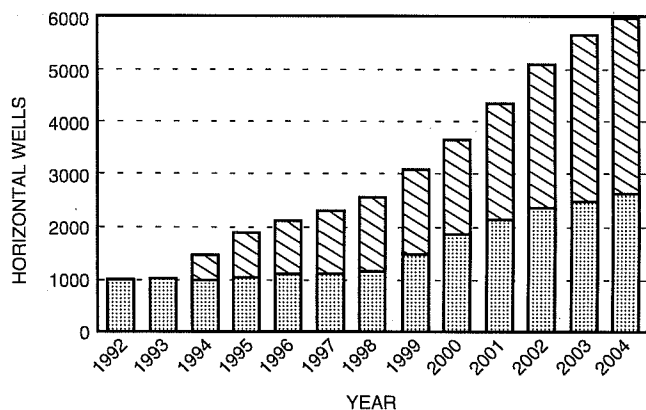


Fig. 2 U.S. horizontal well forecast. ▨, flat oil price. ▩, increasing oil price.

Analysis of Canadian Horizontal Well Experience

A major objective of the project is to forecast the future application of horizontal technology in historically less-popular formation types, including clastics (heavy oil and gas). Because of sparse data from the United States, the study

was expanded to include Canadian horizontal well application data. Canadian operators have exploited a wide variety of formation types with horizontal wells, including unconsolidated sands, fractured carbonates, tight reservoirs, and enhanced oil recovery (EOR) projects (steam and miscible fluids and bitumen production).

Production surveys similar to those distributed to domestic operators were sent to Canadian operators. More than 110 were returned and analyzed by the project team. Eighty-eight unique formations were described. Avoiding coning and favorable economics were the most popular Canadian applications, each at 48% of the pools. Along with intersecting fractures, these applications (fractures, coning, and economics) were the most popular in both the United States and Canada.

Technical and economic success rates of Canadian horizontal projects have been high. Technical success has been above 90% in all formation types. Economic success has generally been greater in Canada than in the United States. Carbonate formations have had much greater economic success in Canada (79% vs. 45%). In clastics, economic success in both countries is about 60%. Heavy oil Canadian projects have been economically successful more often than any other group (92%).

Production ratios for Canadian horizontal projects (Table 5) have been generally higher than those for United States projects. Cost ratios are similar for both countries (U.S. = 2.0). The highest production-to-cost benefit has been for Canadian heavy oil and clastics.

Reserves increases for Canadian formation attributed to horizontal technology are similar to those for the United States. The average increase is 9.5%. The distributions for light-oil clastics, carbonates, and heavy oil formations are shown in Fig. 3. Canadian heavy oil reservoirs showed the highest percentage of large reserves increases: 27% in the greater than 25% range. The average reserves increase for heavy oil is 11%, for clastics is 9%, and for carbonates is 7%.

The outlook for Canadian horizontal drilling is optimistic for the next few years. Canadian activity is expected to exceed that of the United States in 1994 by about 150 wells. Several factors contribute to the rapid increase in Canada in annual well counts. The forecast for the next decade was made on the

TABLE 5

Production and Cost Ratios for Canadian Horizontal Projects

Lithology	Production ratio	Cost ratio	Benefit index
Light-oil clastics	5.1	2.3	2.22
Carbonates	3.1	2.0	1.55
Heavy oil	5.6	2.5	2.24
Gas	3.4	1.8	1.89
All reservoirs	4.1	2.2	1.86

basis of ongoing and planned activity levels by operators. The annual well count (Fig. 4) is expected to peak at about 1400 wells/yr because of limitations imposed by supply and demand of rigs, trained personnel, and specialized equipment.

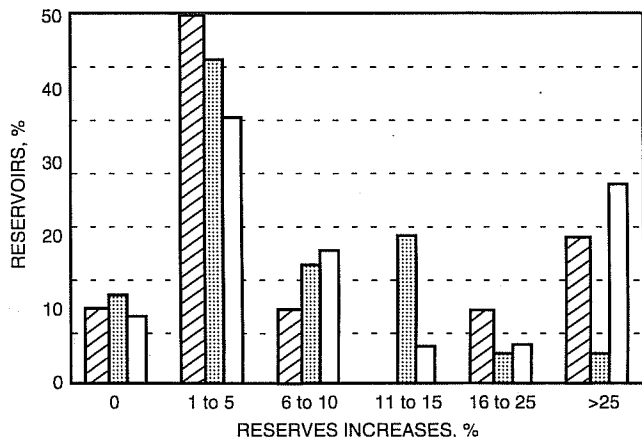


Fig. 3 Reserves increases for Canadian reservoirs. ▨, clastic (light). ▩, carbonates. □, heavy oil.

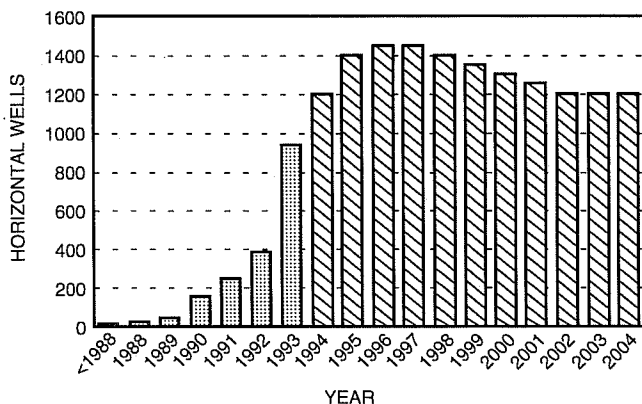


Fig. 4 Canadian horizontal well forecast. ▨, predicted level. ▩, historic level.

IMPROVED EFFICIENCY OF MISCIBLE CO₂ FLOODS AND ENHANCED PROSPECTS FOR CO₂ FLOODING IN HETEROGENEOUS RESERVOIRS

Contract No. DE-FG22-94BC14977

New Mexico Institute of Mining and Technology
Petroleum Recovery Research Center
Socorro, N. Mex.

Contract Date: Apr. 14, 1994
Anticipated Completion: Apr. 13, 1997
Government Award: \$320,000

Principal Investigators:
Reid B. Grigg
John P. Heller
David S. Schechter

Project Manager:
Jerry Casteel
Bartlesville Project Office

Reporting Period: July 1–Sept. 30, 1994

Objective

The objective of this work is to improve the effectiveness of carbon dioxide (CO₂) flooding in heterogeneous reservoirs. The intent is to investigate new concepts that can be applied by field operators within the next 2 to 5 yr. Activities will consist of experimental research in three closely related areas: (1) further exploration of the applicability of selective mobility reduction (SMR) in the use of foam flooding, (2) possible higher economic viability of floods at slightly reduced CO₂ injection pressures, and (3) taking advantage of gravitational forces during low interfacial tension (IFT), CO₂ flooding in tight, vertically fractured reservoirs.

Task 1 of this project is based on work performed during the recent *Field Verification of CO₂ Foam* (Report DOE/MC-26031) and on a previous project, *Improvement of CO₂ Flood Performance* (Report DOE/MC-21136). In these research projects, as well as in projects reported by other researchers, evidence was found for SMR when using certain surfactants in mobility experiments in which CO₂ and surfactant solution were pumped simultaneously through core samples cut from rocks of different permeabilities. Experiments that would decisively define the conditions under which SMR could be reliably realized in CO₂ floods could result in an increase in present productivity and add millions of barrels to the reserves of many oil fields in the Permian Basin and elsewhere where CO₂ is available.

The objective of Task 2 of the project is to demonstrate the feasibility of decreasing CO₂ requirements for CO₂ flooding. This objective can be achieved by using one or both of

two approaches. First, at a constant temperature, the density of CO₂ decreases with decreasing pressure and thus achieves reservoir fill volume with less mass at a lower pressure. The density of CO₂ is always less at the minimum miscibility pressure (MMP) than at several hundred pounds pressure higher, where most systems are being flooded. The density difference can be as high as 50%. Second, foaming agents can be used in conjunction with the injection scheme of water alternating with CO₂ as a mobility control agent. If these two concepts are used together, a synergistic effect should be provided by greatly reducing CO₂ requirements while maintaining or increasing the sweep efficiency of the process. This concept should be particularly applicable in the New Mexico–Texas region where many of the present and potential reservoirs for CO₂ miscible flooding are located. The concept should also be applicable to any gas injection scheme. All the experimental tests and modeling work in this study are designed to increase understanding and to test concepts related to this process.

Task 3 of the project falls under the broad topic “low IFT processes” and is directly related to all enhanced oil recovery (EOR) techniques that rely on the reduction of IFT for mobilization of residual oil. Miscible or near-miscible oil recovery processes, whether surfactant flooding or gas injection processes near the MMP, ultimately depend on the reduction of IFT between the resident and injected fluids. The approach to miscibility from an initially immiscible situation involves important consequences regarding dynamic lowering of the IFTs and subsequent alteration of the capillary pressure, P_c , and the Leverett J-function. These important parameters, in turn, determine the relative permeability function used for reservoir simulation.

Knowledge of the mechanism of IFT lowering is important for the simulation of EOR processes; for instance, the parachor method is currently being used as a prediction tool of IFT in multicomponent mixtures. The accuracy of the parachor method is limited and has been the subject of criticism, although there has been no rigorous study demonstrating the success or failure of the parachor method under widely differing conditions. The IFT and the density difference between the phases as miscibility is approached are the measured parameters in the evaluation of the parachor method. The IFT vs. density difference is also crucial when evaluating capillary–gravity equilibrium in fractured reservoirs, yet there is little understanding of the theory behind the parachor method and almost no literature concerning measurement of low IFT CO₂–crude oil mixtures. Plans are to refine the use of the parachor method and apply the results to the prediction of measured IFTs of crude oil–CO₂ mixtures with the use of only an equation of state (EOS) and ultimately correlate IFTs with the MMP of selected oils. A supplementary, but equally valuable, task to the proposed research will be the creation of a CO₂–crude oil database, which will eventually be necessary for future CO₂ floods. The following plan is a list of activities for Task 3: (1) design a pendant-drop apparatus for measuring IFTs (oil–water, oil–gas, and gas–water) under a

wide range of reservoir conditions; (2) analyze the ability of flash routines to predict liquid and vapor densities for the calculation of IFTs (parachor method) of near-miscible, multicomponent mixtures (CO₂–oil, nitrogen (N₂)–oil, and gas condensate); and (3) correlate IFT and MMP in simple systems and crude oils from measured IFTs (pendant-drop) and slim-tube experiments.

Summary of Technical Progress

Task 1: SMR Study in CO₂ Foam

Progress in Search for Applicability of SMR in CO₂ Foam

For the efficient screening of surfactants to assess their potential for SMR, the standard high-pressure mobility experiment was modified to speed up the measurements of the mobility of CO₂ foam through rock samples with different permeability. In the new modified experiment, two coreholders were assembled in a series in the path of the CO₂ foam such that the pressure across each of them could be measured at the same time. The total volumetric flow rate of CO₂ foam was kept constant during the experiment by withdrawing the output fluid with another Ruska pump downstream. In this way the same flow rate of CO₂ foam through each core at steady state was assured, and the mobilities in high- and low-permeability rock samples were determined simultaneously.

So that the validity of this new design in mobility measurement could be checked, a few experiments were first conducted to study the effect of core position on the mobility measurement. Baker dolomite and fired Berea sandstone were used in these tests with Chevron surfactant Chaser CD1050®. Preliminary results showed that there is no significant effect of the core position by interchanging the position of the core in the flow path on the mobilities of either CO₂–surfactant-free brine or CO₂ foam.

Mobility measurements of CO₂ foam were then continued to investigate the effect of surfactant type, concentration, and rock type as well as the permeability of the rock to the SMR of CO₂ foam. Chevron’s surfactant Chasers CD1045 and CD1050 and rock samples cut from Baker dolomite and Berea sandstone were used in the test. Two surfactant concentrations, 500 ppm [near or below the critical micelle concentration (CMC) of each surfactant] and 1000 ppm (above the surfactant’s CMC) were used to generate the foam. All tests were conducted at 101 °F and 2100 psi.

Chaser CD1050 was one of the surfactants previously identified to show considerable SMR in a carbonate reservoir rock [East Vacuum Grayburg/San Andres Unit (EVGSAU)] when the standard high-pressure mobility experiment was conducted. In the tests with the quarry rocks in which the modified design was used, the SMR was also observed with the use of Baker dolomite rock samples (permeability ranging from 30 to 110 mD) and the fired

Berea sandstone (permeability ranging from 130 to 900 mD). The SMR as observed in the Berea sandstone, however, is less favorable than that in the Baker dolomite. Conversely, surfactant CD1045 exhibits slightly more favorable SMR in Berea sandstone than in Baker dolomite. Overall, surfactant CD1050 shows a better SMR in Baker dolomite rock samples, whereas surfactant CD1045 exhibits a better SMR in Berea sandstone rock samples. All the results suggest that lithology of rock affects the foam behavior and its SMR to some extent. In addition to this, results also reveal that a better SMR is exhibited at low-flow velocity of CO₂ foam (4.7 ft/d) than at high-flow velocity (9.4 ft/d).

These surfactants are being tested with the EVGSAU (carbonate) reservoir rocks. Because these reservoir rocks are preserved rock samples, the existence of residual oil is likely to affect the surfactant's property and the foam behavior. By the use of the modified high-pressure mobility experiment, previous findings by the standard high-pressure mobility measurements may be quickly confirmed or denied. Once this experimental design is verified to be valid for mobility measurements, it will be used to screen commercially available surfactants for a better SMR observable with reservoir rock at the reservoir conditions.

A sample of carbonate outcrop rock has been obtained from the San Andres formation that contains a very sharp permeability contrast. From the several cores that had already been cut from this sample, it was possible to see that the surface separating high and low permeabilities was relatively plane. Two more core samples were cut, the diametral planes of which were roughly coincident with the dividing surface between high and low permeabilities. The ends of the two cores, which were designated TX1 and TX2, were cut perpendicular to the axes. Both of these samples are vuggy and apparently not well-connected; most of the vugs are small, but a few are larger and intersect the surface. The density of the small vugs is less on the low permeability side and greater on the other side of the dividing plane.

With the Petroleum Recovery Research Center (PRRC) scanning minipermeameter, 1089 permeabilities were measured on each of the four faces on a 0.025-in.-square grid. These were measured over the largest possible square fields (0.8 × 0.8 in.) on the end faces. The permeabilities on the low side of this surface are mostly between 0.04 and 2.2 mD, whereas those on the high side lie mostly between 5 and 100 mD. Figure 1 is a gray-scale permeability map made with data obtained from core TX1 on face B. Although the dividing line between the high- and low-permeability sides is quite evident, it is also obvious that the permeabilities are far from uniform on either the high- or low-permeability side. This is very much in accord with other fine-scale measurements with the scanning minipermeameter that have shown large variations between closely spaced locations on most rocks.

Because of the high-permeability contrast in these rock samples, they will provide an interesting test of SMR;

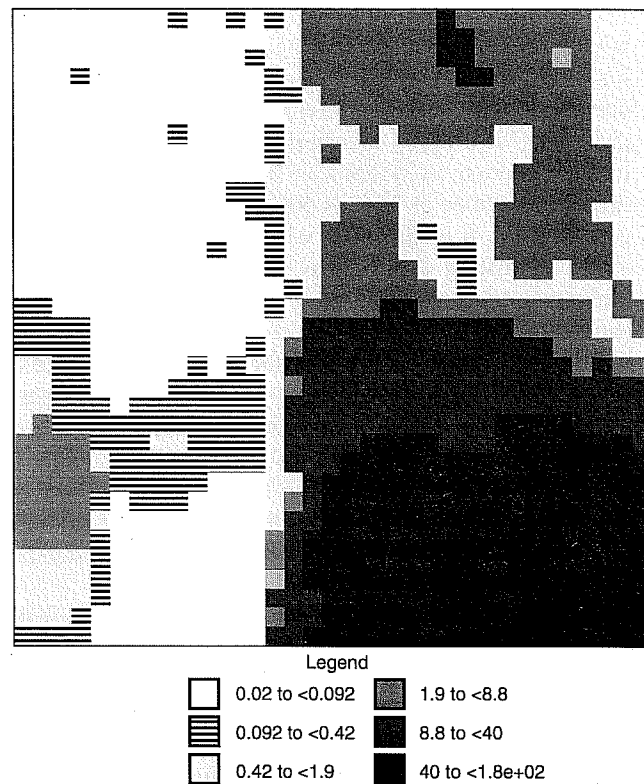


Fig. 1 Permeability map of data from core TX1 on face B.

however, they will require time-consuming experimental work just to achieve saturation equilibrium before each test. Work is under way to design the coreholder for the CO₂ foam experiments and the end cap that will divide the exit flow from the two sides. Plans are to coat the cores with thick (high-viscosity) epoxy and to use a heavy brass tube for pressure containment with solidified, thin epoxy filling the annulus.

Task 2: Reduction of the Amount of CO₂ Required in CO₂ Flooding

Experimental Phase Behavior Tests

In support of sensitivity studies with the use of reservoir simulators with a foam-flooding option, coreflooding tests with the use of reservoir rock are being run. The foam model has been found to be sensitive to gas and water saturations. A series of tests are in progress in which the effects of foam quality and flow velocity on foam formation and, in particular, on mobility control are being examined. Earlier tests were performed on a range of foam qualities found near an injection well.¹ In this study the entire range of foam qualities that will occur in the reservoir is being examined. This additional information will provide guidelines for mobility control vs. foam quality over the entire quality range.

The continuous-phase equilibrium (CPE) apparatus examines composition, density, and viscosity changes in a

dynamic system during continuous injection of a fluid into a reservoir oil at reservoir conditions.² A series of tests on a Permian Basin reservoir fluid has been completed at pressures ranging from below the MMP to well above. This work is being analyzed and will be presented at the SPE International Symposium on Oilfield Chemistry to be held in San Antonio, Tex., February 14–17, 1995.

Reservoir Simulation Studies

During this quarter the focus has continued on the adequacy of foam features that were previously incorporated into the reservoir simulators UTCOMP and MASTER. Sensitivity analysis on a number of foam parameters has been performed on a three-dimensional quarter of a five-spot pattern model. The limiting gas saturation for foam generation was found to have a significant effect on the response time of production. The effect of the limiting gas saturation will continue to be examined both numerically and experimentally. The production history from some of the tests has shown behavior similar to the response of the EVGSAU field pilot.

A new multiphase flash calculation algorithm, which is more efficient and robust than the standard hybrid algorithm, has been developed. In addition, an algorithm has been developed to improve the solution convergence in critical and three-phase regions. Tests are being run at different conditions to assess the validity and applicability of the phase equilibrium calculation algorithms.

Task 3: Low IFT Processes and Gas Injection in Fractured Reservoirs

Construction of the pendant-drop apparatus is in the final stages. The first pressure tests are expected to commence in the coming quarter, and hardware and software for drop digitization and data analysis will be developed.

Two papers are nearing completion that will provide a theoretical basis for use of the parachor method and outline an application of this method for the calculation of multicomponent crude oil IFTs. All the measured data in the literature have been assimilated, and a determination has been made that the method proposed as a result of this research is the most accurate method for calculating IFTs of complicated crude oil systems. Because of the lack of reservoir gas–oil and CO₂–oil data in the literature, however, verification of the accuracy for the method proposed is incomplete. The measurements that will be conducted with the new apparatus will further clarify reservoir IFT calculations, especially for systems that contain water.

References

1. S.-H. Chang and R. B. Grigg, *Laboratory Flow Tests Used to Determine Reservoir Simulator Foam Parameters for EVGSAU CO₂ Foam Pilot*, paper SPE 27675 presented at the SPE Permian Basin Oil and Gas Recovery Conference, Midland, Tex., March 16–18, 1994.
2. R. M. Lansangan and J. L. Smith, Viscosity, Density, and Composition Measurements of CO₂/West Texas Oil Systems, *SPE Reserv. Eng.*, 8(3): 175-182 (August 1993).

THERMAL RECOVERY— SUPPORTING RESEARCH

**STUDY OF HYDROCARBON MISCIBLE
SOLVENT SLUG INJECTION PROCESS
FOR IMPROVED RECOVERY OF HEAVY
OIL FROM SCHRADER BLUFF POOL,
MILNE POINT UNIT, ALASKA**

Contract No. DE-FG22-93BC14864

**University of Alaska
Fairbanks, Alaska**

**Contract Date: Dec. 1, 1992
Anticipated Completion: June 30, 1996**

**Principal Investigator:
G. D. Sharma**

**Project Manager:
Thomas Reid
Bartlesville Project Office**

Reporting Period: July 1–Sept. 30, 1994

Objective

The ultimate objective of this 3-yr research project is to evaluate the performance of the hydrocarbon miscible solvent slug process and to assess the feasibility of this process for improving recovery of heavy oil from Schrader Bluff reservoir. This will be accomplished through measurement of pressure–volume–temperature (PVT) and fluid properties of Schrader Bluff oil, determination of phase behavior of Schrader Bluff oil solvent mixtures, asphaltene precipitation tests, slim-tube displacement tests, coreflood experiments, and reservoir simulation studies. The expected results include determination of optimum hydrocarbon solvent composition suitable for hydrocarbon miscible solvent slug displacement process, optimum slug sizes of solvent needed, solvent recovery factor, solvent requirements, extent and timing of solvent recycle, displacement and sweep efficiency to be achieved, and oil recovery.

Summary of Technical Progress

During this quarter more displacement experiments in slim-tube and miscible coreflood experiments were conducted. After reviewing the results of carbon dioxide (CO₂) and enriched CO₂ as solvents in slim-tube displacement experiments in the previous quarter, attention was focused

on abundantly available natural gas [Prudhoe Bay natural gas (PBG)] and enrichment of this natural gas by natural gas liquids as solvents.

Slim-Tube Experiments

Three slim-tube experiments were performed.

1. *100% PBG at 1300 psia and 82 °F.* The first run in this set was conducted with PBG obtained from the Prudhoe Bay reservoir. This experiment resulted in a recovery of 45.01% (Fig. 1), and solvent breakthrough occurred after 0.46 pore volume (PV) injection. The slim-tube simulation resulted in the recovery of 48.46%, and solvent breakthrough occurred at 0.35 PV injection (Fig. 1). From sight glass observations, it is clear that a two-phase region is present. This clearly shows that there is no miscibility development.

2. *70% PBG and 30% natural gas liquid (NGL) at 1300 psia and 82 °F.* In this run, PBG was enriched with 30% NGL and used as a solvent. This run resulted in a recovery of 83.63% after 1.2 PV solvent injection (Fig. 2). The solvent breakthrough occurred after 0.92 PV of solvent injection. The ultimate recovery from slim-tube simulation is 85.56%. Sight glass observations clearly indicate the presence of two phases. Thus miscibility is not achieved in this run. The density K-value plots (Fig. 2) clearly show that

there is no development of miscibility. Figure 2 also shows the liquid and gas fractions at various contacts during multicontact test (MCT) run.

3. *60% PBG and 40% NGL at 1300 psia and 82 °F.* Further enrichment of PBG by increasing the NGL content to 40% resulted in a recovery of 92.57% (Fig. 3). The solvent breakthrough occurred after 0.97 PV injection. The slim-tube simulation recovery after 1.2 PV injection was 94.55% (Fig. 3). The sight glass observations did not indicate a clear two-phase region. On the basis of recovery, it is concluded that miscibility has not developed completely. The density and K-value plots (Fig. 3) obtained from MCT runs do not indicate the presence of miscibility.

Coreflood Experiments

Pressure-drop data analysis for four runs reported previously, which were conducted to evaluate the effect of slug size on recovery, is being conducted. A coreflood was conducted to study the effect of water-alternating-gas (WAG) ratio. The solvent used was a mixture of 50% PBG + 50% NGL, and the slug size was 0.05 PV.

WAG ratio of 11

In this run, two slugs of 0.05 PV size were injected, separated by water slugs of 0.55 PV. The run resulted in a

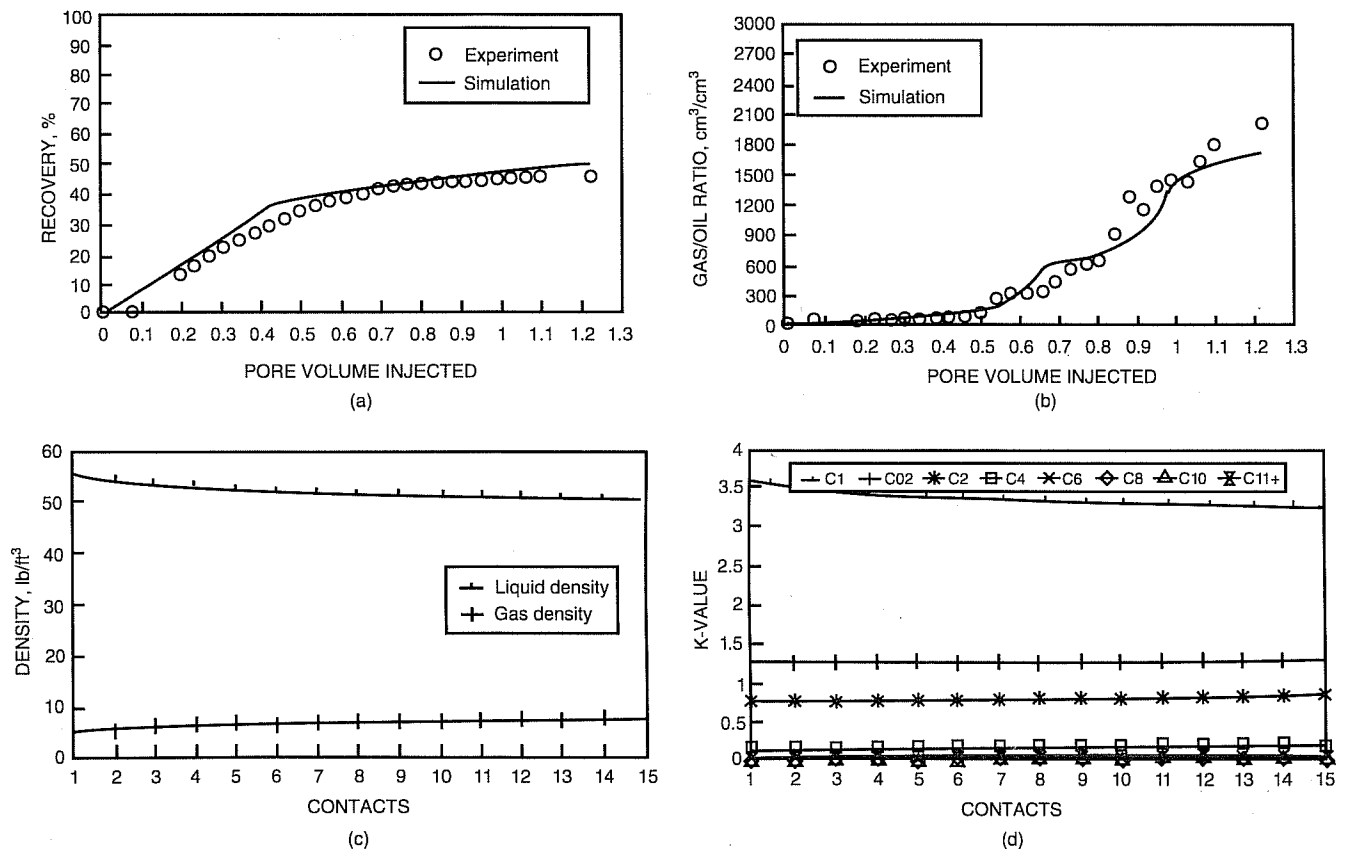


Fig. 1 Slim-tube displacement experiment and simulation results for 100% Prudhoe Bay natural gas at 1300 psia and 82 °F. (a) Recovery vs. pore volume (PV) injected. (b) Density vs. number of contacts. (c) Gas/oil ratio vs. PV injected. (d) K-values vs. number of contacts.

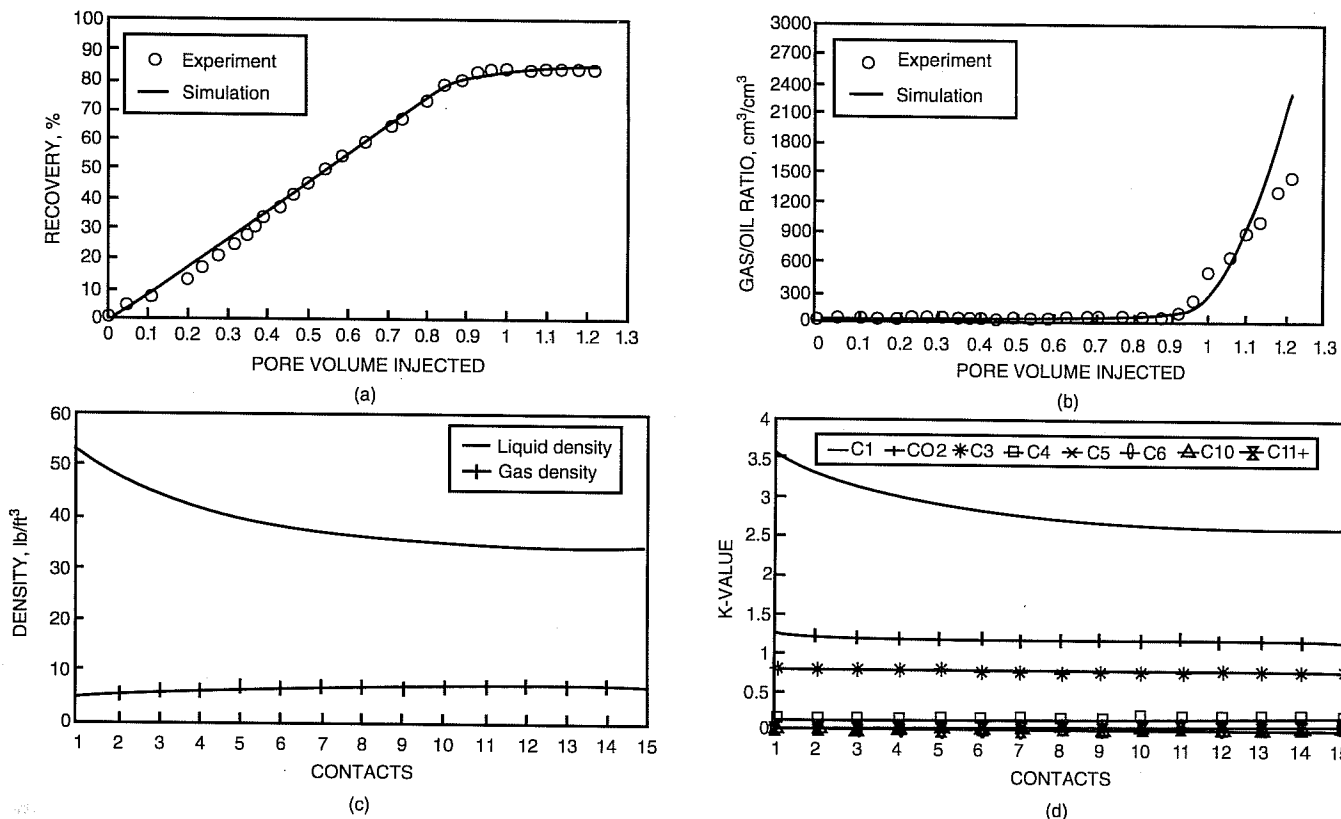


Fig. 2 Slim-tube displacement experiment and simulation results for 70% Prudhoe Bay natural gas/30% natural gas liquid at 1300 psia and 82 °F. (a) Recovery vs. pore volume (PV) injected. (b) Density vs. number of contacts. (c) Gas/oil ratio vs. PV injected. (d) K-values vs. number of contacts.

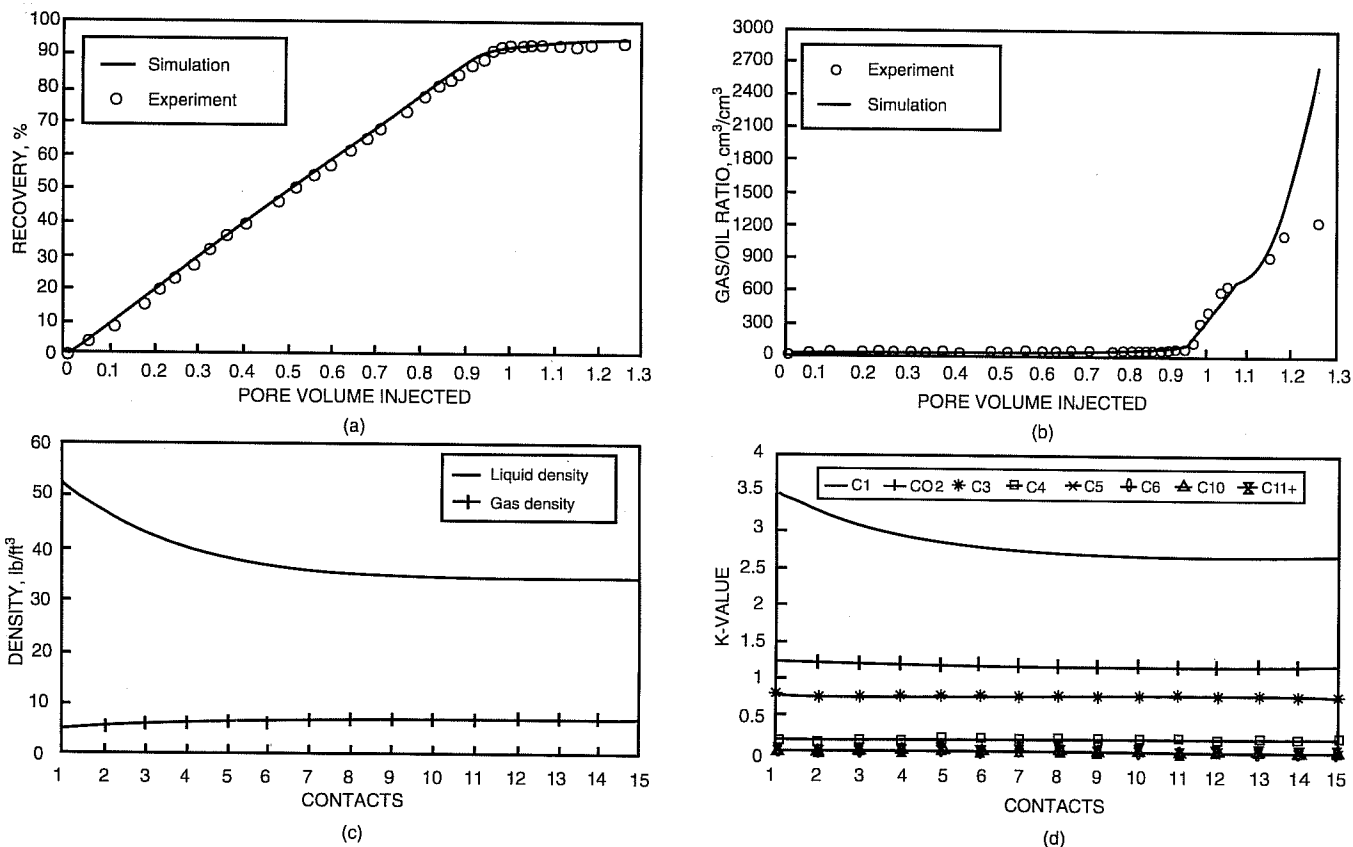


Fig. 3 Slim-tube displacement experiment and simulation results for 60% Prudhoe Bay natural gas/40% natural gas liquid at 1300 psia and 82 °F. (a) Recovery vs. pore volume (PV) injected. (b) Density vs. number of contacts. (c) Gas/oil ratio vs. PV injected. (d) K-values vs. number of contacts.

recovery of 74.67% at 1.2 PV injection (Fig. 4). From the water/oil ratio (WOR) plot (Fig. 5) and the gas/oil ratio (GOR) plot (Fig. 6), the formation of oil bank in front of both the solvent slugs is evident. The second oil bank is produced

at 0.09 PV injection, which results in a sharp decrease in WOR and a marked increase in recovery. Two water breakthroughs are identified from the WOR plot, the first occurring at 0.36 PV injection and the second occurring at 1 PV injection.

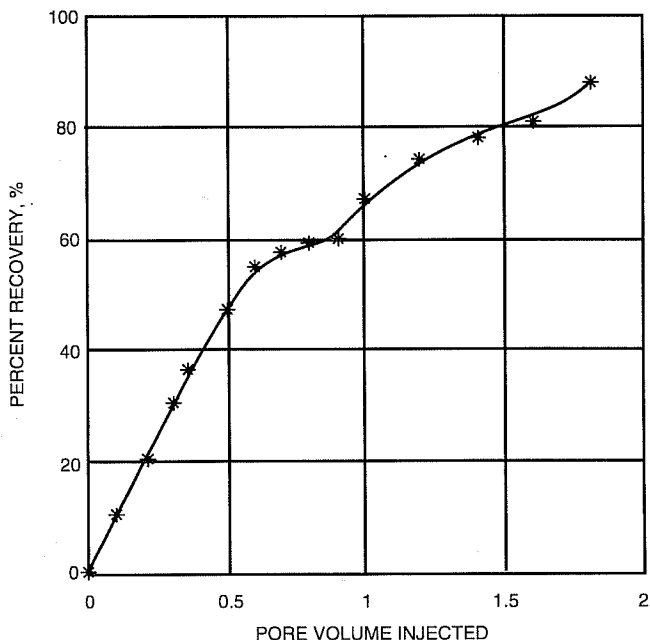


Fig. 4 Oil recovery vs. pore volume (PV) injected, multiple water-alternating-gas (WAG) ratio: 11; multicontact miscible solvent: 50% Prudhoe Bay natural gas + 50% natural liquid gas. —*—, percent recovery.

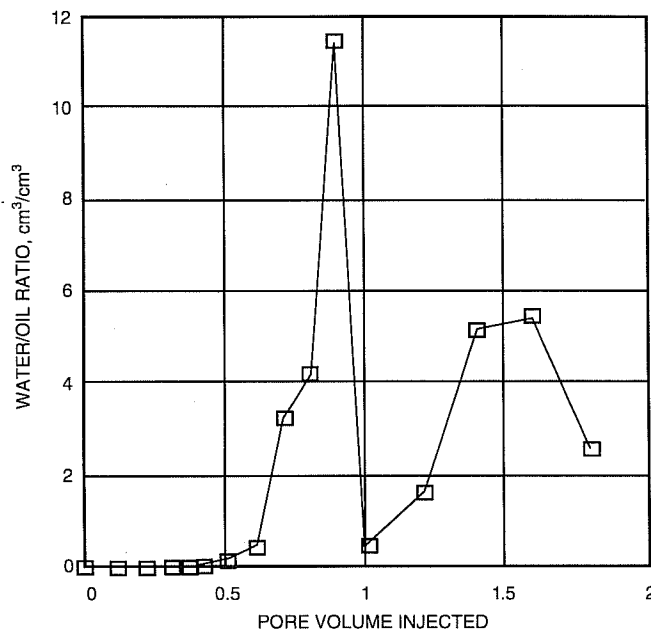


Fig. 5 Water/oil ratio vs. pore volume (PV) injected, multiple water-alternating-gas (WAG) ratio: 11; multicontact miscible solvent : 50% Prudhoe Bay natural gas + 50% natural gas liquid. —□—, water/oil ratio, cm³/cm³.

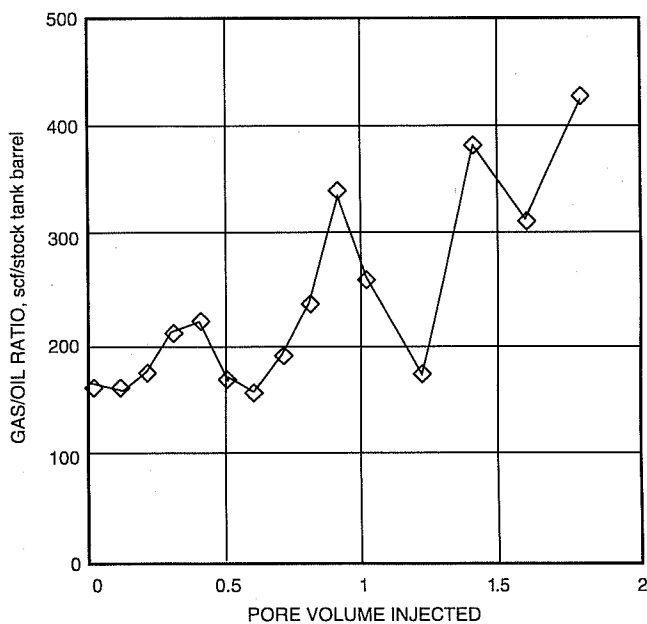


Fig. 6 Gas/oil ratio vs. pore volume (PV) injected, multiple water-alternating-gas (WAG) ratio: 11; multicontact miscible solvent : 50% Prudhoe Bay natural gas + 50% natural gas liquid. —◇—, gas/oil ratio, scf/stock tank barrel.

OIL FIELD CHARACTERIZATION AND PROCESS MONITORING USING ELECTROMAGNETIC METHODS

Lawrence Livermore National Laboratory
Livermore, Calif.

Contract Date: Oct. 1, 1984
Anticipated Completion: Oct. 1, 1994
Government Award: \$350,000

Principal Investigator:
Mike Wilt

Project Manager:
Thomas Reid
Bartlesville Project Office

Reporting Period: July 1–Sept. 30, 1994

Objectives

The objectives of this project are to apply surface and borehole electromagnetic (EM) methods for oil field characterization and monitoring of in situ changes in the electrical conductivity during enhanced oil recovery (EOR) operations and to develop practical tools for geophysical characterization of oil strata and monitoring of EOR processes in a developed field. Crosshole and borehole-to-surface (BTS) EM methods are being applied to map oil field structure and to provide images of subsurface electrical conductivity changes associated with EOR operations.

Summary of Technical Progress

The EM system was used in a waterflood monitoring project at the University of California (UC) Richmond Field Station test facility. For this test a slug of salt water was injected, and the BTS array was applied to determine if the body could be detected by deploying instruments in a single well and at the ground surface. Preliminary results showed that an anomaly caused by an injected saltwater plume could be easily detected but less easily isolated from the effects of surface geological and cultural noise. These data will be interpreted.

A 3-yr experiment to study the effect of steel well casing on crosshole EM was initiated during this quarter. The experiment consists of laboratory-scale measurements to determine the properties of the casing, a series of EM measurements within the casing to determine the effect of signal propagation, and a series of crosshole surveys to determine if the casing and formation effects are easily separable.

Waterflood Monitoring at UC Richmond Field Station

In many problem oil fields and environmental situations, only one borehole is available for geophysical measurements. In an oil field, this may be one of several widely spaced observation wells; in an environmental spill area, this may be the initial monitoring well. It is important to use this well to determine the electrical resistivity distribution beginning at the wellbore and extending outward. This may help determine the direction of steamflood migration or the movement of an underground spill. One technique, in which a single well is used, is the BTS array, where an EM transmitter is located in the borehole and data are collected on the surface. The method allows for multicomponent measurements along any surface profile; the subsurface investigation can thus be focused without the requirement of an additional well. The disadvantage is that the data are less sensitive to the subsurface resistivity than the crosshole array because of the increased source–receiver separation; the array is also more sensitive to the effect of surface geological and cultural noise.

So that the applicability of this method to waterflood monitoring could be tested, a test was designed at the Richmond Field Station facility. This experiment consisted of injecting a slug of salt water into a shallow aquifer and collecting BTS EM data before and after injection. With the use of boreholes along the same profiles, crosshole EM data were also collected at the same frequency as the BTS data. The crosshole data will be used to supplement the BTS measurements for improved inversion resolution and for comparison with the BTS data. Numerical inversion will be applied to both data sets to determine the in situ resistivity distribution and the direction of saltwater migration.

The measurements consist of deploying a borehole transmitter in the injection well and several other observation holes and collecting horizontal and vertical component

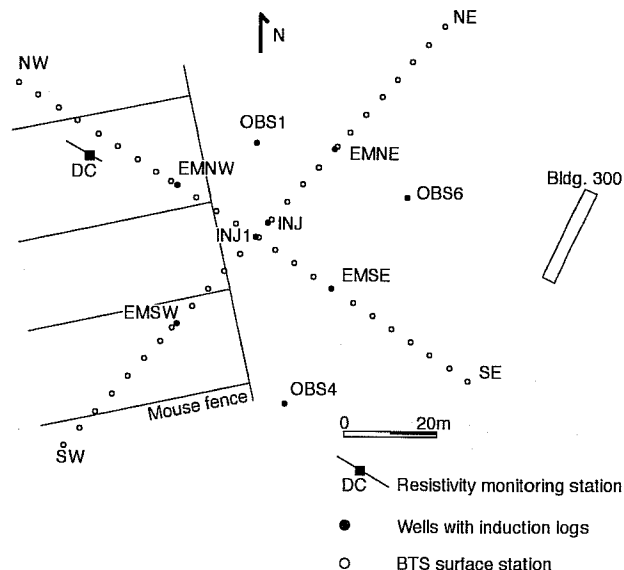


Fig. 1 Base map for the Richmond Field Station waterflood experiment.

magnetic fields on the surface on a densely sampled grid (Fig. 1). A series of temporary stations were established and outfitted with small pipes for placement of the surface detectors to ensure that measurements were repeatable. A complete survey was done before and after saltwater injection. The baseline data for this experiment were collected in December 1993, and the saltwater was injected in late December. Postinjection data were collected during the last week of December 1993 and in January 1994. Early analysis of these data showed significant distortion as the result of leakage of

current from the transmitter. This was subsequently repaired, and new data were collected in March 1994 before saltwater withdrawal. A final data set was collected in April 1994, after saltwater withdrawal.

The data, in general, were of excellent quality. The average repeatability error was 1 or 2%. The EM anomaly, although only half the size of the crosshole anomaly, was easily discernible, and these data may be used for imaging the subsurface plume. Indications of cultural and external noise in the data set persisted even after considerable effort to reduce these effects.

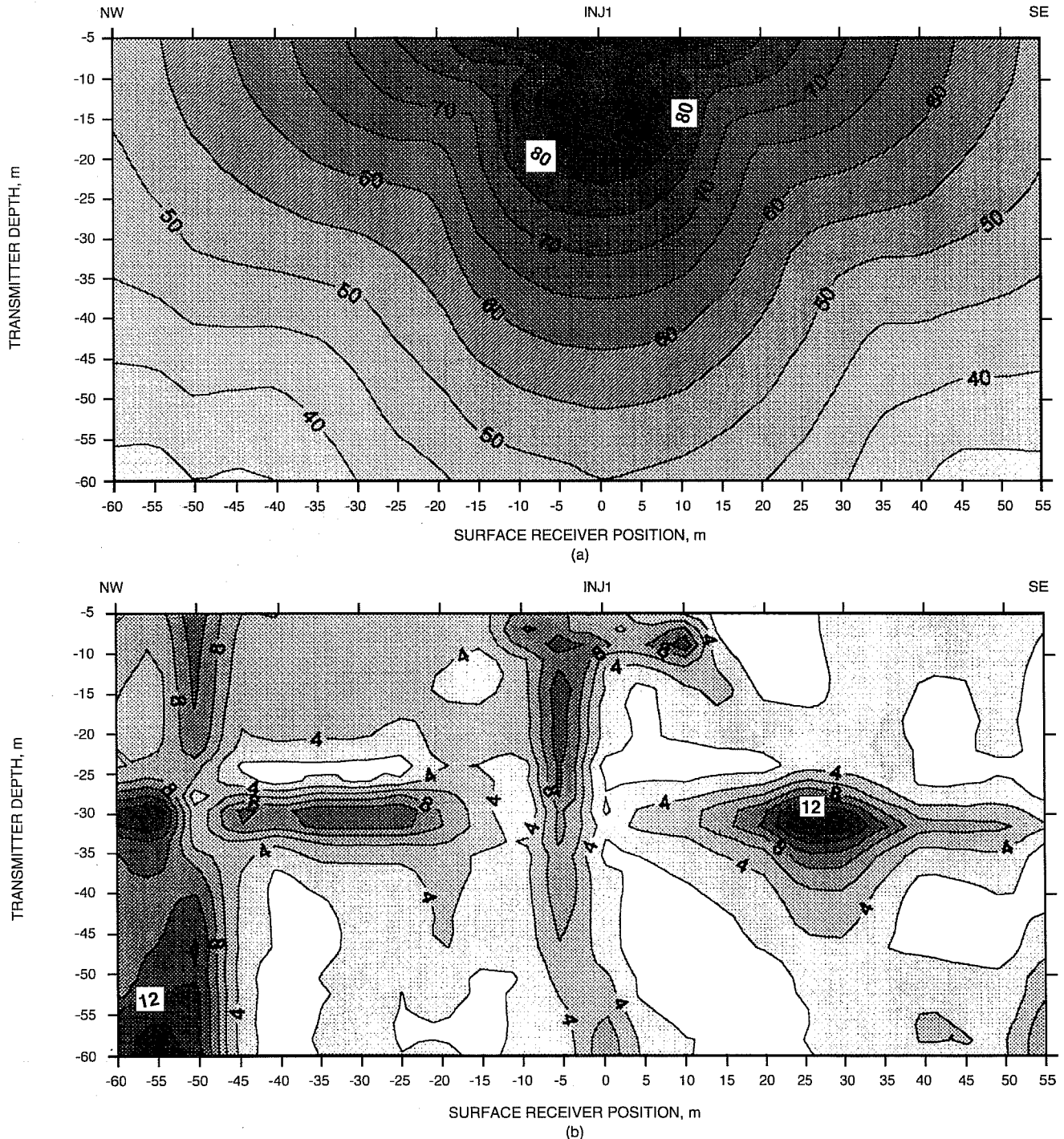


Fig. 2 Borehole-to-surface electromagnetic field data (a) and observed percent differences before and after saltwater flood (b) for profile NW-SE.

Figure 2 shows baseline vertical field magnitudes and differences (in percent) between data collected before and after saltwater injection. The field data, which are plotted below the surface receivers in part a of Fig. 2, show a smooth continuous amplitude distribution with the field steadily decreasing with distance from the source borehole. The difference plot (part b of Fig. 2) indicates several zones where the field changed after the injection of saltwater; the most prominent are the horizontal bands located at a depth of 30 m between stations 15 and 50 and between stations -45 and -5. Forward modeling shows that these differences are due to the saltwater slug. Preliminary indications are that the causative body is a roughly horizontal feature offset to the north of the injection well.

The plot also shows two vertically oriented anomalies, one near the borehole INJ1 and the other at -55. Experience indicates that this type of anomaly is due to a surficial body or some external source of noise. The central anomaly, near the injection borehole, may have been caused by residual current leakage in the transmitter tool or the supply cable. Although steps were taken to minimize this leakage, some residual current could be measured, and this clearly affects data at stations close to the source well. The second anomaly, near -55, was probably caused by a grounded metallic fence used in an earlier biological experiment. Although much of this structure was removed before measurement, some of the effects remain.

Because the plot in part b of Fig. 2 presents the difference in fields, it is expected that the effect of current leakage or a grounded fence would be the same for both surveys and therefore subtract to zero when a difference is taken. This unfortunately was not the case because the near-surface resistivity changed (as the result of rainfall) between the measurement times. It therefore affected the EM coupling to the surface features. This type of variation in geological and cultural noise is the rule, however, and not the exception. The challenge is to engineer the measurement system to be insensitive to this.

Even with the preceding effects, the data set is of excellent quality and is suitable for inversion. Interpretation of these data is under way as part of the Ph.D. thesis for a UC student. The student will initially apply some simple two-dimensional (2-D) models and later interpret the data with a three-dimensional (3-D) code being developed.¹

EM Measurements Through Steel Well Casing

Figure 3 shows some experimental EM data collected in an observation well at the South Belridge oil field in central California; the borehole is steel-cased from the surface to a depth of 150 m but fiberglass-cased below this. The data were collected, at a frequency of 540 Hz, with the use of the BTS array with a loop source situated above the measurement borehole. The plot shows that amplitude

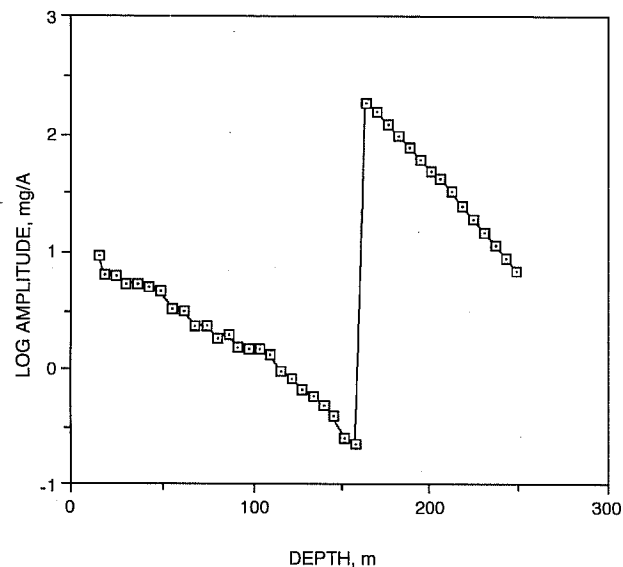


Fig. 3 Surface-to-borehole electromagnetic data in a partially steel-cased well at the South Belridge oil field. Frequency, 540 Hz.

decreases with depth until the receiver reaches a depth of 150 m, where it increases by a factor of 1000 as the coil emerges from the steel casing. The plot shows both the problem and promise of working in steel casing. The problem is that the signal is greatly attenuated, especially at high frequencies (for example, these results indicate that it will probably not be possible to collect EM data through casing at frequencies much above 500 Hz); this limits the resolution. Regardless of the attenuation, however, the fields are well behaved within the casing, and it may be possible to remove the casing effect by a simple arithmetic correction.

A project to understand EM propagation through steel casing was initiated in 1994 through the Lawrence Berkeley Laboratory/Lawrence Livermore National Laboratory (LBL/LLNL) industrial sponsors consortium. The goals of the experiment are to determine the limits and applications for crosswell EM surveys through steel well casing. The work consists of three parts. First, the properties of the casing will be determined from EM measurements. Next, the fields from a borehole transmitter will be measured through segmented steel casing. Finally, a set of crosshole measurements will be made in fiberglass-cased boreholes and a second set will be made with steel pipe inserts in the same wells to determine if the casing effect can be easily removed.

Reference

1. H. W. Tseng, A. Becker, M. Dezcz-Pan, and M. Wilt, *Fluid Injection Monitoring with a Borehole-to-Surface Electromagnetic Method*. Report to sponsors of the Lawrence Berkeley Laboratory/INDUSTRY Research Consortium on Subsurface Electromagnetics.

GEOSCIENCE TECHNOLOGY

**GEOSCIENCE/ENGINEERING
CHARACTERIZATION OF THE
INTERWELL ENVIRONMENT IN
CARBONATE RESERVOIRS BASED
ON OUTCROP ANALOGS,
PERMIAN BASIN,
WEST TEXAS AND NEW MEXICO**

Contract No. DE-AC22-93BC14895

**University of Texas
Austin, Tex.**

**Contract Date: Sept. 29, 1993
Anticipated Completion: Sept. 28, 1996
Government Award: \$354,400**

Principal Investigators:

**F. J. Lucia
C. Kerans**

Project Manager:

**Robert Lemmon
Bartlesville Project Office**

Reporting Period: July 1–Sept. 30, 1994

Objectives

The primary objective of this project is to investigate styles of reservoir heterogeneity that occur in low-permeability pelleted wackestone–packstone facies and mixed carbonate–clastic facies found in Permian Basin reservoirs by studying similar facies exposed in the Guadalupe mountains. Specific objectives for the outcrop study include construction of a stratigraphic framework, petrophysical quantification of the framework, and testing the outcrop reservoir model for effects of reservoir heterogeneity on production performance. Specific objectives for the subsurface study parallel objectives for the outcrop study.

Summary of Technical Progress

Outcrop Activities

Fieldwork on Plowman Ridge established the Grayburg stratigraphic and cyclic framework and documented facies variation along this 3.5-mile-long, dip-oriented ridge. Canyons west of Plowman Ridge expose the Grayburg formation on adjacent fault blocks and provide a unique opportunity to assess the three-dimensional (3-D) variability of depositional sequences, high-frequency cycles, and component facies. The initial 3-D analysis focused on the Grayburg sequence 2 highstand systems tract, which is comprised of 5 ooid grainstone-dominated cycles.

These cross-bedded ooid grainstones have high porosity (10 to 20%) and permeability (50 to 1500 mD).

Closely spaced (150 to 250 ft apart) sections were used to document reservoir-scale heterogeneity at the interwell scale given typical well distances of 660 ft (10 acre spacing) to 1320 ft (40 acre spacing). To date, detailed correlations among 36 measured sections on Plowman Ridge and 25 measured sections in West Dog Canyon, 3000 ft west of Plowman Ridge, extend the high-frequency cycle correlations for 1.5 miles along dip and 3000 ft across strike. Isopach maps generated from these data illustrate the strike and dip dimensions of individual grainstone bodies. Grainstones are oriented parallel to the regional depositional strike and thin landward into peloidal-ooid packstones and dolomitic sandstones. The grainstone bodies range up to 14 ft in thickness, attain a dip width of 4000 ft, and extend across strike for more than 3000 ft. Preliminary results of outcrop studies were presented to industrial associates on a field trip in October 1994.

Subsurface Activities

Stratigraphic studies of the Grayburg formation in South Cowden field are almost complete. Sequence stratigraphic analysis of the Grayburg, combined with regional study of the Grayburg, indicates that the succession represents part of a long-term, transgressive-regressive sequence that can be further subdivided into four high-frequency sequences. The upper two, highstand-dominated sequences, contain higher frequency cycles that can be correlated across the field. Most of the production in the field comes from the upper two high-frequency sequences.

Rock fabrics have been calibrated to capillary pressure data and used to generate rock-fabric-petrophysical classes. The presence of gypsum (which is especially abundant along the eastern margin of the field) in the reservoir complicates the determination of rock-fabric-petrophysical relationships. Because the presence of gypsum affects wireline log response, its distribution must be determined and accounted for when making accurate petrophysical models for wells in these areas.

Studies of production data show that field production is predominantly from intercrystalline and intergranular pore types. Permeability is locally enhanced by anhydrite dissolution, which produces a touching-vug pore geometry composed of open fractures and vugs.

A comparison of production trends with stratigraphic architecture suggests that porosity and permeability development in much of the field is the result of diagenesis. The reservoir can be subdivided into three parts: a western part where flow units reflect facies control, an eastern part where flow units crosscut depositional facies boundaries, and an intermediate part where elements of both are apparent.

Analysis of 3-D seismic data acquired by Unocal Corp. for the Moss Unit has revealed that data are not of sufficiently high resolution to define variations in facies, mineralogy, porosity, or fluid content in the South Cowden field area. Studies of the 3-D data have, however, helped to define the pre-Grayburg depositional history of the area and have resulted in a better

understanding of the depositional controls on facies distribution across the field. The present structural configuration of the field, as well as Grayburg facies distribution patterns, is the result of topography created by the ancestral Clear Fork platform margin, located in the northwest corner of the field, and a middle San Andres progradational wedge, over which the field is centered. An update of the progress of subsurface studies was presented to field operators, Fina Oil and Chemical Co., Inc., Unocal Corp., and Phillips Petroleum Co., in October 1994.

GEOLOGICAL AND PETROPHYSICAL CHARACTERIZATION OF THE FERRON SANDSTONE FOR THREE-DIMENSIONAL SIMULATION OF A FLUVIAL-DELTAIC RESERVOIR

Contract No. DE-AC22-93BC14896

**Utah Geological Survey
Salt Lake City, Utah**

**Contract Date: Sept. 29, 1993
Anticipated Completion: Sept. 28, 1996
Government Award: \$321,042**

**Principal Investigator:
M. Lee Allison**

**Project Manager:
Robert Lemmon
Bartlesville Project Office**

Reporting Period: July 1-Sept. 30, 1994

Objective

The project objective is to develop a comprehensive, interdisciplinary, and quantitative characterization of a fluvial-deltaic reservoir that will allow realistic interwell and reservoir-scale modeling to be developed for improved oil field development in similar reservoirs worldwide. The geological and petrophysical properties of the Cretaceous Ferron sandstone in east-central Utah (Fig. 1) will be quantitatively determined. Both new and existing data will be integrated into a three-dimensional (3-D) representation of spatial variations in porosity, storativity, and tensorial rock permeability at a scale appropriate for interwell to regional-scale reservoir simulation. Results could improve reservoir management through proper infill and extension drilling strategies, reduce economic risks, increase recovery from existing oil fields, and provide more reliable reserve calculations. Transfer of the project results to the petroleum industry will be an integral component of the project.

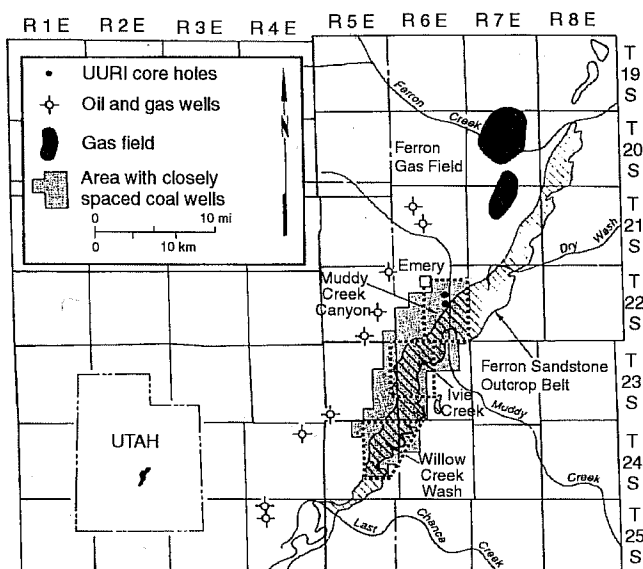


Fig. 1 Location map of the Ferron sandstone study area (cross-hatched) showing detailed case study sites (outlined by heavy dashed lines).

Summary of Technical Progress

Technical progress is divided into several sections corresponding to subtasks outlined in the regional stratigraphy task and the case studies task sections of the original proposal. The primary objective of the regional stratigraphy task is to provide a more detailed description and interpretation of the stratigraphy of the Ferron sandstone outcrop belt from Last Chance Creek to Ferron Creek (Fig. 1). This regional study will include the determination of the dimensions and depositional environment of each sandstone body and the nature of its contacts with adjacent rocks or flow units. The study will provide a basis for selecting prime outcrops for detailed case studies of the major reservoir types (meander belt, mouth-bar complex, wave-dominated delta front, bar-finger sands, distributary channel, and tidal channels). The morphological framework established from the case studies will be used to generate subsequent flow models for the reservoir types.

The primary objective of the case studies task is to develop, at a well-sweep or smaller scale, a detailed geological and petrophysical characterization of the primary reservoir lithofacies typically found in a fluvial-dominated deltaic reservoir. Sedimentary structures, lithofacies, bounding surfaces, and permeabilities measured along closely spaced traverses (both vertical and horizontal) will be combined with data from core drilling to develop a 3-D view of the reservoirs within each case study area.

Regional Stratigraphy

Surface Mapping/Interpretation of the Outcrop Belt

The Ferron sandstone outcrop belt within the study area (Fig. 1) has been obliquely photographed. These photographs

[a total of 1823 depicting 80 mi (130 km) of outcrop] have been digitized and transferred to compact discs (CD). Image-editing software is being used to assemble the photographs from the CDs into reproducible photomosaics. Lithofacies, measured sections, vertical and horizontal scales, and other data are being plotted on the photomosaics in the field for both the regional and case study analysis.

Collection and Interpretation of Existing Surface and Subsurface Data

The Utah Geological Survey (UGS) continues to collect and compile published and unpublished maps, measured sections, well logs, core descriptions, reports, and other data. There are 481 wells in the study area, of which 412 were cored. As of Sept. 30, 1994, the UGS had acquired 138 geophysical logs and 1800 ft (550 m) of core or core descriptions from these wells (Table 1). Information from 232 wells has been entered into ASCII files; 305 of the 481 total wells were also entered into the UGS INTEGRAL database for the Ferron project (Table 1). Interpretations (thickness, type of lithology, and geologic description) have been completed for 343 wells.

Base maps have been digitized for the Willow Springs, Short Canyon, Johns Peak, Mesa Butte, Walker Flat, and Geyser Peak quadrangles. These base maps show drill-hole locations (petroleum exploratory and development wells and coal core holes), measured sections, coal outcrops, coal mined-out areas, drainages, and the top and base of the Ferron sandstone.

Preliminary Regional Stratigraphic Interpretation

Regionally, the Ferron sandstone consists of up to seven delta-front sandstone bodies or parasequence sets. The focus of this work is two parasequence sets in the lower part of the Ferron. These have been designated as the Nos. 1 and 2 sets. Recognizable sequences within the sets have been designated with lowercase letters (for example, No. 1a). Most fit the definition of a parasequence, being bounded above and below by transgressive surfaces (flooding surfaces in the sequence stratigraphic terminology). In some cases the divisions may lack transgressive surfaces, yet they are recognizable by changes in sedimentary styles. In the Ivie Creek area, the No. 1a, b, and c parasequences are well exposed and are interpreted as low-wave-energy subdelta deposits. The uppermost carbonaceous mudstone or ash-rich coal is the sub-A coal zone. A flooding surface has been identified at the top of the sub-A. The boundary with the overlying No. 2 parasequence set is drawn at this flooding surface. The No. 2a, b, and c parasequences are initially interpreted as low-wave-energy subdelta deposits.

As the result of regional work in the northern part of the Ivie Creek area (Fig. 1), a marine sand, which developed out of the brackish water lithofacies found to the south in the Ivie Creek case study area, has been identified. Stratigraphically, this sand is between the No. 1c and the top of the sub-A coal zone and has been tentatively designated the No. 1d parasequence.

TABLE 1

Summary of Well, Geophysical Log, and Core Data Collected for the Ferron Sandstone Study Area

Source of wells	No. of wells with geophysical logs	No. of logs obtained by the UGS*	No. of wells cored/ footage cored	Core obtained by the UGS,* ft	No. of wells recorded in ASCII files*	No. of wells recorded in INTEGRAL*
Oil and Gas						
University of Utah Research Institute	2	2	2/800	800	0	0
ARCO Oil and Gas Company	7	7	7/3527	Descriptions only	0	0
British Petroleum	5	5	5/1000	1000	0	0
Other	58	41	0	0	0	0
Coal						
CONSOL Inc.	357	62	356/unknown	Descriptions only	232	305
U.S. Geological Survey	33	15	29/1402	Descriptions only	0	0
Bureau of Land Management	0	0	6/1156	Descriptions only	0	0
Western States Mineral Corporation	12	0	0	0	0	0
Hidden Valley Coal Company	7	6	7/463	Descriptions only	0	0
Total	481	138	412/8348	1800	232	305

*Obtained by Utah Geological Survey (UGS) as of Sept. 30, 1994.

This parasequence may emerge to the northeast. In the No. 2c, a large channel system is exposed with a predominantly west-to-southwest directed paleoflow. This system has been tentatively interpreted to be a tidal channel complex, which flooded back into the bay deposits that are well defined in the Ivie Creek case study area. The marine sands found proximal to the channel system were interpreted as deposits of the flood-tidal delta.

Case Studies

Field Work

Forty-six sections have been measured and described in the Ivie Creek and Willow Creek Wash case study areas. Descriptions of the individual units in the measured sections include the following information: primary and secondary lithologies; rock composition, color, and grain size; bed size, shape, and degree of induration; sedimentary structures; biologic structures; fossils; bounding surfaces; and depositional environment. Sections were correlated to develop preliminary interpretations of the stratigraphy and lithofacies. Over 500 paleocurrent measurements have been made at these and other localities. Lithologic and paleocurrent data are being entered into the UGS INTEGRAL database for use in constructing statistical models, strip logs, and lithofacies maps.

Eleven core-hole locations have been permitted from the Utah Division of Oil, Gas, and Mining in the Ivie Creek area (Fig. 2); five or six core holes will be drilled. Water use and right-of-way permits have also been obtained. The total depth of the core holes will be approximately 550 ft (150 m). The Nos. 1 and 2 parasequence sets will be cored [approximately 160 ft (50 m)] in each hole. The No. 1 represents a river-dominated delta deposit that changes from proximal to distal

(where the sandstone pinches out) from east to west across the Ivie Creek area. The No. 2 contains more and cleaner sand, which indicates a more wave-influenced environment of deposition. The core holes will be located downdip 200 to 1200 ft (60 to 365 m) from the Ferron outcrop. The pattern of the core holes is similar to that in an oil field.

Outcrop Gamma-Ray Measurements

The objectives of outcrop gamma-ray measurements for the Ferron sandstone in the Ivie Creek case study area are threefold: to determine variations in clay-mineral content (or sand-shale), to permit detailed correlation among outcrop traverses and between these traverses and drill-hole gamma-ray logs, and to detect possible diagenetic changes associated with precipitation of uranium. The equipment used for field measurements is a portable 256-channel gamma-ray spectrometer that is capable of determining total natural gamma counts as well as concentrations of potassium, thorium, and uranium. The spectrometer was tested in the lab and in the field to determine its vertical resolution and replicability. Test measurements in the field were found to be unreliable in rough topography because gamma rays enter the sides of the detector. This problem was corrected by covering the sides of the detector with lead shielding.

Field measurements showed that the total gamma-ray count is not always a reliable indicator of clay content. Potassium and thorium covary, probably because they are present primarily in clays. Uranium, however, commonly is not correlated with potassium and thorium. This indicates that uranium is present in minerals other than clays. Consequently, for reliable determination of clay content, potassium and thorium must be measured rather than just total gamma rays. It was decided to make 1-min measurements, which is almost five times as long as is needed for good total gamma values but

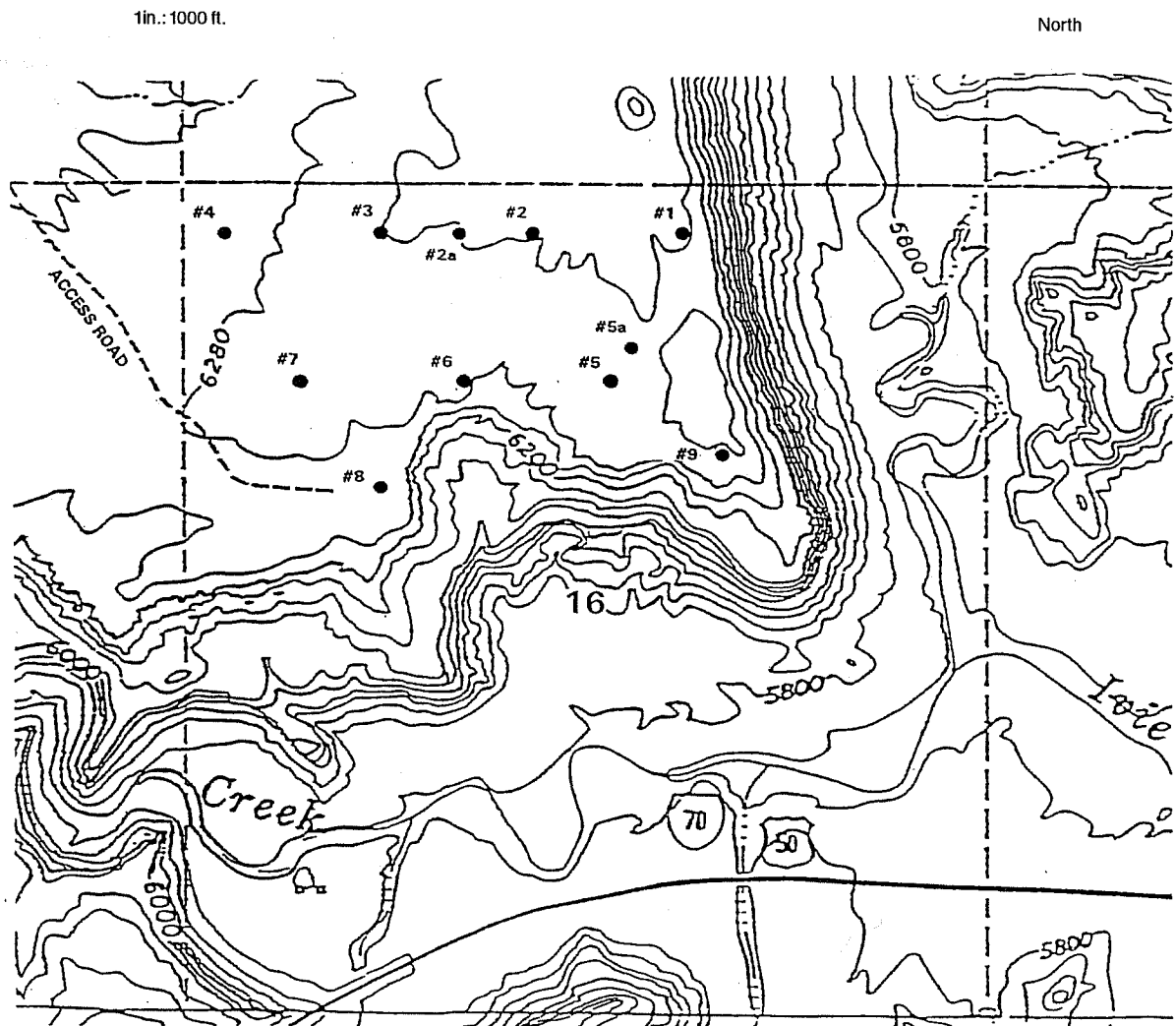


Fig. 2 Location of eleven proposed core holes permitted in the Ivie Creek case study area, sec. 16, T. 23 S., R. 6 E., Emery County, Utah, to core the Nos. 1 and 2 sandstones. Base map from U.S. Geological Survey topographic maps of Mesa Butte and Walker Flat; contour interval is 40 ft (12 m).

barely enough for reliable potassium, thorium, and uranium measurements.

All gamma-ray logging was in the form of vertical or near-vertical (depending on access) traverses. In all, 15 gamma-ray traverses were undertaken, each consisting of 200 to 400 measurements at 0.5- to 1.0-ft (0.15- to 0.3-m) intervals. All traverses included the entire No. 1 parasequence set, and most also included all or part of the No. 2 parasequence set. Most traverses corresponded to measured sections. The traverses are useful for correlation and quantitative determination of sand-shale percentage (Fig. 3).

Core-Plug Sampling

The objective of core-plug sampling in the Ivie Creek case study area was to characterize vertical and lateral variations of a number of petrophysical properties (velocity, density, porosity, permeability, and mineralogy) and to determine the interrelations among these properties. The technique used

involved drilling a 1- to 4-in. (2.5- to 10-cm)-long core plug, 1 in. (2.5 cm) in diameter, with a portable gas-powered motor and diamond bit. The geographic orientation of each sample was determined, and the sedimentary structure of the bed was noted or photographed. All core plugging was along vertical or near-vertical (depending on access) traverses. In all, 283 samples were taken from 9 traverses. Most traverses corresponded to measured sections. Various lithofacies from both the Nos. 1 and 2 sandstones were sampled.

Mini-Permeameter Measurements

Seven permeability transects, four vertical and three sub-horizontal (parallel to bedding), were made on the outcrop at the Ivie Creek case study site (Fig. 4). The transects span the proximal, middle, and distal portions of the delta-front rocks of the No. 1 sandstone. Transect locations, jointly established by the geological and engineering teams, were designed to encompass the majority of the lithofacies present in the

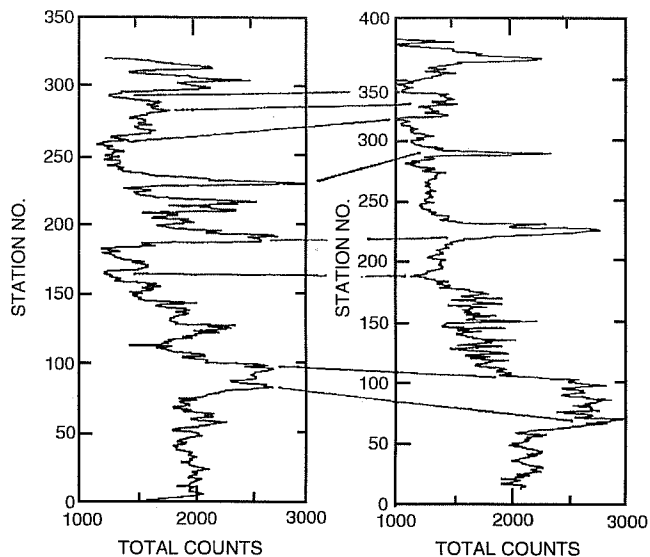


Fig. 3 Typical gamma-ray profiles from traverses in the Ivie Creek case study area. Preliminary correlations are shown.

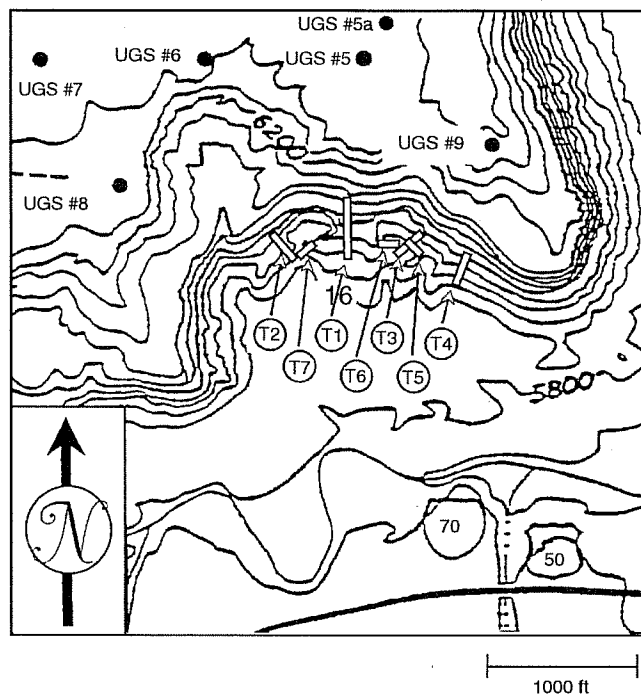


Fig. 4 Location of seven permeability transects (vertical and parallel to bedding) in the Ivie Creek case study area, sec. 16, T. 23 S., R. 6 E., Emery County, Utah. Proposed core-hole sites are shown by heavy dots. Base map from U.S. Geological Survey topographic maps of Mesa Butte and Walker Flat; contour interval is 40 ft (12 m).

delta-front sequence. Data from these transects will be used to determine the statistical structure of the spatially variable permeability field within the delta front, to investigate how geological processes control the spatial distribution of permeability, and to evaluate permeability measurement techniques.

The four vertical transects were approximately 600 ft (200 m) apart and 100 to 200 ft (30 to 60 m) long. Measurements were made at 0.3-ft (0.1-m) intervals (station spacing) along all the vertical transects. From west to east (distal to proximal), the transects were: T-2, T-1, T-3, and T-4. The three sub-horizontal, bed-parallel transects were approximately 50 ft (15 m) long. From west to east, the transects were T-7, T-6, and T-5. Station spacing was 0.5 ft (0.2 m) on the bed-parallel transects. After general sedimentologic and stratigraphic interpretation of the area encompassing the vertical transects, a window approximately 300 ft (90 m) wide was selected for detailed geologic description. Three stratigraphic sections (at the center and two ends of the window) were measured in detail, noting lithologies and grain size, primary and secondary sedimentary structures, and bed thicknesses. Lateral and vertical variations of these parameters within units were also described. Units as thin as 0.01 ft (0.2 cm) were described.

Within the window, a representative succession of several adjacent clinoforms in the No. 1a was chosen to expand documentation of lateral variation of these parameters within individual clinoforms. Clinoform characterization was continued past the proximal window boundary to incorporate additional variation. Locations along the clinoforms, termed mini-windows, were photographed at approximate 50-ft (15-m) intervals to document lateral variation in lithology, bed thickness, and sedimentary structures along clinoforms. Several mini-windows outside the window were also interpreted. These were in a more proximal position and allowed documentation of additional change in clinoforms. The mini-windows were approximately 4 ft (1 m) high by 6 ft (2 m) wide at the distal ends of the window and approximately 10 ft (3 m) high by 6 ft (2 m) wide at the proximal end of the clinoforms. This detailed geologic information will allow the reservoir modeler to develop rules and constraints on lateral variation within the delta front.

Core plugs roughly 0.75 in. (0.3 cm) in diameter and 1 to 3 in. (2.5 to 7.5 cm) long were drilled from the outcrop at each transect station (where possible) to ensure that permeability measurements could be made on fresh, unweathered rock surfaces. Drilling experience and examination of the core plugs indicates that chemical weathering extends less than 0.5 in. (1.3 cm) into the rock. Whole plugs were typically recovered only from sandstone beds greater than 2 in. (5 cm) thick. Useful plugs could usually not be obtained from thinner sandstone beds or from thinly bedded sandstones, siltstones, and mudstones. Core recovery rates range from 50 to nearly 100%. Where core plugs could not be recovered, small rock samples were taken except where the outcrop is buried under colluvium.

Permeability was measured in the laboratory on the unweathered end of the core plugs after the unweathered end of the plug was trimmed flat with a rock saw. The thin disks trimmed from the plug ends were saved for possible future petrographic analysis. At those stations where a good hole was drilled but a broken core was recovered, permeability was measured in the

hole. Before field permeability in a core hole was measured, the back of the hole was prepared with the use of a screwdriver and a rock hammer to chip away rough spots and thus provide a flat surface for the mini-permeameter probe tip. The hole was sprayed out with water and allowed to dry for at least 24 hr before permeability testing. The hole was also cleaned by a blast of compressed gas immediately before testing.

An electronic miniprobe permeameter (EMP) supplied to the project by Mobil Research and Development Corp. was used to make laboratory permeability measurements on the trimmed, whole core plugs and field measurements in core holes (Fig. 5). This instrument is accurate to within 1 to 12% and precise to within 1 to 3% on homogeneous core plugs with permeabilities ranging from 1 to 4500 mD. A rack was used to secure the probe in the laboratory; an expansion packer was used to secure the probe in a core hole in the field. In both cases, an air-actuated piston pushes the probe tip against the center of the sample, which provides a consistent coupling between the probe tip and the rock.

The seven transects contain 1236 stations; of these, 1000 were drilled and 900 whole core plugs were recovered for laboratory permeability testing. The permeability measurements made so far are too sparse to make any definitive statements about the spatial pattern of permeability in the

delta front of the No. 1 sandstone. The early data suggest that a substantial fraction of the rocks are low permeability, less than 10 mD. This holds true for both the mudstones and siltstones as well as the sandstones. The majority of the permeabilities obtained thus far, however, are field measurements made in transects T-1 and T-2, situated in the middle and distal portions of the delta front, where siltstones and mudstones are common and lower permeabilities are expected. Less than 50 permeability measurements have been made thus far in the laboratory. The majority of these samples are more proximally located, fine-grained, well-cemented sandstones; permeability of these sandstones is usually less than 10 mD. At a few stations, however, permeabilities greater than 100 mD have been measured in coarser grained, poorly cemented sandstones.

Several stations were occupied multiple times in the field in order to obtain statistics to verify the precision of the mini-permeameter. In addition, several stations from which good whole core plugs were recovered were also field tested in the core hole to provide a comparison between field and laboratory measurements of permeability. The permeability of these core plugs will also be measured with conventional Hassler sleeve techniques to evaluate the accuracy of the mini-permeameter.



Fig. 5 Electronic miniprobe permeameter measuring permeability at a core hole in the Ivie Creek case study area.

INTEGRATION OF ADVANCED GEOSCIENCE AND ENGINEERING TECHNIQUES TO QUANTIFY INTERWELL HETEROGENEITY

Contract No. DE-AC22-93BC14893

New Mexico Institute of Mining and Technology
Petroleum Recovery Research Center
Socorro, N. Mex.

Contract Date: Sept. 29, 1993

Anticipated Completion: Sept. 30, 1996

Government Award: \$249,850

Principal Investigator:

F. David Martin

Project Manager:

Robert Lemmon

Bartlesville Project Office

Reporting Period: July 1–Sept. 30, 1994

Objective

The objective of this project is to integrate advanced geoscience and reservoir engineering concepts with the goal of quantifying the dynamics of fluid–rock and fluid–fluid interactions as they relate to reservoir architecture and lithologic characterization. This interdisciplinary effort will integrate geological and geophysical data with engineering and petrophysical results through reservoir simulation. Subcontractors from Stanford University and the University of Texas at Austin (UT) are collaborating on the project. The Department of Geophysics at Stanford is supervising the geophysical research and the Center for Petroleum and Geosystems Engineering at the UT is supervising the hydrologic and tracer research. Several members of the Petroleum Recovery Research Center (PRRC) staff are participating in the development of improved reservoir description by integrating the field and laboratory data as well as developing quantitative reservoir models to aid performance predictions.

Summary of Technical Progress

Laboratory Studies

Interfacial Tension of Sulimar Queen Oil

Interfacial tensions (IFTs) between crude oil and brine solutions of varying pH and ionic strength reflect changes in surface charge of the oil–brine interface. So that charged oil species that can interact with rock surfaces to alter-wetting could be studied, measurements of IFT between sodium

chloride (NaCl) brine solutions of varying pH and ionic strength and crude oil from the Sulimar Queen reservoir were made by the du Nouy ring method. Samples of brine and oil were not preequilibrated in these preliminary tests. The results for two levels of ionic strength (0.1 and 1.0M) and for measurements made with the ring initially in the brine phase as well as initially in oil are shown in Fig. 1.

Variations in the higher pH measurements appear to be related to mixing that occurs at the interface during repeated measurements. Measurements are under way for preequilibrated oil and brine samples as well as for the simulated reservoir brine.

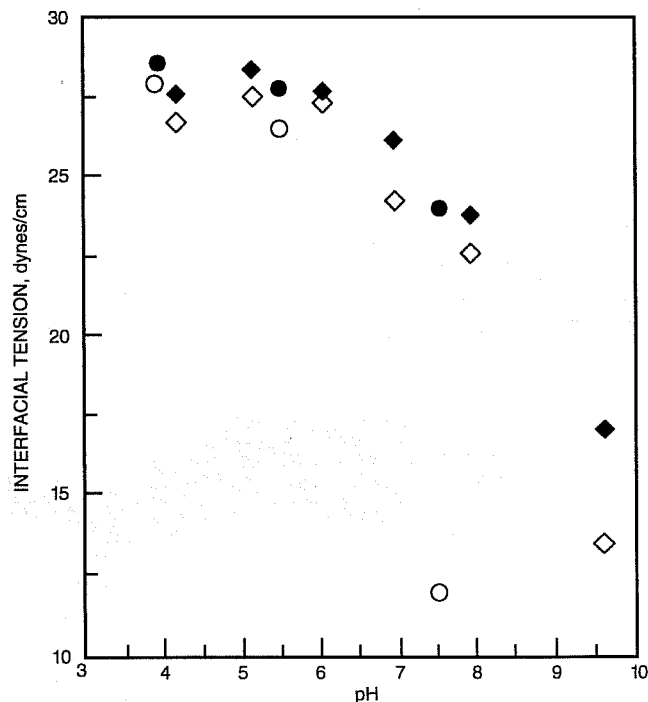


Fig. 1 Interfacial tension between Sulimar Queen crude oil and sodium chloride brines. \diamond , 0.1M, oil \rightarrow brine. \blacklozenge , brine \rightarrow oil. \circ , 1.0M oil \rightarrow brine. \bullet , brine \rightarrow oil.

Preserved Core

One section of preserved Sulimar Queen core (Sulimar Queen No. 1–16, Eddy Co., N. Mex., Core No. 1, Box No. 2, Interval 1995.0 to 1995.5 ft, depth 1995.25 ft) was opened and a core plug was cut. The 1.5-in.-diameter plug was cut from the long dimension of the preserved core and was originally about 6 in. long; the axis of the plug would be oriented vertically in its original position in the reservoir. The plug was highly nonuniform with obvious layering of dark-colored material (presumably shale) separating sandstone layers. A shorter section (about 2 in.) that appeared to be free of these dark layers was cut for further testing.

The core plug was mounted in a Hassler holder for cleaning by flushing with toluene. Flow along the axis of this sample represents vertical flow in the reservoir. Permeability in this plug appears to be very limited, and little cleaning has been

accomplished thus far. Horizontal plugs will be cut for future work.

Hydrologic and Tracer Research

Preliminary design calculations for a single-well wettability tracer test (SWWTT) have been conducted. These calculations considered the behavior of both the reactant and the product tracers, producing cuts, and bottomhole pressures under two different wetting conditions (namely, strongly water-wet and strongly oil-wet conditions) as characterized by different relative permeabilities, capillary pressures, and residual phase saturations. For these simulations, both a homogeneous reservoir and a two-layer reservoir using radial geometry and the average reservoir and fluid properties of the Sulimar Queen formation producing at 94% water-cut were considered. No fluid drift was considered, and capacitance was neglected.

As expected, these preliminary simulations show distinct and characteristic behavior of the tracers, producing cuts, and bottomhole pressures under different wetting conditions. Many more concerns remain, however, before an optimal SWWTT design can be obtained; for example,

- End-point relative permeabilities and fluid saturations to be obtained from preserved core studies of the Sulimar Queen reservoir are very important because relative permeability is a wettability-dependent property.
- Wettability studies currently in progress at the PRRC, part of which will focus on estimation of wettability in the area to be contacted by the SWWTT, alteration of wetting with

reservoir core and fluids, and variation of wetting with geology and fluid saturation history.

- Maximum injection and withdrawal rates possible from the well from which the SWWTT will be conducted because they will affect the total duration of the test and sampling-related issues.

The issue of the maximum injection and production rates is expected to be resolved with the completion of the single-well, pump-in, pump-out tracer test with the use of sodium thiocyanate. Some preliminary calculations have been made to estimate the amount of tracer and the total duration of this test.

Geophysical Research

The objective of the travel-time inversion research is to develop a parameterization for seismic velocity that is consistent with the model required for amplitude reflection mapping. To this end, a nodal model has been developed wherein the velocity is determined on an irregularly spaced grid of nodes. The code has been written and tested on synthetic data. The final phase of this particular effort is to develop a preprocessor to adaptively select the location of the nodes on the basis of heterogeneity or ray coverage or other consideration.

Cross-well imaging, as performed to date, has two separate and distinct steps: travel-time inversion for velocity and reflection imaging of amplitudes. Travel-time inversion normally uses rectangular pixels as velocity basis functions, whereas reflection imaging uses a one-dimensional stratified velocity model. The goal in this project is to combine these

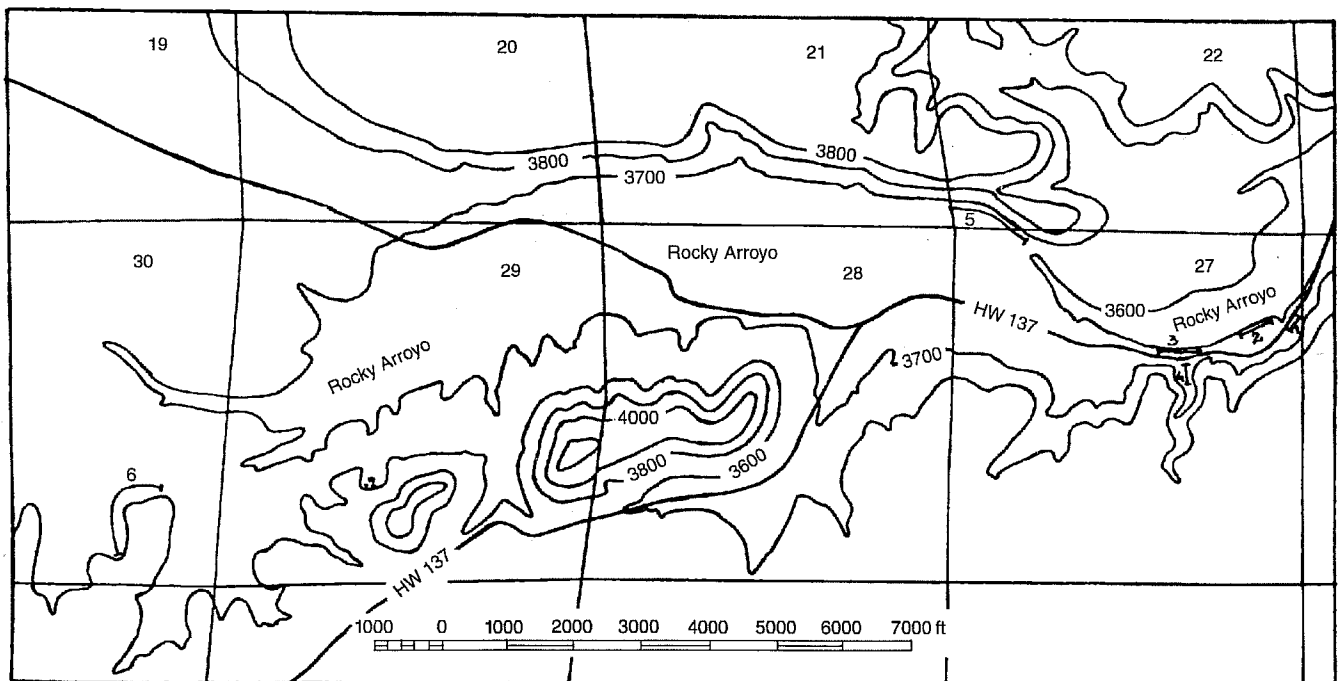


Fig. 2 Location map of measured sections along Rocky Arroyo (T. 21 S., R. 24 E.), Eddy County, N. Mex.

two steps in an iterative manner that results in a more consistent model for both velocity and reflection amplitudes.

Field Activities

Outcrop Study of the Queen Formation (Shattuck Member) in Eddy County, New Mexico

The outcrop study of the Queen formation in Eddy County, N. Mex., will provide more quantitative information on the dimensions and geometries of the sand bodies, the possible presence of barriers to fluid flow that might cause compartmentalization, the distribution of permeability and porosity in three dimensions, and the factors controlling their distributions. Reconnaissance work has been done in several areas, and a more detailed study has been made of exposures present along and adjacent to Rocky Arroyo (T. 21 S., R. 24 E.) (Fig. 2). This area is about 40 miles southwest of the Sulimar Queen field. Detailed study includes the collection of permeability data using a field minipermeameter supplied by Temco, Inc., collection of rock samples for further analysis, and construction of measured sections.

Permeability in all samples is fairly low, ranging between 7 and 108 mD. This is consistent with permeability measurements made on reservoir core samples. Generally, rocks with low permeabilities are of two types: finely laminated siltstones and shales or massively bedded and tightly cemented fine-grained sandstones. The permeability distribution does appear to be a function of depositional environment. Qualitative observations suggest that the sandstone units deposited in subaqueous environments show higher permeabilities than those deposited as eolian dunes, and the permeability heterogeneities are higher within units than between units.

Field Tests

Field development of the inverse drill stem test (DST) method for estimating permeability continued. The proper setting for pressure tolerance and power-source filtering of the pressure-time recording equipment were better defined during this reporting period. Well No. 1-16 was retested without wellhead pressure, and permeability was estimated to be 4.5 mD with a 2.6 skin. New signal transmitting cable and transducers have been ordered.

GYPSY FIELD PROJECT IN RESERVOIR CHARACTERIZATION

Contract No. DE-FG22-94BC14970

**University of Oklahoma
Norman, Okla.**

**Contract Date: May 19, 1994
Anticipated Completion: May 18, 1995
Government Award: \$348,000
(Current year)**

**Principal Investigator:
Daniel J. O'Meara, Jr.**

**Project Manager:
Robert Lemmon
Bartlesville Project Office**

Reporting Period: July 1-Sept. 30, 1994

Objective

The overall objective of this project is to use the extensive Gypsy field laboratory and data set as a focus for developing and testing reservoir characterization methods that are targeted at improved recovery of conventional oil. The Gypsy field laboratory¹ consists of coupled outcrop and subsurface sites that have been characterized to a degree of detail not possible in a production operation. Data from these sites entail geological descriptions, core measurements, well logs, vertical seismic surveys, a three-dimensional (3-D) seismic survey, cross-well seismic surveys, and pressure-transient well tests.

The project consists of four interdisciplinary sub-projects that are closely interlinked: (1) modeling depositional environments, (2) integrated 3-D seismic interpretation, (3) sweep efficiency, and (4) tracer testing.

The first of these aims at improving the ability to model complex depositional environments that trap movable oil. The second is a development geophysics project that proposes to improve the quality of reservoir geological models through

better use of 3-D seismic data. The third investigates the usefulness of a new numerical technique for identifying unswept oil through rapid calculation of sweep efficiency in large reservoir models. The fourth explores what can be learned from tracer tests in complex depositional environments, particularly those which are fluvial dominated.

Summary of Technical Progress

Research this quarter involved three sub-projects.

- *Modeling depositional environments.* The use of thin-plate and tension splines for detecting discontinuities in geological or petrophysical properties was examined. In an example derived from the Gypsy outcrop, tension splines were clearly superior.

- *Integrated 3-D seismic interpretation.* A 3-D geological model of the Gypsy subsurface site was constructed with the use of 3-D seismic data constrained by well log and core data. Eight seismic horizons were mapped on the basis of seismic data, which yielded geometrical information on major sand and shale zones.

- *Sweep efficiency.* As a first step in the examination of the cubature method as an alternative to implicit pressure, explicit saturation (IMPES) schemes, the equations and a numerical scheme were formulated for two-dimensional (2-D) flow in heterogeneous reservoirs. A computer program for implementing this numerical scheme is being developed.

Modeling Depositional Environments

It is well known that reservoirs are highly heterogeneous and have properties that may possess large spatial variations. Moreover, properties are often known in detail only at wells. In interwell regions, if data are available at all, there is far less detail. A fundamental problem in any attempt to predict recovery behavior involves the extraction of relevant geological and petrophysical information from relatively sparse measurements.

In the present study, a function space approach² is adopted by formulating problems in Hilbert spaces. Instead of explicitly characterizing representative elements, the focus is on the variational boundary value problems that occur as Euler conditions associated with the minimization problems and their finite element solution. Simple bicubic B-spline functions are used as basis elements for finite dimensional approximating spaces.³ Constraints are also incorporated by means of penalty and augmented Lagrangian methods. Although data that are realized as equality constraints are considered here, many of the techniques used carry over to inequality constraints as well.

Linear constraints are treated with the goal of obtaining approximating functions from data that may have discontinuities. A computational example shows that the thin-plate spline method appears to be inadequate for obtaining functions that are capable of modeling discontinuities, at least for a case in which

data are distributed as in the Gypsy outcrop site. The regularization is then weakened by replacing the thin-plate functional with a membrane-potential energy functional corresponding to the tension term described by Mitsova and Mitsova.⁴ This approach provides a more flexible function that can accommodate sudden changes better while still smoothing.

Linear Functional Constraints

The case is which data z_i are associated with points x_i , in an open domain $\Omega \subset \mathcal{R}^n$, where $n = 2$, with a Lipschitz boundary Γ is considered here. Further, the data z_i represent measurements of some attribute z that is defined on Ω . The problem is to determine a function u_0 that is defined on the entire region Ω while it remains close to the data. Hence

$$Q_{ad} = \{u \in Q : \langle \phi_i, u \rangle = z_i \text{ for } i = 1, \dots, N_0\} \quad (1)$$

where ϕ_i for $i = 1, \dots, N_0$ are continuous linear functionals on Q . Here $\langle \cdot, \cdot \rangle$ represents the duality pairing between Q and Q^* , where H is designated as the pivot space. Hence $Z = \mathcal{R}^{N_0}$ and

$$C_0 u = [\langle \phi_1, u \rangle, \dots, \langle \phi_{N_0}, u \rangle] \quad (2)$$

The subspace Q_0 is given by

$$Q_0 = \{u \in Q : \langle \phi_i, u \rangle = 0 \text{ for } i = 1, \dots, N_0\} \quad (3)$$

The penalized problems take the form

$$\text{Minimize } N(u) + K \sum_{i=1}^{N_0} [\langle \phi_i, u \rangle - z_i]^2 \quad (4)$$

subject to $u \in Q$. For the linearized case, the variational optimality conditions give necessary and sufficient conditions for the solution of the preceding. Hence, on taking the variation of the functional of Eq. 4, one obtains

$$\left(u \left| v \right. \right) + K \sum_{i=1}^{N_0} \langle \langle \phi_i, u \rangle - z_i \rangle \phi_i, v \rangle = 0 \quad (5)$$

for any $v \in Q$.

Variational problems such as those just shown are weak forms of elliptic boundary value problems. The associated boundary conditions are so-called variational boundary conditions and typically are not imposed on approximating finite-element basis functions. Thus, as approximations to solutions of weak boundary value problems, finite-element solutions need not satisfy the variational boundary values. Nevertheless, the imposition of the boundary values on approximating basis functions allows a more accurate solution. Hence the use of bicubic B-splines with the tension functional may be adjusted to include zero flux boundary conditions.

With the use of these optimality conditions solutions to approximating problems over finite dimensional subspaces of Q may be obtained. To this end, let $\{\psi\}_{j=1}^n$ be a set of linearly independent functions in Q . Denote by

$$Q^n = \text{span}\{\psi_j : j = 1, \dots, n\} \text{ and set } u^n = \sum_{j=1}^n c_j \psi_j$$

$$(G_D)_{kj} = \sum_{i=1}^{N_0} \langle \phi_i, \psi_k \rangle \langle \phi_i, \psi_j \rangle \quad (6)$$

and

$$(G)_{kj} = (\psi_k | \Psi_j) \quad (7)$$

for $k, j = 1, 2, \dots, n$ and the vector

$$(\zeta)_j = \sum_{i=1}^{N_0} z_i \langle \phi_i, \psi_j \rangle \quad (8)$$

for $j = 1, 2, \dots, n$. The discrete analog of Eq. 5 is

$$(K G_D + G) c = K \zeta \quad (9)$$

For $n = 2$, consider the thin-plate functional

$$N(u) = \int_{\Omega} (u_{xx}^2 + 2u_{xy}^2 + u_{yy}^2) dx dy \quad (10)$$

Also consider the functional

$$N(u) = \int_{\Omega} |\nabla u|^2 dx \quad (11)$$

as in the case of a membrane tensional functional. In the first case, take $Q = H^2(\Omega)$, whereas in the second case, $Q = H^1(\Omega)$.

Boundary value problems that are associated with these formulations can be obtained. The resulting boundary conditions in the thin-plate case involve second and third derivatives. Alternately, in the tension case, the boundary value problem is obtained:

$$\begin{aligned} -\nabla \cdot \nabla u &= K \sum_{i=1}^{N_0} (\langle \phi_i, u \rangle - z_0^i) \phi_i \text{ in } \Omega \\ \frac{\partial u}{\partial z} &= 0 \text{ on } \Gamma \end{aligned} \quad (12)$$

Of significance here is that the variational boundary condition involves only first-order derivatives. Thus these conditions may be imposed on the boundary values of approximating basis functions constructed from bicubic B-splines. Their inclusion helps to control the oscillation of the approximating functions.

Example with Gypsy Outcrop Data

This example is aimed at understanding the ability to detect discontinuities in geological or petrophysical properties because of channels, as are found in the Gypsy formation. Consider the case of a function that has two linear discontinuities over a rectangular region, Ω , shaped like the area behind the main Gypsy roadcut. At Gypsy, this region has 22 boreholes, as shown in Fig. 1. For simplicity, the following data function was chosen.

$$z(x, y) = \begin{cases} 2, & 0 \leq y < 3 \\ 4, & 3 \leq y < 6 \\ 2, & 6 \leq y < 10 \end{cases} \quad (13)$$

The ability to detect the discontinuities at $y = 3$ and $y = 6$ is investigated given measurements at the 22 boreholes. Note the density of borehole information is high for $y < 6$, and there are only 3 boreholes for which $y > 6$. Ω is partitioned with a grid that is determined by dividing the sides of Ω into $N = 5$ subintervals of equal length. This determines a set of 64 B-splines as described by Schultz.³

The results of computations for the thin-plate spline are shown in Fig. 2, and the results for the tension spline are shown in Fig. 3. In this case, the tension spline clearly does better at detecting the discontinuities.

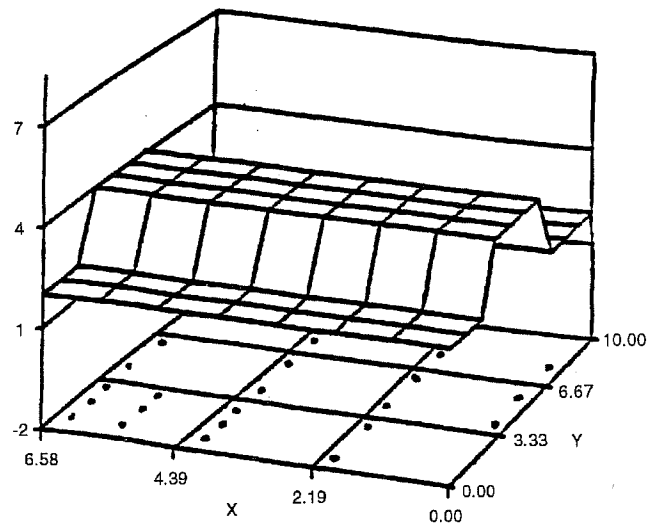


Fig. 1 Test data function showing discontinuities at $y = 3$ and $y = 6$. Locations of 22 boreholes are shown on the base plane.

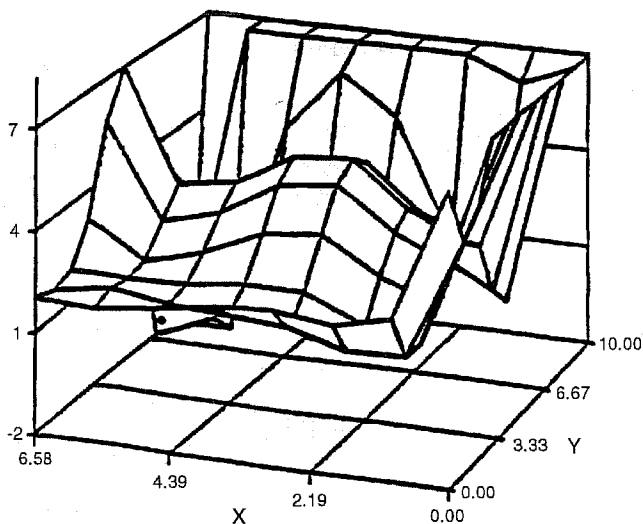


Fig. 2 Fit of test data function with the use of thin-plate spline with measurements at 22 boreholes, only 3 of which occur at $y > 6$.

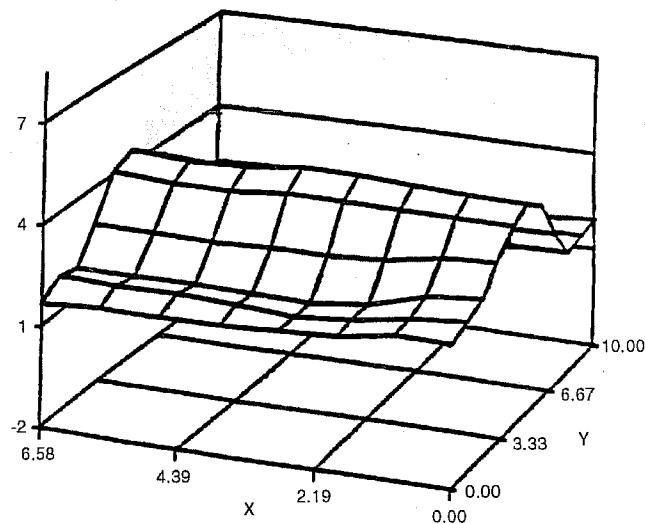


Fig. 3 Fit of test data function with the use of tension spline with measurements at 22 boreholes, only 3 of which occur at $y > 6$.

Integrated 3-D Seismic Interpretation

Three-dimensional seismic data constrained by well log and core data were used to construct the geological model of the Gypsy subsurface site. The objectives of this study are to assess the value of the Gypsy high-resolution 3-D seismic data in delineating channels; to integrate 3-D seismic data with well logs and core data; and to construct a working 3-D geological model of the Gypsy subsurface, on which seismic forward modeling and fluid-flow modeling can be based. The geology is tied to the seismic data by constructing and matching synthetic seismograms to the seismic record sections. In three phases of seismic interpretation, major horizons are mapped and used to develop a detailed 3-D geological model of the Gypsy reservoir.

The upper and lower boundaries of the Gypsy interval were identified on the lithodensity logs of each of the wells. The gamma-ray logs were used to discriminate sand units from shale units within the interval; however, correlation of the Gypsy sand units between wells is difficult because the shape of the curves differs substantially. Core photographs were used to compare the lithologies of individual channel sands and guide their correlation. Thus the Gypsy interval was subdivided into three to five fluvial channels with a composite thickness ranging from 8.5 m (28 ft) to 18.6 m (61 ft). These channels are encased and sometimes separated by shales.

The densities of the channel sands are generally much lower ($\rho = 2.25 \text{ g/cm}^3$) than the densities of the shales because of much higher porosities of the channel sands (up to 26%, derived from petrophysical data); however, the channel sands exhibit lower sonic travel times (higher velocities). This compensation of lower densities by higher velocities decreases the contrast in acoustic impedance, the product of density and velocity. Consequently reflections are not very strong at interfaces between sand and shale. Thus it is difficult to match the synthetic seismograms to the actual seismic data, and an exact fit cannot be made.

The 3-D data set consists of 52 in-lines and 52 cross-lines covering an area approximately 161,768 m^2 (40 acres). The data were acquired with dynamite charges at hole depths of 36.5, 33.5, 30.5, and 27.4 m (120, 110, 100, and 90 ft, respectively). Geophones were arranged in groups of 12 in a circular array 7.6 m (25 ft) in diameter and 12 groups per swath. The data were acquired and processed by Western Geophysical.

The dominant frequencies within the Gypsy interval were estimated to be between 78 and 168 Hz by measuring the periods on the seismic section at three different positions within the Gypsy interval. With the use of velocities determined by seismic logs, 3,021 to 3,413 m/s (9,917 to 11,200 ft/s), the bed resolution ranges from 4.6 to 11 m (15 to 36 ft), and the range of detectability is from 0.6 to 4.6 m (2 to 15 ft) in thickness. Because most of the channels are 3.0 to 9.1 m (10 to 30 ft) thick (as derived from well log data), the definition of the three to five channels on the well logs is at the limit of seismic resolution.

Figure 4 shows a North-South cross section through the seismic data with all mappable horizons labeled. For the three interpretation phases, relevant horizons are identified by picking the characteristics shown on the synthetic seismograms (e.g., upper part of the peak or trough). Unfortunately, it is impossible to pick these characteristics accurately because of errors in synthetic seismograms caused by uncertainty in velocities, inaccuracy of visual picking, and the fact that the thickness of the units is close to the limits of resolution. Consequently the Δt 's (isochrons) are off by a certain amount, which then results in thickness estimates that are different from the well log data. Furthermore, during computation of the isopachs, one average velocity was applied to each interval.

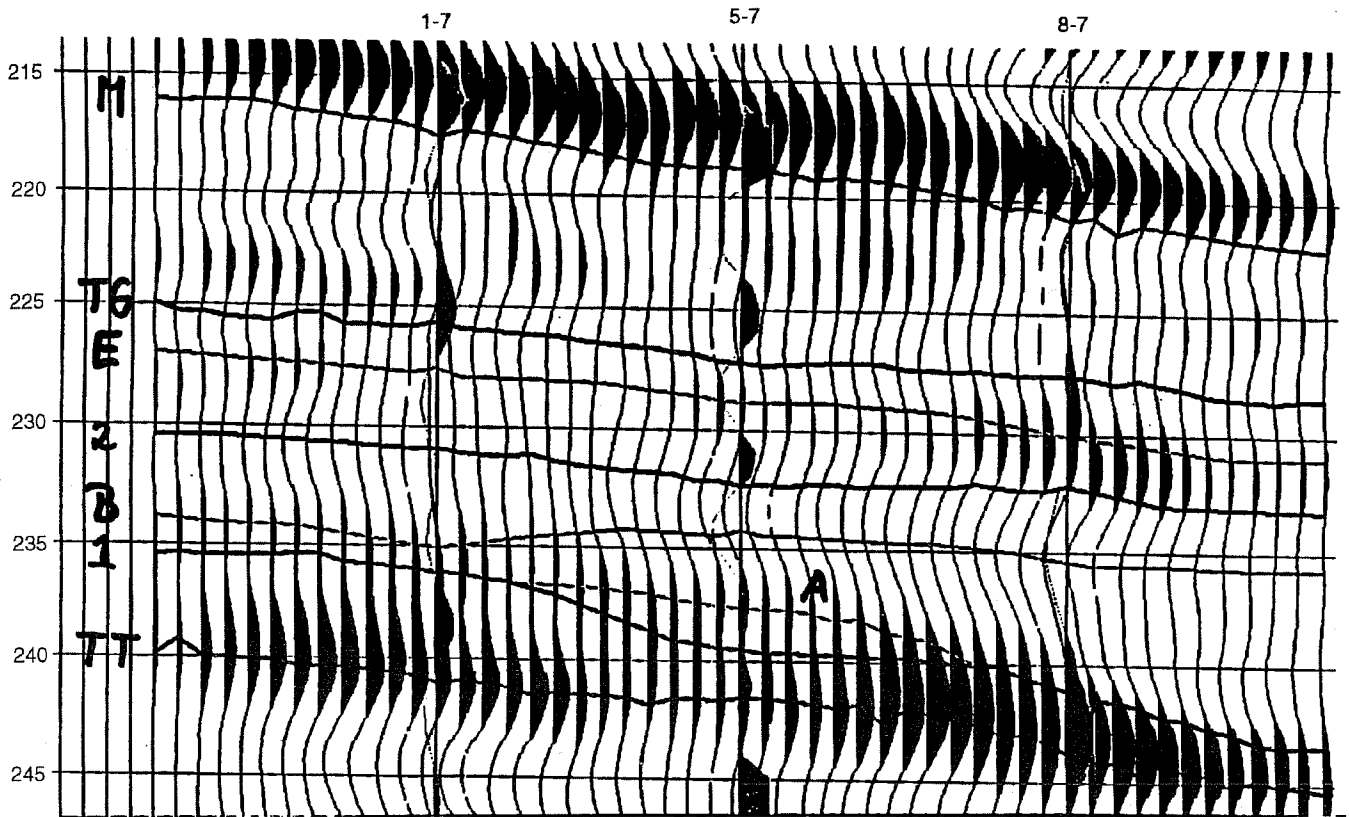


Fig. 4 North-South 3-D seismic cross section, showing eight surfaces. "A" denotes a channel that was discernible from seismic data.

During this quarter a portion of the Gypsy dataset was analyzed and integrated to develop a comprehensive geological model of the subsurface. The data analyzed include well logs, core photographs, vertical seismic profiles, and the 3-D seismic survey. Eight seismic horizons were mapped on the basis of seismic data, which gave geometrical information on major sand and shale zones.

Sweep Efficiency

The cubature method, as developed by Civan,⁵⁻⁷ has been applied to the problem of unit mobility, incompressible flow in a heterogeneous reservoir. A unique feature of the cubature method is that the whole of an equation can be discretized instead of term-by-term discretizing as used in the conventional approach. As a result of including both the temporal and spatial derivative terms in this discretization, a transient-state problem can be solved like a steady-state problem. By virtue of this feature, the cubature solutions are significantly more rapid and less computationally intensive than IMPES schemes, and thus produce numerical solutions that are more accurate.

As a first step, thickness-averaged porosity, permeability, and saturation were used to formulate the equations and a numerical scheme for 2-D flow. For the numerical solution of this 2-D model, the time-space numerical scheme of Civan⁵⁻⁷ has been implemented. This scheme leads to stable numerical solutions for relatively large spatial grids and time

increments. A computer program is under development for the implementation of this numerical scheme.

For numerical discretization purposes, the local computational molecules in t , x , and y were represented by a general irregular-shaped cube containing 64 nodes with variable spacing. The cubature weights associated with these nodes were calculated. Next, the linear control volume equations were linearized by means of Newton's method with the use of Frechet derivatives. The matrix equations resulting from this exercise have 64-element, banded, coefficient matrices.

References

1. J. D. Doyle, D. J. O'Meara, Jr., and E. J. Witterholt, *The Gypsy Field Research Program in Integrated Reservoir Characterization*, paper SPE 24710 presented at the 67th Annual SPE Technical Conference and Exhibition, Washington, D.C., October 4-7, 1992.
2. R. L. Parker, *Geophysical Inverse Theory*, Princeton University Press, Princeton, N.J., 1984.
3. M. Schultz, *Spline Analysis*, Prentice Hall, Englewood Cliffs, N.J., 1973.
4. H. Mitasova and L. Mitas, Interpolation by Regularized Spline with Tension: I. Theory and Implementation, *Math. Geol.*, 25: 641-655 (1993).
5. F. Civan, Finite Analytic Method for Numerical Solution of Mathematical Models, in *Integral Methods in Science and Engineering* (90), Series in Computational and Physical Processes in Mechanics and Thermal Sciences, pp. 270-281, A. Haji-Sheikh et al. (Eds), Hemisphere Publishing Co., New York.
6. F. Civan, Quadrature and Cubature Methods for Numerical Solution of Integro-Differential Equations, in *Integral Methods in Science and*

INTERDISCIPLINARY STUDY OF RESERVOIR COMPARTMENTS

Contract No. DE-AC22-93BC14891

Colorado School of Mines
Golden, Colo.

Contract Date: Sept. 29, 1993
Anticipated Completion: Sept. 30, 1996
Government Award: \$753,266

Principal Investigator:
Craig W. Van Kirk

Project Manager:
Robert Lemmon
Bartlesville Project Office

Reporting Period: July 1-Sept. 30, 1994

Objective

The objective of this research project is to document the integrated team approach for solving reservoir engineering problems. A field study integrating the disciplines of geology, geophysics, and petroleum engineering is the mechanism for documenting the integrated approach. The goal is to provide tools and approaches that can be used to detect reservoir compartments, reach a better reserve estimate, and improve profits early in the life of a field.

Summary of Technical Progress

Six tasks were in progress during the third quarter of 1994.

Reservoir/Outcrop Selection and Evaluation

Data Gathering and Checking

During the quarter the project team agreed on a tentative area for reservoir simulation (Fig. 1). Most of the data have been gathered, input into the database, and checked for quality. Data will be added to the database on an as-needed basis. Some additional data will be needed now that the preliminary area for reservoir simulation has been selected.

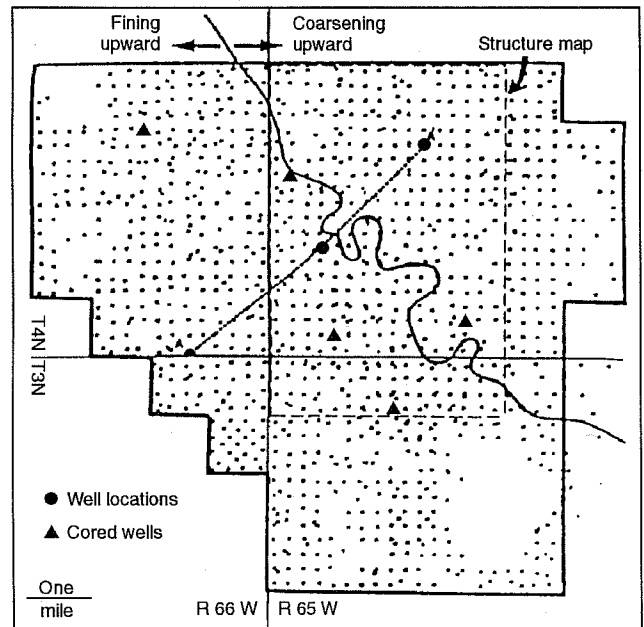


Fig. 1a Map of Hambert-Aristocrat Field area showing wells and boundary between vertical sequences.

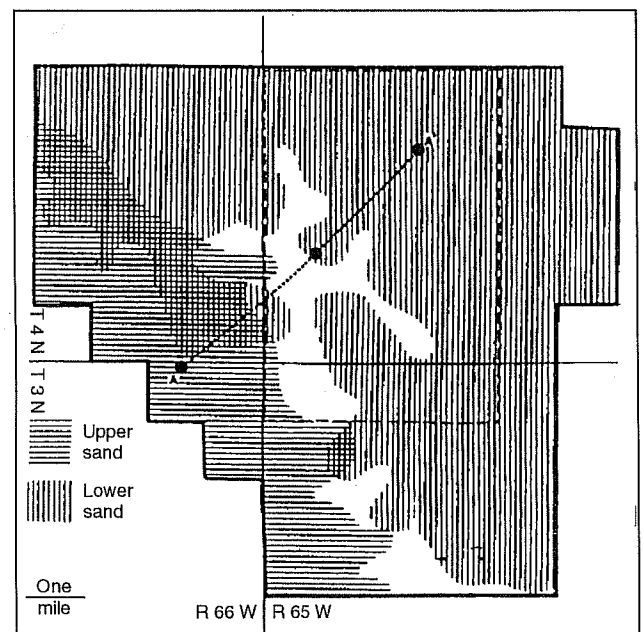


Fig. 1b Map of areal distribution of lower and upper sandstones. Middle sandstone occurs throughout the area.

The application of quality control data checking has helped identify correlation problems in some of the initial correlation work. The iterative nature of the integrated approach has been noted as more information is gathered and assimilated.¹

Outcrop/Core/Log Analysis and Correlations

Conclusions reached on the basis of the log analysis work include:

- Bulk volume water (BVW) is a better parameter for discriminating pay from non-pay than porosity, water saturation, or shale volume cutoffs. In addition, BVW helps to distinguish the thinly laminated sands that commonly occur above the basal sand.
- 104 wells have been digitized and processed in the regional Aristocrat–Hambert field area. Plates have been printed for the wells to check the quality of the digitization and to graphically present data on a common set of scales along with results of the processing and a pay indicator.
- Correlation is aided with these Plates because all the log traces are presented on a common format with common scales.
- With the data analyzed to date, the clay mineralogy is still considered to be illite with some montmorillonite–smectite and possibly traces of kaolinite. All these clays are hydrous and swell (to varying degrees) when in contact with fresh water.²

Internal Architecture Description

The internal architecture of the reservoir was studied, and a series of cross sections were constructed. Twelve NE–SW cross sections were constructed along with one NW–SW cross section. These cross sections coupled with a detailed analysis of the log shapes lend insight into the reservoir internal architecture. The complex stratigraphic sequence has been described as follows:

In the western part of the area, the facies are arranged in a fining-upward or blocky sequence. By contrast, in the eastern part of the area they are arranged in a coarsening-upward sequence. The complex pattern of sequences is interpreted to be a result of westward shingling (paleolandward) of three separate sandstone intervals—termed lower, middle, and upper (see Fig. 2).³

Detailed structure and isopach mapping and log analysis indicate that the field area is also structurally complex. The evidence to date suggests that faults are common. A study of the gas/oil ratio (GOR) data and preliminary results of pressure buildup data suggest that the faults are sealing.

Seismic Analysis

The geophysical components of the integrated study are also being addressed. Landmark’s SeisWorks software is being used to interpret the seismic data. Synthetic seismograms have been used to locate the Sussex, Niobrara, and J sandstone formations.

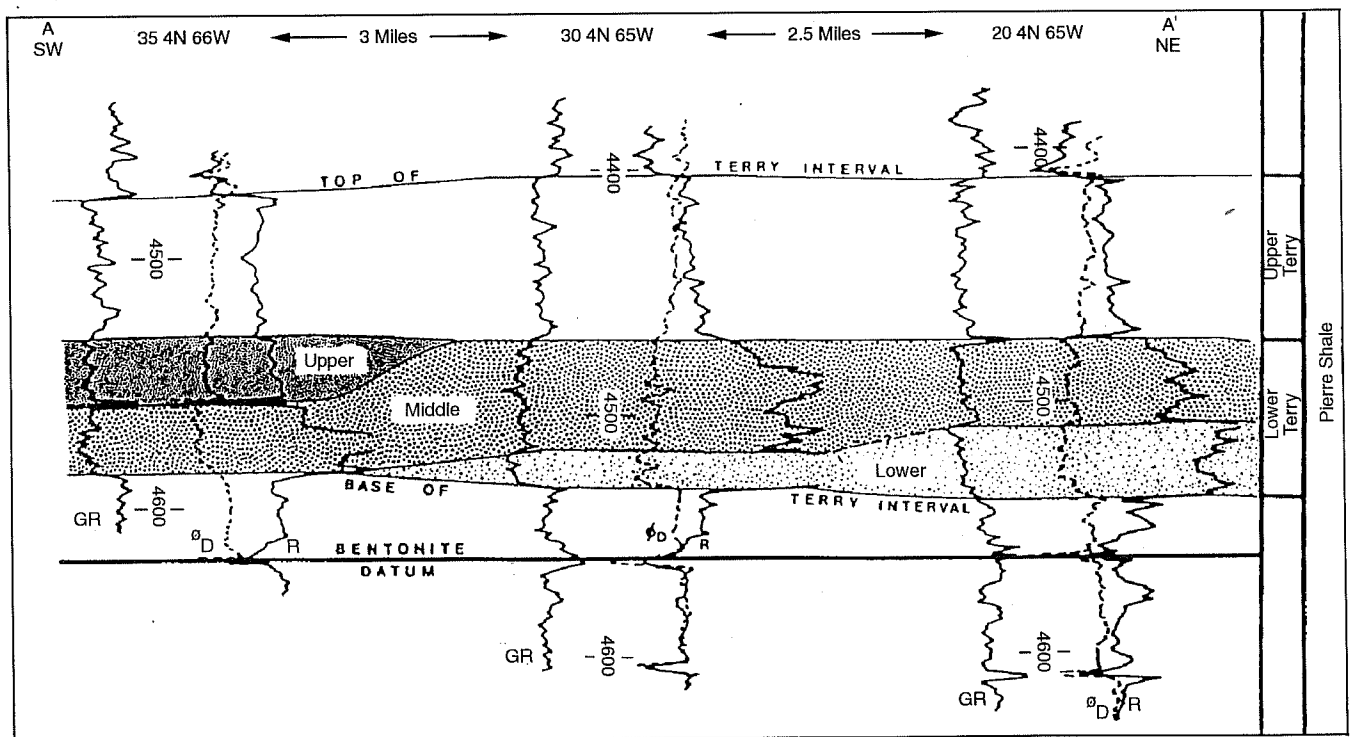


Fig. 2 Southwest-northeast stratigraphic cross section.

Figures 3 and 4 show preliminary time structure maps on the Niobrara and Sussex formations. The current focus of the interpretation process is to map the faulting in the survey area. The results will be integrated with the geologic interpretation and engineering data.

Detailed Reservoir Engineering Evaluation

The results of the detailed reservoir engineering evaluation indicate that two wells have sufficient pressure buildup data to

be analyzed. Preliminary analysis supports flow boundaries within the area of investigation. This information will be used in conjunction with the geologic and three-dimensional seismic interpretations to better characterize the reservoir.

Experimental Investigation

Permeability Experimental Work

On the basis of experimental work conducted during the quarter, it is noted that the effect of increasing the net

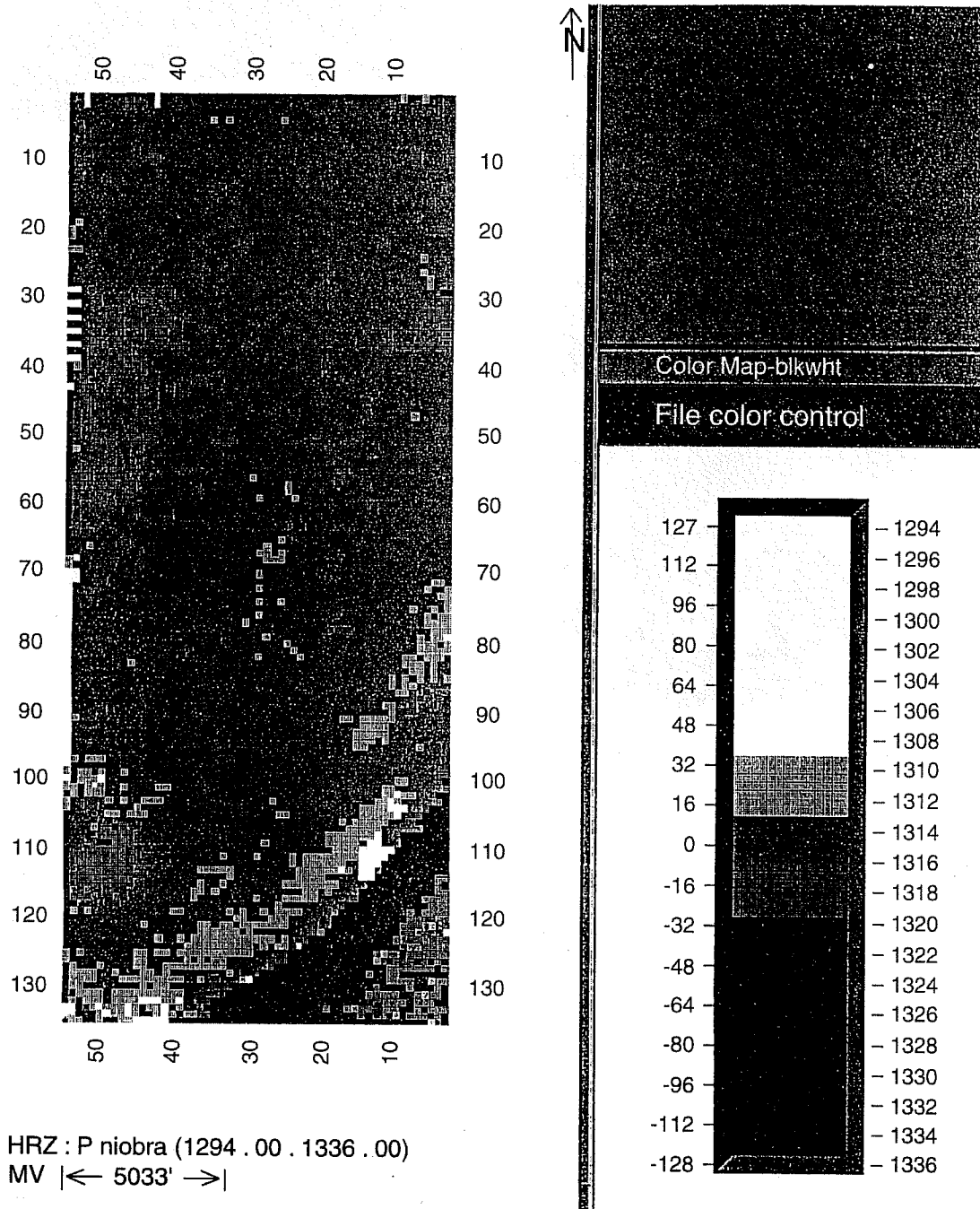


Fig. 3 Niobrara formation time structure map. Note the SW-NE trending fault in the SE corner of the seismic survey. (Art reproduced from best available copy.)

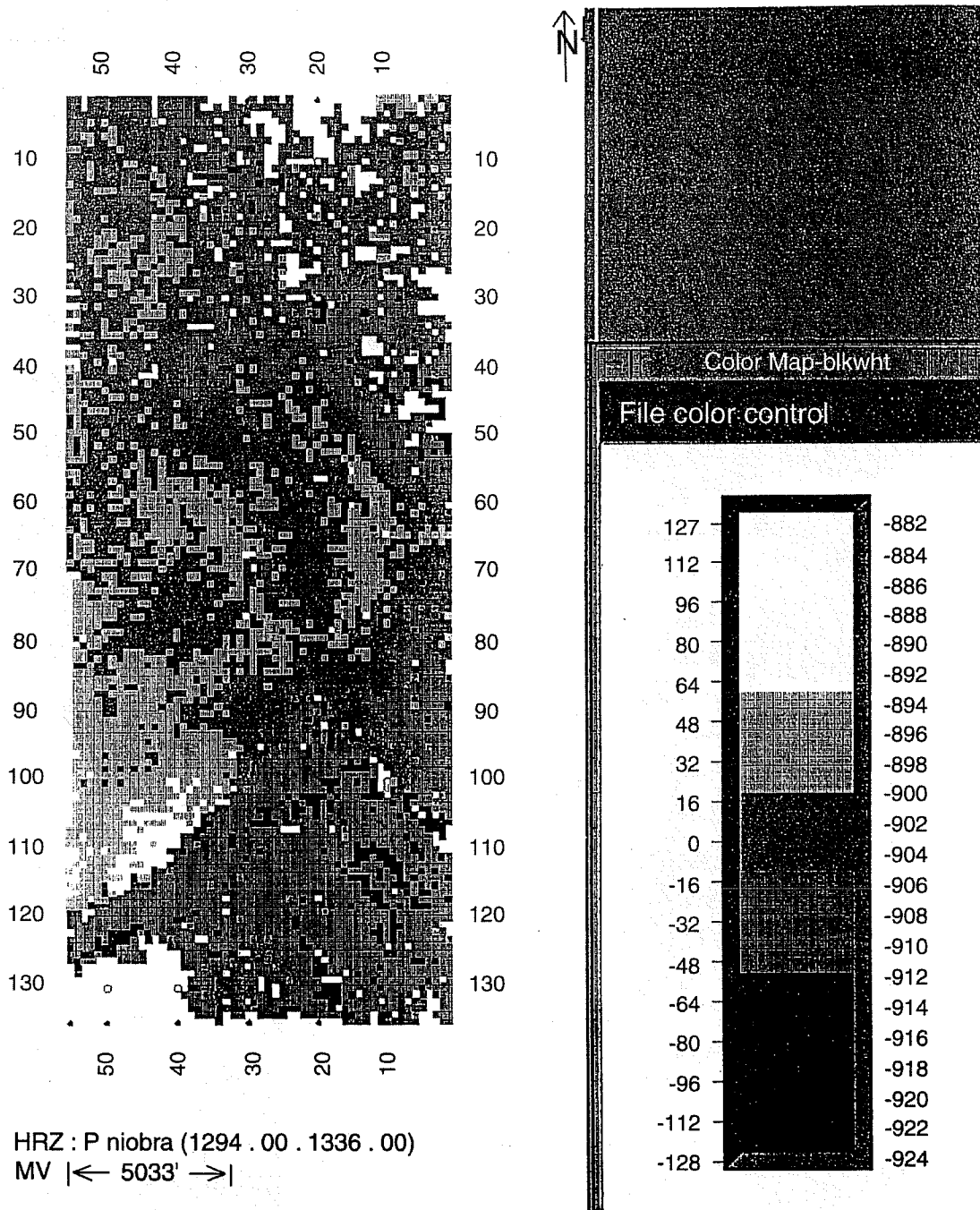


Fig. 4 Sussex formation time structure map. (Art reproduced from best available copy.)

confining stress from 100 to 3500 psig and the temperature from 70 to 140 °F causes only a minor shift in the end points and the shape on the relative permeability curves. These variations could easily be within the limits of experimental procedures, the equipment, and data smoothing techniques. Figures 5 to 7 are examples.

Information/Technology Transfer

Two abstracts^{3,4} were presented at the First Biennial Conference on Natural Gas in the Western United States in Golden, Colo., October 17–18, 1994.

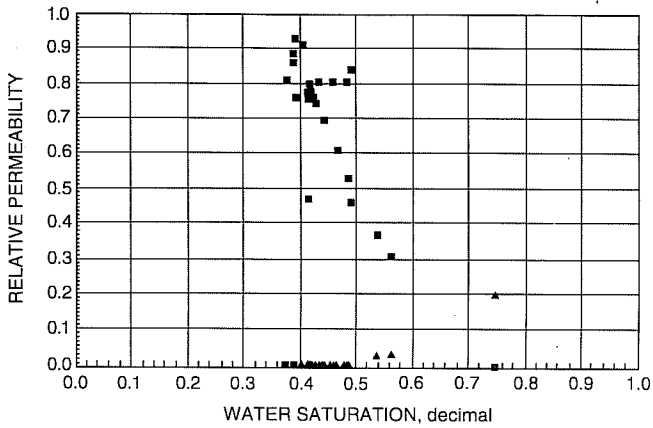


Fig. 5 Oil displacing water relative permeability Experiment 11, second drainage cycle. Core plug Berea 2. Net confining stress $\sigma = 100$ psig. $T = 70$ °F. Johnson-Bossler-Naumann (JBN) data reduction method results. \blacktriangle , k_{rw} , relative permeability of water. \blacksquare , K_{ro} , relative permeability of oil.

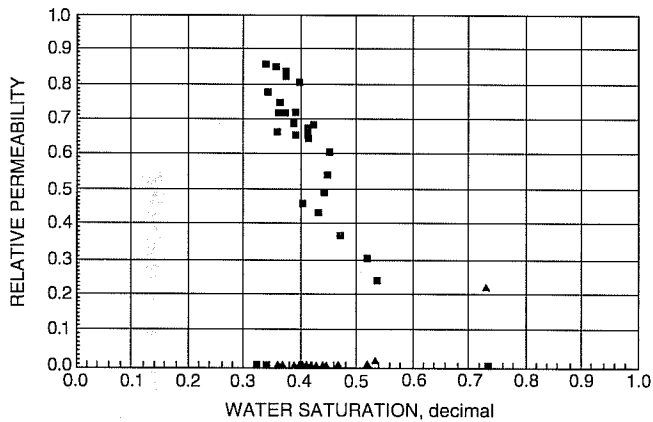


Fig. 6 Oil displacing water relative permeability experiment 14, second drainage cycle. Core plug berea 2. Net confining stress 3500 psig. $T = 70$ °F. Johnson-Bossler-Naumann (JBN) data reduction method results. \blacktriangle , k_{rw} , relative permeability of water. \blacksquare , K_{ro} , relative permeability of oil.

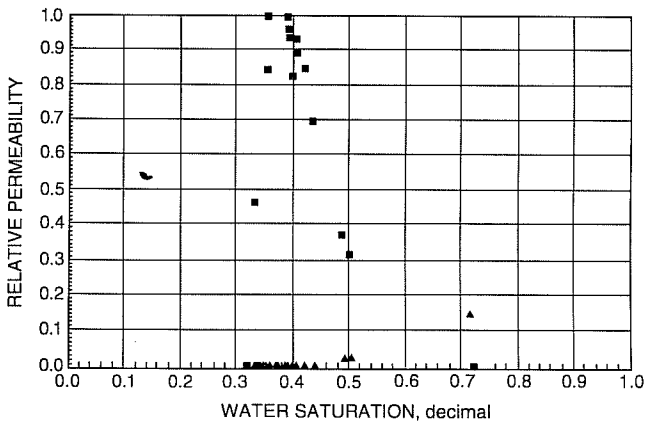


Fig. 7 Oil displacing water relative permeability experiment 17, second drainage cycle. Core plug Berea 2. Net confining stress 3500 psig, $T = 140$ °F. Johnson-Bossler-Naumann (JBN) data reduction method results. \blacktriangle , k_{rw} , relative permeability of water. \blacksquare , K_{ro} , relative permeability of oil.

References

1. D. Edington, *Data Gathering, Correlation, and Internal Architecture Description*, Colorado School of Mines, Sept. 30, 1994.
2. A. Prestridge and J. M. Jalaludin, *Log Analysis and Correlations*, Colorado School of Mines, Sept. 30, 1994.
3. Edington, Slatt, and Araujo, *Structural and Stratigraphic Compartmentalization of the Terry Sandstone and Effects on Reservoir Fluid Distributions: Part II, Lambert-Aristocrat Fields, Denver Basin, Colorado*, abstract presented at the First Biennial Conference on Natural Gas in the Western United States, Golden, Colo., October 17-18, 1994.
4. Al-Raisi, Slatt, and Decker, *Structural and Stratigraphic Compartmentalization of the Terry Sandstone and Effects on Reservoir Fluid Distributions: Part I, Latham Bar Trend, Denver Basin, Colorado*, abstract presented at the First Biennial Conference on Natural Gas in the Western United States, Golden, Colo., October 17-18, 1994.

LAWRENCE BERKELEY LABORATORY/ INDUSTRY HETEROGENEOUS RESERVOIR PERFORMANCE DEFINITION PROJECT

Lawrence Berkeley Laboratory
University of California
Berkeley, Calif.

Contract Date: Apr. 1, 1992
Anticipated Completion: Sept. 1995
Government Award: \$275,000

Principal Investigators:

J. C. S. Long
E. L. Majer
L. R. Myer

Project Manager:

Robert Lemmon
Bartlesville Project Office

Reporting Period: July 1-Sept. 30, 1994

Objective

The overall objective is to develop a methodology that can be used by the petroleum industry in a variety of heterogeneous regimes for characterizing and predicting the performance of petroleum reservoirs. The purpose of this work is to validate geophysical and hydrological techniques for characterizing heterogeneous reservoirs in the most optimal (economic) manner. This will be accomplished through a cooperative research program between Lawrence Berkeley Laboratory (LBL), British Petroleum, Inc. (BP), and the University of Oklahoma (OU), which is focused on the characterization of heterogeneous reservoirs in a meander-belt porous-medium formation. BP has done characterization and data integration at several test facilities. The present program will continue BP's multiyear efforts at the Gypsy site in northeastern Oklahoma. The resulting research will integrate various geophysical and hydrological

methods and apply them at a well-calibrated and characterized site where their utility can be assessed. This cooperation will allow techniques developed for waste storage and geothermal energy to be adapted for use in heterogeneous and fractured reservoirs. The work will be coordinated with the cross-well electromagnetic (EM) research and development project and the LBL/Morgantown Energy Technology Center (METC) reservoir performance definition project.

Summary of Technical Progress

Hydrologic-Related Work

Three tasks related to the hydrological inversion of the pilot-site well tests were in process this quarter: single-test inversions of all the well tests conducted in the upper and middle sand channels were completed; co-inversions of several combinations of upper/middle sand channel well tests were begun; and well test analysis results were compared with well log lithologic information.

Single-Test Inversions of Upper/Middle Sand Channel Well Tests

Single-test inversions have been done for all five of the 1990 well tests conducted in the upper and middle sand channels: tests 90/S1/T2 (well No. 11 middle interval pumped), 90/S2/T2 (well No. 9 middle interval pumped), 90/S2/T3 (well No. 9 upper interval pumped), 90/S3/T2 (well No. 8 upper/middle interval pumped), and 90/S4/T2 (well No. 1 middle interval pumped). There are insufficient observed data available to complete single-test inversions for the two 1989 tests that pumped from well No. 5. Figure 1 shows schematically the well tests analyzed.

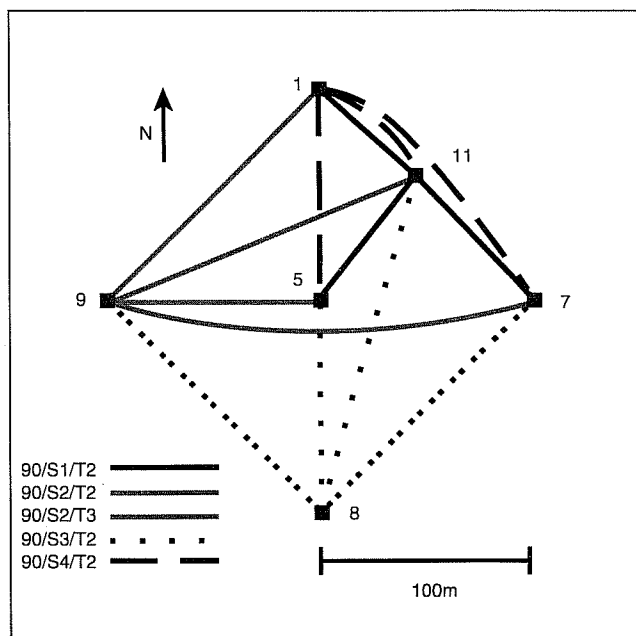


Fig. 1 Gypsy pilot-site upper and middle sand channel well test schematic for 1990 well tests.

For two of the tests, 90/S2/T2 and 90/S2/T3, the reported flow rates for the second pulse were about twice the size of the other pulses, but the pressure responses in the pumping well did not confirm a larger second pulse for either test. For test 90/S2/T2, the pressure response to the second pulse was unusually small; for test 90/S2/T3, the pressure response to the second pulse was comparable to that for the other pulses. For these two tests, the second-pulse flow rates were modified as shown in Table 1 to give the correct relative magnitude for the pressure response in the pumping well.

TABLE 1
Second Pulse Flow Rates

Test	Pulse	Reported flow rate	Modified flow rate
90/S2/T2	1	230	230
	2	575	57.5
	3	287	287
	4	282	282
90/S2/T3	1	263	263
	2	430	230
	3	240	240
	4	288	288

A three-layer model in which the upper and lower layers consist of horizontal elements that represent the upper and middle sand channels and have uniform properties and an intermediate layer that consists of vertical elements, which connects the upper and lower layers and has variable properties, was used for the inversions. In most of the inversions, the intermediate layer has low (clay-like) background permeability, and the effect of the attractor is to increase the permeability; thus the attractor shows the region where the clay layer is missing. An alternative approach would be to give the intermediate layer high (sand-like) background permeability and let the attractor act to decrease permeability and thus represent the region where the clay layer is present. The approach was chosen on the basis of the well log information, which suggests that the clay layer is present in the western, northern, and eastern portions of the well field (well Nos. 1, 7, 9, and 11) but absent in the central and southern portions (well Nos. 5 and 8). As shown in Fig. 2, the gap in the clay layer can be represented simply as a convex polygon, whereas the clay layer itself would require a more complicated shape. This enables iterated function systems (IFS) with fewer parameters to be used and thus simplifies the inversion because fewer unknown parameters must be searched for.

In test 90/S1/T2, well No. 11 was pumped, and pressures were observed in well Nos. 1, 5, and 7. Eleven inversions of test 90/S1/T2 have been done. Most successfully match the main features in the pressure transients for the three observation wells. The clay layer is required to be present between well Nos. 1, 7, and 11, which yields different responses in the upper and lower model layers, but absent around well No. 5, which yields the same pressure response in the upper and lower model layers. The energy (E) for successful inversions ranges from about 14.5 to 16.5.

In test 90/S2/T2, well No. 9 was pumped, and pressures were observed in well Nos. 1, 5, 7, and 11. Early inversions of test 90/S2/T2 yielded energies over $E=100$ with pressure

transients that grossly mismatched the observed values, as illustrated in Fig. 3. After some study, the determination was made that the inversion program was not broken but that

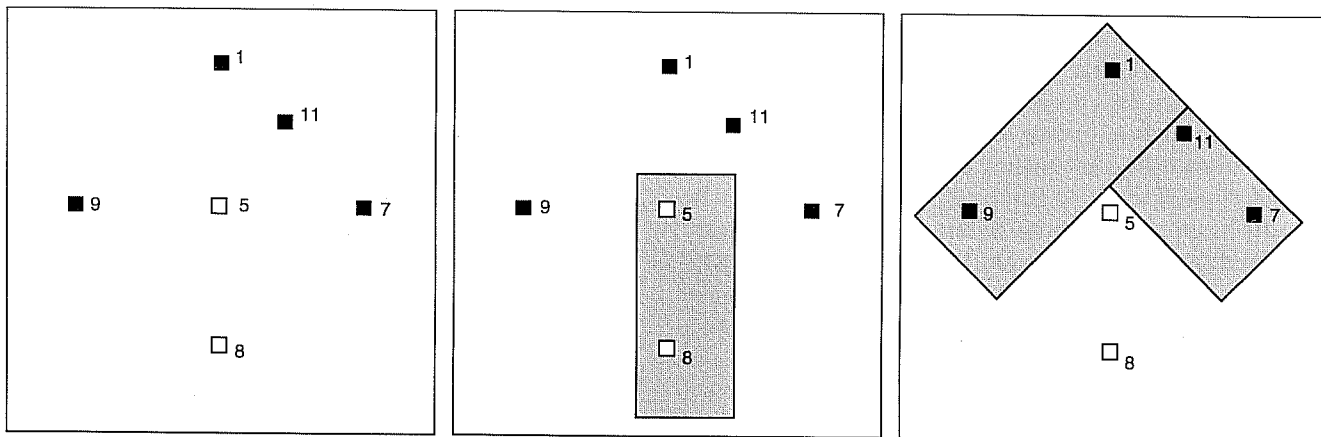


Fig. 2 Lithologic information on the location of the upper clay layer and possible inversion schemes. (a) ■, upper clay present. □, upper clay absent. (b) Inversion check for gap in upper clay. (c) Inversion check for upper clay.

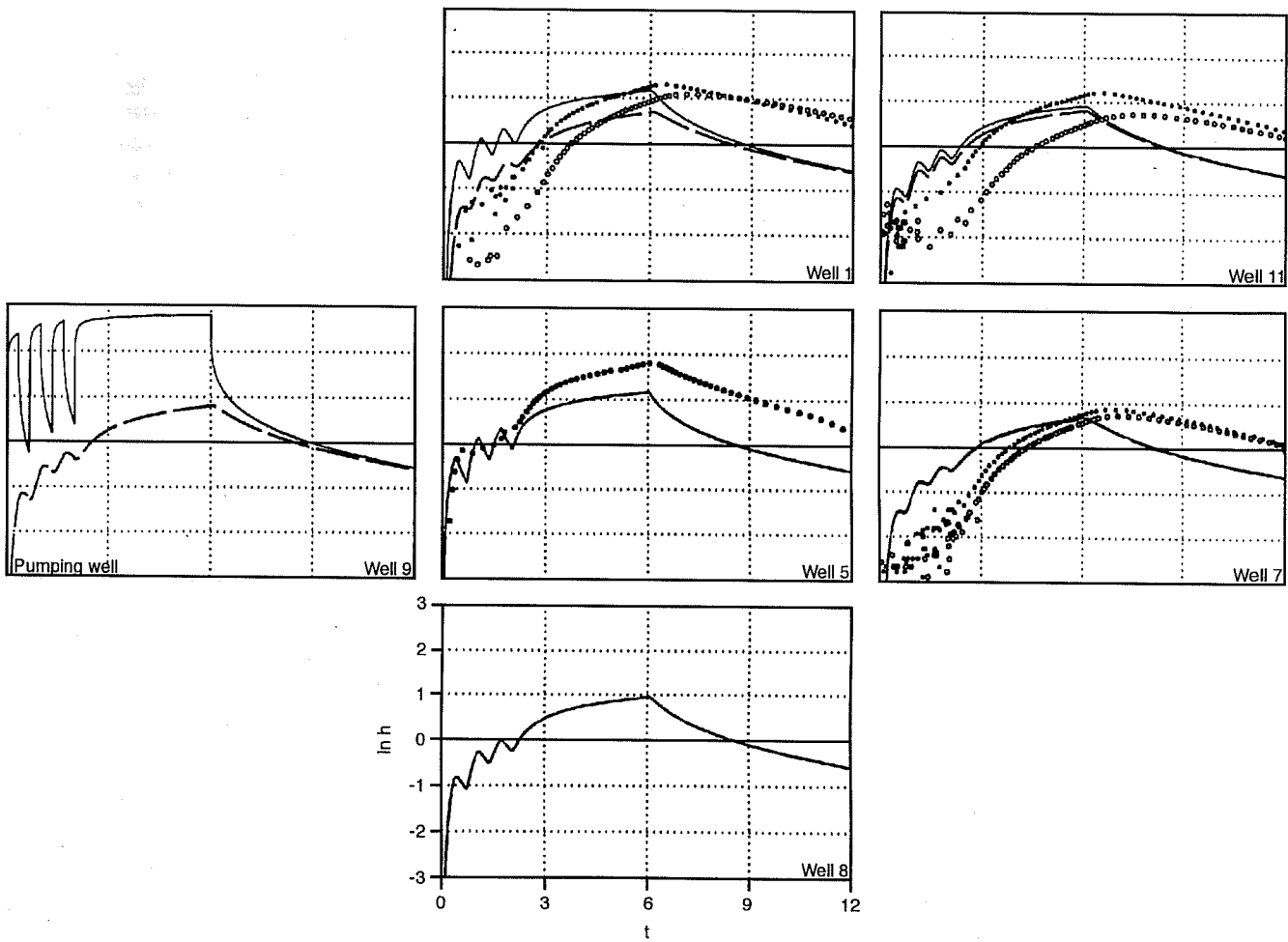


Fig. 3 Observed and modeled pressure transients for an inversion of test 90/S2/T2 (gum15 $E=100.86$) before observed data had been edited. ●, modeled middle. —, observed middle, ○, modeled upper. ---, observed upper.

strongly scattered early-time observed pressures were dominating the matching procedure. In general, not all the observed pressure data are used for the well test analysis because pressures are recorded far more frequently than is necessary to discern most trends. A preprocessing program is used to select enough points to resolve pressure variations that correspond to the step-flow rate changes that occur during the tests. This program, however, is not very sophisticated and tends to include too many data points when the observed pressure data contains too much scatter. Therefore, for all the well tests, the observed pressure transients to be inverted were edited by hand to remove many of the widely scattered data points; this made the density of points similar for early and late times. Although with these changes the inversions of test 90/S2/T2 improve significantly, yielding energies around $E = 10$, none of the inversions done thus far show the correct difference between upper sand channel response and the middle sand channel response for all four observation wells. Figure 4 shows the pressure transients for a typical example, and Fig. 5 shows the corresponding attractor. The match is acceptable for all the wells except

well No. 1, for which the calculation shows the same response for the upper and middle sand channels, whereas the observed data show a significant difference. This comparison suggests that the high-permeability region shown in Fig. 5 just to the north of well No. 1 should not be present.

In test 90/S2/T3, well No. 9 was pumped, and pressures were observed in well Nos. 1, 5, 7, and 11. Test 90/S2/T3 is the only test in which the upper sand channel interval of the pumping well was pumped. In all the other upper/middle tests, the middle sand channel was pumped, and a greater pressure change was observed in the middle channel interval of the observation wells than in the upper channel interval, as would be expected for two partially connected channels. Unexpectedly, test 90/S2/T3 also showed greater pressure changes in the middle sand channel than in the upper sand channel for observation well Nos. 1, 7, and 11. This suggests that the transmissivity of the upper sand channel is less than that of the middle sand channel and that a model that assigns the equal values of transmissivity to each sand layer is inadequate. After some trial and error, a transmissivity in the middle sand channel that was 10 times as great as that in the

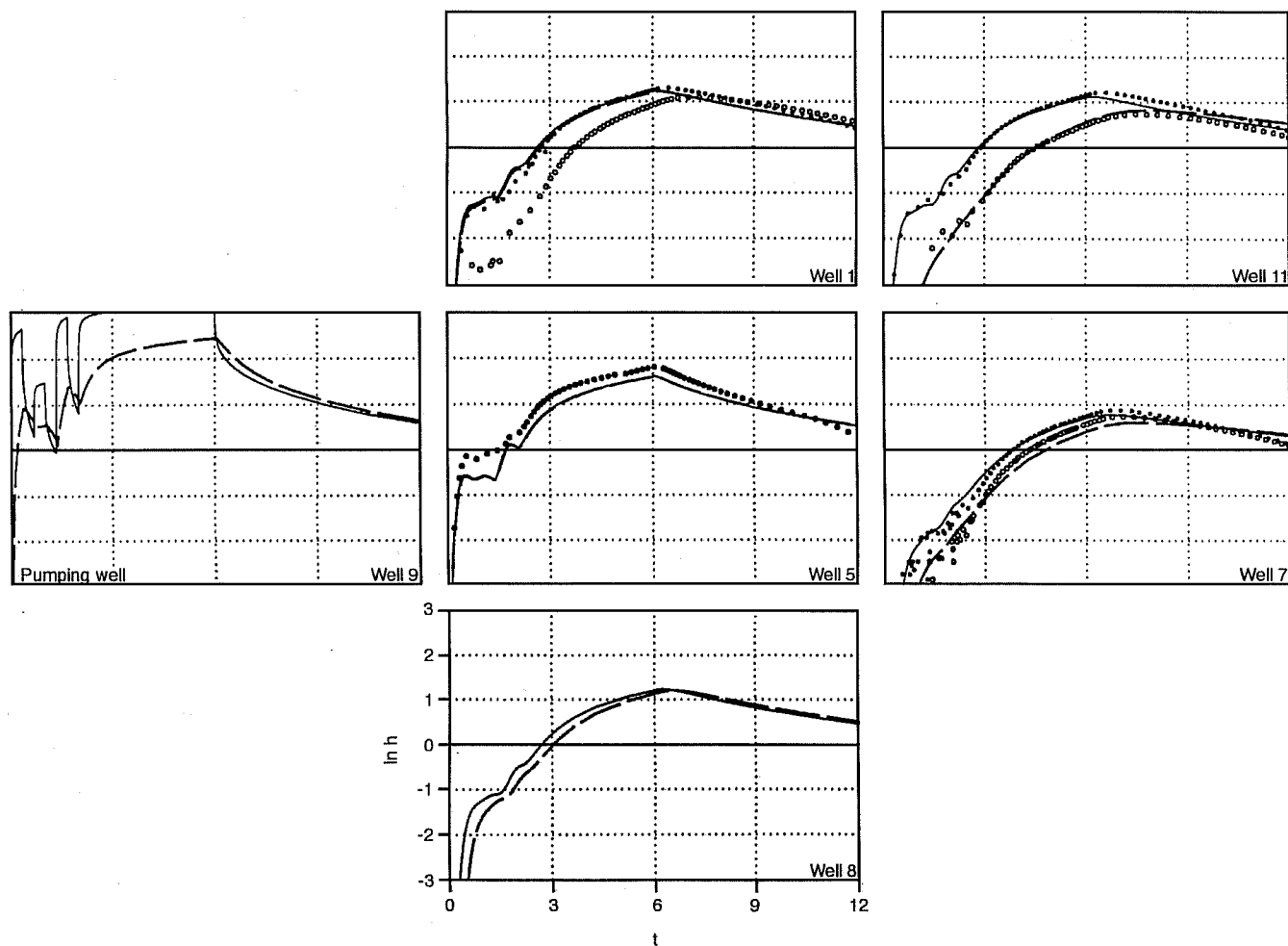


Fig. 4 Observed and modeled pressure transients for an inversion of test 90/S2/T2 (gum39a $E = 8.72$) after observed data had been edited. ●, modeled middle. —, observed middle. ○, modeled upper. ---, observed upper.

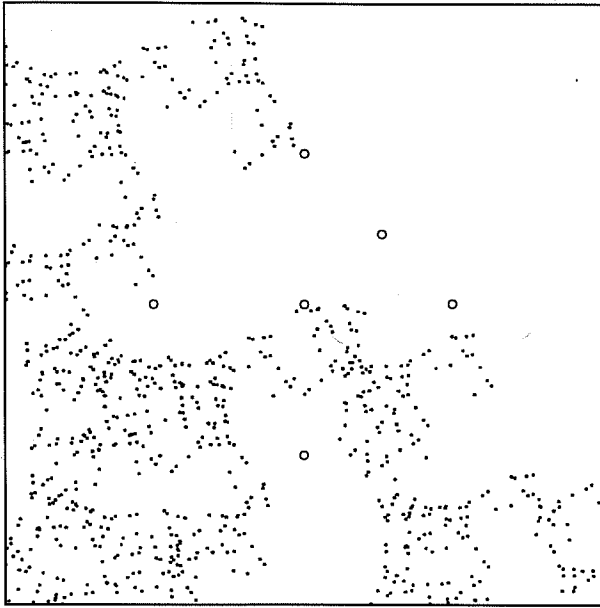


Fig. 5 The final attractor for an inversion of test 90/S2/T2 (gum39a $E = 8.72$). Attractor points identify locations of high permeability (gaps in the clay layer) in the intermediate layer between the upper and middle sand channels.

upper sand channel was used for the inversion of test 90/S2/T3. This modification is at least qualitatively supported by the well log information, which suggests that the upper sand channel is thinner and/or produces a weaker sand signal than the middle sand channel for well Nos. 1, 9, and 11. With this change in the conceptual model, several inversions successfully matched the difference between the middle and upper sand channel pressure transients. Figure 6 shows the pressure transients for a typical example, and Fig. 7 shows the corresponding attractor. This modified conceptual model, with different transmissivities for the upper and middle sand channels, will be used for inversions of all the upper/middle well tests. It will be useful to do cross validation between tests 90/S2/T2 and 90/S2/T3 with the use of the model developed by inverting one test to try to match the response of the other test.

In test 90/S3/T2, well No. 8 was pumped, and pressures were observed in well Nos. 5, 7, 9, and 11. In each observation well, there was no difference between the upper and middle sand channel responses. This is not surprising because the upper clay layer is absent in well No. 8; therefore no distinction could be made between the upper and middle sand channels there. Four inversions of this test successfully

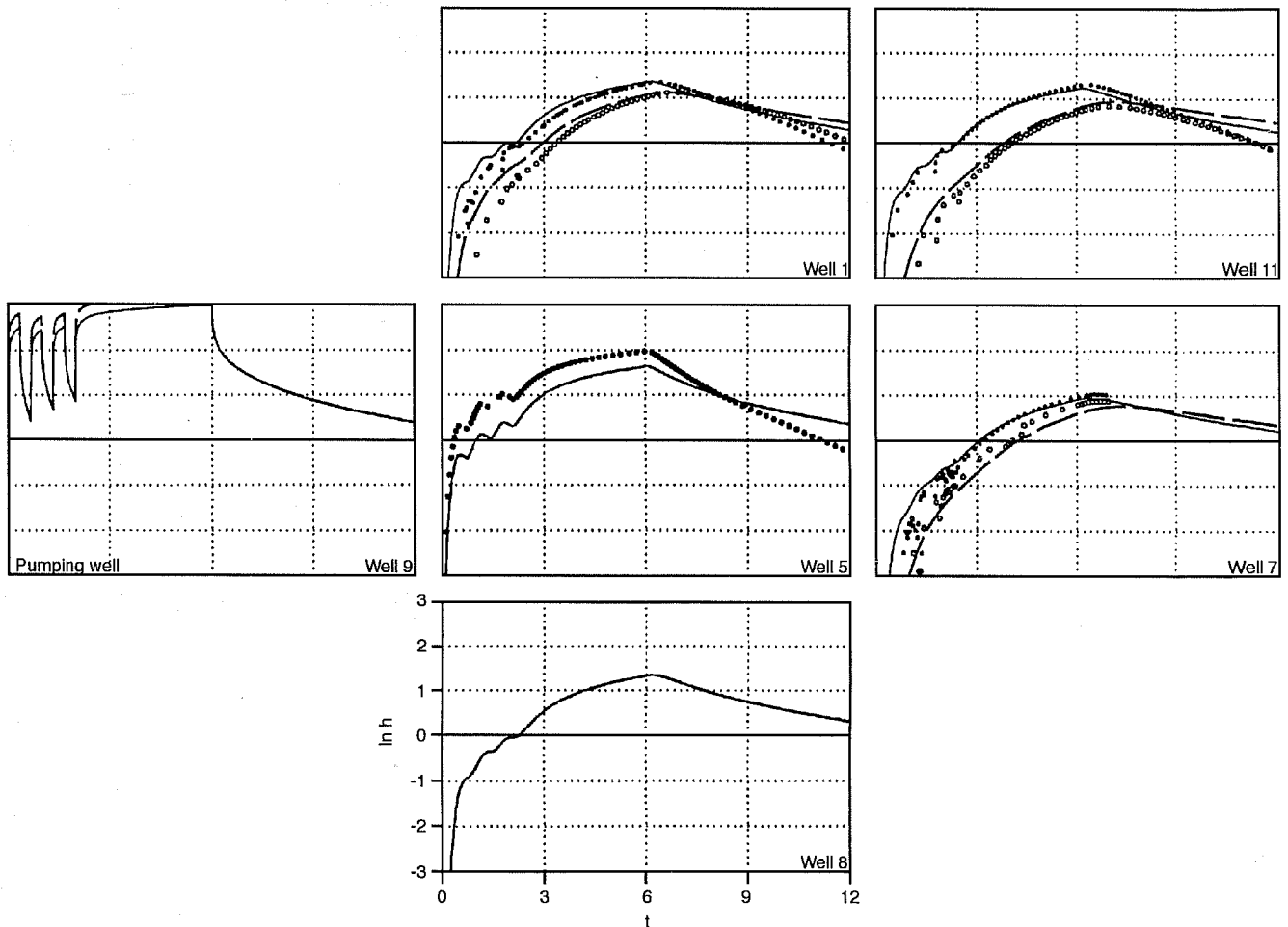


Fig. 6 Observed and modeled pressure transients for an inversion of test 90/S2/T3 (gum21 $E = 15.16$). ●, modeled middle. —, observed middle. ○, modeled upper. ---, observed upper.

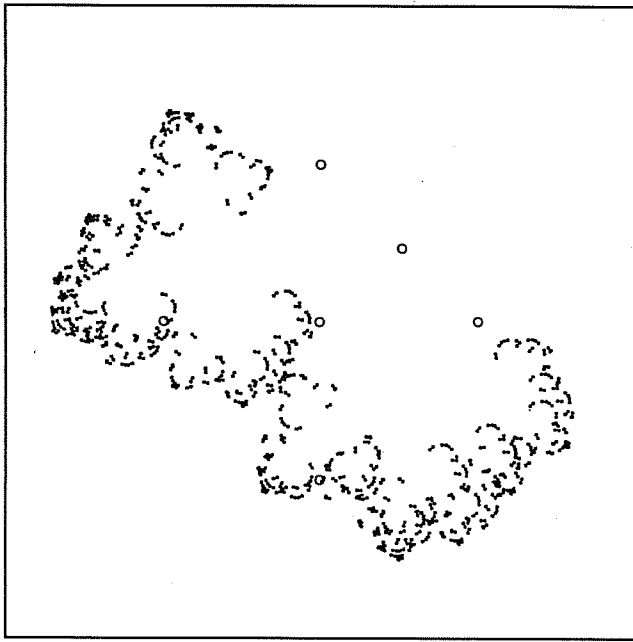


Fig. 7 The final attractor for an inversion of test 90/S2/T3 (gum21 $E = 15.16$). Attractor points identify locations of high permeability (gaps in the clay layer) in the intermediate layer between the upper and middle sand channels.

matched this pressure response; however, they did not yield consistent permeability distributions. If gaps are placed in the clay layer either at the pumping well (as the well log lithology suggests) or at each of the observation wells (in contradiction to the well log lithologies), or both places, the pressure responses can be matched equally well. Including the pressure response at the pumping well as part of the observed data to be inverted would help the inversion to place gaps at the pumping well, but there would still be no reason to avoid placing gaps other places. In conclusion, the pressure responses for test 90/S3/T2 do not provide enough information about the reservoir to be useful in single-test inversions, but they can be an important contribution to a co-inversion of multiple well tests.

In test 90/S4/T2, well No. 1 was pumped, and pressures were observed in well Nos. 5, 7, and 11. This is the same set of wells used in test 90/S1/T2, and not surprisingly the results are similar. All three inversions yielded good matches to the pressure transients and placed a gap in the clay layer between the pumping well and well No. 5 or a gap localized around well No. 5. It will be useful to do cross validation between tests 90/S1/T2 and 90/S4/T2 with the use of the model developed by inverting one test to try to match the response of the other test.

Co-inversions of Upper/Middle Sand Channel Well Tests

The goal of co-inversion is to use multiple tests that provide complementary information about the reservoir. Because the forward calculation becomes slower as more

tests are added, however, it is also desirable to minimize the number of tests to be co-inverted (for example, it would not be worthwhile to co-invert tests 90/S1/T2 and 90/S4/T2 because they both contain information about the northwest quadrant of the well field. Similarly, tests 90/S2/T2 and 90/S2/T3 are not co-inverted when the inversion is looking for gaps in the clay layer, although if the inversion were searching for variability within each sand layer, a co-inversion of tests 90/S2/T2 and 90/S2/T3 would be useful. Two pairs of tests (tests 90/S1/T2 and 90/S3/T2 and tests 90/S2/T3 and 90/S4/T2, and three tests (90/S1/T2, 90/S2/T2, and 90/S3/T2) have been co-inverted. The two tests were more or less co-inverted for practice because it seems that three tests are really the minimum number needed to include all independent information about the reservoir. Figure 8 shows the observed data for the three-test co-inversion. If only one pressure transient shows for a given segment of the test, it means that the upper and middle sand channels responded identically. In inversions that look for clay-layer gaps, the key features to try to match are the differences between middle and upper sand channel responses for each observation well (for example, there is a large difference in upper and middle responses in well Nos. 1 and 7 when well No. 11 pumps but a much smaller difference when well No. 9 pumps).

A three-stage sequence was followed during most of the co-inversions. In the first stage, simulated annealing was used with simple attractors determined by only six unknown parameters to get a rough picture of heterogeneity. In simulated annealing, alternate permeability distributions are tried at random, so a great variety of distributions are tested. Next, the inversion was restarted with the use of the final attractor of the first stage, but nine parameters were considered as unknowns, which allows more variability in the permeability distribution. In the final stage, the inversion was restarted with the use of the final attractor of the second stage; simplex annealing rather than simulated annealing was used as the optimization algorithm. Simplex annealing makes smaller non-random changes in the trial permeability distributions, which are specifically designed to move to lower energy (mismatch) values.

Figure 9 shows an example of the attractors resulting from each stage for the three-test co-inversion. Figure 10 shows the pressure transients at the end of the final stage. With the exception of the response in well No. 11 when well No. 8 is pumped, the difference between upper and middle sand channel responses is matched. None of the three-test co-inversions has produced a completely satisfying match to all the pressure transients. It may be that a more sophisticated conceptual model that allows variability in both the intervening clay layer and the sand channels will be necessary to achieve this. In light of the lower sand channel inversions, which required significant heterogeneity within one sand channel to match all pressure responses, this is not an unreasonable expectation.

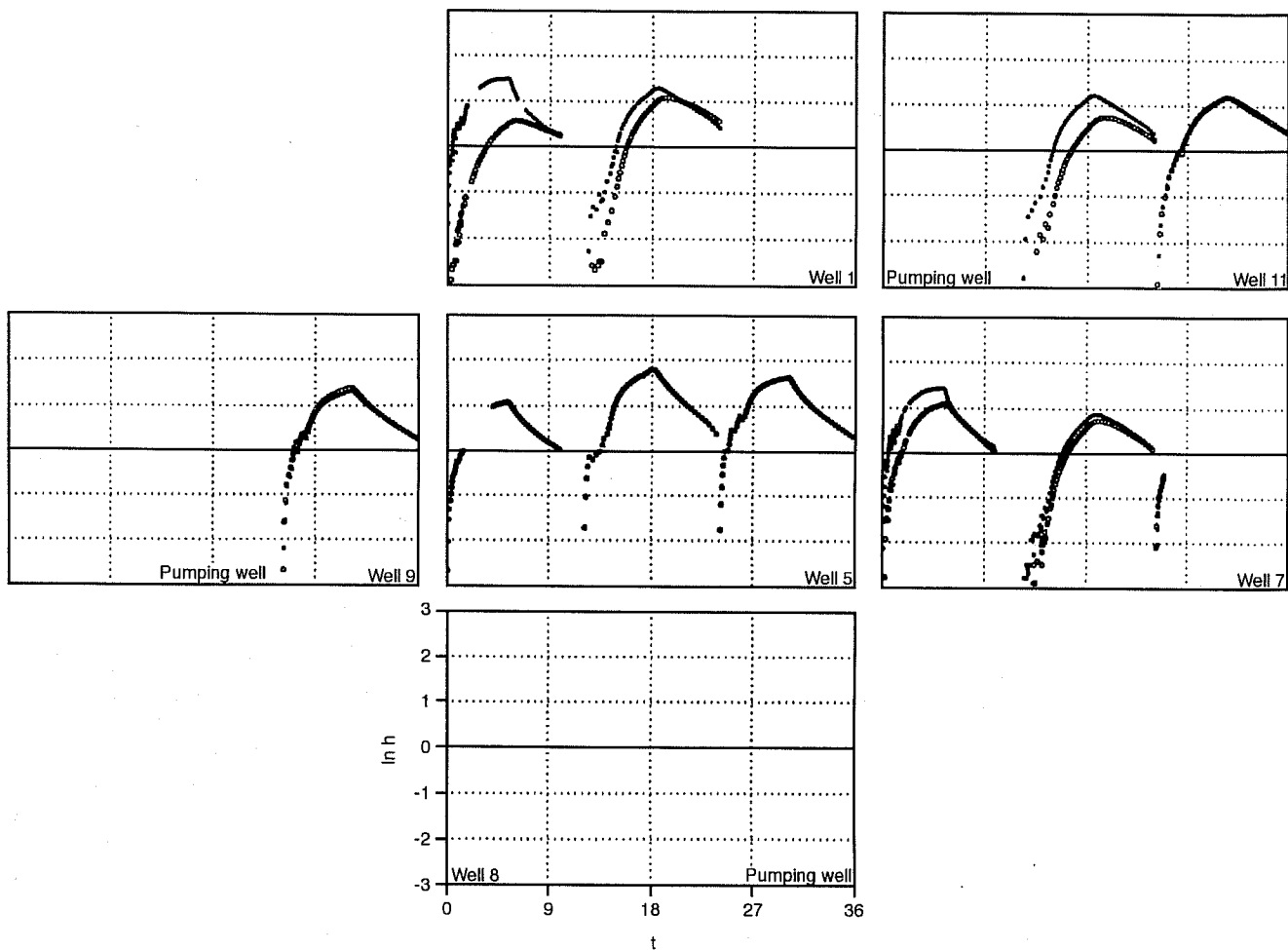


Fig. 8 The observed data for the three-test co-inversion of tests 90/S1/T2, 90/S2/T2, and 90/S3/T2. ●, observed middle. ○, observed middle.

Comparison of Well Test Analysis and Well Log Lithology

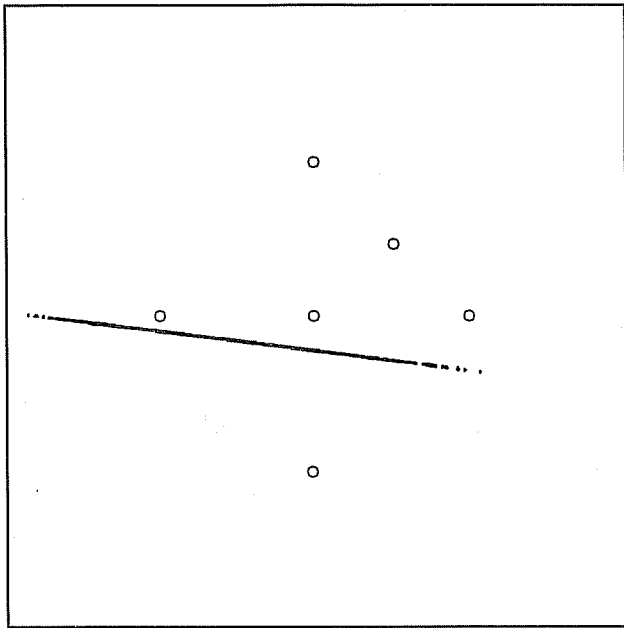
In view of the difficulty in achieving good matches to the observed pressure responses described previously, an alternate approach that makes use of both well log lithologic data and interference data is being explored. The well log data indicate the presence or absence of the upper clay layer at six points, the well locations, only. This point information can be interpolated in a variety of ways to create a complete picture of the clay layer and its gaps, as suggested in Fig. 11. Each of these interpolations has been used to simulate the sequence of three tests: 90/S1/T2, 90/S2/T2, and 90/S3/T2. The strong variation in energy, the integrated mismatch between the observed and calculated pressure transients, indicates that a large clay gap is much more probable than a small one. The configuration with the lowest energy also provides guidelines for a good starting shape for further inversions or co-inversions. The first few accepted attractors and the corresponding energies for one such co-inversion of tests 90/S1/T2, 90/S2/T2, and 90/S3/T2 are shown in Fig. 12.

Seismic-Related Work

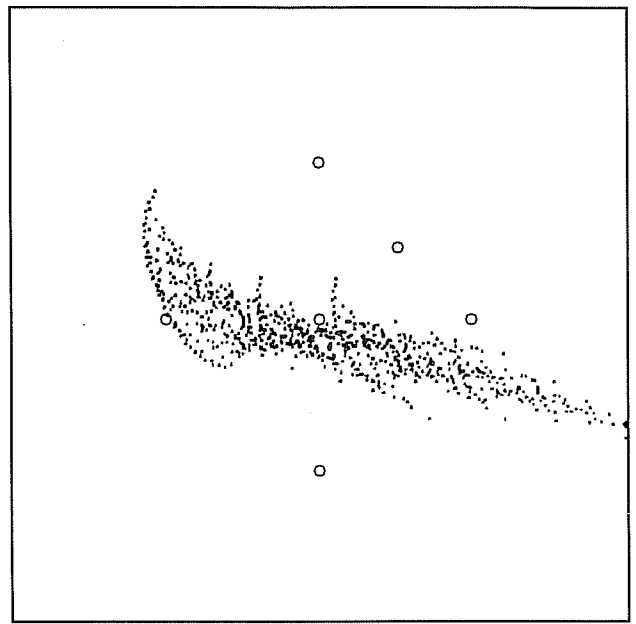
The travel/time tomography for the pilot-site cross-well seismic data is complete. A draft of the report describing the work has been submitted for publication.¹

Integration of Hydrologic and Seismic Work

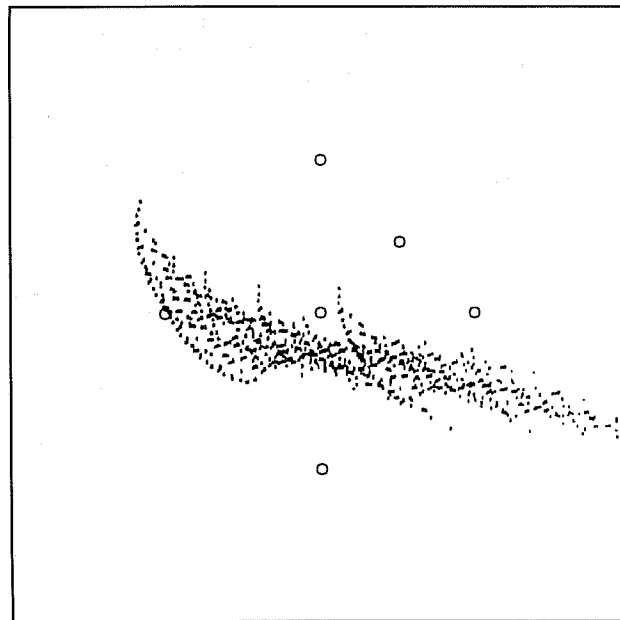
The travel-time tomography described previously for well Nos. 5 and 7 confirms the conclusions drawn from the first-arrival time analysis done by hand for well Nos. 5 and 1 (namely, that although the first arrivals indicate a pronounced low-velocity zone at the depth of the Gypsy sand channels, they cannot provide any information about the thin clay layers within the Gypsy formation). On the other hand, the inference from the reflection analysis that the upper clay layer may not extend very far from well No. 1 toward well No. 5 (because no reflections off it were observed in the common source/multiple receiver gathers) seems to be corroborated by the upper/middle sand channel well test analyses described previously, which suggest that the gap in the clay layer observed at well No. 5 is not just a small localized feature.



(a)



(b)



(c)

Fig. 9 Attractor at the end of each stage of a co-inversion of tests (a) 90/S1/T2 (s123 gum36 E = 26.24), (b) 90/S2/T2 (s123 gum36a E = 23.02), and (c) 90/S3/T2 (s123 gum36b E = 22.86). Attractor points identify locations of high permeability (gaps in the clay layer) in the intermediate layer between the upper and middle sand channels.

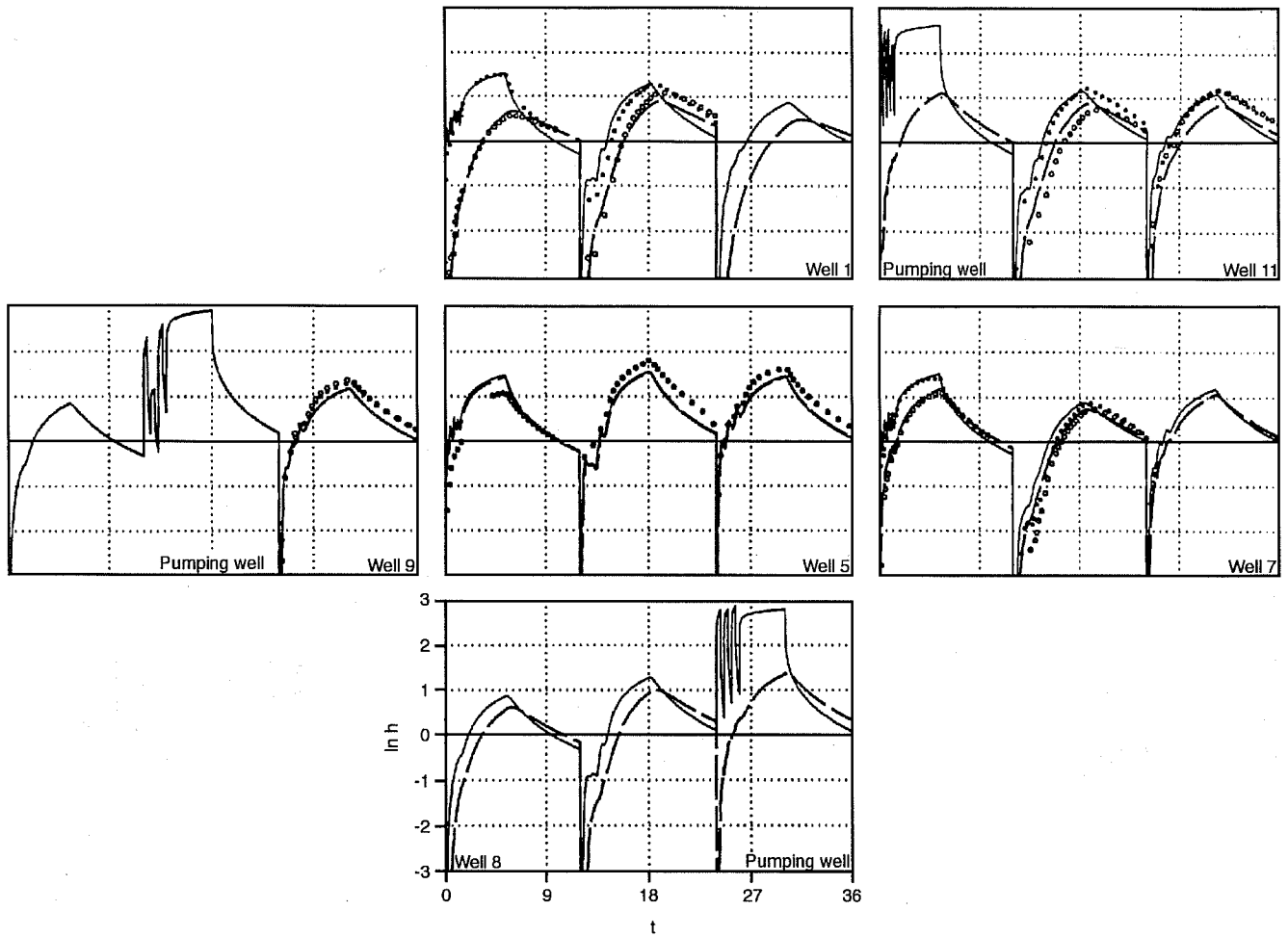


Fig. 10 Observed and modeled pressure transients for a co-inversion of tests 90/S1/T2, 90/S2/T2, and 90/S3/T2 ($s_{123} \text{ gum36b } E = 22.86$). Only one-third of the observed data points used in the match are shown to enable the calculated curves to be more visible. ●, modeled middle. —, observed middle. ○, modeled upper. ---, observed upper.

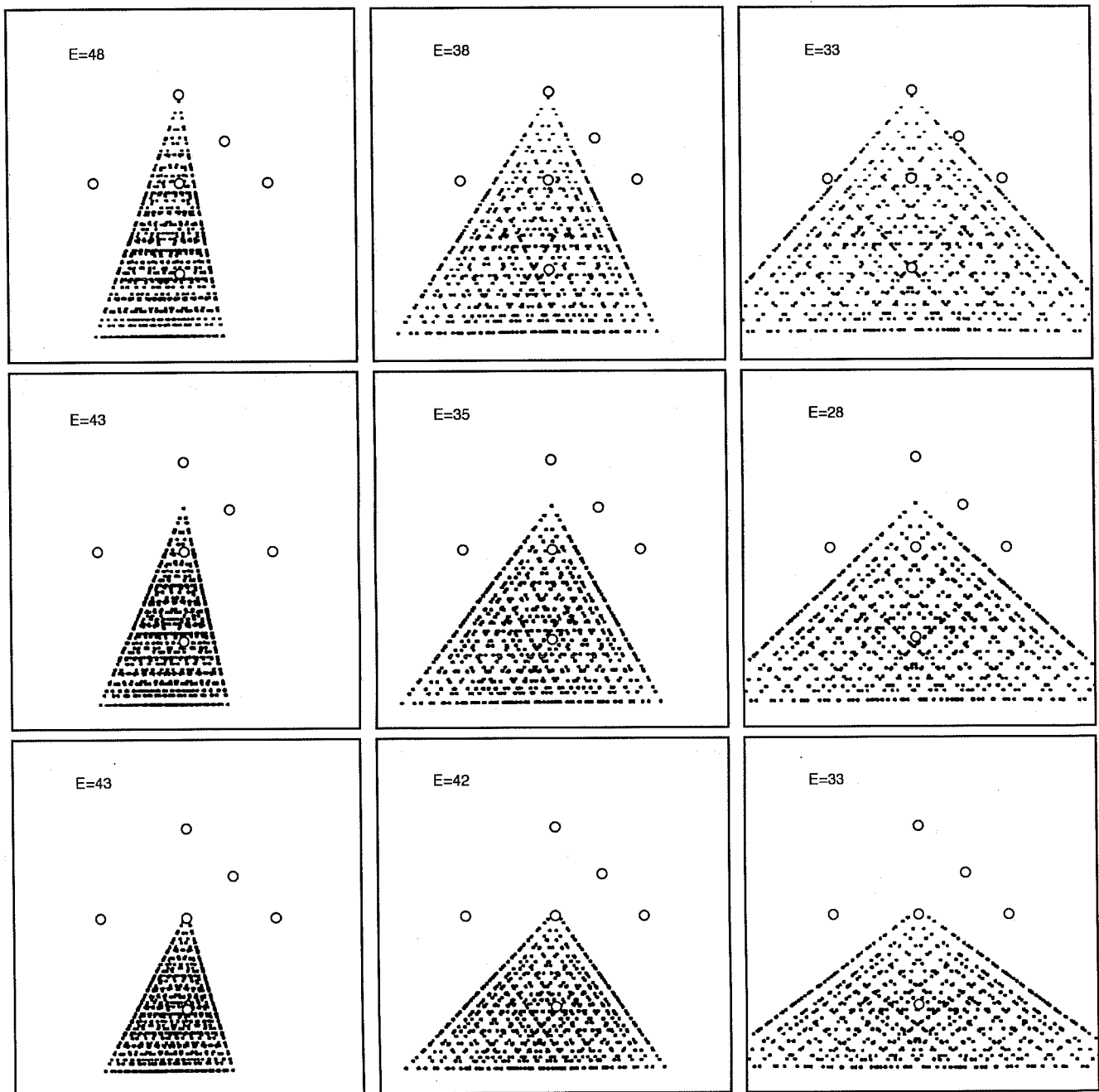


Fig. 11 Nine possible interpolations of the point lithologic data obtained from well logs. The dark regions represent gaps in the intermediate clay layer between the upper and middle sand channels. The energy values show the mismatch between each of these models and the observed data for tests 90/S1/T2, 90/S2/T2, and 90/S3/T2, shown in Fig. 8.

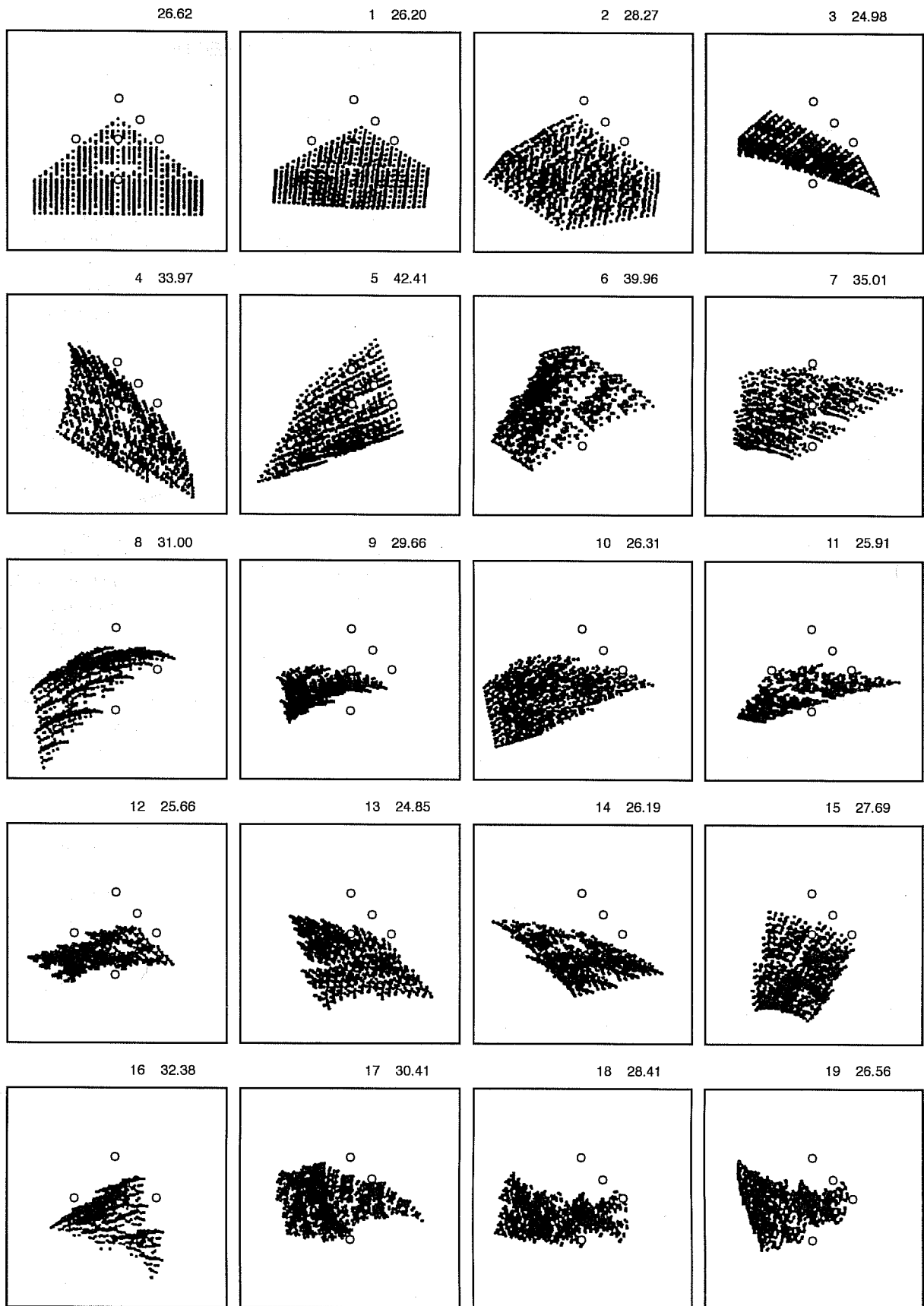


Fig. 12 The initial attractor, the first 19 accepted attractors, and the corresponding energies for a co-inversion of tests 90/S1/T2, 90/S2/T2, and 90/S3/T2.

Reference

1. D. W. Vasco, J. E. Peterson, Jr., and E. L. Majer, Beyond Ray Tomography: Ensemble Inference and Cluster Analysis, *Geophysics*, in press, 1996.

RESEARCH PROGRAM ON FRACTURED PETROLEUM RESERVOIRS

Contract No. DE-FG22-93BC14875

**Reservoir Engineering Research Institute
Palo Alto, Calif.**

**Principal Investigator:
Abbas Firoozabadi**

**Project Manager:
Robert Lemmon
Bartlesville Project Office**

Reporting Period: July 1–Sept. 30, 1994

Objective

The objective of this project is to quantify the physics of multiphase flow in fractured porous media. Because the roles of capillary, diffusive, gravity, and viscous forces will be addressed, the topics of natural depletion, gas injection (both miscible and immiscible), and water injection in light and heavy oil reservoirs will be studied in a unified approach.

Summary of Technical Progress

Crossflow across the interface of layered reservoirs and between matrix blocks and fractures in fractured reservoirs may be pronounced. The literature emphasizes viscous crossflow, whereas gravity crossflow even for dip angles of 5 to 15° may be more significant.

The results of work on crossflow in layered porous media are presented. The examples selected show that most of the oil is first transferred to the high-permeability layer and then produced. The crossflow and no-crossflow cases do not show significant recovery difference however. The small difference may be attributed to the examples selected. Other example problems will be tested.

Crossflow of fluids between fracture network and rock matrix in fractured reservoirs and between different layers in layered reservoirs could be very pronounced in certain gas injection schemes. The crossflow could be caused by gravity, capillary, viscous, and fluid compressibility effects. At high pressures, phase-behavior effects reduce surface tension significantly, and therefore the effect of capillary pressure on crossflow can be neglected.

It has been demonstrated that the crossflow of the injected fluid from the fracture to the matrix and the crossflow of the matrix oil to the fracture strongly affects the recovery efficiency.¹ Crossflow caused by gravity² is the dominant mechanism for first-contact miscible fluid injection in fractured porous media. The investigation of crossflow processes at conditions other than first-contact miscibility is one purpose of this project.

In layered reservoirs, which are similar to fractured reservoirs, crossflow across layers is expected to be important. Because of strong crossflow, the recovery from tight layers may be improved. Because the crossflow in both fractured and layered porous media is often a localized phenomenon, reservoir simulators cannot capture its basic features.

Zapata and Lake³ studied viscous crossflow in layered media for immiscible fluid systems. Pande and Orr⁴ also studied viscous crossflow in a two-layer system incorporating transfer of components between gas and liquid phases but neglecting gravity and volume changes caused by mixing. In a recent study, Tan and Firoozabadi² included the effect of gravity in the study of crossflow between a matrix medium and a fracture medium. In all these studies, the effect of volume change on mixing was neglected. When an injected gas dissolves in the oil phase, the volume of the total system reduces significantly.

The subject of viscous crossflow has received considerable attention.³⁻⁴ Crossflow caused by viscous forces, however, may be small. Gravity contribution to crossflow, however, may be very pronounced for fractured reservoirs and for layered reservoirs with tilt angles in the range of 5 to 15°. Phase-behavior effects, which include component transfer and volume change caused by mixing, and the incorporation of these effects in the crossflow term may also be important. The purpose of this project is to conduct a comprehensive study of crossflow in fractured and layered reservoirs incorporating gravity, compressibility, phase behavior, and viscous effects. So that the effect of the crossflow term can be understood, formulation of the problem will be done in two steps. First, the formulation for a homogeneous medium is presented, and then the formulation for flow in systems with two distinct media—fracture and matrix or layers (with and without crossflow)—is presented.

Homogeneous Medium

A homogeneous medium can be represented with one set of properties (permeability, porosity, relative permeability, etc.). The governing component mass-balance equations for

one-dimensional (1-D) multiphase multicomponent systems are given by

$$A\phi \frac{\partial}{\partial t} \sum_{j=1}^{n_p} x_{ij} \rho_j S_j + \frac{\partial}{\partial x} q_T \sum_{j=1}^{n_p} x_{ij} \rho_j f_j = 0 \quad (i = 1, \dots, n_c) \quad (1)$$

Symbols are defined in the nomenclature list on page 77. Equation 1 is based on the following assumptions: instantaneous local chemical equilibrium, isothermal flow, homogeneous medium along the displacement length, and negligible dispersion.

The component material balances can be written in a more compact form by using the following notation:

$$G_i = G_i(\bar{Z}) = \sum_{j=1}^{n_p} x_{ij} \rho_j S_j \quad (i = 1, \dots, n_c) \quad (2)$$

and

$$F_i = F_i(\bar{Z}, q_T) = \sum_{j=1}^{n_p} x_{ij} \rho_j S_j \quad (i = 1, \dots, n_c) \quad (3)$$

Thus Eq. 1 becomes

$$A\phi \frac{\partial G_i}{\partial t} + \frac{\partial q_T F_i}{\partial x} = 0 \quad (i = 1, \dots, n_c) \quad (4)$$

G_i and F_i represent number of moles of component i per unit pore volume (PV) and molar fractional flow of component i , respectively; $q_T F_i$ represents the molar flux of component i . In Eq. 4, the flow rate, q_T , is not constant because of volume change on mixing, even though the total injection at the inlet is constant.

The equation system (Eq. 4) is a Riemann problem where the initial data are described by two constant composition states connected by a discontinuity at the origin.⁵⁻⁶

$$\bar{Z}(x, 0) = \begin{cases} \bar{Z}_{inj} & x \leq 0 \\ \bar{Z}_{ini} & x \geq 0 \end{cases} \quad (5)$$

The two constant compositions are injection composition, (\bar{Z}_{inj}) and initial composition (\bar{Z}_{ini}), respectively.

The solution of Eq. 4 subject to the initial data in Eq. 5 is self-similar. In other words, solution is a function of a similarity variable (x/t). The solution of Eq. 4 consists of continuous variations, shocks, and constant states. The shock speed (Λ) is given by

$$\Lambda = \frac{(q_T F_i)^{II} - (q_T F_i)^I}{A\phi (G_i^{II} - G_i^I)} \quad (i = 1, \dots, n_c) \quad (6)$$

where superscripts I and II refer to opposite sides of the shock, downstream and upstream, respectively. Equation 6 can be obtained by a material balance across the shock.⁷⁻⁸

Two-Media Flow

Consider a two-media flow—one medium-low permeability and the other medium-high permeability. Each medium could represent a layer in layered media or a fracture or matrix in fractured media. Two cases are considered, one case in which the two layers communicate (crossflow case) and the other case in which there is no crossflow between the two media (no crossflow case).

Crossflow Case

For this case, the problem becomes significantly simplified if the powerful crossflow equilibrium (CE) assumption is invoked between the two layers.^{3,9} Crossflow equilibrium means that the pressures in both layers are equal along the displacement length. This is an appropriate assumption for geometries with $R_L = L/H (k_v/k_h)^{1/2} > 10$, where k_v is thickness-weighted harmonic vertical permeability and k_h is thickness-weighted average horizontal permeability.³ L and H are the total system length and the total system thickness, respectively. The crossflow equilibrium assumption is appropriate for this study.

The material-balance equations for a two-layer system with CE assumption is similar to those for homogeneous systems with the inclusion of a crossflow (source/sink) term, depending on the direction of crossflow. The crossflow term represents the transverse communication of the two layers.

Crossflow term. The mass flow equations for the two layers are given by

$$A^1 \phi^1 \frac{\partial G_i^1}{\partial t} + \frac{\partial (q_T^1 F_i^1)}{\partial x} - CR_{iM} = 0 \quad (i = 1, \dots, n_c) \quad (7)$$

$$A^2 \phi^2 \frac{\partial G_i^2}{\partial t} + \frac{\partial (q_T^2 F_i^2)}{\partial x} + CR_{iM} = 0 \quad (i = 1, \dots, n_c) \quad (8)$$

$$\text{where } G_i^k = \sum_{j=1}^{n_p} x_{ij}^k \rho_j^k S_j^k$$

$$F_i^k = \sum_{j=1}^{n_p} x_{ij}^k \rho_j^k f_j^k$$

$$CR_{iM} = \text{molar crossflow flux of component } i \text{ from layer 1 to layer 2 (per length)}$$

$$k = 1, 2 = \text{layer superscript}$$

$$k = 1 = \text{more-permeable layer in this study}$$

For crossflow from layer 2 to 1, the sign of the last term in Eqs. 7 and 8 changes. The relationship between molar crossflow

flux of component i and volumetric crossflow flux, CR_{TV} , is given by

$$CR_{iM} = F_i^1 CR_{TV} \quad (i=1, \dots, n_c) \quad (9)$$

when crossflow is from layer 1 to layer 2. The combination of Eqs. 7 and 9 and the summation over all components yields

$$CR_{TV} = \frac{1}{\sum_{i=1}^{n_c} F_i^1} \sum_{i=1}^{n_c} \left[A^1 \phi^1 \frac{\partial G_i^1}{\partial t} + \frac{\partial(q_T^1 F_i^1)}{\partial x} \right] \quad (10)$$

Note that the crossflow term given by Eq. 10 depends not only on $\partial q_T^1 / \partial x$ but also varies with $\partial G_i^1 / \partial t$ and $\partial F_i^1 / \partial x$. These last two terms are due to the volume change on mixing and can be viewed as compressibility effects.

Rewriting the mass flow (Eqs. 7 and 8) with the expression of crossflow gives

$$A^1 \phi^1 \frac{\partial G_i^1}{\partial t} + \frac{\partial(q_T^1 F_i^1)}{\partial x} - \frac{F_i^1}{\sum_{i=1}^{n_c} F_i^1} \sum_{i=1}^{n_c} \left[A^1 \phi^1 \frac{\partial G_i^1}{\partial t} + \frac{\partial(q_T^1 F_i^1)}{\partial x} \right] = 0 \quad (i=1, \dots, n_c-1) \quad (11)$$

$$A^2 \phi^2 \frac{\partial G_i^2}{\partial t} + \frac{\partial(q_T^2 F_i^2)}{\partial x} + \frac{F_i^1}{\sum_{i=1}^{n_c} F_i^1} \sum_{i=1}^{n_c} \left[A^1 \phi^1 \frac{\partial G_i^1}{\partial t} + \frac{\partial(q_T^1 F_i^1)}{\partial x} \right] = 0 \quad (i=1, \dots, n_c-1) \quad (12)$$

In Eq. 11 because the summation over all components in Eq. 7 was used to obtain the crossflow term, there will be only $n_c - 1$ independent equations.

The following dimensionless variables and parameters are defined:

$$x_D = \frac{x}{L} \quad (13)$$

$$t_D = \frac{q_{T,inj} t}{\phi A_T L} \quad (14)$$

$$q_{TD}^k = \frac{q_T^k}{q_{T,inj}} \quad (15)$$

$$\rho_{jD} = \frac{\rho_j}{\rho_{ini}} \quad (16)$$

$$R^k = \frac{\phi^k A^k}{\phi A_T} \quad (17)$$

$$\bar{\phi} = \frac{\sum_{k=1}^2 \phi^k A^k}{A_T} \quad (18)$$

$$A_T = \sum_{k=1}^2 A^k \quad (19)$$

The dimensionless form of the material-balance equations (Eqs. 11 and 12) becomes

$$R^1 \frac{\partial G_i^1}{\partial t_D} + \frac{\partial(q_{TD}^1 F_i^1)}{\partial x_D} - \frac{F_i^1}{\sum_{i=1}^{n_c} F_i^1} \sum_{i=1}^{n_c} \left[R^1 \frac{\partial G_i^1}{\partial t_D} + \frac{\partial(q_{TD}^1 F_i^1)}{\partial x_D} \right] = 0 \quad (i=1, \dots, n_c-1) \quad (20)$$

$$R^2 \frac{\partial G_i^2}{\partial t_D} + \frac{\partial(q_{TD}^2 F_i^2)}{\partial x_D} + \frac{F_i^1}{\sum_{i=1}^{n_c} F_i^1} \sum_{i=1}^{n_c} \left[R^1 \frac{\partial G_i^1}{\partial t_D} + \frac{\partial(q_{TD}^1 F_i^1)}{\partial x_D} \right] = 0 \quad (i=1, \dots, n_c) \quad (21)$$

Material-balance equations are written more simply in terms of G_i and F_i , and their functional dependence on the overall mole fractions and the total layer rates is as follows:

$$G_i^k = G_i^k(\bar{Z}^k) = \sum_{j=1}^{n_p} x_{ij}^k \rho_{jD}^k S_j^k \quad (i=1, \dots, n_c; k=1,2) \quad (22)$$

$$F_i^k = F_i^k(\bar{Z}^1, \bar{Z}^2, q_{TD}^k) = \sum_{j=1}^{n_p} x_{ij}^k \rho_{jD}^k S_j^k \quad (i=1, \dots, n_c; k=1,2) \quad (23)$$

The total mass balance for component i is the sum of Eqs. 20 and 21

$$\frac{\partial[(R^1 G_i^1 + R^2 G_i^2)]}{\partial t_D} + \frac{\partial[(q_{TD}^1 F_i^1 + q_{TD}^2 F_i^2)]}{\partial x_D} = 0 \quad (i=1, \dots, n_c-1) \quad (24)$$

or

$$\frac{\partial G_i^T}{\partial t_D} + \frac{\partial F_i^T}{\partial x_D} = 0 \quad (i=1, \dots, n_c-1) \quad (25)$$

where $G_i^T = R^1 G_i^1 + R^2 G_i^2$ and $F_i^T = q_{TD}^1 F_i^1 + q_{TD}^2 F_i^2$.

The total mass of all the components can be obtained by summing Eq. 25 over $i = 1$ to n_c ,

$$\frac{\partial \left[\sum_{i=1}^{n_c} G_i^T \right]}{\partial t_D} + \frac{\partial \left[\sum_{i=1}^{n_c} F_i^T \right]}{\partial x_D} = 0 \quad (26)$$

or

$$\frac{\partial G^T}{\partial t_D} + \frac{\partial F^T}{\partial x_D} = 0 \quad (27)$$

where $F^T = \sum_{i=1}^{n_c} F_i^T$ and $G^T = \sum_{i=1}^{n_c} G_i^T$.

Equations 20, 25, and 27 are then solved instead of Eqs. 20 and 21, which do not contain the crossflow term.

Initial and boundary conditions. The initial data for the problem are prescribed by two different constant states connected by a discontinuity at the origin, as in the case of

homogeneous systems, and are given by Eq. 5. Crossflow equilibrium assumption requires that

$$\frac{dP^1}{dx_D} = \frac{dP^2}{dx_D} \quad (28)$$

From Darcy's law, the total flow rate of layer k at point x_D is given by

$$q_{TD}^k = -\frac{k^k A^k}{L} \lambda_T^k \frac{dP^k}{dx_D} - A^k k^k g \sin \theta \sum_{j=1}^{n_p} \lambda_j^k M_j^k \rho_j^k \quad (k=1,2) \quad (29)$$

The pressure-gradient term in Eq. 29 can be eliminated by using Eq. 28. Thus the relationship between the dimensionless flow rates in the layers can be obtained

$$q_{TD}^k = C_R \frac{\lambda_T^k}{\lambda_T^\ell} \left(q_{TD}^\ell + \frac{A^\ell k^\ell g \sin \theta}{q_{T,inj}} \sum_{j=1}^{n_p} \lambda_j^\ell M_j^\ell \rho_j^\ell \right) - \frac{A^k k^k g \sin \theta}{q_{T,inj}} \sum_{j=1}^{n_p} \lambda_j^k M_j^k \rho_j^k, \quad k, \ell = 1, 2, \quad k \neq \ell \quad (30)$$

where the capacitance ratio (C_R) is defined as

$$C_R = \frac{A^k k^k}{A^\ell k^\ell} \quad (31)$$

Equation 30 can be used to calculate q_{TD}^k once q_{TD}^ℓ ($\ell \neq k$), \bar{Z}^k , and \bar{Z}^ℓ are known.

No-Crossflow Case

The equations for the no-crossflow (NC) case are identical to the equations for homogeneous systems (Eq. 4) or the equations for the CE case without the crossflow terms (Eqs. 20 and 21). The only difference between homogeneous systems and the NC case is the boundary conditions. In NC, the rates of the layers are dependent through the pressure-drop boundary condition across the displacement length, $0 \leq x_D \leq 1$

$$\Delta P^1 = \Delta P^2 \quad (32)$$

Pressure gradients are given by the Darcy law

$$\frac{dP^k}{dx_D} = -\frac{q_{TD}^k q_{T,inj}}{A^k k^k \lambda_T^k} - \frac{g \sin \theta}{\lambda_T^k} \sum_{j=1}^{n_p} \lambda_j^k M_j^k \rho_j^k \quad (k=1,2) \quad (33)$$

The pressure differences, ΔP^1 and ΔP^2 , can be obtained by integrating Darcy's equation

$$\int_{x_{D=0}}^1 dP^k = -\frac{q_{TD,inj}^k}{A^k k^k} \int_{x_{D=0}}^1 \frac{q_{TD}^k q_{Tinj}^k}{q_{TD,inj}^k \lambda_T^k} dx_D - g \sin \theta \int_{x_{D=0}}^1 \frac{\sum_{j=1}^{n_p} \lambda_j^k M_j^k \rho_j^k}{\lambda_T^k} dx_D \quad (k=1,2) \quad (34)$$

Combining Eqs. 32 and 34 with the constant total injection rate condition at the inlet, $q_{TD,inj}^1 + q_{TD,inj}^2 = 1$, yields Eq. 35

$$q_{TD,inj}^1 = \frac{\frac{A^1 k^1 g \sin \theta}{q_{T,inj}} \left(\int_{x_{D=0}}^1 \frac{\sum_{j=1}^{n_p} \lambda_j^2 M_j^2 \rho_j^2}{\lambda_T^2} dx_D - \int_{x_{D=0}}^1 \frac{\sum_{j=1}^{n_p} \lambda_j^1 M_j^1 \rho_j^1}{\lambda_T^1} dx_D \right) + \frac{A^1 k^1}{A^2 k^2} \int_{x_{D=0}}^1 \frac{q_{TD}^2}{q_{TD,inj}^2 \lambda_T^2} dx_D}{\int_{x_{D=0}}^1 \frac{q_{TD}^1}{q_{TD,inj}^1 \lambda_T^1} dx_D + \frac{A^1 k^1}{A^2 k^2} \int_{x_{D=0}}^1 \frac{q_{TD}^2}{q_{TD,inj}^2 \lambda_T^2} dx_D} \quad (35)$$

Equation 35 indicates that the individual layer injection rates can vary as the displacement process continues. The dependence of rate on other parameters (e.g., layer compositions) is implicit. Equation 35, however, can be solved explicitly for $q_{TD,inj}^1$ over a time step. In the explicit scheme, the parameters at the right-hand side of Eq. 35 are calculated from the old time step. Composition profiles of each layer will still be similar to the profiles of homogeneous systems. Qualitatively, NC solutions are identical to the solutions for homogeneous systems. Each layer is treated separately at a given time step, and the solution is obtained with the use of the same procedure as homogeneous systems. The solution procedure for homogeneous systems can be found elsewhere.⁸

Solution Technique

For the solution of 1-D material-balance equations with Riemann initial data, the method of characteristics is used.¹⁰ The system given by Eqs. 20, 25, and 27 was selected, with the initial data given in Eq. 5 and the crossflow equilibrium condition given by Eq. 30. The system is self-similar and is a function of x_D/t_D . If the chain rule is used for differentiation and $\lambda_D = x_D/t_D$ is defined as the characteristic wave speed, Eqs. 20, 25, and 27 can be written as

$$([F] - \lambda_D [G]) \bar{X} = \bar{0} \quad (36)$$

Similarity transform ($\tau = x_D/t_D$) does not affect the initial data because the initial data consist of two constant states

(Eq. 5). Equation 36 is an eigenvalue problem where λ_D is the eigenvalue and \bar{X} is the eigenvector of the system; $[G]$ contains the derivatives of the accumulation term, and $[F]$ contains the derivatives of the overall molar flux term. Explicit definitions and the calculation procedure of the entries in Eq. 36 are given in the section on binary systems. Eigenvectors are the directions in the composition space in which the eigenvalues are the characteristic wave speeds of compositions. Composition variations along the eigenvectors satisfy the material-balance equations.

For a given point in the rate-composition space, continuous variations can be obtained by integrating along the eigenvectors of Eq. 36. The integration along an eigenvector requires a starting rate-composition vector, \bar{U}^0 . The solution procedure is as follows: Calculate all the eigenvalues

(λ_{Dn}) and the associated eigenvectors (\bar{X}_n) and take a sufficiently small step (s) along a selected eigenvector to update the starting rate-composition, $\bar{U}^1 = \bar{U}^0 + s \bar{X}_k$. The full composition path (if permitted) can be obtained by using the same relationship recursively as $\bar{U}^m = \bar{U}^{m-1} + s \bar{X}_k$.

Discontinuities

The composition path cannot always be described by Eq. 36. The solution of the system (Eqs. 20, 25, and 27) consists of a combination of continuous variations, shocks, and constant states. The shocks or discontinuities arising in such systems must be treated differently. Discontinuities or shock waves are required in solution construction when continuous variations are not possible (i.e., faster upstream compositions than downstream compositions—multivaluedness). In strict terms, Eqs. 20, 25, and 27 carry information about continuous variations. If the system in Eqs. 20, 25, and 27 yields multivalued solutions, then Eqs. 20, 25, and 27 fail to describe the physical process because at a given x_D and t_D , there is only one value per dependent variable. Furthermore, spatial derivatives may diverge to infinity in the material-balance equations. Shocks or discontinuities are introduced to alleviate this problem.

When the material transport equations fail to describe a physically correct single-valued flow process, shocks are introduced in the solution. The shocks are resolved with the use of material-balance equations across them. The shock balance equation with the crossflow term for crossflow from layer 1 to layer 2 is derived in Appendix A (Appendix A not included in

this report). Equation A-4 corresponds to Eq. 20, which has a similar crossflow term. On the basis of Eq. A-4 of Appendix A, the dimensionless form of the shock balance for Eq. 20 is

$$\Lambda_{D_i}^k = \frac{(q_{TD}^k F_i^k)^{II} - (q_{TD}^k F_i^k)^I - \alpha_i^k \left[\sum_{i=1}^{n_c} (q_{TD}^k F_i^k)^{II} - \sum_{i=1}^{n_c} (q_{TD}^k F_i^k)^I \right]}{R^k \left\{ (G_i^k)^{II} - (G_i^k)^I - \alpha_i^k \left[\sum_{i=1}^{n_c} (G_i^k)^{II} - \sum_{i=1}^{n_c} (G_i^k)^I \right] \right\}} \quad (i=1, \dots, n_c-1) \quad (37)$$

The shock balances without the crossflow term are derived elsewhere.^{8, 11-12} Therefore the shock balances for the rest of the equations are

$$\Lambda_D^T = \frac{(F^T)^{II}}{(G^T)^{II}} - \frac{(F^T)^I}{(G^T)^I} \quad (38)$$

and

$$\Lambda_{D_i}^T = \frac{(F_i^T)^{II}}{(G_i^T)^{II}} - \frac{(F_i^T)^I}{(G_i^T)^I} \quad (i=1, \dots, n_c-1) \quad (39)$$

Different symbols for the shock speeds are used to distinguish the right-hand sides of the shock balances. The shock speeds ($\Lambda_{D_i}^k, \Lambda_D^T$, and $\Lambda_{D_i}^T$) are all equal to each other. The shock balances in Eqs. 38 and 39 are similar to those for homogeneous systems (Eq. 6). In general, Eqs. 37, 38, and 39 are coupled. The solution of Eqs. 37, 38, and 39 could only yield a maximum of $2n_c - 1$ unknowns. Depending on the information at the upstream and downstream of the shock, Eqs. 37, 38, and 39 could be coupled with other equations. Different types of shocks entail different types of treatment.

A gravity term appears in both the fractional flow function of the phases f_j and the crossflow terms of the transport equations. Such dependence on gravity complicates the numerical computations (e.g., fractional flow function becomes an implicit function of the compositions of both layers because of rate dependence). The formulation presented along with the method of characteristics solution procedure and shock balances is for systems with any number of components. As the number of components increases, however, the degrees of freedom in the composition space increase. Thus the solution construction becomes very complex.

This study is restricted to binary solutions. Even in binary systems, the solution usually includes more than two shocks and can be very complicated. In general, the shocks with intermediate speeds (intermediate shocks) are difficult to resolve and require iterative schemes. As the qualitative features of the solution change, the solution construction algorithm needs to be modified. The solution of systems with volume change on mixing needs an extra level of trial-and-error procedure because the total flow velocity in front of the fastest shock is also an unknown.

Binary Flow

The simplest case of displacement is the binary flow, where the injected gas and the in situ oil consist of two

components when they are mixed. Equations 20, 25, and 27 can be reduced for binary systems. For binary systems, equations of crossflow only from layer 1 to layer 2 will be presented because the formulation for the reverse crossflow direction can be deduced by using the same approach as that shown in Eqs. 7 to 12.

Material-balance equations for crossflow from layer 1 to layer 2 are

$$R^1 \frac{\partial G_1^1}{\partial t_D} + \frac{\partial q_{TD}^1 F_1^1}{\partial x_D} - \frac{F_1^1}{\sum_{i=1}^2 F_i^1} \sum_{i=1}^2 \left(R^1 \frac{\partial G_i^1}{\partial t_D} + \frac{\partial q_{TD}^1 F_i^1}{\partial x_D} \right) = 0 \quad (40)$$

$$\frac{\partial G^T}{\partial t_D} + \frac{\partial F^T}{\partial x_D} = 0 \quad (41)$$

$$\frac{\partial G_1^T}{\partial t_D} + \frac{\partial F_1^T}{\partial x_D} = 0 \quad (42)$$

The associated eigenvalue problem is

$$\begin{bmatrix} a & b & c \\ \frac{\partial F^T}{\partial Z_1^1} & \frac{\partial F^T}{\partial Z_1^2} & \frac{\partial F^T}{\partial q_{TD}^2} \\ \frac{\partial F_1^T}{\partial Z_1^1} & \frac{\partial F_1^T}{\partial Z_1^2} & \frac{\partial F_1^T}{\partial q_{TD}^2} \end{bmatrix} - \lambda_D \begin{bmatrix} d & 0 & 0 \\ \frac{\partial G^T}{\partial Z_1^1} & \frac{\partial G^T}{\partial Z_1^2} & 0 \\ \frac{\partial G_1^T}{\partial Z_1^1} & \frac{\partial G_1^T}{\partial Z_1^2} & 0 \end{bmatrix} \begin{bmatrix} \frac{dZ_1^1}{d\eta} \\ \frac{dZ_1^2}{d\eta} \\ \frac{dq_{TD}^2}{d\eta} \end{bmatrix} = \begin{bmatrix} 0 \\ 0 \\ 0 \end{bmatrix} \quad (43)$$

where the eigenvectors are defined by

$$\vec{X} = \left(\frac{dZ_1^1}{d\eta} \quad \frac{dZ_1^2}{d\eta} \quad \frac{dq_{TD}^2}{d\eta} \right)^T \quad (44)$$

and explicit definition of the top-row elements are

$$a = \frac{\partial q_{TD}^1 F_1^1}{\partial Z_1^1} - \frac{F_1^1}{\sum_{i=1}^2 F_i^1} \frac{\partial \sum_{i=1}^2 q_{TD}^1 F_i^1}{\partial Z_1^1} \quad (45)$$

$$b = \frac{\partial q_{TD}^1 F_1^1}{\partial Z_1^2} - \frac{F_1^1}{\sum_{i=1}^2 F_i^1} \frac{\partial \sum_{i=1}^2 q_{TD}^1 F_i^1}{\partial Z_1^2} \quad (46)$$

$$c = \frac{\partial q_{TD}^1 F_1^1}{\partial q_{TD}^2} - \frac{F_1^1}{\sum_{i=1}^2 F_i^1} \frac{\partial \sum_{i=1}^2 q_{TD}^1 F_i^1}{\partial q_{TD}^2} \quad (47)$$

$$d = R^1 \left(\frac{\partial G_1^1}{\partial Z_1^1} - \frac{F_1^1}{\sum_{i=1}^2 F_i^1} \frac{\partial \sum_{i=1}^{n_c} G_i^1}{\partial Z_1^1} \right) \quad (48)$$

The eigenvalues (λ_{D1} and λ_{D2}) are the roots of the equation

$$\begin{vmatrix} (a - \lambda_D d) & b & c \\ \left(\frac{\partial F^T}{\partial Z_1^1} - \lambda_D \frac{\partial G^T}{\partial Z_1^1} \right) & \left(\frac{\partial F^T}{\partial Z_1^2} - \lambda_D \frac{\partial G^T}{\partial Z_1^2} \right) & \frac{\partial F^T}{\partial q_{TD}^2} \\ \left(\frac{\partial F_1^T}{\partial Z_1^1} - \lambda_D \frac{\partial G_1^T}{\partial Z_1^1} \right) & \left(\frac{\partial F_1^T}{\partial Z_1^2} - \lambda_D \frac{\partial G_1^T}{\partial Z_1^2} \right) & \frac{\partial F_1^T}{\partial q_{TD}^2} \end{vmatrix} = 0 \quad (49)$$

Equation 49 has two roots, (λ_{D1} and λ_{D2}). Each eigenvalue (λ_{Dn}) has an associated eigenvector (\bar{X}_n) (Eq. 44) that describes the direction in composition–rate space. Each eigenvalue yields one potential composition path. The first and second rows of the eigenvector (Eq. 44) provide the changes in layer 1 and layer 2 compositions, respectively. The last row in Eq. 44 ($dq_{TD}^2/d\eta$) provides the changes in q_{TD}^2 along a selected eigenvector direction. The rate in layer 1 (q_{TD}^1) can be updated from the crossflow equilibrium condition stated in Eq. 30 once the changes in Z_1^1 , Z_1^2 , and q_{TD}^2 are known.

Solution Construction

A correct physical solution consists of compatible waves where velocity constraint is satisfied. Velocity constraint requires monotonic wave velocities, which increase from upstream to downstream. Shocks are included in the solution when the condition of monotonicity is violated. In addition, the phase boundaries are crossed via shocks.

The shocks in binary flow are always associated with phase appearance and disappearance in one or both of the layers. In other words, the shocks appear in the solution when the phase boundaries are crossed in at least one of the

layers. In the solutions, path switch is allowed so long as velocity constraint is satisfied. The solution is constructed by combining separate segments (zone of constant states, shocks, and continuous variations), which satisfies both material balance and velocity constraint.

Computation of Eigenvalues and Eigenvectors

The computation of eigenvalues and eigenvectors entails calculation of the entries in Eq. 49. Each entry of this determinant is coupled with the phase equilibrium calculations. Therefore a phase behavior model must be used in the calculations. The Peng–Robinson¹³ equation of state has been selected to represent phase equilibrium calculations.

For the flow of each phase in porous medium, simple functional forms of relative permeabilities are used. For the gas phase, the assumption is

$$k_{rg} = k_{rg}^0 \left(\frac{S_g}{1 - S_{or}} \right)^{n_g} \quad (50)$$

and for the liquid phase, the assumption is

$$k_{rl} = k_{rl}^0 \left(\frac{1 - S_g - S_{or}}{1 - S_{or}} \right)^{n_l} \quad (51)$$

The fractional flow equation for the gas phase without capillary pressure effect is

$$f_g^k = \frac{1 - N_{gr}^k k_{rl}^k}{1 + \left(\mu_g^k / \mu_l^k \right) \left(k_{rl}^k / k_{rg}^k \right)} \quad (52)$$

where N_{gr}^k is the gravity number defined by

$$N_{gr}^k = \frac{k^k A^k (M_g^k \rho_g^k - M_l^k \rho_l^k) g \sin \theta}{\mu_l^k q_T^k} \quad (53)$$

The gravity number defined by Eq. 53 is a function of time and position; however, the gravity number at the inlet is constant at all times. The gravity number can be increased by increasing the permeability area product, by increasing the tilt angle, and by density difference between the two phases. The parameters at the denominator of the gravity number have a similar effect (for instance, decreasing the flow rate or liquid viscosity would increase the gravity number). Therefore one particular gravity number could correspond to a spectrum of parameters. At a given pressure and fixed geometry, N_{gr} is proportional to $\sin \theta / q_T^k$; therefore tilt angles in the range of 5 to 15° have a substantial effect on gravity number. In Eqs. 52 and 53, phase viscosities are calculated with the use of the equilibrium phase compositions from the Lohrenz et al.¹⁴ correlation.

Relative permeabilities are functions of vapor saturation. Vapor saturation is a function of overall composition. For two-phase equilibrium conditions,

$$S_g = \frac{V}{V + (\rho_g / \rho_l)(1 - V)} \quad (54)$$

and the mole fraction of vapor can be calculated with equilibrium phase compositions

$$V = \frac{Z_i - x_{il}}{x_{ig} - x_{il}} \quad (55)$$

After phase behavior and flow relations have been established, the entries in the matrices of Eq. 43 can be calculated. Partial derivatives are performed numerically because of implicitness of the phase behavior and flow relations in the quantities to be differentiated. The numerical derivatives are calculated with the central difference formulation. For a generic function H,

$$\frac{\partial H}{\partial Z_1} = \frac{H(Z_1 + \Delta Z_1, Z_2, Z_1^1, Z_2^2, q_{TD}^2) - H(Z_1 - \Delta Z_1, Z_2, Z_1^1, Z_2^2, q_{TD}^2)}{2\Delta Z_1} \quad (56)$$

Conclusions

Regardless of very pronounced crossflow caused by gravity, the total recovery with and without crossflow is surprisingly close for the example cases studied; however, with crossflow, the bulk of the oil is transferred to the more-permeable layer. The effects of various parameters are being investigated to examine the fundamental differences between the crossflow and NC cases. On the basis of the present study, the following conclusions are drawn:

1. An analytical model has been developed (method of characteristics) for the calculation of viscous and gravity crossflow in a layered/fractured porous medium including the effects of volume change. Features of crossflow in fractured media will be reported later.

2. The breakthrough recovery (at the arrival of leading shock) of CE solution is higher than that of NC solution.

3. The gravity dominant cases yield higher total recoveries for the total system. Beneficial effects of gravity are essential to recovery enhancement when large contrasts between the layers are considered.

4. The gravity dominant case includes a single-phase spreading segment in the solutions because of strong crossflow from layer 2.

5. Crossflow between the layers increases with the gravity number, but the total recovery is affected slightly by the crossflow, as shown by a comparison with NC solutions for the cases examined.

Additional information on this research is on file at the Bartlesville Project Office, U.S. Department of Energy.

Nomenclature

- A = flow area
- A_k = flow area of layer k
- A_T = total flow area (Eq. 19)
- C_R = capacitance ratio (Eq. 31)
- f_j = fractional flow function of phase j
- F_i^k = molar fractional flow of component i (Eq. 23)
- g = acceleration of gravity
- G_i^k = number of moles of component i per unit volume (Eq. 22)
- k = absolute permeability
- k_{ro} = relative permeability of liquid phase (oil)
- k_{ro}^o = relative permeability coefficient of liquid phase (oil)
- k_{rg} = relative permeability of vapor phase (gas)
- k_{rg}^o = relative permeability coefficient of vapor phase (gas)
- L = system length
- M_g^k = molecular weight of gas phase
- M_l^k = molecular weight of liquid phase
- n_o = relative permeability exponent of liquid phase (oil)
- n_g = relative permeability exponent of vapor phase (gas)
- n_p = number of phases
- n_c = number of components
- P = pressure
- q_{gr}^k = gravity drainage rate of layer k, $q_{gr}^k = k^k A^k (M_g^k \rho_g^k - M_l^k \rho_l^k) g \sin \theta / \mu_l^k$
- q_T = total rate of injection
- $q_{T,inj}^k$ = total rate of injection in layer k at the inlet
- $q_{TD,inj}^k$ = total dimensionless rate of injection in layer k at the inlet
- q_T^k = total rate of injection in layer k
- q_{TD}^k = total dimensionless rate of injection in layer k
- R^k = fractional pore volume of layer k (Eq. 17)
- S_j = saturation of phase j, fraction
- S_o = liquid phase (oil) saturation, fraction
- S_g = gas phase (vapor) saturation, fraction
- S_{or} = residual saturation of liquid phase (oil), fraction
- t = time
- t_D = dimensionless time (Eq. 14)
- x = spatial dimension
- x_D = dimensionless distance (Eq. 13)
- x_{ij} = mole fraction of component i in phase j
- \bar{X} = eigenvector
- Z_i = overall mole fraction of component i
- \bar{Z} = composition vector

Greek Symbols

- ϕ = porosity
 ϕ^k = porosity of layer k
 $\bar{\phi}$ = volume-averaged porosity (Eq. 18)
 μ_j = viscosity of phase j
 ρ_j = molar density phase j
 ρ_{jD} = dimensionless molar density of phase j
 θ = tilt angle
 Λ = shock speed
 Λ_D = dimensionless shock speed
 λ = eigenvalue (characteristic velocity)
 λ_D = dimensionless eigenvalue (dimensionless characteristic velocity)
 λ_j^k = mobility of phase j in layer k, $\lambda_j^k = k_{rj}^k / \mu_j^k$
 λ_T^k = total fluid mobility in layer k, $\lambda_T^k = \sum_{j=1}^{n_p} k_{rj}^k / \mu_j^k$

References

1. J. C. T. Tan and A. Firoozabadi, *Miscible Displacement in Fractured Porous Media: Part II—Analysis*, paper SPE 27837 presented at the Ninth SPE/DOE Symposium on Improved Oil Recovery, Tulsa, Okla., April 17–20, 1994.
2. C-T. Tan and A. Firoozabadi, Theoretical Analysis of Miscible Displacement in Fractured Porous Media by a One-Dimensional Model: Part I—Theory, *J. Can. Pet. Technol.*, 17-35 (February 1995).
3. V. J. Zapata and L. W. Lake, *A Theoretical Analysis of Viscous Crossflow*, paper SPE 10111 presented at the 56th Annual Society of Petroleum Engineers Technical Conference, San Antonio, Tex., October 5–7, 1981.
4. K. K. Pande and F. M. Orr, Jr., *Composition Paths in Binary CO₂-C₁₀ Displacements: Effects of Reservoir Heterogeneity and Crossflow on Displacements with Limited Solubility*, paper presented at the 1990 Second European Conference on the Mathematics of Oil Recovery, Arles, France, September 11–14, 1990.
5. P. D. Lax, Hyperbolic Conservation Laws II, *Commun. Pure Appl. Math.*, 10: 537-566 (1957).
6. H. Rhee, R. Aris, and N. R. Amundson, *First-Order Partial Differential Equations: Volume I*, Prentice-Hall, Englewood Cliffs, N.J., 1986.
7. J. M. Dumore, J. Hagoort, and A. S. Risseuw, An Analytical Model for One-Dimensional, Three-Component Condensing and Vaporizing Gas Drives, *SPE Soc. Pet. Eng. J.*, 24: 169-179 (April 1984).
8. B. Dindoruk, *Analytical Theory of Multiphase Multicomponent Flow in Porous Media*, Ph.D. Dissertation, Stanford University, Stanford, Calif., June 1992.
9. K. H. Coats, J. R. Dempsey, and J. H. Henderson, The Use of Vertical Equilibrium in Two-Dimensional Simulation of Three-Dimensional Reservoir Performance, *Trans. Am. Inst. Min., Metall. Pet. Eng.*, 251: 63-71 (1971).
10. H. Rhee, R. Aris, and N. R. Amundson, *First-Order Partial Differential Equations: Volume II*, Prentice-Hall, Englewood Cliffs, N.J., 1989.
11. J. Smoller, *Shock Waves and Reaction-Diffusion Equations*, first edition, Springer-Verlag, New York, N.Y., 1983.
12. T. Myint-U and I. Debnath, *Partial Differential Equations for Scientists and Engineers*, third edition, North Holland, New York, N.Y., 1987.
13. D. Y. Peng and D. B. Robinson, A New Two-Constant Equation of State, *Ind. Eng. Chem. Fundam.*, 15: 59-64 (1976)
14. J. Lohrenz, B. C. Bray, and C. R. Clark, The Viscosity of Pure Substances in Dense Gaseous and Liquid Phases, *J. Pet. Technol.*, 1171-1176 (1964).

RESOURCE ASSESSMENT TECHNOLOGY

**CONTINUED SUPPORT OF THE
NATURAL RESOURCES INFORMATION
SYSTEM FOR THE STATE OF
OKLAHOMA**

Contract No. DE-FG22-92BC14853

**Oklahoma Geological Survey
University of Oklahoma
Norman, Okla.**

**Contract Date: May 18, 1992
Anticipated Completion: Sept. 30, 1994
Government Award: \$350,000
(Current year)**

**Principal Investigators:
Charles J. Mankin
Terry P. Rizzuti**

**Project Manager:
R. Michael Ray
Bartlesville Project Office**

Reporting Period: July 1–Sept. 30, 1994

Objective

The objective of this research program is to continue developing, editing, maintaining, using, and making publicly available the Oil and Gas Well History File portion of the Natural Resources Information System (NRIS) for the state of Oklahoma. This contract funds the development work as a continuation of earlier contract numbers DE-FG19-88BC14233 and DE-FG22-89BC14483. The Oklahoma Geological Survey (OGS), working with geological information systems (GIS) at the University of Oklahoma (OU) Sarkeys Energy Center, has undertaken the construction of this information system in response to the need for a computerized, centrally located library containing accurate, detailed information on the State's natural resources. Particular emphasis during this phase of NRIS development is being placed on computerizing information related to the energy needs of the Nation, specifically oil and gas.

Summary of Technical Progress

The NRIS Well History File contains historical and recent completion records for oil and gas wells reported to the Oklahoma Corporation Commission (OCC) on Form 1002-A. At the start of this quarter, the Well History File contained

369,231 records, providing geographical coverage for most of Oklahoma (all but Osage County). Data elements on this file include American Petroleum Institute (API) well number, lease name and well number, location information, elevations, dates of significant activities for the well, and formation items (e.g., formation names, completion and test data, depths, and perforations). In addition to the standard Well History File processing, special projects are undertaken to add supplemental data to the file from well logs, scout tickets, and core and sample documentation.

A large portion of the Well History File work involves photocopying the completion reports for use in coding before data entry. All new completion reports are copied as soon as they are received from the OCC or the Osage Tribal Council (OTC). More than 410,000 completion reports had been copied by the end of the quarter, which represents all the historical 1002-A completion reports available through the OCC, as well as several thousand additional completion reports obtained from Sooner Well Log and the OTC.

Processing the OCC's oil and gas well completion reports (Form 1002-A and the Osage County form) is proceeding smoothly. Well records are being prescanned, keyed, and edited for Osage County and for all new records obtained from the OCC. Approximately 9000 well records were keyed and added to the file this quarter. Thus, as of September 1994, the database contained 378,243 records. The Well History File progress is shown by NRIS Regional Division in Table 1. The current status of county coverage and the total record counts by county are shown in Figs. 1 and 2 respectively.

Both general and specialized edit procedures were continued on the well data. Search strategies are used to research well records with incorrect township-range-section (TRS) or county location data and well records that should be cross-referenced. Oklahoma Tax Commission (OTC) lease numbers are being assigned to well records through a combined machine and manual matching process between the lease and well files. The statewide Lease File/Well File match used to identify sections with significant discrepancies in the lease and well counts has been facilitated by cooperation from NRIS users and from Sooner Well Log Service, Oklahoma City, Okla. Since the start of the contract, efforts to locate missing 1002-A forms for areas identified through these methods have been successful.

TABLE 1

Well History File Progress by Regional Division

Area of coverage	Start of grant	Start of quarter	Current
Southeast region	65,712	67,485	67,883
Southwest region	69,453	72,385	72,955
Northeast region	23,467	133,432	140,766
Northwest region	32,507	33,700	34,103
North-central region	40,883	62,229	62,536
Total	232,022	369,231	378,243

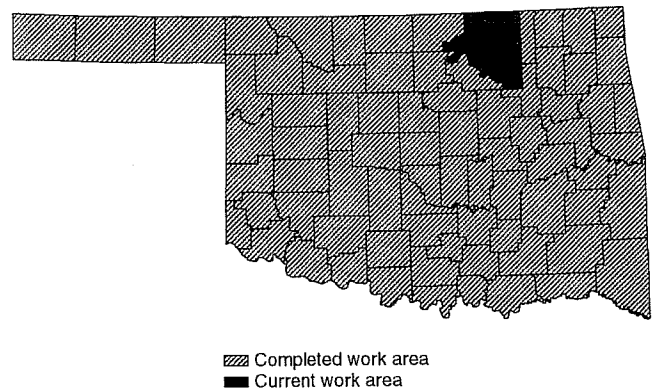


Fig. 1 Status of well history database project by county as of Sept. 30, 1994.



Fig. 2 Status of well history database project as of Sept. 30, 1994. Total well records, 378,243.

During the second quarter of this budget year, all the completion reports available in-house had been processed, which resulted in approximately 350,000 forms on the File. Work efforts have since emphasized three areas of research to obtain the remaining records, estimated to be an additional 70,000 forms; for example, the Lease File/Well File matching efforts continued as a means of identifying areas with missing 1002-A forms. Another method involved implementing research efforts whereby well records currently on file were matched against hard-copy scout tickets available through the Lawrence Youngblood Energy Library at OU. Initial efforts concentrated in the northeastern part of the State on a township-by-township basis. Scout tickets identified for wells not on the Well History File were sent to Sooner Well Log Service and any missing 1002-A forms available through their collection were added to the file. Those scout tickets for which no corresponding 1002-A records could be identified were added to the Well History File to ensure a more complete file.

Additionally, efforts were finalized during the second budget quarter and procedures were established to obtain access to Osage County records available through the Osage Tribal Agency. By the close of the quarter, records for the entire county had been copied and sent to be recopied, coded,

keyed, and entered into the Well History File. Forms from the first shipment of Osage records were reviewed to ascertain how many different form layouts were used to report well completions. It was determined that five layouts would require new keying formats, reformatter programs, and processing job streams. The five formats were reviewed to identify what data elements were unique to the Osage County forms. As a result of this review, 62 labels were identified and added to the data dictionary. Coding procedures for these data elements and formats were established and coding began. Data-entry keying formats, reformatter programs, and processing job streams were developed and tested. Data entry began early in the third quarter.

It was previously determined that the goal of having 400,000 forms on file by the close of the contract in May 1994 would not be met. The processing of the Osage County records is proceeding at approximately half the pace as processing of the 1002-A forms because of the increased amount of data recorded on the Osage County forms. However, a no-cost extension was requested of the U.S. Department of Energy (DOE) and granted through September 1994, at which point it was estimated that approximately 375,000 forms would be contained in the file. That goal was met and surpassed, as shown in Table 1. The remaining 42,000 forms (estimated) required additional funding, so an unsolicited proposal seeking \$300,000 in DOE funding for a 1-yr project to complete Osage County was submitted during the no-cost extension. That request was approved during this quarter.

Efforts to standardize the formation names on the Well History File are continuing. A personal computer (PC)-based program uses a conversion table to standardize spellings and allows the user to build interactively new entries for the conversion table as new spelling variations are encountered. In the southeast, southwest, and northwest regions, over 99% of the reported names have been standardized. Efforts to standardize formation names in the northeast region are complete with 97% standardized. Efforts to standardize formation names in the north-central region were resumed with 95% of the region standardized. This formations-editing process is further enhanced by the addition of a table to determine the standard Franklized abbreviation for each reported name following the convention with which industry users are familiar.

One goal of the NRIS system involves efforts to assign leases and wells to fields on the basis of the official field outlines as designated by the Midcontinent Oil and Gas Association's Oklahoma Nomenclature Committee (ONC). Some areas exist where significant field extension drilling has taken place, but the ONC has had insufficient resources to update the field boundaries accordingly. To assist the ONC in updating their field outlines, information packages are produced from the NRIS system for selected areas. These packages include well data listings and well spot maps. On the basis of this input, the ONC began by first updating several gas-field boundaries; emphasis has shifted to oil-field boundaries as work proceeds on a separate DOE project involving the identification and evaluation of Oklahoma's fluvial-

dominated deltaic reservoirs. Overall, unassigned gas production remains at 12% of annual average production and unassigned oil production at 17%.

During the second budget quarter, 28 new data elements were added to accommodate the new 1002-A completion report forms for 1992. A new reformatter program was written as well as a processing job stream. Keying of the new forms began during the third quarter and continues to proceed smoothly. Efforts to prepare and distribute the July 1994 data release were delayed until August, and all new data elements (definitions and coding instructions) were documented for inclusion in the NRIS Data Manual. It is anticipated that the 92 new data elements for the 1992 forms and the Osage County records will be included in the January 1995 data release.

Public Data Release

Since early 1991 efforts have been made to disseminate NRIS information through meetings, workshops, OGS annual reports, and mass mailings to numerous individuals, companies, and organizations. As a result, a dramatic response to the release of NRIS data began during the summer of 1991 and has continued. Feedback from the public continues to reflect enthusiasm about this new resource for the oil and gas industry in Oklahoma. Data and analyses have been provided that would not have been feasible before construction of the NRIS system.

Two commercial firms subscribe to the Well History File, and several inquiries are received each quarter from small companies and independents who typically acquire NRIS subsets to evaluate within their specific computer systems before committing to larger data acquisitions.

Also, as previously reported, NRIS well data have been made available through the Oklahoma City Geological Library with positive results. The high level of interest by library members has led to the acquisition of several thousand records by several members as well as constructive feedback on user-detected data anomalies. The Library, which is cataloging their extensive well-log collection and tying each log to the corresponding NRIS well record, will be able to provide a listing of logs for which no NRIS records are on file. This should greatly enhance efforts to locate missing well records.

The OGS is establishing a computing facility to promote user access to the NRIS data, initially by staff and eventually by the public. A PC-level relational database management system called Advanced Revelations is being used to develop a menu-driven retrieval system customized to NRIS data. Negotiations are also under way to obtain Oracle as a database manager to facilitate use of the lab. A large digitizer, large plotter, and desktop scanning equipment enhance the capabilities available through GeoGraphix and Radian CPS/PC contour mapping software as well as through ARC/INFO, a GIS spatial analysis tool. Additionally, Platte River Associates has agreed to donate their land-grid and associated cultural data for use in the lab.

The NRIS data are a significant factor in several projects; for example, the lab will become the central location for NRIS data access and distribution in the OGS's forthcoming role as Regional Lead Organization for the Southern Midcontinent under the Petroleum Technology Transfer Council program. Another project, funded by DOE, involves the study of Oklahoma's

fluvial-dominated deltaic reservoirs. A third project, completed this quarter and involving cooperative research with the School of Civil Engineering and Environmental Science, is the creation of a GIS database (with a wellhead protection component) containing current and potential waste sites located on Oklahoma's Cheyenne/Arapaho tribal lands.



MICROBIAL TECHNOLOGY

***THE USE OF INDIGENOUS MICROBES
TO SELECTIVELY PLUG THE MORE
POROUS ZONES TO INCREASE OIL
RECOVERY DURING WATERFLOODING***

Contract No. DE-FC22-94BC14962

**Hughes Eastern Corporation
Jackson, Miss.**

**Contract Date: Jan. 1, 1994
Anticipated Completion: June 30, 1999
Government Award: \$508,835
(Current year)**

**Principal Investigators:
Lewis R. Brown
Alex A. Vadie**

**Project Manager:
Rhonda Lindsey
Bartlesville Project Office**

Reporting Period: July 1–Sept. 30, 1994

Objective

The objective of this work is to demonstrate the use of indigenous microbes as a method of profile control in waterfloods. It is expected that, as the microbial population is induced to increase, the expanded biomass will selectively block the more permeable zones of the reservoir and thereby force injection water to flow through the less permeable zones, which will result in improved sweep efficiency.

This increase in microbial population will be accomplished by the injection of a nutrient solution into four injectors. Four other injectors will act as control wells. During Phase I, two wells will be cored through the zone of interest. Special core analyses will be performed in order to arrive at the optimum nutrient formulation. During Phase II, nutrient injection will begin, the results will be monitored, and adjustments to the nutrient composition will be made, if necessary. Phase II also will include the drilling of three wells for postmortem core analysis. Phase III will focus on technology transfer of the results. One expected outcome of this new technology will be a prolongation of economical waterflooding operations (i.e., economical oil recovery should continue for much longer periods in the producing wells subjected to this selective plugging technique).

Summary of Technical Progress

Phase I: Planning and Analysis

The concepts for the new technology to be evaluated in this project are considered to be scientifically sound and have been proven to be effective in laboratory experiments. Laboratory tests on live cores from the reservoir of interest must be performed nevertheless. Two wells will be drilled for this purpose, and special core analyses will be conducted in order to fine-tune the exact concentration of and schedule for additions of nutrients to the injection water.

While the main purpose for drilling the two wells is to obtain cores suitable for use in the laboratory work, a secondary purpose is to obtain production data that will indicate the sweep efficiency of the existing waterflood. The two core wells ultimately will be converted to injection if this project is successful and the program is expanded. At the conclusion of Phase I, a specific feeding regime will have been formulated for each of the injection wells. Since the injection wells all vary in terms of years of service, differences in channeling are anticipated and a different feeding regime may be needed for each well.

The work for Phase I of the project has been divided into seven tasks:

Task 1.1: Drilling of Two New Injection Wells for the Acquisition of Cores and Other Data

Work on this task is complete.

Task 1.2: On-Site Handling of Cores

Work on this task is complete.

Task 1.3: Core Analysis to Determine Microbial Enhanced Oil Recovery (MEOR) Requirements

On the basis of the laboratory tests conducted under Task 1.5, the concentrations of nutrients to be used on the field have been established. The tentative schedule for the addition of nutrients has been established. On the basis of these concentrations and the present water injection rate in the 2-14 No. 1 well, the first nutrient injection skid has been designed and is under construction in the field. The skid is designed to pump 200 to 300 gal/d of nutrient solution at a constant rate into the injection stream.

Task 1.4: Microbial Analyses of Cores

Work on this task is complete.

Task 1.5: Laboratory Waterflooding Test of Live Cores

Ten live cores were prepared for the waterflooding tests. Initially, simulated injection water was allowed to flow through each core for 48 h to determine the flow rate of each core. There were four feeding regimes (each with a duplicate core) and two controls with simulated injection water only. The duplicate feeding regimes were potassium nitrate (KNO₃), disodium

phosphate (Na₂HPO₄), ethanol (ETOH), and hydrogen peroxide (H₂O₂), hereinafter referred to as N, P, C, and O, respectively. Each symbol indicates additions for a 24-h period.

Feeding Regimes:

core 1 and core 2:	N P P P P
core 3 and core 10:	C N P P P
core 4 and core 9:	N P O P O
core 5 and core 7:	Injection water only
core 6 and core 8:	C N P O P O

The effluent from each core was collected and the following observations made daily: plugging of the core, volume of effluent, presence of oil, odor, presence of sediment, and pH. The following tests were conducted on the effluents collected after the initial 48-h run and on the effluent collected after a complete feeding regime sequence: Nitrate (NO₃), phosphate (PO₄), and plate counts on PCA and Oil agar (both aerobic and anaerobic). With the exception of the two controls, plugging was observed in all the cores. Sediment and slight oily odor were observed in several of the effluents collected from the test cores, but no oil was collected from any of the cores. Microbial populations from the oil cores were facultative anaerobes with the populations from the 10 different cores appearing to be similar. The experiment with these 10 cores is complete.

Two additional cores were set up for waterflooding tests. The feeding regimes for cores 11 and 12 were as follows:

core 11:	Injection water only (hereinafter referred to as I)
core 12:	N I P I P I P I

The nitrate and phosphate influents were the same concentrations as those used in the first 10 cores. Plugging, oil, and sediment were observed in both cores 11 and 12. The experiment with these two cores is complete.

Two additional cores were set up for waterflooding tests. The feeding regimes for cores 13 and 14 were as follows:

core 13:	Injection water
core 14:	N P P I I I I I

Core 14 received the same concentration of phosphate as cores 1 to 10, but the nitrate concentration was doubled. There was no plugging in either core 13 or 14. A slight variation in the flow rates of the two cores was observed; however, there were no drastic changes. An increase in the number of oil-degrading microorganisms from effluents collected from the test core was noted, whereas the size of the microbial population in the control core remained constant. The microbial populations from these two additional cores appeared to be similar. The waterflooding experiment with these two cores is complete.

Work on Task 1.5 is complete.

Task 1.6: Acquisition of Baseline Data

Work on this task is continuing with chemical and microbiological analyses of injection water and production fluid.

Task 1.7: Analysis of Baseline Data

This task will begin when the data in Task 1.6 have been collected.

RESERVOIR CLASS FIELD DEMONSTRATIONS

WEST HACKBERRY TERTIARY PROJECT

Contract No. DE-FC22-93BC14963

**Amoco Production Company
Houston, Tex.**

**Contract Date: Sept. 3, 1993
Anticipated Completion: April 2, 1997
Government Award: \$6,017,500**

**Principal Investigator:
Travis H. Gillham**

**Project Manager:
Gene Pauling
Metairie Site Office**

Reporting Period: July 1–Sept. 30, 1994

Objective

The objective of this project is to demonstrate the technical and economic feasibility of combining air injection with the double displacement process (DDP) for tertiary oil recovery. The DDP is the gas displacement of a water-invaded oil column for the recovery of oil through gravity drainage. The novel aspect of this project is the use of air as the injection fluid. The

target reservoir for the project is the Camerina C-1,2,3 sand located on the West Flank of West Hackberry field in Cameron Parish, La. If successful, this project will demonstrate that the use of air injection in the DDP can economically recover oil in reservoirs where tertiary oil recovery is presently uneconomic.

Summary of Technical Progress

During this quarter Amoco Production Co. has proceeded with project implementation. Areas of progress include construction of surface facilities, well workovers, reservoir monitoring program, Louisiana State University's (LSU) modeling study and laboratory tests, and Tulsa Research Center support.

Construction of Surface Facilities

The first major goal of this project is to initiate air injection into the target reservoir, the Camerina C-1,2,3 sand on the West Flank of West Hackberry field. Delays associated with the fabrication of the reciprocating compressor package moved the target date for initial air injection from June 1994 to October 15, 1994.

Air Compressors

The reciprocating compressor package was completed, tested, and shipped to the Hackberry site. The limited access and physical constraints of the installation site require the larger reciprocating compressor to be installed before the screw

compressor. This prevented installation of the screw compressor. A 2-d operating and maintenance school on the screw compressor was conducted for the Hackberry operating personnel by the compressor vendor.

Compressor Foundation

The concrete addition to the existing foundation for installation of the screw compressor cooler and receiver is complete. Holes were cored in the existing concrete foundation for installation of the anchor bolts for the compressors and building. A pollution trough was also cut in the old section of the foundation. Existing grout was removed and the depressions were filled. The foundation is ready for installation of the compressors.

Injection and Purge Facilities

The injection, purge, and scrubber dump lines from the facilities to the Gulf Land D No. 51 injection well are complete. All major equipment items were delivered, including the high-pressure purge pump, the wellhead scrubbers, the screw compressor afterscrubber, the compressor building, and all valves. Gulf States Utilities completed the upgrade of the electrical distribution lines. Installation of the electrical and automation equipment is 60% complete. The purge, injection, and wellhead skids were designed and constructed.

Well Workovers

Gulf Land D No. 51 (Air Injection Well)

The Gulf Land D No. 51 was successfully recompleted from the Bol 3 sand to the Cam C-1,2,3 sands so that the well could serve as the air injection well for Fault Block IV. A pulsed neutron log and five cased-hole formation pressures were taken.

The pulsed neutron log will be used as a baseline log for comparison with future pulsed neutron logs during the life of the project. The Gulf Land D No. 51 will be loaded with nitrogen before air injection begins. The nitrogen will serve as a buffer between the reservoir fluids and the initial air injected into the well.

Gulf Land D No. 52 (Monitor Well)

The Gulf Land D No. 52 was originally completed in the Cam C-2 sand. During this quarter perforations were added in the Cam C-1 sand and a shut-in bottomhole pressure survey was run.

Reservoir Monitoring Program

During this quarter shut-in bottomhole pressure surveys were run in the Gulf Land D Nos. 51 and 52. The bottomhole pressures from these two wells supported the assumption that both wells are in pressure communication. In Fault Blocks IV and V, these surveys also confirmed that the average reservoir pressure (at 9000 ft below sea level) is approximately 2600 psi whereas the average reservoir pressure in Fault Blocks I and II is about 3200 psi. A plot of reservoir pressure vs. time is given in Fig. 1.

In Fault Block IV in the Gulf Land D No. 51, a series of five cased-hole formation pressures indicated that the pressure in Cam C-1,2 is currently 270 psi higher than that in Cam C-3. The original open-hole logs in the Gulf Land D No. 51 showed that the Cam C-1,2 sands were wet (residual hydrocarbon saturation), whereas the Cam C-3 was gas productive. The pulsed neutron log in the Gulf Land D No. 51, which was run during July 1994, was wet in the Cam C-1,2, gas productive in one lobe of the Cam C-3, and oil productive in two other lobes of the Cam C-3. A posted induction log is shown in Fig. 2. An oil

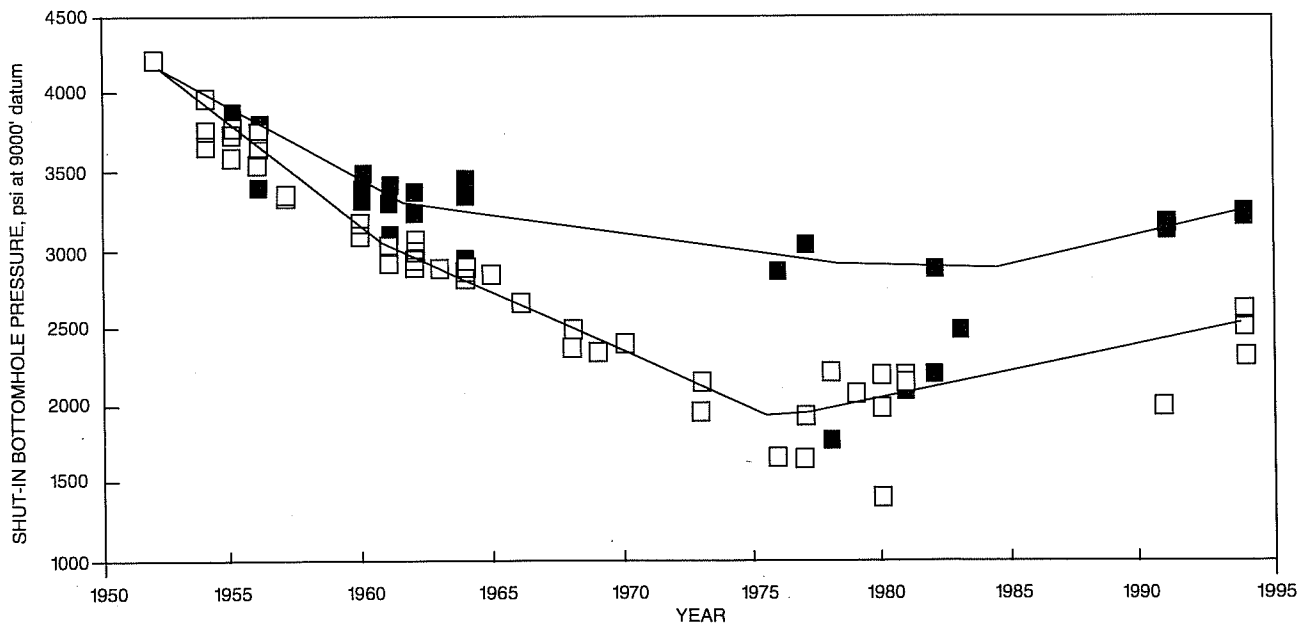


Fig. 1 Shut-in bottomhole pressure vs. time (Cam C-1,2,3 sands). ■, Fault Blocks I and II. □, Fault Blocks III, IV, and V.

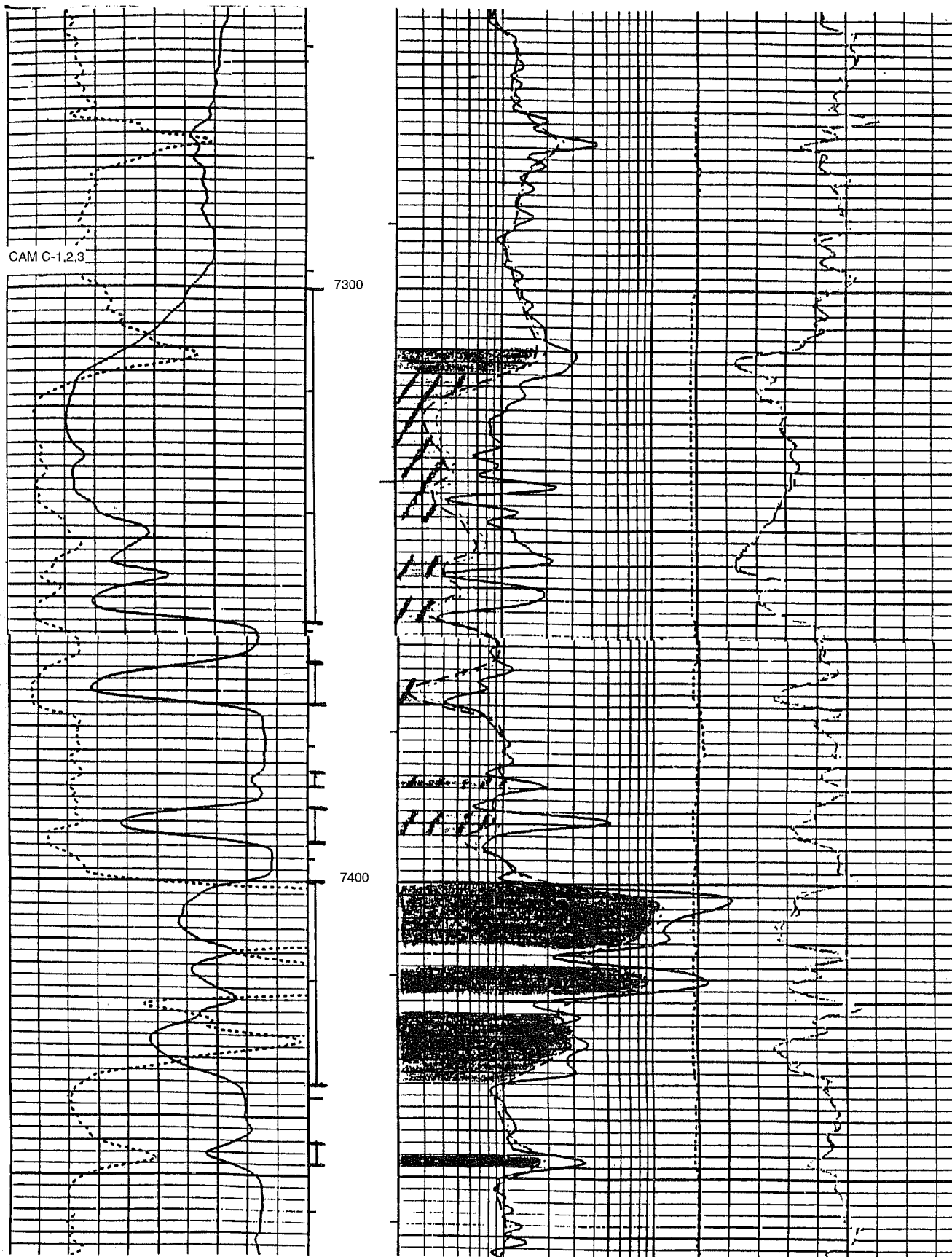


Fig. 2 Posted induction log from the Gulf Land D No. 51. (Art reproduced from best available copy.)

sample was taken from the Cam C-3 with a cased-hole formation tester. The oil sample confirmed the suspected presence of an oil rim in the Cam C-3 in Fault Block IV.

The oil rim in the Cam C-1,2 in Fault Block IV is believed to be located upstructure to the Gulf Land D No. 51. The importance of the existence of an oil rim is related to the relative permeability effects that cause oil to be more mobile in the presence of high oil saturations. In other words, the preexistence of an oil rim is expected to facilitate the growth of the rim during the project.

Along with the bottomhole pressure data, the maximum recorded bottomhole temperature was also measured during the shut-in surveys in the Gulf Land D Nos. 51 and 52. The maximum recorded temperatures in the Gulf Land D Nos. 51 and 52 were 186 °F and 193 °F, respectively. The differences in temperature are directly related to depth.

Louisiana State University's Modeling Study and Laboratory Tests

An informal meeting was held between LSU and Amoco personnel to review the work that has been done thus far and to discuss plans for the upcoming year.

A reservoir modeling study is being prepared for the project. The goals are to predict future performance and to define the controlling parameters for tertiary oil recovery. Laboratory core tests are being performed on consolidated Berea core and sandpacks to measure the mobilization of residual oil (in a water-swept core) caused by gas injection and subsequent gravity drainage and on a transparent micromodel that was constructed for observing and filming the mechanics of the gravity drainage process. A black oil model is being used to develop screening criteria for future projects. Parameters such as dip angle, vertical permeability, thickness, injection rate, and proximity of injectors to producers will be modeled to determine their effect on production rates and ultimate recovery.

The laboratory core tests and the development of screening criteria for future projects are essentially 50% complete, whereas the reservoir modeling study is in its earliest stages. Louisiana State University plans to study the project in its early stages and to perform further study and technology transfer in the middle and latter stages of the project.

Tulsa Research Center Support

Earlier in the project, oil samples were gathered from the North Flank of West Hackberry field because there was no remaining oil production from the project reservoirs on the West Flank of the field. The oil sample recently taken with a cased-hole formation tester in the Gulf Land D No. 51 was sent to Amoco's Tulsa Research Center for testing. The oil sample was analyzed, and it was determined that the North Flank oil was almost identical to that of the West Flank. Therefore, static pressure-volume-temperature tests and combustion tube tests previously run on samples of North

Flank oil will be representative of West Flank oil from the project reservoir.

The thermal model (THERM) is being used to history match the results of the combustion tube runs to calibrate the model for the Hackberry project. This work is expected to be completed by the end of September.

GREEN RIVER FORMATION WATERFLOOD DEMONSTRATION PROJECT, UINTA BASIN, UTAH

Contract No. DE-FC22-93BC14958

**Lomax Exploration Company
Salt Lake City, Utah**

**Contract Date: Oct. 21, 1992
Anticipated Completion: Oct. 20, 1995
Government Award: \$1,304,000**

Principal Investigators:

**John D. Lomax
Dennis L. Nielson
Milind D. Deo**

Project Manager:

**Edith Allison
Bartlesville Project Office**

Reporting Period: July 1–Sept. 30, 1994

Objective

The project is designed to increase recoverable petroleum reserves in the United States. The Green River Formation in Utah's Uinta Basin contains abundant hydrocarbons that are hard to recover by primary means. The successful Lomax Monument Butte Unit waterflood will be evaluated under this contract, and, on the basis of this information, waterfloods will be initiated in nearby Travis and Boundary units. In 1987, Lomax Exploration Company started a waterflood in the Monument Butte Unit of a Douglas Creek member of the Green River Formation. This was a low-energy, geologically heterogeneous reservoir producing a waxy crude oil. Primary production yielded about 5% of the original oil in place

(OOIP). As a result of the waterflood project, total production will yield an estimated recovery of 20% OOIP.

Summary of Technical Progress

Field Activity

Monument Butte Unit

As of June 30, 1994, the Monument Butte Unit No. 10-34 (project well), which was put on production the last quarter of 1992, had produced 12,325 bbl of oil and 16,320 Mcf of gas and the Monument Butte No. 9-34 (project well), which was drilled and completed in December 1993, had produced a total of 12,002 bbl of oil and 8,757 Mcf of gas. As of Sept. 30, 1994, the Monument Butte Unit production from the inception of the U.S. Department of Energy (DOE) project (October 1992) has increased from 781,095 to 970,672 bbl of oil, or a 189,577 bbl (24%) increase. As of June 30, 1994, total gas production had increased from 2,052,978 to 2,158,385 Mcf of gas, or a 90,903 Mcf (5.1%) increase. As of Sept. 30, 1994, approximately 2.8 million bbl of water has been injected into the unit. Currently, approximately 37,000 bbl of water is being injected on a monthly basis.

Travis Unit

Travis well No. 14a-28 (project well) was completed in the last quarter of 1992. Even though the primary sand target was the Lower Douglas Creek zone, commercial D-sands were identified by the use of advanced logging methods. As the result of the success of well No. 14a-28, well Nos. 14-28 and 10-28 in the Travis Unit were completed in D-sands. Well No. 14a-28 produced 7,953 bbl of oil and 23,045 Mcf of gas before it was converted into a water injection well in October 1993. After recompletion, well No. 14-28 has produced 9,047 bbl of oil and 67,672 Mcf of gas, whereas well No. 10-28 has produced 5,985 bbl of oil and 21,374 Mcf of gas. The cumulative water injection in the Travis Unit as of Sept. 30, 1994, is 579,225 bbl. The total Travis Unit production from the inception of the DOE project (October 1992) has increased from 257,242 bbl to a total of 284,008 bbl of oil as of Sept. 30, 1994, or a 26,766 bbl (10%) increase. As of Sept. 30, 1994, the total gas production has increased from 1,195,570 to 1,303,782 Mcf of gas, or a 108,212 Mcf (9%) increase. Currently, approximately 17,000 bbl of water is being injected on a monthly basis.

Geologic Characterization

The reevaluation of the stratigraphy for the Travis, Monument Butte, and Boundary areas is complete. Most changes involved minor differences in the elevations of unit tops and bottoms. The redefined zones are available for input into reservoir models.

The Lower Douglas Creek sandstones continue to be an area of research interest because of the large quantities of oil

they contain and their unique geologic relationships. The conclusion was reached that these sandstones were deposited by turbidity currents. This conclusion is supported by textures seen in both core and the borehole imaging logs. Depositional sites are probably controlled by fault-bounded troughs. There is a direct relationship between the thickness of the net sandstone reservoirs and the vertical separation of overlying and underlying marker beds. Results of this work were presented in a poster session at the 1994 meeting of the American Association of Petroleum Geologists (AAPG).¹

The imaging logs for the Monument Federal No. 9-34 well have been processed and are ready for detailed analysis with the use of the workstation.

Reservoir Simulations

Detailed reservoir simulations for the Travis Unit continued. The response to the waterflood in Travis has been slower than expected. Hence three different reservoir models were constructed to analyze the ongoing waterflood in Travis: a homogeneous reservoir model with locally adjusted permeabilities; a fractured dual-porosity, dual-permeability model; and a model with hydraulically fractured wells.

The homogeneous model. This model is a variable-thickness, variable-depth model. The reservoir parameters are summarized in Table 1. The D-sands, the Lower Douglas Creek (LDC) sands, and the Castle Peak sands were represented by two benches of sandbodies each. The injection and production field operations were duplicated in the simulations. The primary production match was satisfactory. If water injection in Travis is continued at a rate of 300 stock tank barrels (STB)/d, the model predicts production rates of 67 STB/d of oil from the unit at the end of 1995 and peak production rates of 104 STB/d.

TABLE 1

Homogeneous Reservoir Parameters

Reservoir extent, ft	5300-6300
Grid	5 × 7 × 8
Grid size (x and y), ft	660
Porosity (constant)	0.132
Initial reservoir pressure, psia	2700
Initial bubble-point pressure, psia	2350
Oil gravity, °API	33
Gas gravity	0.77
Initial oil saturation	0.76 to 0.78
Bottomhole pressure, psi	900
Permeabilities, mD	10 to 40

Fractured reservoir model. A description of this model was included in previous quarterly reports and in the yearly report. The dual-porosity, dual-permeability option was used. This model does not permit inclusion of limited fracturing. With continued injection of 300 STB/d, this model predicts peak production rates of 51 STB/d at very high water cuts (>80%).

Hydraulically fractured model. This model was constructed specifically to see if hydraulic fractures were responsible for the waterflood behavior being observed in Travis. The hydraulic fractures were represented by thin, essentially vertical blocks around wells. The widths of the smallest grid blocks were either 0.5 or 1 ft. The block widths were then progressively increased. Permeability of the hydraulically fractured zone was of the order of 100 darcys (D), in contrast to permeabilities of 5 to 10 mD in the surrounding blocks. The reservoir parameters used are summarized in Table 2. In this particular model, the sands (D, LDC, and Castle Peak) were lumped into single sections (to reduce computation time). The peak production rates predicted by this model were only half the rates predicted by the homogeneous model, and the water cuts were higher. This model essentially illustrates that hydraulic fractures could have provided conduits for water channeling in the Travis Unit.

TABLE 2

Hydraulically Fractured Reservoir Parameters

Grid	7 × 53 × 5
Grid size (x and y), ft	varying from 660 to 0.5
Porosity (constant)	0.132
Initial reservoir pressure, psia	2700
Initial bubble-point pressure, psia	2350
Oil gravity, °API	33
Gas gravity	0.77
Initial oil saturation	0.76
Bottomhole pressure, psi	900
Reservoir permeabilities, mD	5 to 10
Hydraulic fracture permeabilities, D	100 to 150

Model comparison. Cumulative oil production results from the three models are compared with the field data in Fig. 1. It is observed that the oil production history match is reasonable for all the models. The cumulative gas production from the field is compared with the model predictions in Fig. 2. Even though the ultimate gas production is well matched by all the models, the rates of gas production over the entire production interval are not well represented. It is theorized that matching gas production in all intervals will require the incorporation of limited fracturing along with more accurate representations of hydraulic fractures. The oil production results from the homogeneous model for well No. 15-28 (which accounted for about 40% of the total field production) are compared with the field results in Fig. 3. Once again, the model performance is reasonable, given its limitations.

Other Work

A preliminary 15-layer reservoir model for the Boundary Unit was constructed. Results will be used to guide the future drilling activity in the unit. A model to assess the effect of

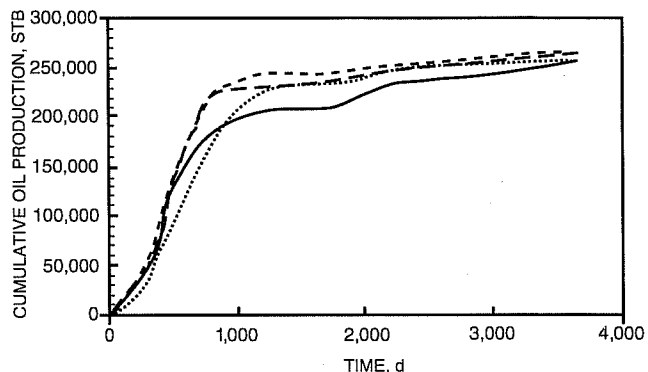


Fig. 1 Comparison of cumulative oil production results from the three models with field data (entire Travis Unit). —, field data. ---, fractured. - · -, homogeneous. ·····, hydraulic fracture.

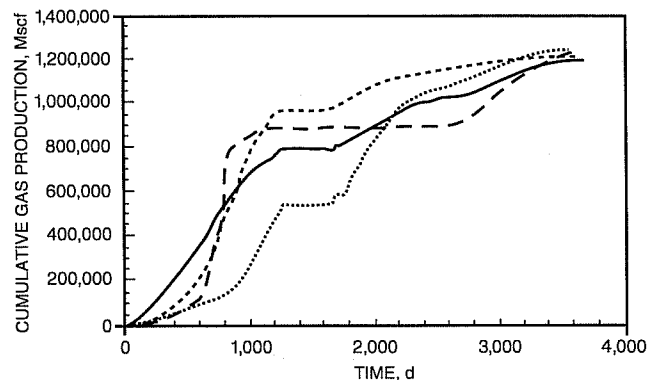


Fig. 2 Comparison of cumulative gas production results from the three models with field data (entire Travis Unit). —, field data. ---, fractured. - · -, homogeneous. ·····, hydraulic fracture.

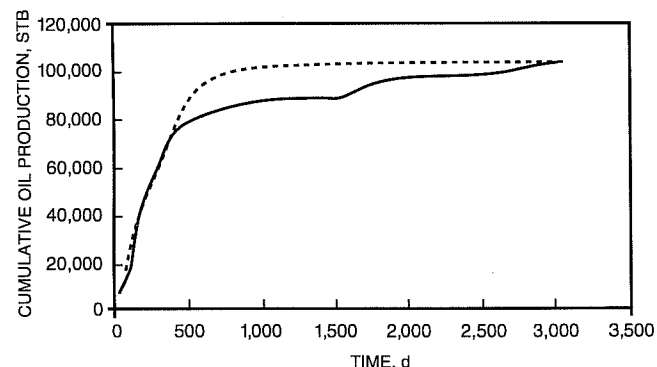


Fig. 3 Comparison of cumulative oil production for well No. 15-28 in the Travis unit with results from the homogeneous model. —, field data. ---, simulations.

paraffin deposition on oil recovery was also completed. Several corefloods were conducted on cores from Travis and Monument Butte in the general-purpose thermodynamic/coreflooding system described previously. The data were used to obtain permeabilities, relative permeabilities, residual saturations, and other rock-fluid properties.

Results of the geologic characterization study on LDC were presented by Lutz et al. at the 1994 AAPG meeting in Denver.¹ The modeling study on the Travis Unit was presented by Deo et al. at the 1994 Society of Petroleum Engineers (SPE) Annual meeting in New Orleans.² A paper on paraffin deposition and its effect on oil recovery has been prepared for presentation at the SPE International Symposium on Oil Field Chemistry in San Antonio in February 1995.³

References

1. S. J. Lutz, D. L. Nielsen, and J. D. Lomax, *Lacustrine Turbidite Deposits in the Lower Portion of the Green River Formation, Monument Butte Field, Uinta Basin, Utah*, paper presented at the American Association of Petroleum Geologists Annual Convention, Denver, Colo., June 12-15, 1994.
2. M. D. Deo, L. A. Neer, E. M. Whitney, D. L. Nielson, J. D. Lomax, and B. I. Pennington, *Description and Performance of a Lacustrine Fractured Reservoir*, paper SPE 28938 presented in the Poster Session of the 69th Society of Petroleum Engineers Annual Meeting, New Orleans, La., September 25-28, 1994.
3. M. D. Deo, *Solids Precipitation in Reservoirs Due to Nonisothermal Injections*, paper SPE 28967 to be presented at the SPE International Symposium on Oil Field Chemistry, San Antonio, Tex., February 1995.

Objective

The overall objective of this project is to integrate research on petroleum reservoir characterization and process monitoring funded by the U.S. Department of Energy (DOE). Specific objectives this quarter include

- Improve the reservoir model by incorporating the new grid.
- Establish carbon dioxide (CO₂) injection into the horizontal well and production from the remaining producers.
- Modify CO₂ injection patterns to allow for optimum CO₂ use by incorporating a standard water-alternating-gas (WAG) injection process if necessary.

Summary of Technical Progress

Production from the Port Neches project has reached a new high of 500 bbl of oil per day (BOPD), as shown in Fig. 1. Changing water and CO₂ injection patterns improved production from several wells. The WAG process appears to be effective in fluvial-dominated deltaic (FDD) reservoirs. The WAG process has improved the oil production rates and simultaneously decreased the CO₂ production rates from wells with high gas/oil ratios (GOR). Material balance calculations indicate that the reservoir pressure remained relatively flat, and a new bottomhole pressure (BHP) will be taken to verify the calculations. Total CO₂ injection is averaging about 9.5 million cubic feet per day (MMCFD), including 3.9 MMCFD purchased from Cardox (Fig. 2), and the balance is recycled from the producing wells. Over 50% of the gas was produced from one well, Kuhn No. 33. A CO₂ injection line was installed to huff 'n' puff well Kuhn No. 6 that did not respond to CO₂ injection in well Kuhn No. 17. After injection of a limited CO₂ volume in well Khun No. 6, a short shut-in period will follow; then the well will be placed on production.

POSTWATERFLOOD CO₂ MISCIBLE FLOOD IN LIGHT OIL, FLUVIAL-DOMINATED DELTAIC RESERVOIR

Contract No. DE-FC22-93BC14960

Texaco Exploration and Production, Inc.
New Orleans, La.

Contract Date: June 1, 1993
Anticipated Completion: Dec. 31, 1997
Government Award: \$3,424,258
(Current year)

Principal Investigator:
Darrel W. Davis

Project Manager:
Chandra Nautiyal
Bartlesville Project Office

Reporting Period: July 1-Sept. 30, 1994

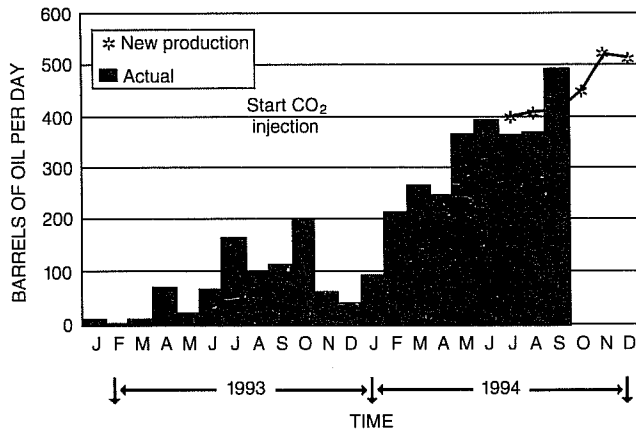


Fig. 1 Port Neches CO₂ Project allocated production.

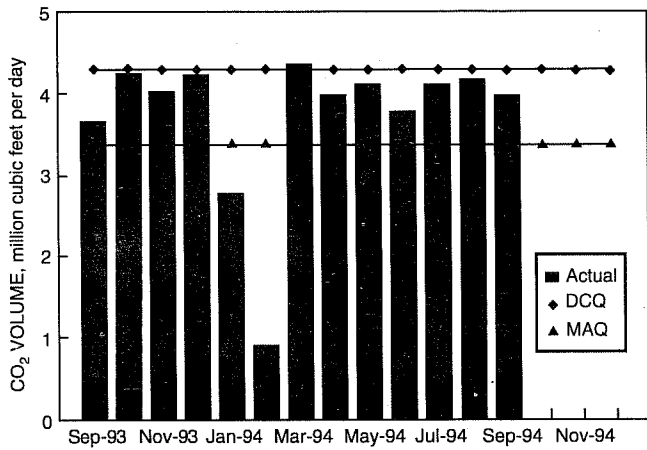


Fig. 2 Port Neches CO₂ delivery (actual vs. contract). DCQ, daily contract quantity. MAQ, minimum annual quantity.

Fourth-Quarter Results

Research in the fourth quarter included altering the injection pattern, monitoring production results, building a strata model, and adjusting the production forecast.

Altering the Injection Pattern

The injection pattern of the CO₂ and water injection wells was altered to allow maximum contact of the reservoir oil to achieve optimum recovery and improve sweep efficiency. In June, wells Kuhn No. 17 and Stark No. 10 were switched to CO₂ and wells Kuhn No. 36 and No. 7 to water injection. Eventually well Marginulina Area No. 1-H was switched to inject water after a nearby well Kuhn No. 33 went to high GOR. The test results indicated that most wells exhibited an increase in oil production and a decrease in CO₂ production; however, some exhibited an increase in water production. Graphs of the daily yields and production for the reservoir and individual wells are shown in Figs. 3–8. The overall results were positive, and the average oil production from the reservoir increased from 400 BOPD to about 500 BOPD during the last month.

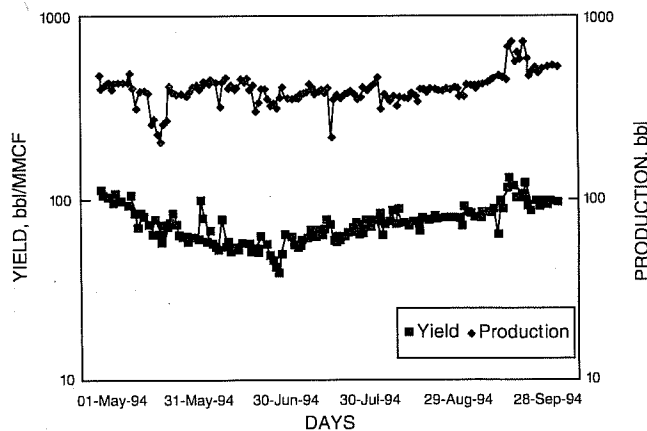


Fig. 3 Port Neches Field reservoir yield and production vs. time.

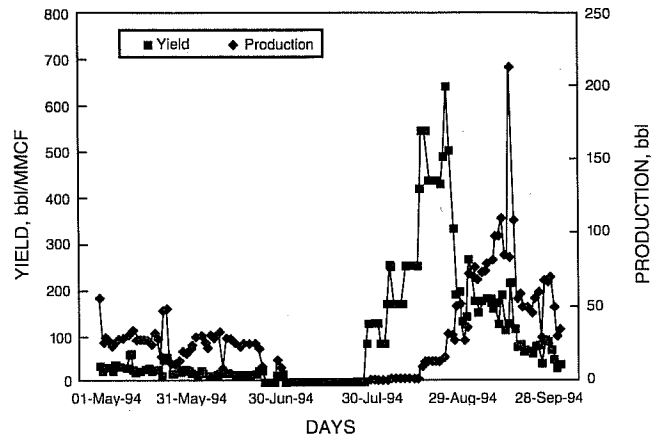


Fig. 4 Port Neches Field well No. 8 yield and production vs. time.

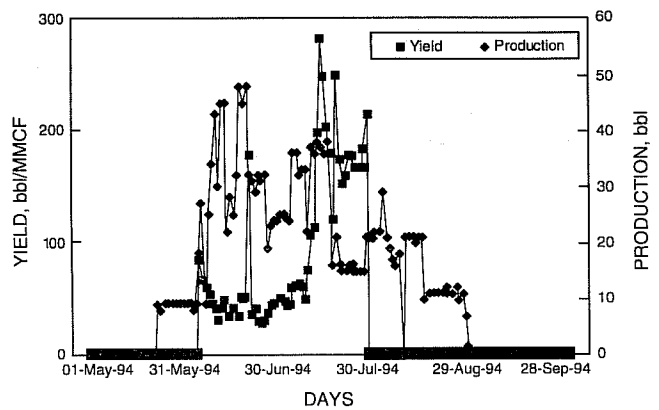


Fig. 5 Port Neches Field well No. 14 yield and production vs. time.

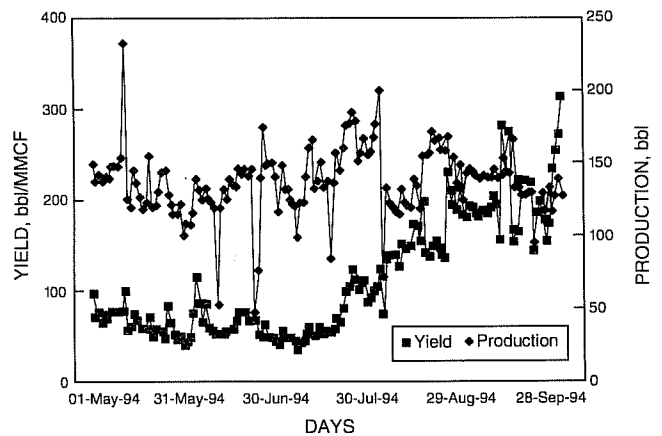


Fig. 6 Port Neches Field well No. 15R yield and production vs. time.

Texaco laid a CO₂ injection line to well Kuhn No. 6 to initiate a huff 'n' puff cycle affecting the part of the reservoir that has not responded to CO₂. CO₂ injection to stimulate the near-wellbore area will begin soon, and the well will be placed on production until a full flooding program is initiated in this part of the reservoir next year.

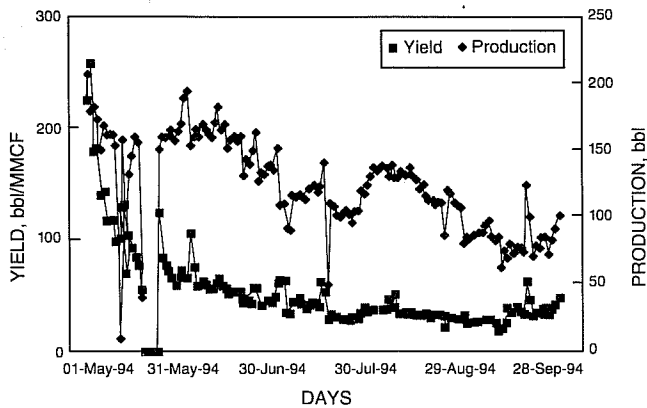


Fig. 7 Port Neches Field well No. 33 yield and production vs. time.

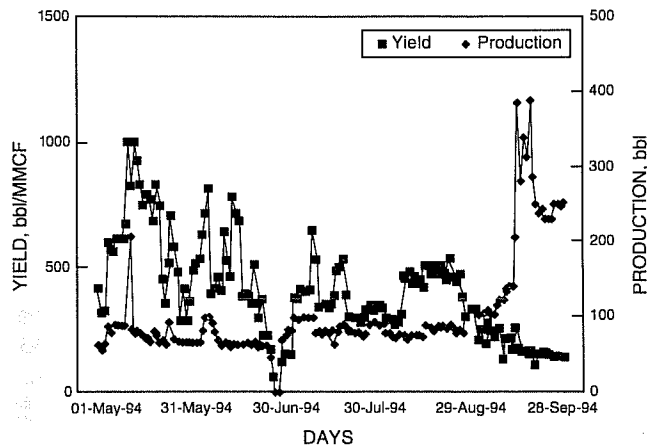


Fig. 8 Port Neches Field well No. 38 yield and production vs. time.

Monitoring Production Results

Production response, reservoir pressure, oil and gas analysis, water injection, and radioactive tracers were monitored to optimize production and to build a more effective reservoir model.

Table 1 lists results of the most recent well tests performed on October 10, 1994, for all the producing and injection wells.

Table 2 lists the average injection and production volumes for this quarter.

The reservoir pressure was not measured during this quarter. Texaco is planning to run a BHP test in October to verify the estimated value of 2900 psi obtained from material balance calculations. The radioactive tracer has not been detected in any of the producing wells. If the tracer cannot be detected during the next 6 months, the monitoring will be discontinued. The water injection volume almost doubled after the recent installation of a new pump; the injection capacity increased by about 1200 BWPD. Additional capacity will be available next year after a disposal facility has been installed for the water produced throughout the field.

Building a Strata Model

The building of a detailed strata model to use in the development of the improved compositional model has been delayed. At this stage the strata model can be used as an input to the reservoir simulator. The strata model incorporates data from well logs, cores, and three-dimensional (3-D) seismic surveys.

TABLE 1

Well Test Results*

Well No.	BOPD	BWPD	MMCFD	Choke	TBG	PSI
Producing wells						
Kuhn No. 15R	125	706	562	18	790	
Kuhn No. 38	252	447	2338	18	1250	
Kuhn No. 33	73	737	1612	18	1160	
Stark No. 8	89	335	1026	26	1026	
Kuhn No. 6	0	330	2	40	100	
Kuhn No. 14	0	430	210	30	75	
Polk No. B5	0	0	0	-	-	
Injection wells						
Marginulina Area No. 1H		1280				400
Kuhn No. 36		922				1530
Stark No. 7		1247				1530
Kuhn No. 17			5227			1400
Stark No. 10			4668			1350

*BOPD, barrels of oil per day; BWPD, barrels of water per day; MMCFD, million cubic feet per day; TBG, tubing pressure (psi); PSI, pounds per square inch.

TABLE 2

Average Injection and Production Volumes*

Oil production	411	BOPD
Water production	3129	BWPD
Gas production	5367	MMCFD
Water injection	2032	BWPD
Gas injection	8986	MMCFD
Reservoir voidage	502	BPD

*BOPD, barrels of oil per day; BWPD, barrels of water per day; MMCFD, million cubic feet per day; BPD, barrels per day.

Adjusting the Production Forecast

The production forecast will be adjusted, if necessary, on the basis actual of reservoir performance. The current reservoir performance closely matches the original forecast submitted to DOE with the project management plan (PMP). This trend will likely continue for the next 6 months. Production from Area 2 is critical in order to continue matching the original forecast. Any changes in the program as to the number of injectors or producers may affect the recovery rate without affecting the ultimate tertiary reserves. Additional information from 3-D seismic data is being evaluated to decide the direction that will be followed in the development of the remainder of Area 2 of this project.

Discussion of Results

Field Operations

The estimated reservoir pressure from material balance remained relatively flat at about 2900 psi, as illustrated in Figs. 9 and 10. Thus the improved reservoir performance (from an average 400 to 500 BOPD) was mainly attributed to the implementation of the WAG process. Further improvement is anticipated by reversing the WAG cycle. Also, the implementation of the huff 'n' puff process in well Kuhn No. 6 will improve the overall reservoir performance.

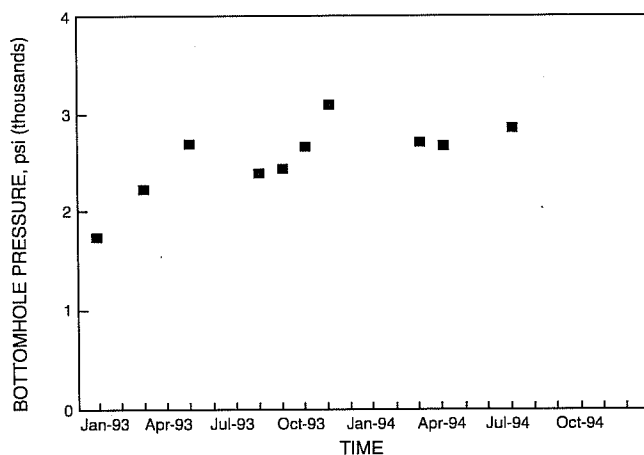


Fig. 9 Port Neches Field reservoir pressure.

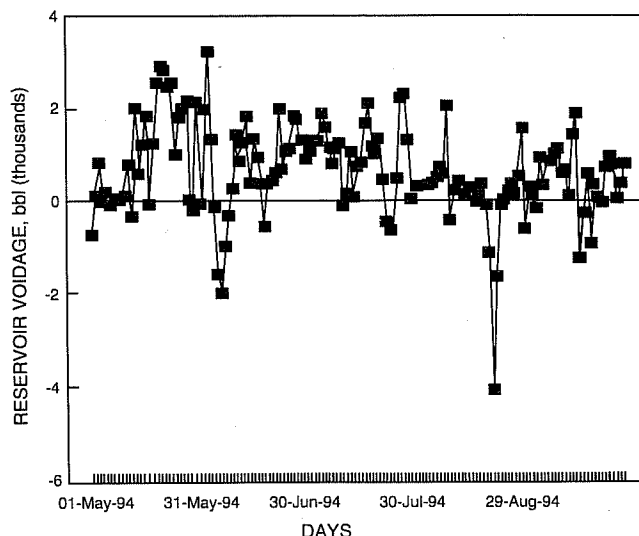


Fig. 10 Port Neches Field reservoir voidage.

Technology Transfer

Science Applications International Corporation (SAIC) has finalized the Environmental Constrain Topical Report for transmittal to DOE in November. Louisiana State University (LSU) is preparing information on FDD reservoirs in the Gulf Coast area. Texaco is planning to meet with LSU personnel to evaluate the progress of the work under way and to plan 1995 objectives.

IMPROVED OIL RECOVERY IN FLUVIAL-DOMINATED DELTAIC RESERVOIRS OF KANSAS—NEAR TERM

Contract No. DE-FC22-93BC14957

**University of Kansas
Lawrence, Kans.**

**Contract Date: June 18, 1993
Anticipated Completion: Dec. 31, 1998
Government Award: \$2,007,450**

**Principal Investigators:
Don W. Green
G. Paul Willhite**

**Project Manager:
Rhonda Lindsey
Bartlesville Project Office**

Reporting Period: July 1–Sept. 30, 1994

Objective

The objective of this project is to address waterflood problems of the type found in Cherokee Group reservoirs in southeastern Kansas and in Morrow sandstone reservoirs in southwestern Kansas. Two demonstration sites operated by different independent oil operators are involved in the project. The Nelson Lease (an existing waterflood), located in Allen County, Kans., in the northeastern Savonburg field, is operated by James E. Russell Petroleum, Inc. The Stewart field (on latter stage of primary production), located in Finney County, Kans., is operated by Sharon Resources, Inc.

General topics to be addressed will be reservoir management and performance evaluation, waterflood optimization, and the demonstration of recovery processes involving off-the-shelf technologies that can be used to enhance waterflood recovery, increase reserves, and reduce the abandonment rate of these reservoir types.

The reservoir management portion of the project will involve performance evaluation and will include such work as reservoir characterization and the development of a reservoir database, identification of operational problems, identification of near-wellbore problems, identification of unrecovered mobile oil and estimation of recovery factors, and identification of the most efficient and economical recovery process. The waterflood optimization portion of the project involves only the Nelson Lease. Optimization will be based on the performance evaluation and will involve design and implementation of a water cleanup system for the waterflood, application of well remedial work such as polymer gel treatments to improve vertical sweep efficiency, and changes in waterflood patterns to increase sweep efficiency. Finally, plans are to implement an improved recovery process, possibly polymer-augmented waterflooding, on both field demonstration sites.

Summary of Technical Progress

Savonburg Field Project

Engineering and Geological Analysis

The computer database has been continually revised with new net and gross picks from core analysis for the two productive sandstones identified as B2 and B3. The black non-productive sandstone was identified and selective non-productive intervals determined. Draft cross sections have been modified on the field. The productive sandstones B2 and B3 have been revised and new maps made.

Water Plant Development

The air flotation unit has been a priority. Tertiary Oil Recovery Project (TORP) and field personnel continuously worked out problems that have plagued the project: changes in water chemistry on the produced side, method of adding cationic chemical to air flotation unit, and achieving steady-state conditions.

Pattern Changes and Well Bore Cleanup

Recommendations were made on the basis of zone potential. From examination of the geological report, zone B-3 was found to be of better quality and higher potential than zone B-2. As a result, work was conducted to better produce Zone B-3. Once this work is implemented, recommendations will be made to better produce Zone B-2. Producing wells have been worked over with the use of fishing tools and jetting with water, acid, and solvents. Each producing well has been placed on production after the workover, and the wells are being monitored. Well workovers included the following:

H-5, found T.D. and cleaned with foam and modified acid.
H-21, found T.D. and cleaned with foam and modified acid.
K-44, found T.D. and cleaned with foam and modified acid.
O-1, found T.D. and cleaned with water and modified acid.
H-9, found T.D. and cleaned with water and modified acid.
K-54, found T.D. and cleaned with water and modified acid.
H-22, found T.D. and cleaned with water and modified acid.

RW-8, gel polymer treatment to plug the upper shale and cleanup with acid and foam; injectivity has been monitored.

KW-51, one-inch tubing has been placed in pipe and injection will be monitored after a proper cleanup has been implemented; the matrix acid treatment has been recommended.

RW-6, a gel polymer treatment has been implemented.

Additional pattern changes will be considered on the basis of identified mobile oil saturation. New injection lines will be placed to converted injection wells, and pumping units will be placed on converted production wells. Wells exhibiting skin problems will be cleaned with appropriate methods. Treatments will be designed on the basis of the problem(s) identified.

Field Operations

Normal field operations have included monitoring wells on a daily basis; repairing water plant, piping, and wells as required; collecting daily rate and pressure data; and solving any other daily field operational problem that might occur. Production statistics are summarized in Table 1.

TABLE 1

Savonburg Field Oil Production

Month	Oil production, BOPD
October 1993	26.4
November 1993	30.7
December 1993	32.0
January 1994	30.8
February 1994	30.9
March 1994	30.3
April 1994	29.1
May 1994	28.5
June 1994	30.3
July 1994	28.9
August 1994	24.6

Stewart Field Project

Engineering and Geological Analysis

The two independent three-dimensional (3-D) simulation studies undertaken by Sharon Resources, Inc., and the University of Kansas have been completed. Some minor corrections to the University of Kansas model are being made to adjust the amount of original-oil-in-place (OOIP) present in the reservoir.

Cost estimates of waterflood investments have been prepared for the purpose of determining a pattern that will optimize net present value. Higher injection volumes will recover secondary reserves sooner, but at a higher capital and operating cost. Price quotes were obtained from supply companies to approximate total costs. Economic analyses were run on all the waterflood patterns investigated in the simulation study. Economics were run based on 100% working interest with an 80% net revenue interest. The price of oil was held constant at \$18.00/bbl. The lease operating expenses were \$1600/month/well for the life of the project. Economics were run using 6-month time units instead of yearly production to more accurately reflect

discounting of future production back to the initial time of investment. When the production profile was subjected to the assumptions of the economic analysis, it was determined that some of the waterflood production is below the economic limit. Therefore, the analysis was conducted on economic reserves. Sensitivity analysis to oil price was also investigated on economic reserves. The net present value of the economic reserves was conducted for discount rates of 10 and 40%.

Laboratory Testing

All laboratory testing work associated with this task has been completed.

Unitization

Regular meetings and correspondence have taken place between the technical committee members and Working Interest Owners (WIO). The proposed Unit Agreement and Unit Operating Agreement has continued to be negotiated between WIOs. Negotiations concerning the selection of the Unit Operator have continued. Equity issues necessary for unitization continue to be debated.

INTEGRATED APPROACH TOWARD THE APPLICATION OF HORIZONTAL WELLS TO IMPROVE WATERFLOODING PERFORMANCE

Contract No. DE-FC22-93BC14951

**University of Tulsa
Tulsa, Okla.**

**Contract Date: Jan. 1, 1993
Anticipated Completion: Dec. 31, 1996
Government Award: \$250,973**

**Principal Investigator:
Balmohan G. Kelkar**

**Project Manager:
Rhonda Lindsey
Bartlesville Project Office**

Reporting Period: July 1–Sept. 30, 1994

Objective

The overall objective of the project is to improve secondary recovery performance of a marginal oil field through the use of a horizontal injection well. The location and direction of the well will be selected on the basis of the detailed reservoir description using an integrated approach. With the use of this method, a recovery of 2 to 5% of original oil in place (OOIP) is expected. This should extend the life of the reservoir by at least 10 yr.

The project is divided into two stages in order to accomplish its goals. In Stage I part of the Glenn Pool field (William B. Self Unit) will be selected and additional reservoir data will be collected by conducting cross-borehole tomography surveys and formation microscanner logs through the newly drilled well. Analogous outcrop data will also be used. The state-of-the-art data combined with conventional core and log data will be used to develop a detailed reservoir description. After extensive reservoir simulation studies are conducted, location and direction of a horizontal injection well will be selected. The well will be drilled on the basis of optimized design, and the field performance will be monitored for at least 6 mo. If the performance is encouraging, the second budget period of the project will begin.

Stage II, the second budget period of the project, will involve selection of part of the same reservoir (Berryhill Unit, Tract 7), development of reservoir description with the use of only conventional data, simulation of flow performance with the use of a developed reservoir description, selection of a location and direction of a horizontal injection well, and implementation of the well followed by monitoring of reservoir performance.

Comparison of the results during two budget periods will allow evaluation of the usefulness of collecting additional data with state-of-the-art technology. The application of horizontal wells in improving secondary recovery performance of marginal oil fields can also be evaluated.

Successful completion of this project will provide new means of extending the life of marginal oil fields using readily available technology. A methodology to integrate various qualities and quantities of measured data to develop a detailed reservoir description will also be presented.

Summary of Technical Progress

The overall report is divided into three sections. In the first section, the new results on the basis of the cross-borehole seismic surveys are discussed. In the second section, the geological description of the Self Unit based on formation microscanner imaging (FMI) analysis is discussed. In the last section, the flow simulation results under different scenarios followed by economic evaluation are presented. On the basis of economic evaluation, it is believed that drilling a horizontal injection well may not be a viable option under the present oil price scenario.

Geophysical Data Collection

A prestack migration algorithm has been applied to the Glenn Pool cross-well data. The method is used to image scatterers in the subsurface. All available digital wireline log data from well No. 82 have been transferred to the Apollo workstations. A program has been developed to extract log data for a given depth interval for synthetic seismogram generation. The deviation survey data were incorporated into the BOMTOM (Bureau of Mines TOMography) input file. However, the resulting tomograms are not available at the present time.

Seismic activity in the Glenn Pool field, Self Unit, has continued during the third quarter of 1994. A zero-offset vertical seismic profile (VSP) and a two-dimensional (2-D) seismic line were shot. These data were acquired to no cost to the project. Nonetheless, the data are valuable in supporting the preliminary results from other reservoir description techniques (i.e., geological, engineering).

A finite difference wavefield propagation code was tested on a simple layer-cake velocity model. Tomogram velocities will be used as input to the code to observe wave propagation in the interwell area, as a forward modeling study.

Cross-Well Seismic Data Migration

Seismic data from three cross-well surveys (63→82, 82→64, 81→82) were migrated using the method of Liner and Lines.¹ The prestack migration, which assumes constant velocity distribution, provided promising results. A detailed discussion on the method together with synthetic and real data examples can be found in the original paper.

The production from cross-well tomography is a distribution of seismic velocities between the survey wells. Migration methods image the reflectors by using these velocities. Migration in general is defined as "an inversion operation involving rearrangement of seismic information elements such that reflections and diffractions are plotted at their true locations."²

Figure 1 shows an overlay of velocity tomogram and migration result for the 82→81 survey. Seismic reflectors associated with areas of strong vertical velocity gradient are expected to be seen. The migrated traces are in close agreement with the velocity tomogram in defining the reflectors.

Wireline Logs and Synthetic Seismograms

A complete suite of wireline logs from well No. 82 is available in digital format. The data have been transferred to the Department of Geosciences Apollo workstation network for analysis. A program is made to view any log by inputting the desired depth interval. The program was designed primarily to generate synthetic seismograms from sonic and density logs. First, the reflection coefficients are calculated using the relationship

$$RC = \frac{\rho_{i+1}V_{i+1} - \rho_iV_i}{\rho_{i+1}V_{i+1} + \rho_iV_i}$$

where ρ is density (gr/cc) from density log and V is P-wave velocity (ft/s) = 1,000,000/slowness (ms/ft).

These reflection coefficients are then placed along an axis corresponding to vertical two-way travel time. Finally, the reflection coefficients are convolved with a wavelet to generate the synthetic seismogram. Figure 2 shows an overlay of gamma ray log, sonic log, and synthetic seismogram on a velocity plot from well No. 82.

Deviation Survey

A deviation survey for all four wells (82, 63, 64, 81) was completed in the first quarter 1994. The data are important for highly deviated wells, since cross-well tomography uses source-receiver coordinates in the borehole to calculate ray paths. Velocities are obtained by inverting travel times, which are related to ray paths. Therefore, the deviation may be critical in tomography where the borehole is significantly curved.

The deviation data consist of horizontal offset of a subsurface point toward North (or South) and East (or West) with respect to the wellhead coordinates. The values are gathered at a 50-ft depth step. Since the sources and the receivers were moved at 8-ft intervals for the cross-well acquisition, the deviation values were interpolated to an 8-ft spacing. A separate program was run to transfer those values into a format acceptable by BOMTOM. Velocity tomograms resulting from the deviation-incorporated BOMTOM input are not available at this time.

Other Geophysical Activity

A zero-offset VSP and a 2-D seismic survey were conducted in August 1994. Amoco's three-component downhole receiver was used for the VSP survey. The data acquisition was at no cost to the project and represents additional information for the current reservoir imaging studies. The data were initially processed at Mercury International Technologies, Tulsa. The data are available on 8-mm digital tape but have not yet been transferred to the Apollo.

Geophysical modeling studies continued in this quarter. A finite difference wavefield propagation code³ was tested on a horizontally layered velocity model. The code generates a

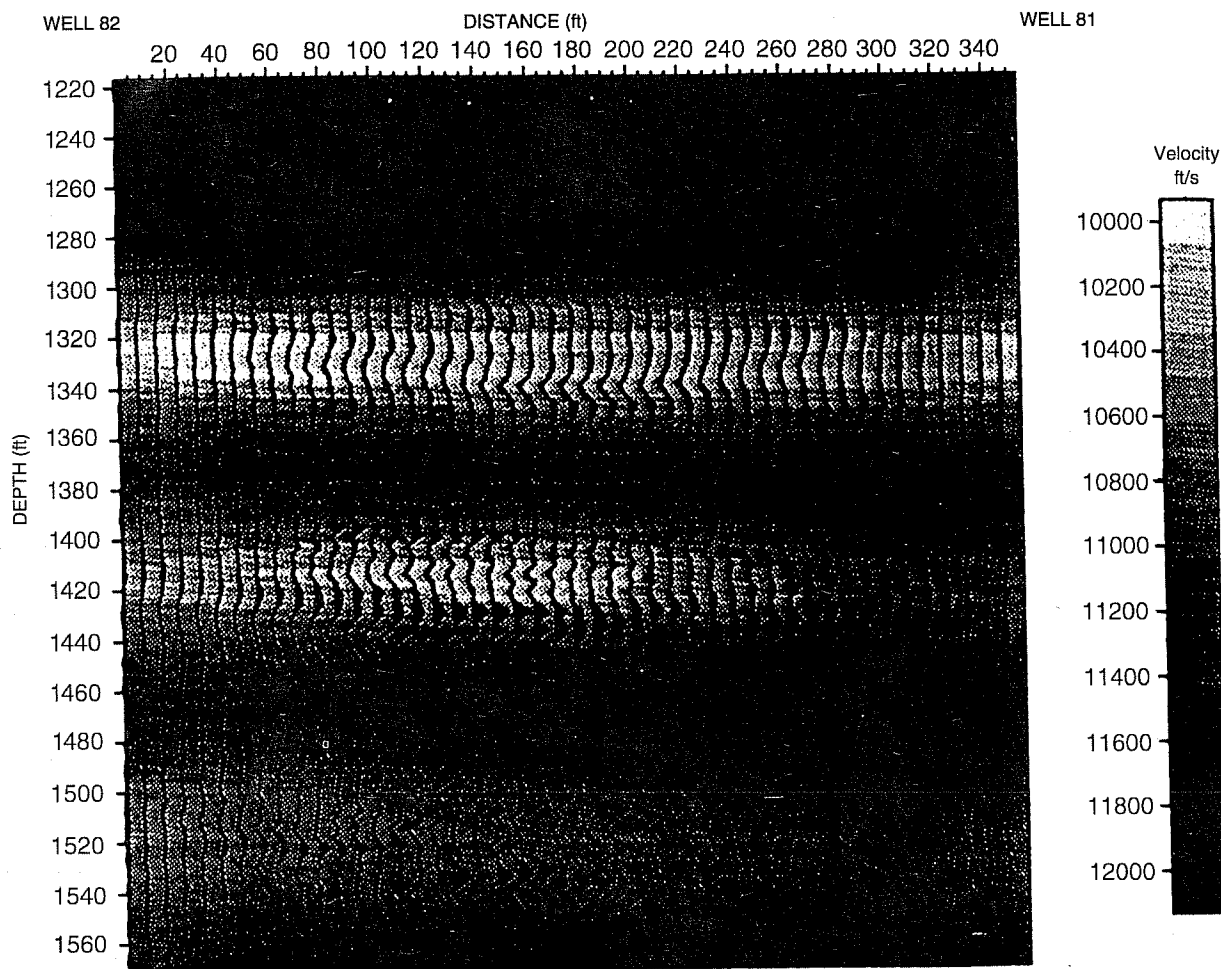


Fig. 1 82 → 81 Survey: velocity and migration overlay. (Art reproduced from best available copy.)

plane wave from the source well and displays snapshots of the propagating wavefield at specified time intervals. The code and accompanying Seismic Unix shell programs are under modification for future use. The tomograms will be input as velocity models for forward modeling. In this way synthetic data can be generated for direct comparison with common-level gathers in the field data. If the velocity field (derived by tomography) is consistent with the field data, then modeled first arrivals should coincide with observed first arrivals.

Interpretation of the initial tomograms is in progress. Work toward establishing a velocity–porosity relationship for the reservoir rocks will begin soon. The analysis has been awaiting core plug velocity measurements.

Geological Description

Refinements of the facies interpretation and reservoir architecture were achieved through FMI analysis (Self No. 82 well) and core and log facies studies. The results show that discrete genetic intervals (DGI) A through E are regarded as delta plain fluvial channel-fill and crevasse splay sandstones and interdistributary mudstones, and F as channel-mouth bar sandstone. At the location of well Self No. 82, DGI C is lateral

accretion bar deposits, DGI D is divided into four splay units, and DGI E is divided into two splay units. Detailed architecture and spatial distribution for each of these units are developed.

According to detailed well log correlation results, a set of new version shale maps has been developed that indicates that DGIs A and B and B and C are very well separated, but the vertical connectiveness between C and D, D and E, and especially E and F is not negligible. High-resolution structure maps constructed for top Inola marker and top DGI D sandstone show that there are local highs and local lows superimposed on the general southeasterly dipping.

Analysis of lab core measurements has shown that the porosity and permeability are strongly DGI related. Descending from DGIs A to F, porosity increases from about 8% to about 22%, and permeability increases from less than 0.1 mD to more than 300 mD.

On August 18, 1994, expert participants from petroleum geology, geophysics, and petroleum engineering gathered at the Amoco Core Facility. A poster exhibition on achievements and progress of the project was given in August 1994 in the University of Tulsa Department of Petroleum Engineering. An expanding study out of the Self Unit using the log and core data is under investigation.

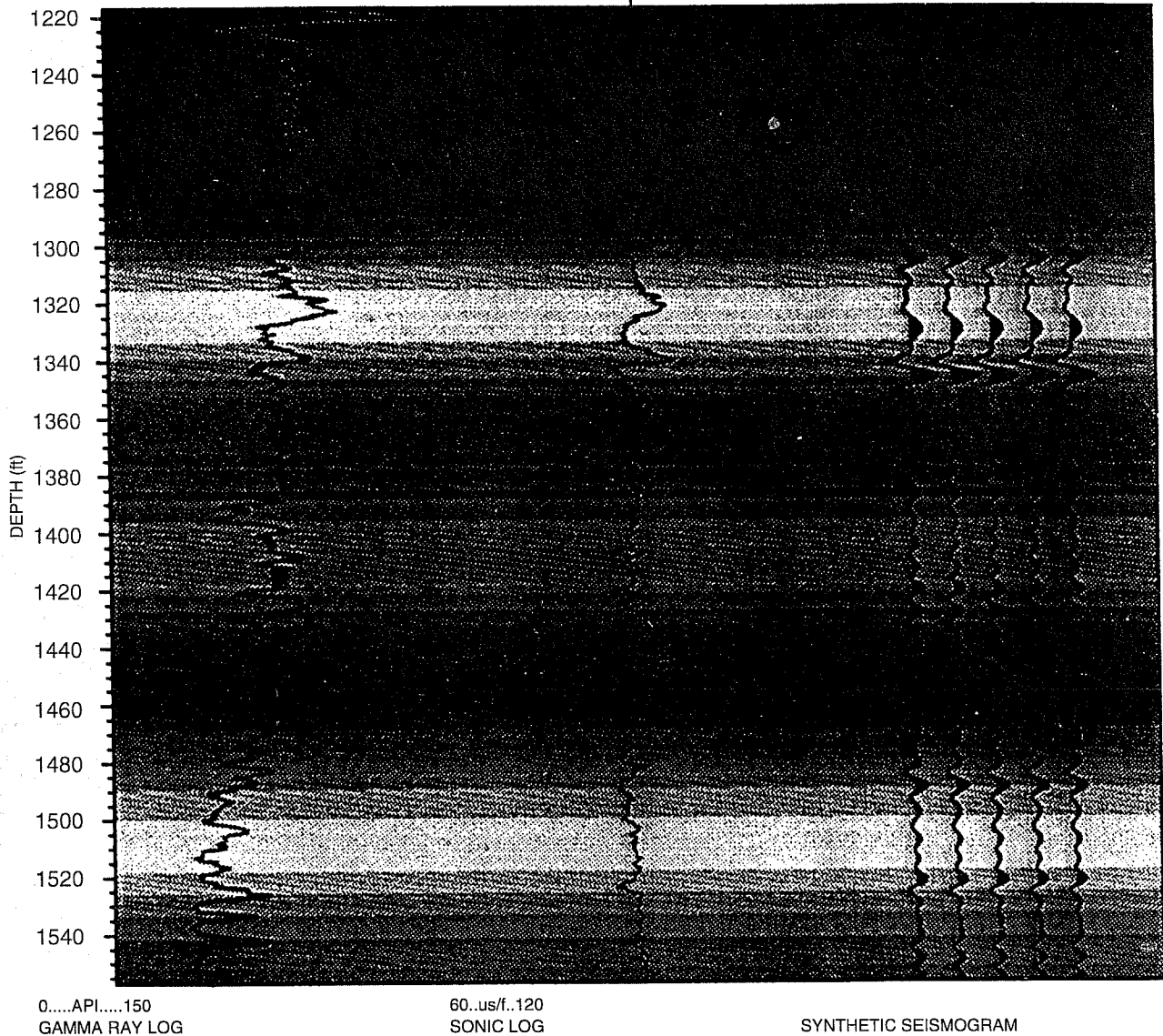


Fig. 2 Well 82 P-wave velocity and well log overlay. (Art reproduced from best available copy.)

Facies Interpretation

Facies distribution has a very important bearing on the issue of reservoir compartmentalization. Oil in the reservoir can be trapped by the contact surfaces between different facies units and hence bypassed by the waterflooding. Facies-subfacies distribution for the whole Self Unit and vicinity has been refined as a result of the detailed correlation and log facies study of all 50 wells in the unit (Fig. 3). In DGIs A through E, facies include channel-fill sandstone, splay sandstone, and interdistributary mudstone. Throughout the whole unit, DGI F is regarded as channel-mouth bar sandstone.

Detailed Architecture

On the basis of the findings from the advanced information collected in Self No. 82 well, detailed facies architec-

ture, especially for DGIs C, D, and E, has been constructed for the immediate vicinity of this well. This detail provides an accurate assessment of the level of heterogeneity for each facies/subfacies and is very useful for developing a reservoir management plan for the Self Unit.

At the location of Self No. 82, DGI C is dominated by subaqueous dune deposits of the lower channel-fill subfacies and lateral accretion bar deposits of the middle channel-fill subfacies. The angle of dip azimuth between cross-strata (121°) and lateral accretion surface (150°) indicates a downstream location. Lateral accretion surface dip azimuth shows progressive upward rotation from 200 to 146° . Lateral accretion surface spacing is averaged at 1.08 ft, and the dip angle is averaged at 4.4° . On the basis of this information, and with the help of net sand isopach and net/gross ratio map, it is inferred that 19 lateral accretion mudstone drapes are present between Self No. 82 and No. 81, and the exact spatial

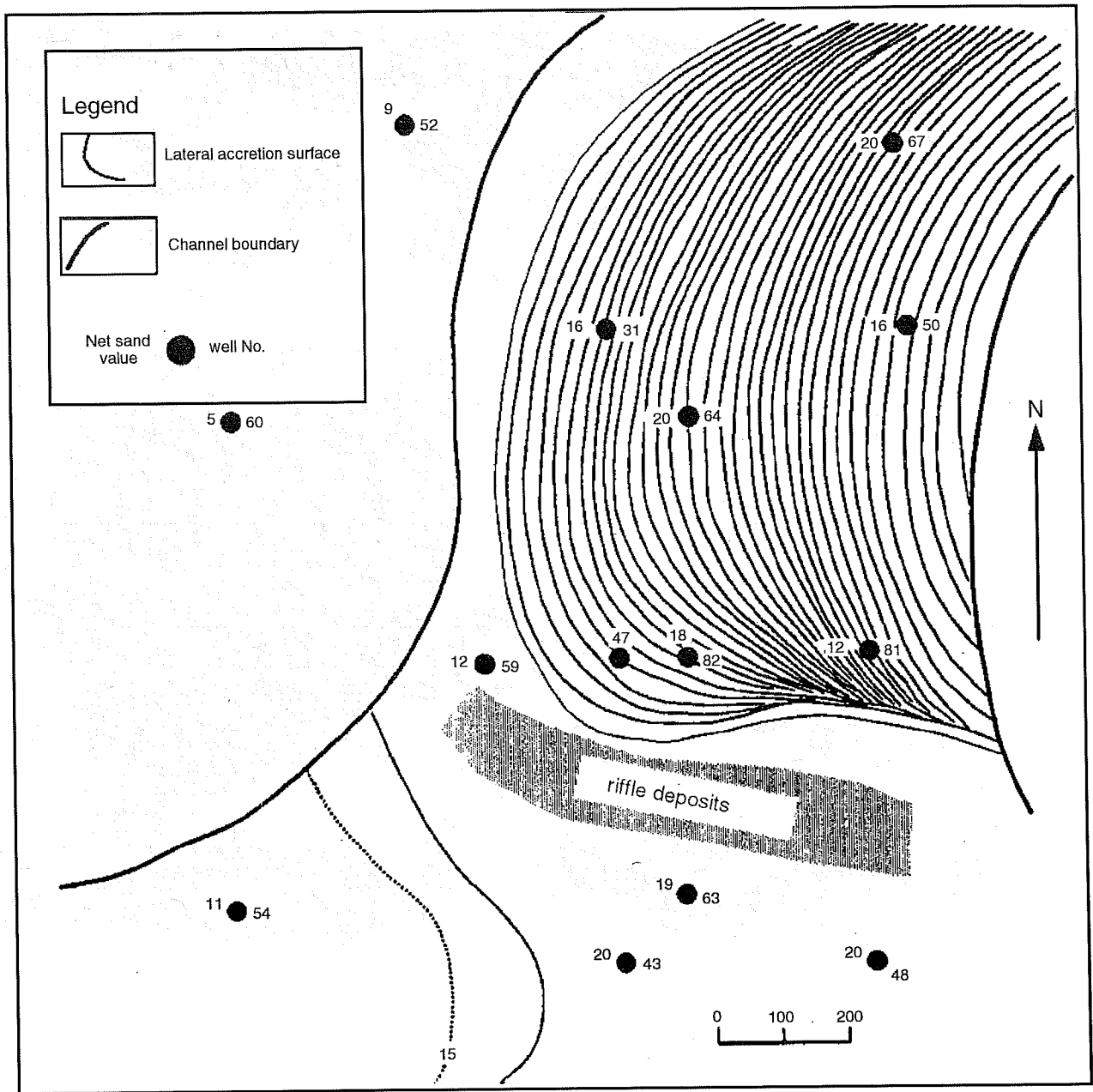


Fig. 3 Detailed reservoir architecture for the point-bar deposits in the vicinity of Self No. 82, Unit C.

configuration of lateral accretion surfaces for these point-bar deposits is known (Fig. 4).

DGIs D and E are composed of splay deposits at the location of Self No. 82. They are divided into four splay units and two splay units respectively (Fig. 5). Formation microscanner imaging (FMI) analysis indicates that dispersal orientations for these six units are, in descending order, 120°, 315°, 70°, 210°, 180°, and 30°, respectively. With this information and through detailed log correlation among surrounding wells, the spatial distribution for each unit is exactly located.

For DGIs A and B, at the location of Self No. 82 well, the foreset direction is the same as the mud drape direction,

indicating that DGIs A and B here are not made of lateral accretion bar but normal channel-fill deposits. DGI F does not show much orientation information because of its massive structure.

Shale Maps

The shale maps constructed in 1993 have been refined as a result of a new correlation scheme to delineate the vertical connection between different DGIs. The following points summarize the results.

- DGIs A and B are totally separated by 3- to 6-ft-thick shale.

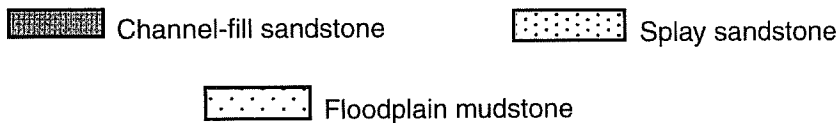
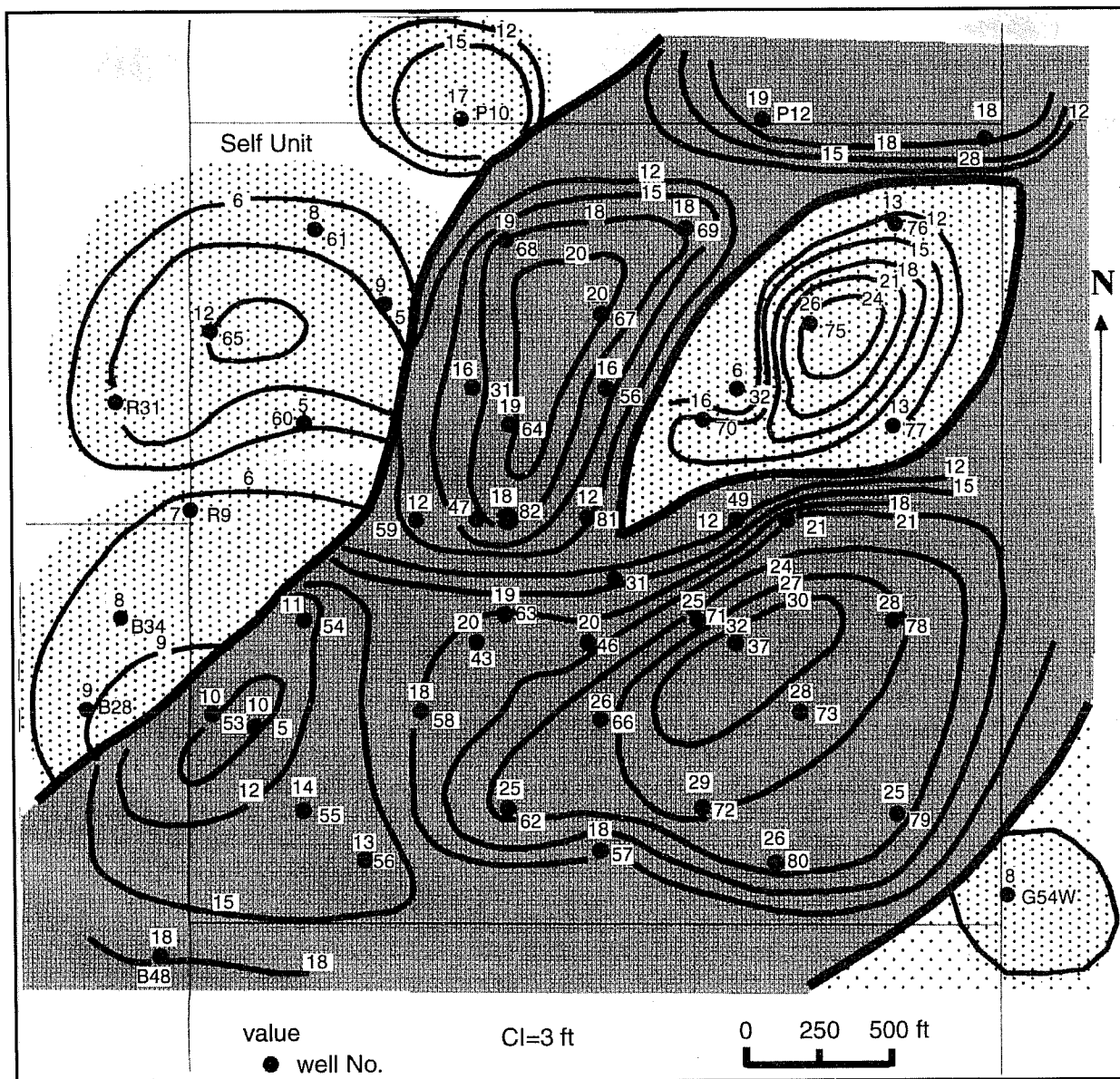


Fig. 4 Glenn Sand Unit C net sand isopach and facies map.

- DGIs B and C are well separated generally, except at locations of four wells (about 10% of the area), where they are directly contacted vertically.

- Between DGIs C and D, and D and E, the connection becomes better; in about 10–15% of the Self Unit there is no shale between them. Both cases have seven wells with zero shale thickness.

- Between DGIs E and F, the connection becomes even more extensive. There are 16 wells (about 40% of the area) with zero shale thickness and seven other wells with only 1-ft-thick shale.

Structure Map

High-resolution structure maps for the top Inola marker bed and top DGI D sandstone were constructed. Both of these maps show that Glenn Sand generally dips in a southeasterly direction about 3–5 degrees. Superimposed on this general trend are local highs and local lows. For example, at the top of DGI D, well Nos. 81, 76, 77, 56, and 62 fall in local highs with about 10–15-ft relief above the general trend, whereas well Nos. 37, 72, 75, 53, and P12 fall in local low area with 10–20-ft relief below the general trend (Fig. 6).

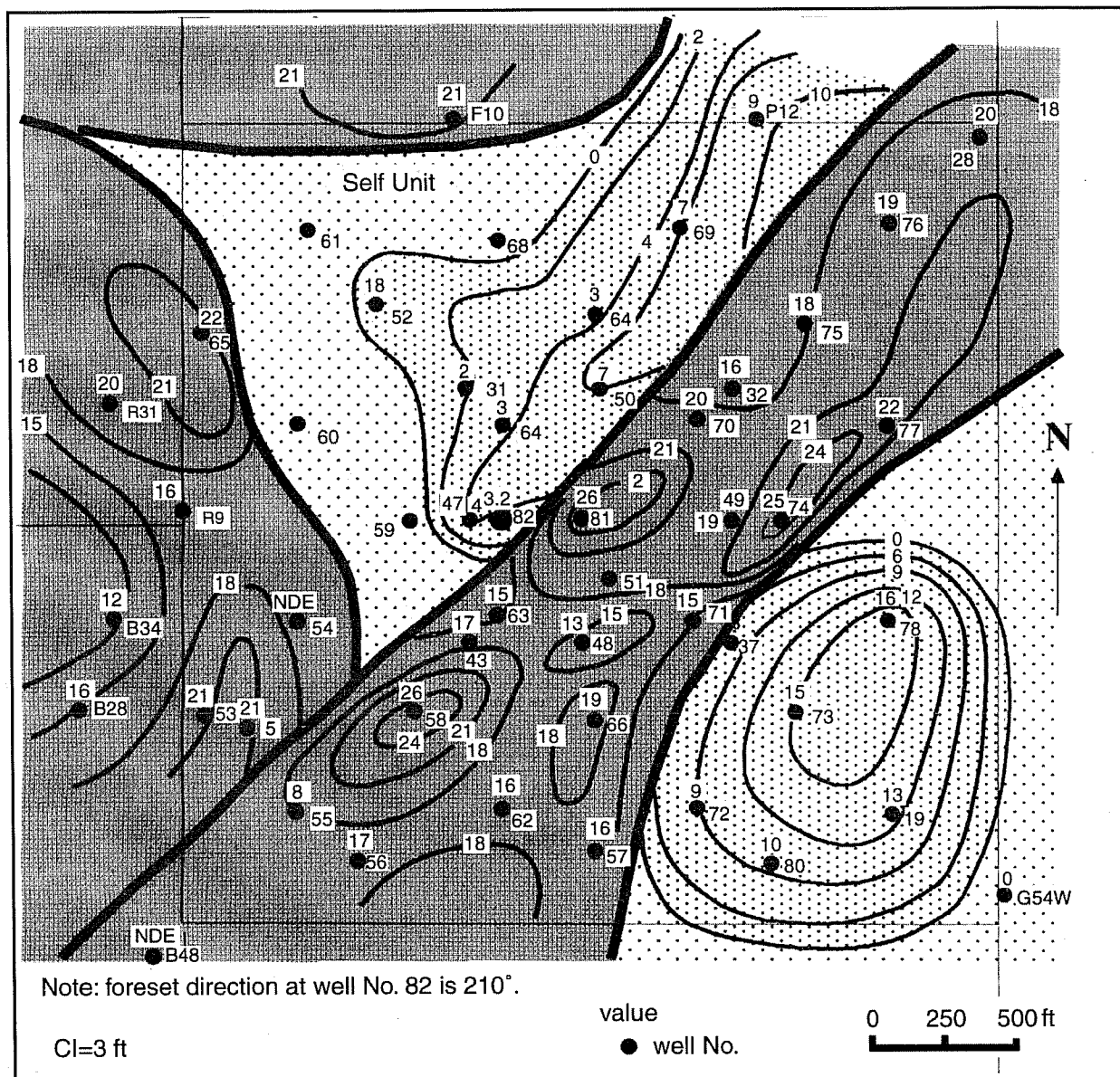


Fig. 5 Unit D No. 1 splay in the vicinity of Self No. 82 as interpreted from formation microscanner imaging (FMI) data.

This information should be useful for analyzing oil-water distribution.

Engineering Description and Simulation

The bases for improvement in reservoir management for the Self Unit comprise flow simulation and economic analysis for future production. The flow simulation was based on the reservoir description reported. The future production estimate is derived from conducted flow simulation until

the year 2000, and the increase of production relative to the current condition is evaluated. The simulation matches the past history of oil production, and the saturation is validated by the log measurement of well No. 82. Three different cases (1, 2, and 3) are used in the simulation to compensate for the uncertainty of the data. The definition of each case is presented in Table 1. For each case three different scenarios are simulated: no additional well/current field configuration, drilling horizontal wells, and drilling extra vertical wells.

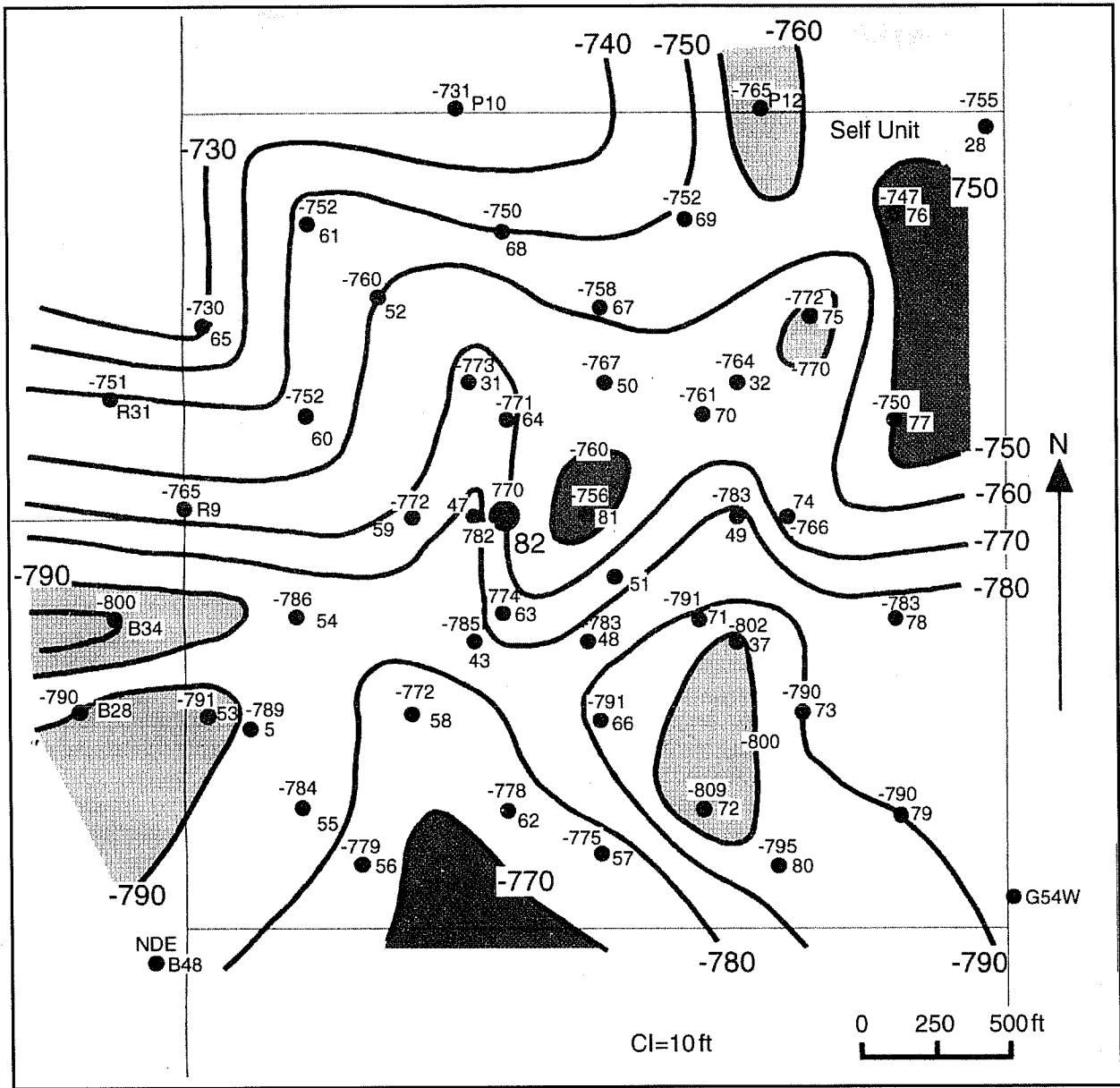


Fig. 6 Structure map top Unit D sandstone.

TABLE 1

Definition of Cases Used in the Flow Simulation and Economic Evaluation

Case 1	Uniform relative permeability, Uniform initial water saturation [S_{wi} (initial water saturation) = S_{wr} (residual water saturation)]
Case 2	Modified relative permeability (modification 1) Variable initial water saturation (modification 1)
Case 3	Modified relative permeability (modification 2) Variable initial water saturation (modification 2)

For every scenario several possibilities related to the well completion and the amount of water injected are simulated. From the core and FMI studies, as well as the flow simulation results, it was determined that the best potential for future production is from DGIs C, D, and E. However, it is observed that only 33 and 11% of DGIs D and E, respectively, had been open for production. Even though DGI C is a good candidate for future production, the permeability is lower in this unit compared to the other two units, D and E, and it has been opened within most of the unit. Thus, it is anticipated that by opening DGIs D and E, production will increase.

Oil production in 1993 showed an increase of 38% from 21 bbl of oil per day (BOPD) to 29 BOPD when the field was flooded with a 125% higher injection rate compared to 1992. This suggests that the field gives a good response to the amount of water injected. Thus, it is hoped that by increasing the water injection rate, production will increase.

The economic analysis is conducted for several selected scenarios that would give the best increase of production. The analysis is based on the data provided by Uplands Resources Inc. Conservative estimates are used for the cost of production to avoid the overoptimistic forecast of profit. The best scenario is determined with the rate of return and the payout time as criteria.

Flow Simulation Scenarios

In flow simulation for the three scenarios mentioned, incremental oil production is calculated as the difference of oil production at a particular scenario with respect to the base case. The base case is the simulation result if the field is operated with the current condition. Several sensitivity studies are conducted for each scenario in seeking the best solution. The definition of each scenario is presented in Table 2.

TABLE 2

Definition of Scenarios Used in Flow Simulation*

Name	Description
Scenario 1A	Open well 82 as producer, convert well 81 as producer
Scenario 1B	Re-open DGIs D and E at all wells, base injection rate
Scenario 1C	Current perforation, double injection rate
Scenario 1D	Re-open DGIs D and E at all wells, double injection rate
Scenario 1E	Re-open DGIs D and E at all wells, triple injection rate
Scenario 2A	Horizontal injection well with injection rate of 1000 BWPd, re-open D and E, double rate at old wells
Scenario 2B	Horizontal injection well with injection rate of 2000 BWPd, re-open D and E, double rate at old wells
Scenario 2C	Horizontal injection well with injection rate of 3000 BWPd, re-open D and E, double rate at old wells
Scenario 2D	Horizontal injection well with injection rate of 3000 BWPd, re-open D and E, base rate at old wells
Scenario 2E	Horizontal producer well, re-open D and E, base rate at old wells
Scenario 3A	Four extra vertical wells (producer), base rate at old wells
Scenario 3B	Four extra vertical wells (producer), double rate at old wells

*BWPd, barrels of water per day.

Figure 7 shows an example of the increase of production using the first scenario (no additional wells). From the sensitivity studies of scenario 1, it is observed that the additional amount of 20–35 BOPD can be expected from the Self Unit.

Figure 8 presents the simulation result for the second scenario (drilling horizontal well). The horizontal well in this study is located in the vicinity of well No. 82. The simulation has been run for three different area locations and six different vertical positions, but no significant difference in the results are observed. From the sensitivity study of this scenario, it is found that the injector horizontal well is preferred over a producer horizontal well. The additional oil production from this scenario ranges between 30–40 BOPD, whereas the range for the first scenario is 20–35 BOPD. It is evident that drilling a horizontal well does not provide significantly better performance compared to the first scenario. Intuitively, it is concluded that this additional oil production will not be able to

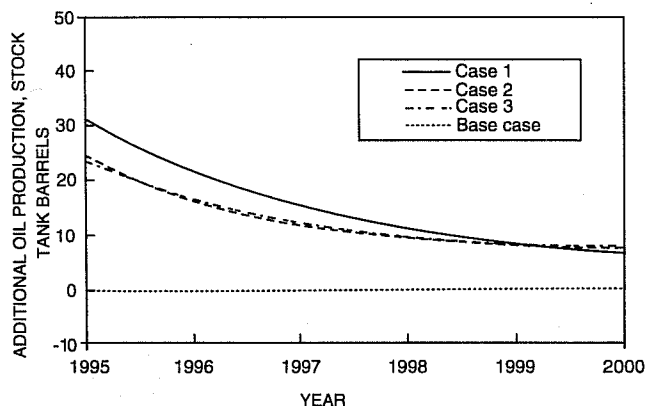


Fig. 7 Increase of oil production with scenario 1 (no additional wells). Re-open DGIs D and E, double injection rate.

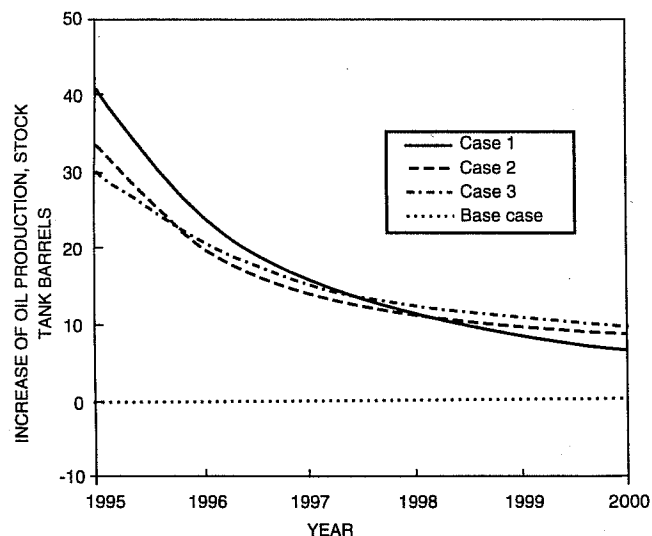


Fig. 8 Increase of oil production with scenario 2 (drilling horizontal well). Horizontal well with injection rate 3000 BWPd, double rate at old injection wells; re-open DGIs D and E.

cover the cost of drilling a horizontal well (cost ~ \$400,000) at the current level of oil prices.

Figure 9 shows the simulation for the third scenario (drilling additional vertical wells). An additional four vertical wells are used in this simulation. The locations of these wells were determined on the basis of the oil saturation map and also by considering the vacant space that exists in the Self Unit. As can be seen from Fig. 9, the additional oil production with this scenario is about the same as the previous scenarios, which ranges from 30 to 36 BOPD. Thus, only scenario 1 is considered for economic evaluation purposes.

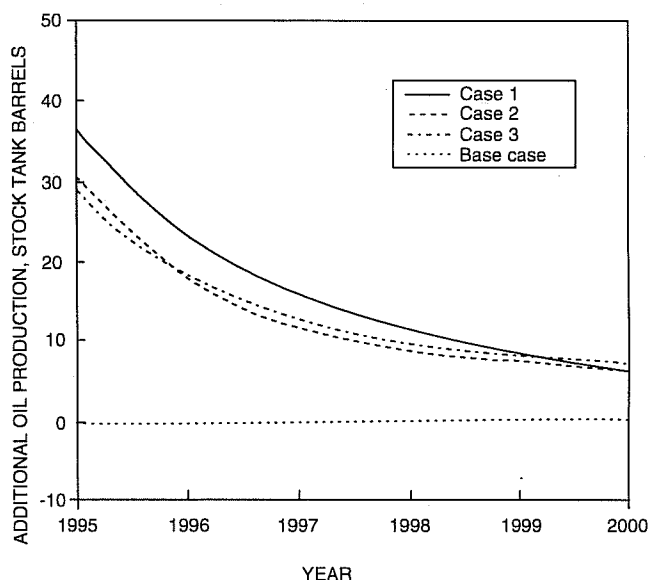


Fig. 9 Increase of oil production with scenario 3 (drilling additional vertical wells). Four extra vertical wells (producers), double rate at old injection wells; re-open DGIs D and E.

Economic Evaluation

The rate of return (ROR) and pay-out time are calculated using the first scenario that can be applied to the Self Unit. Before this calculation is performed, scenarios 1B through 1E were re-run for another 4 yr, so that a 10-yr projection could be made. The revenue is calculated using the constant oil price of \$17/bbl. The capital and operating costs are provided by Uplands Resources Inc. The cost to re-perforate DGIs D and E is predicted as \$61,600, whereas the cost to increase the water injection rate is \$87,495.

The operating cost is made on the basis of chemical treatment of water, electrical, and maintenance costs. This cost varies significantly for the Self Unit (it ranged between \$6/bbl of oil to \$9/bbl of oil during 1993–1994). The value of \$9.50/bbl of the produced oil is considered to be a conservative estimate under current conditions. In this report, this value is used for the condition where no increase of injection rate is applied (scenario 1B). For the scenarios where the injection rate is to be doubled (scenarios 1C and 1D), the operating cost of \$10.50/bbl of produced oil is used. For

scenario 1E (tripled injection rate), the operating cost is assumed to be \$11.50/bbl of produced oil.

Figure 10 presents the different RORs for the four scenarios evaluated. The pay-out time calculated was between 3 and 5 yr. The highest ROR comes from scenario 1B, because it has the lowest capital income. But the uncertainty among the three case studies is significant. In case 3, the ROR is equal to zero. To further examine the effect of the operating cost, a sensitivity study is conducted by increasing the operating cost by \$1/bbl, so that it becomes \$10.50/\$11.50/\$12.50 for no increase in injection rate, double injection rate, and triple injection rate, respectively. The result is shown in Fig. 11. It can be seen that scenario 1B is not very stable (negative ROR for case 2 and 3) and very sensitive to the operating cost. The other three scenarios show a consistently positive ROR. The sensitivity of the result with respect to the oil price has also been studied. In order for this scenario to work, the oil price cannot be lower than \$15.00 per barrel.

Conclusions

On the basis of the flow simulation and economic evaluation conducted, several conclusions can be reached:

- Opening DGIs D and E at all wells and increasing the water injection rate will cause the oil production from Self Unit to increase.
- Increasing the oil production by drilling a horizontal well is not significantly superior compared to the method of re-perforating and increasing the injection rate; thus, it is not feasible to drill a horizontal well at the present oil price.
- Additional oil production of about 20–30 BOPD can be recovered by re-perforating and doubling the injection rate.
- The ROR is expected to be 10–25% with pay-out time of 3–5 yr.

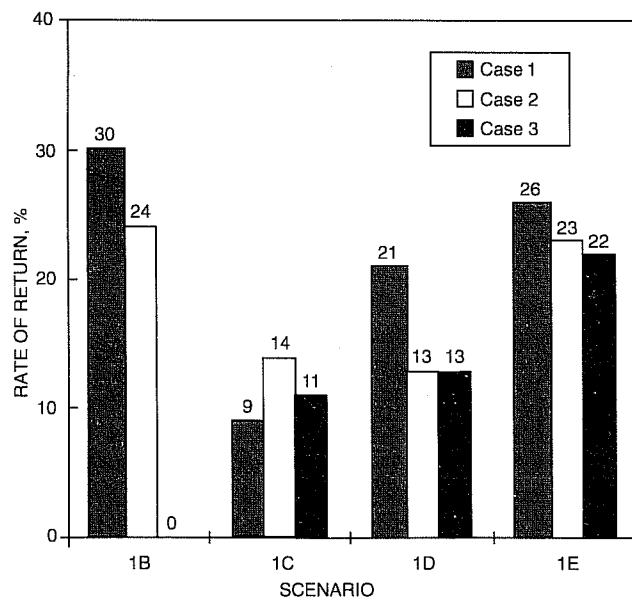


Fig. 10 Rate of return prediction. Operation cost: 1B, \$9.50; 1C and 1D, \$10.50; 1E, \$11.50.

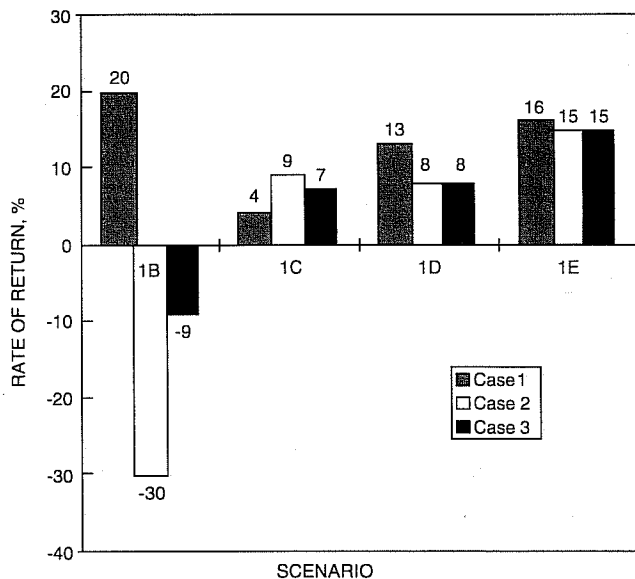


Fig. 11 Rate of return prediction for higher operation cost. Operation cost: 1B, \$10.50; 1C and 1D, \$11.50; 1E, \$12.50.

References

1. C. L. Liner and L. R. Lines, Simple Prestack Migration of Crosswell Seismic Data, *J. Seismic Explor.*, 3: 101-112 (1994).
2. R. E. Sheriff, *Encyclopedic Dictionary of Exploration Geophysics: Geophysical Reference Series 1*, Third Edition (1991).
3. R. P. Bording, A Finite Difference Wave Field Propagation Computer Algorithm, personal communication, 1994.

Objective

The objective of this project is to demonstrate the effectiveness of geologically targeted infill drilling and improved reservoir management in obtaining maximum oil recovery from the Sooner Unit (SU) in the Denver-Julesburg (D-J) Basin. The Sooner Unit Field is located about 100 miles northeast of Denver, Colo., and produces from the fluvial-deltaic Cretaceous D Sand formation at an average depth of 6200 ft.

The first phase of the project will involve multidisciplinary reservoir characterization and recovery identification in which high-density three-dimensional (3-D) seismic, detailed stratigraphy and engineering analysis will be used to identify optimum infill well sites and production and withdrawal schedules. One well will be drilled during this phase to obtain data pertinent to seismic activities.

The second phase will involve implementation of the selected technologies by drilling geologically targeted infill wells and establishing production and injection schedules. Evaluation of results from the second phase will be performed with reservoir simulation, transient well tests, and careful production tests of producing wells. A comparison of the prediction of ultimate recovery resulting from the implementation of these technologies with that which would have occurred in the absence of these technologies will be made.

The third phase of the project will involve technology transfer through a series of technical papers and presentation of a short course. Emphasis will be on the economics of the project and implemented technologies. Small- to medium-sized independents will be targeted. The success of this project and effective technology transfer should prompt re-appraisal of older waterflood projects and implementation of new projects in oil provinces such as the D-J Basin.

The project finished activities for Budget Period 1 in June 1993. At that time, the prime contractor, Research & Engineering Consultants, Inc., withdrew. Diversified Operating Corp. is the operator of the Sooner Unit and elected to assume responsibility as prime contractor. Negotiations to assign Diversified Operating Corp. as prime contractor continued until May 1994. Since that time, the project has proceeded with targeted infill drilling and completion demonstration activities.

Summary of Technical Progress

Field Operations

The Sooner Unit Field is located about 100 miles northeast of Denver, Colo., and produces from the fluvial-deltaic Cretaceous D Sand formation. The Unit has been under secondary recovery operations since 1989. Both water injection and gas recycling have been employed during secondary operations. Figure 1 shows the Unit area and well locations. The current production rate at the Unit for August 1994 was about 242 bbl of oil per day (BOPD), 1218 bbl of water per day (BWPD), and 552 thousand cubic feet per day (MCFD) (Fig. 2). Cumulative

ADVANCED SECONDARY RECOVERY DEMONSTRATION FOR THE SOONER UNIT

Contract No. DE-FC22-93BC14954

Diversified Operating Corporation
Denver, Colorado

Contract Date: Oct. 21, 1992
Anticipated Completion: Mar. 31, 1995

Principal Investigators:
Mark Sippel

Project Manager:
Edith Allison
Bartlesville Project Office

Reporting Period: July 1-Sept. 30, 1994

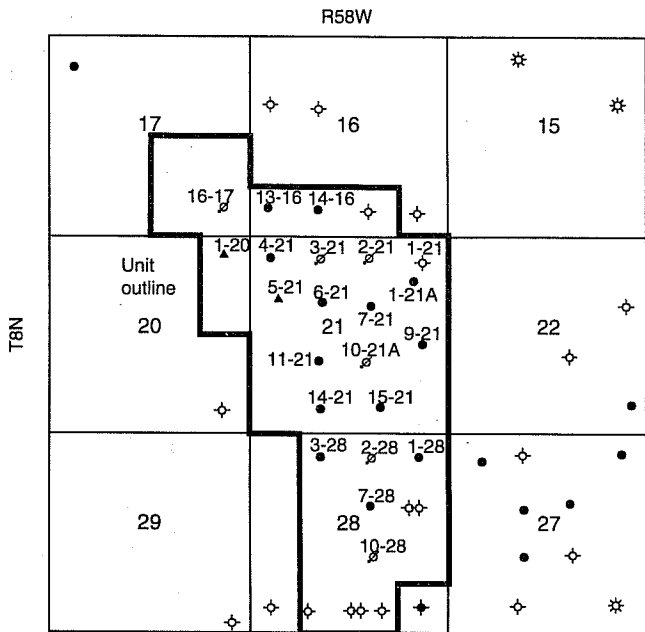


Fig. 1 The Sooner D Sand Unit area and wells. Grid is regular sections of one square mile.

oil produced, both primary and secondary, is 1,264,000 bbl as of August 1994. This is 19% of the original oil in place (OOIP) contacted by the existing wells. The target ultimate recovery is 34% of the OOIP or 2,244,000 bbl.

The following summarizes the current well status:

Active production	9 wells
Active water injection	4 wells
Active gas injection	1 well
Inactive production	1 well
Inactive water injection	1 well
Total	16 wells

Reservoir management of injection and voidage balancing began in February 1993. At that time, it was determined that the combined voidage of liquids with gas was exceeding injection, and reservoir pressure was decreasing at some wells. The positive results that started in the second quarter of 1993 from the balancing of injection and voidage are shown in Fig. 2. Oil production stabilized and slightly increased until February 1994, when the average daily oil production was 341 BOPD. At that time, shut-in and injecting well pressures indicated the reservoir pressure was increasing; however, an

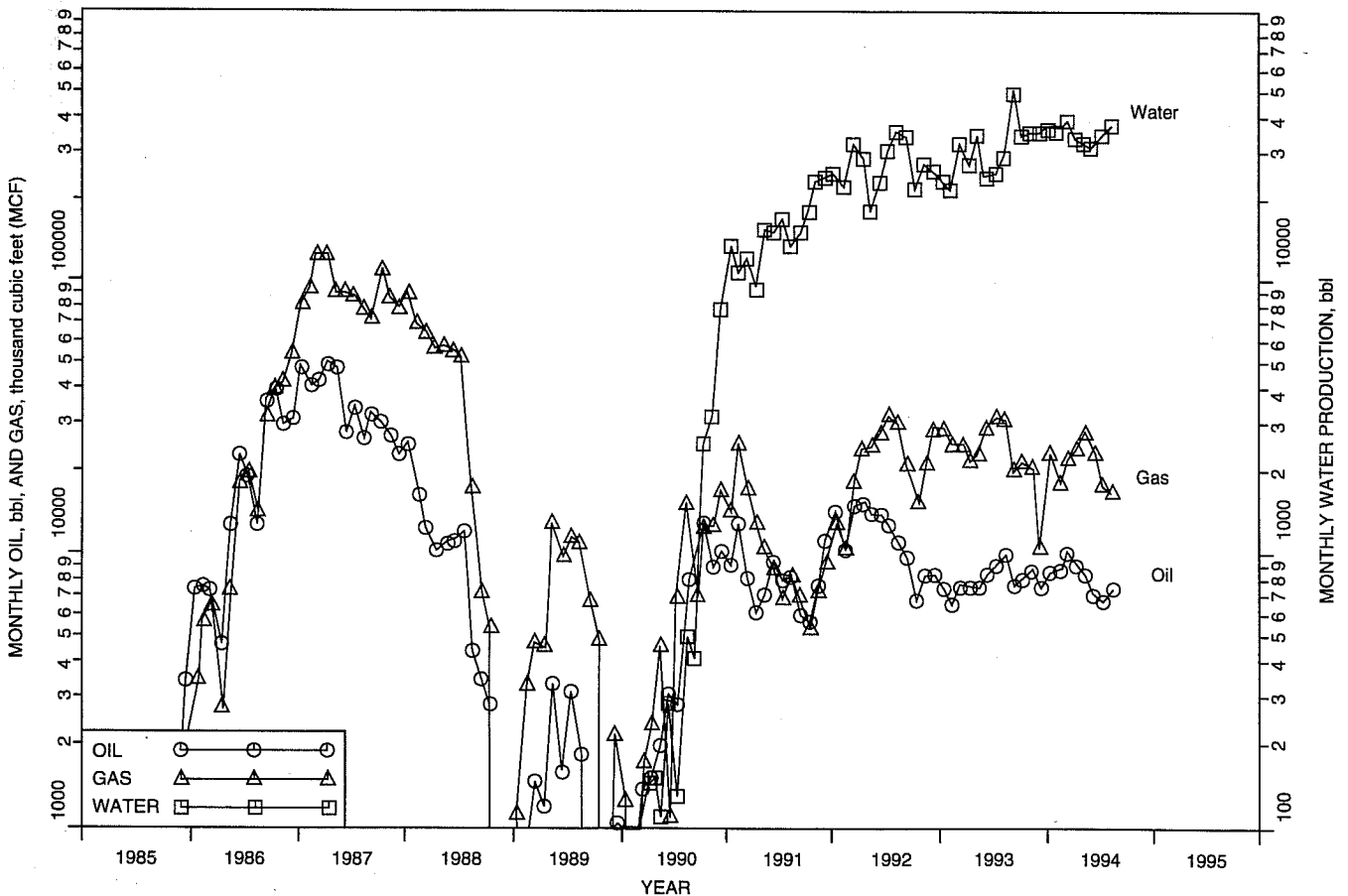


Fig. 2 Sooner D Sand Unit production history since discovery. Average oil production was 341 BOPD in February 1994.

injection flowline leak interrupted operations. Figure 3 shows the pressure increases observed at SU No. 2-28 gas injection well after water injection was balanced by compartment and increased to overcome voidage losses. The higher reservoir pressure also affected gas injection and recycling because compressor loads reached maximum ratings. The injection flowline leak and compressor limits have hindered attempts to further increase the average reservoir pressure. These problems are reflected in the production decline since February 1994, which is readily observed in Fig. 2.

Gas recycling has been determined to be an impediment to further improvement in production because the equipment effectively limits raising the reservoir pressure to optimal levels of 1500 to 1800 psi. Negotiations to resume gas sales have begun and plans have been made to convert the SU No. 2-28 gas injection well to production.

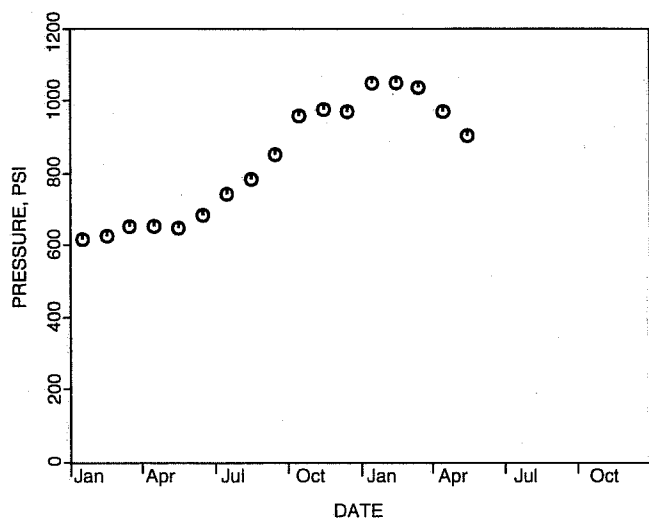


Fig. 3 Sooner Unit No. 2-28 gas injection wellhead pressure history. The wellhead pressure (●●●) indicates an increase in reservoir pressure achieved by balancing water injection and voidage.

Horizontal Recompletions

It was concluded at the end of Budget Period 1 that using the existing wellbores and infrastructure would be environmentally prudent and the most economic course of action in an infill development plan.

Area A, shown in Fig. 4, is identified as having the greatest OOIP from volumetric and computer simulation studies of contacted oil during primary production. The minimum contacted OOIP for area A is 3,090,000 bbl, which represents nearly 47% of the OOIP contacted by all existing wells in the Unit area. The cumulative oil production for this 200-acre area is 417,000 bbl as of August 1994. This is a recovery factor of only 13.5% of the OOIP. By analogy and five-spot computer simulations, the ultimate recovery after waterflooding should be 34% of the OOIP. Using 34% as a target recovery factor, an OOIP of 3,090,000 bbl, and cumulative of 417,000 bbl, the remaining recoverable reserves for area A is 633,000 bbl.

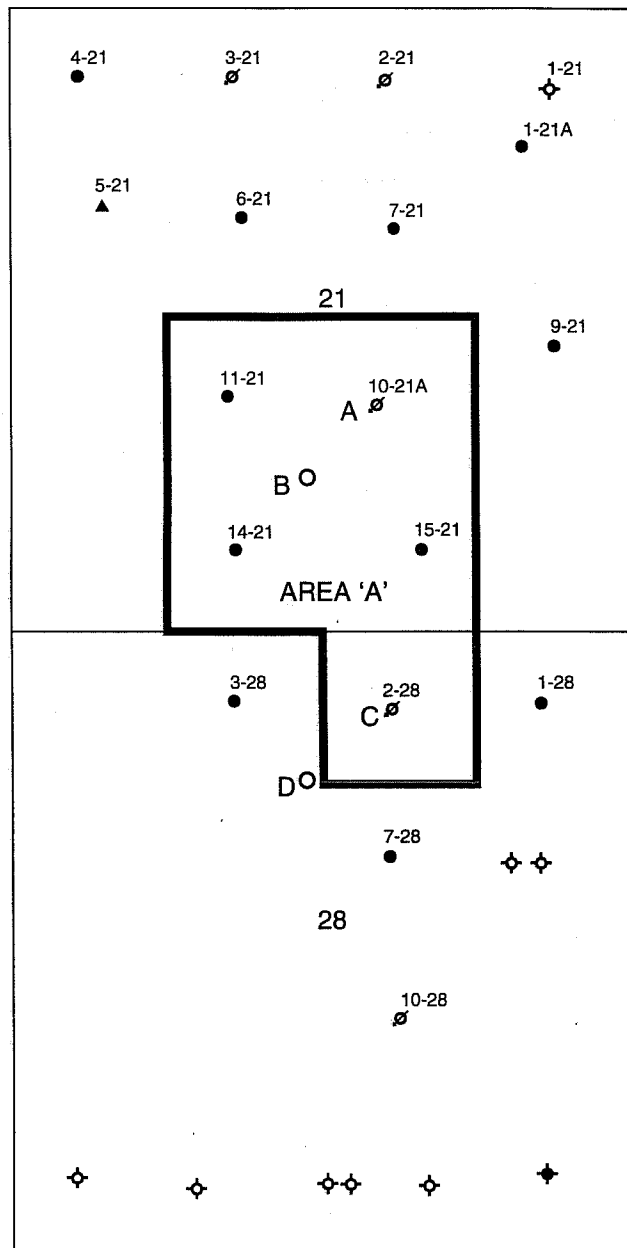


Fig. 4 Area A and field demonstration activities: (A) lateral recompletions. (B) vertical infill injection well. (C) conversion to production. (D) vertical infill well.

The reasons for low recovery from Area A are concluded to be lack of water injection and low reservoir pressure. Area A is adjacent to the SU No. 10-21A water injection well but has not experienced pressure or fluid influx from this or any other water injection well. The SU No. 10-21A was in obvious communication with the SU No. 15-21 well (Fig. 1) and had excellent injectivity. An injection profile survey indicated all water was confined to the perforated intervals in the D Sand. Geological heterogeneity was concluded to be a reason for poor reservoir sweep and anisotropic flow. The decision was made to drill a lateral drain-hole completion from the SU

No. 10-21A well southwest toward the center of Area A and attempt to overcome the north-south permeability orientation.

Ultra-short radius (USR) drilling of laterals from existing well bores was attempted with the technology described by Warren et al.¹ This technology consists of a rotary-guided short-radius curve drilling system. The curve-drilling assembly is composed of an anti-whirl polycrystalline-diamond bit, flexible joint, eccentric deflection sleeve, orientation indicator, and flexible drill string (Fig. 5). The system is used to drill drainholes with curvatures of approximately 30 ft from existing well bores.

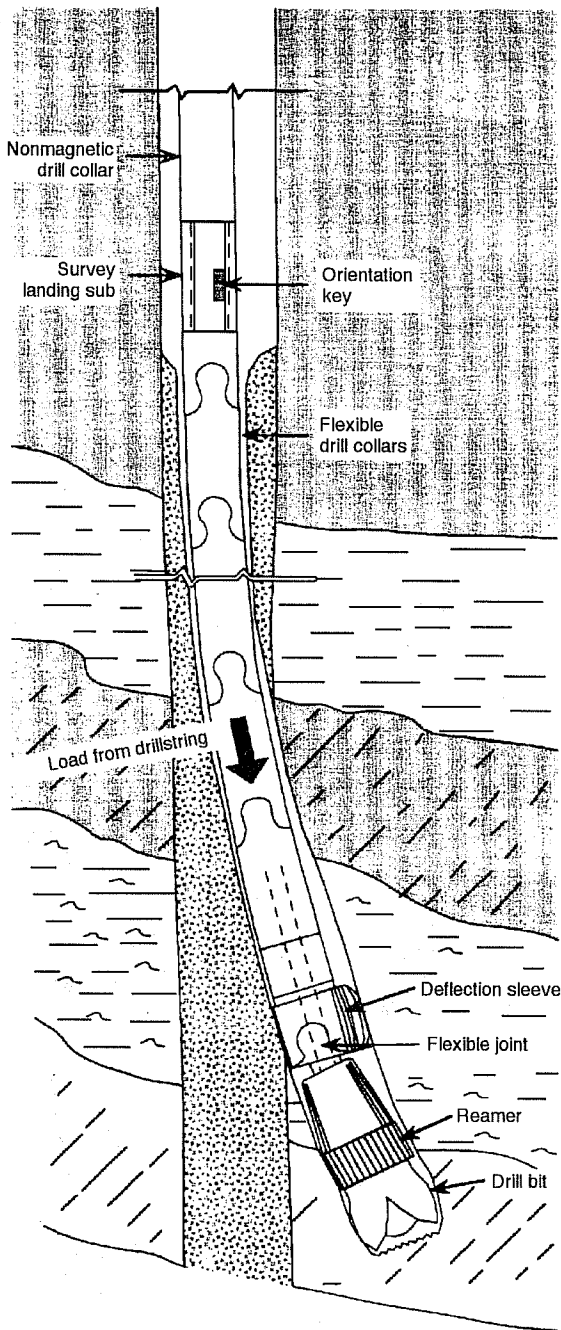


Fig. 5 Ultra-short radius curve-drilling bottomhole assembly. The assembly is turned via shouldered drill pipe and a power swivel.

Lateral recompletions from injection wells can help contact unswept oil and redirect sweep in directions dictated by well spacing and geological heterogeneity.

The use of this technology was anticipated to result in significantly lower cost compared to mud motor and measuring while drilling (MWD) horizontal drilling, and the system has been successfully used elsewhere at depths of less than 4000 ft. Two unsuccessful attempts to drill a 300-ft lateral to the southwest from the SU No. 10-21A well were made with this technology. The USR drilling system was uncontrollable at a depth of 6200 ft, and the steering and navigation system was too slow at this depth, especially for daylight-only operations. Inconsistent curvature and inaccurate directional control were problems in early development and testing of the USR system.¹ These problems may be resolved satisfactorily for shallow completions of 4000 ft or less, but they are still significant impediments at the depth of 6200 ft required for the D Sand at the Sooner Unit.

Efforts continued to determine if use of existing wells and infrastructure could be accomplished in the infill drilling and completion program. A more conventional mud motor with steering system and conventional drill rig were mobilized to the SU No. 10-21A well. A cement plug was placed in the well bore across the casing window used for USR and a second 100-ft section of casing was milled for short-radius (less than 150 ft) lateral drilling. Again, two unsuccessful attempts were made to drill horizontally. Final displacement of the second lateral was 680 ft (185 ft south and 655 ft west) at 6239 ft total vertical depth (TVD). The horizontal drilling was unsuccessful because the Graneros shale overlying the D Sand was unstable, and the horizontal hole collapsed during trips despite careful attention to mud properties and hydraulics. The Graneros shale section is not a problem during conventional vertical drilling operations.

Despite the failure to complete a lateral extension from the SU No. 10-21A well, it was determined that a significant lithological or fault barrier exists at about 250 ft west from the well. At a horizontal reach of 254 ft from the well bore (94 ft south and 236 ft west with a TVD of 6239 ft), the mud motor stalled and drilling angle changed abruptly. This barrier is in agreement with distance-to-barrier calculations made from a pressure falloff test performed on the well during Budget Period 1. The pressure transient behavior of this test indicates channel-like flow with a width of 400 to 500 ft. The 3-D seismic also indicates a change west from the SU No. 10-21A well. The amplitude and isochron attributes of the D Sand waveform indicate rapid thickening of the section in the westerly direction.

Technology Transfer

The 3-D survey results and methodologies have been presented seven times since May 1993. One of these presentations was made in this quarter to the Society of Exploration Geophysicists (SEG) Development and Production Forum on Economic Impact of Geophysical and Geostatistical Reservoir Characterization, Big Sky, Mont., July 1994.²

Synthetic Seismic Stratigraphic Modeling

Detailed synthetic seismic modeling was performed to determine resulting seismic signature and seismic frequency content necessary to resolve the internal stratigraphic architecture within the D Sand interval and to confirm the mapping and interpretation methodologies from earlier work during the project. Detailed stratigraphic cross sections of the D Sand interval were constructed across the central portion of the unit, running west to east. Stratigraphic correlation of well log data suggests that the D Sand interval can be subdivided into a series of vertically stacked reservoir flow units that may be related to sequence stratigraphic events or surfaces. This detailed reservoir unit correlation scheme was subsequently employed as a geometric control for two-dimensional (2-D) synthetic seismic modeling in order to determine the impact of the internal stratigraphic architecture on seismic response and potential vertical and lateral resolution limitations.

A detailed seismic cross-section model was built across the Sooner valley channel trend with data from the SU Nos. 16-20, 5-21, 6-21, 7-21, 1-21A, and 1-21 wells (Fig. 1).

Synthetic seismograms were generated for each well with the use of available sonic log data or Faust-transformed resistivity log data. All correlations between well locations and stratigraphic boundary conditions for the 2-D seismic cross-section modeling were based on the stratigraphic correlations. As a result, the synthetic seismic model geometry represents the D Sand internal stratigraphic architecture as interpreted from log correlation and production behavior.

A series of Ricker wavelet filters, at different frequencies, were applied to the synthetic cross-section model to determine the frequency necessary to resolve internal stratigraphy. Ricker wavelets were used on all models and at all frequencies for simplicity and to remove any possibility of wavelet side-lobe interference in the modeled seismic response. Wavelet extraction from the Sooner 3-D seismic data over the Niobrara to Dakota interval reveals broad frequency spectra with central frequencies in the 45- to 50-Hz range and with usable, high-end frequencies in the range of 70 to 85 Hz.

Generation of the 50-Hz model (Fig. 6) shows that internal D Sand stratigraphy is not resolvable into separate seismic events at this frequency. A general broadening of the seismic

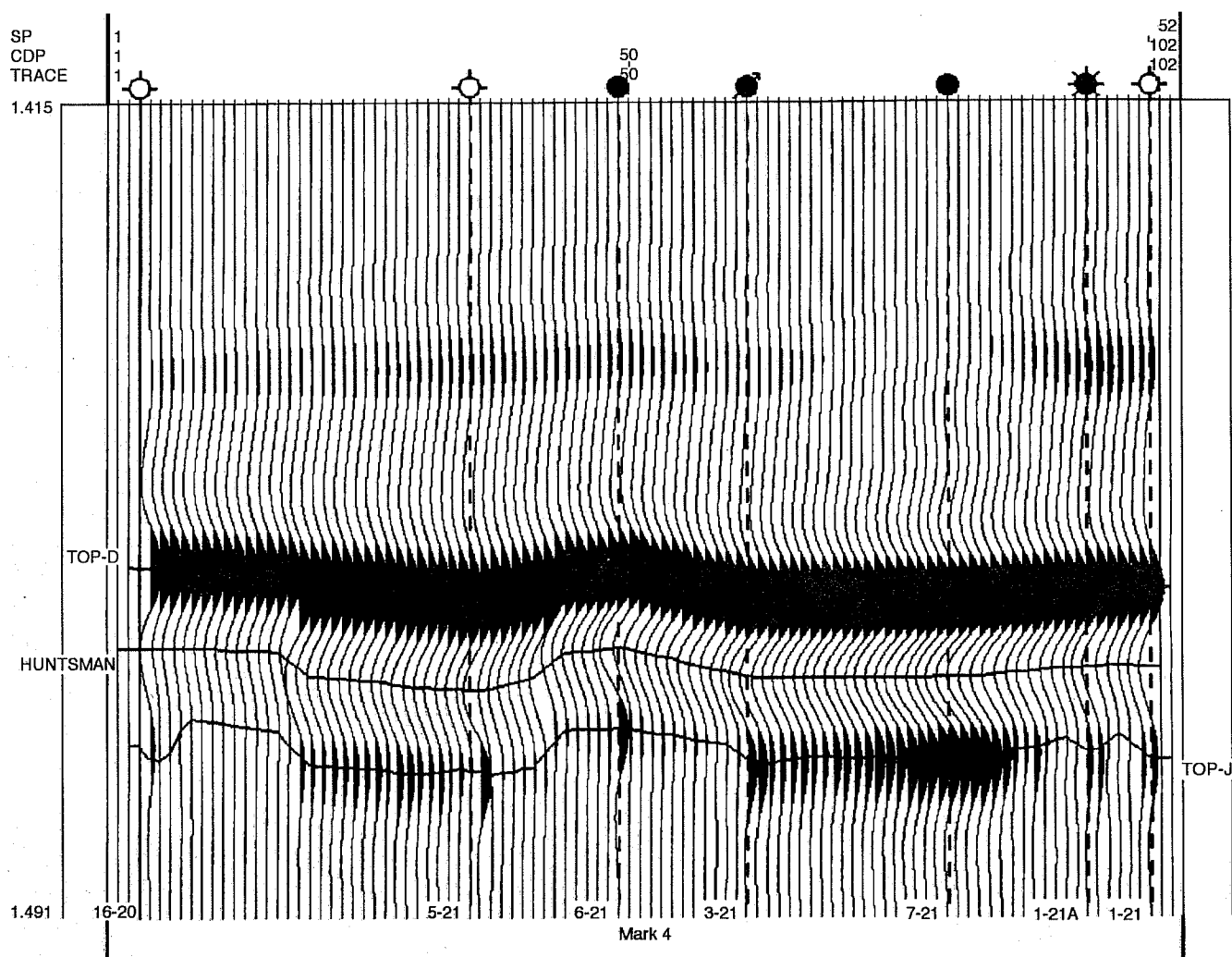


Fig. 6 Sooner synthetic seismic model—50 Hz.

peak associated with the D Sand is observed where the gross sand thickness is greatest in the stratigraphic cross section. The model generated at 75 Hz does not differ greatly from the 50-Hz model. No appreciable increase in resolution is gained at these slightly higher frequencies. Detailed modeling at 50 and 75 Hz shows results similar to those exhibited by the initial generalized Sooner synthetic seismic modeling effort. As gross sand thickness increases, a corresponding increase in D Sand peak amplitude associated with negative amplitude increase in the Huntsman Shale seismic horizon is observed. Isochron thicks are also observed between the D Sand and Huntsman events. As 50- to 75-Hz seismic data were recorded during the 3-D acquisition at Sooner, observations from the synthetic seismic modeling offer the most reasonable and cost-effective methodologies for D Sand development and exploitation.

Additional modeling at higher frequencies was done to establish the seismic parameters necessary to seismically resolve internal stratigraphy. The 100-Hz model begins to show resolution of D Sand stratigraphy with initial development of a lower, secondary seismic peak within the D Sand

interval at the SU No. 5-21 location (Fig. 2). At 125 Hz, the modeling shows full development of the secondary peak and trough pair coincident with location of increased incision and thicker D Sand fill in the valley system (Fig. 7). This model also exhibits lower valley channel development with sharp lateral boundaries truncating the lower D Sand seismic peak. This sharp valley channel boundary is also observed in the dramatic isochron thinning of the Huntsman trough to J Sand peak interval.

A final model was run at 300 Hz that fully resolves the internal D Sand stratigraphy. Tops and bottoms of individual sandbodies are observable as separate seismic events (Fig. 8). Abrupt valley channel boundaries are observable as sharp character and phase changes in the synthetic model. At 300 Hz, a significant amount of background noise is evident in the modeling, both within and outside of the valley trend.

The 2-D synthetic seismic modeling, constrained by detailed stratigraphic correlation, shows that D Sand internal stratigraphic architecture can be resolved into individual seismic events with data frequencies of 125 Hz or greater. At less than 125-Hz frequencies, D Sand stratigraphy cannot be

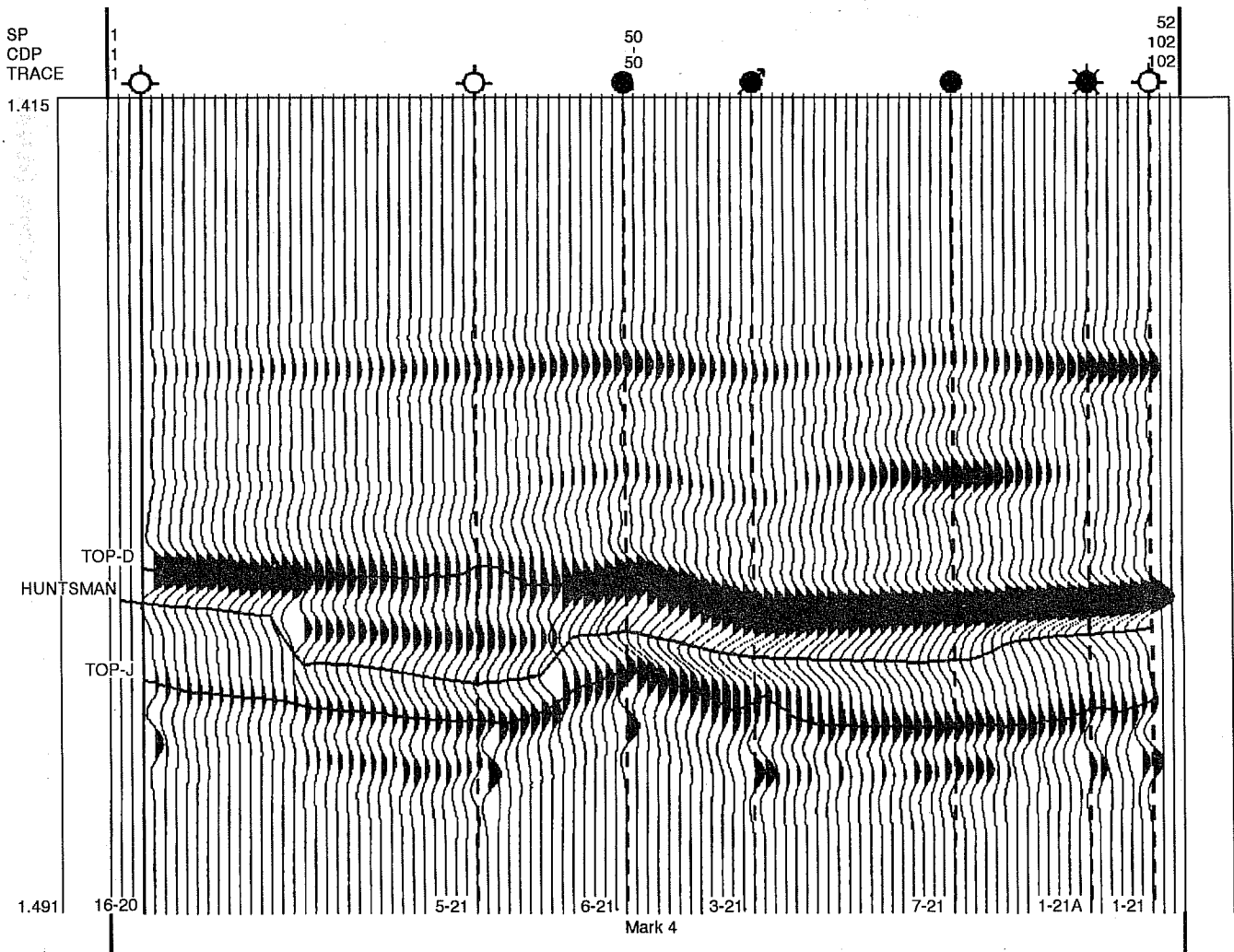


Fig. 7 Sooner synthetic seismic model—125 Hz.

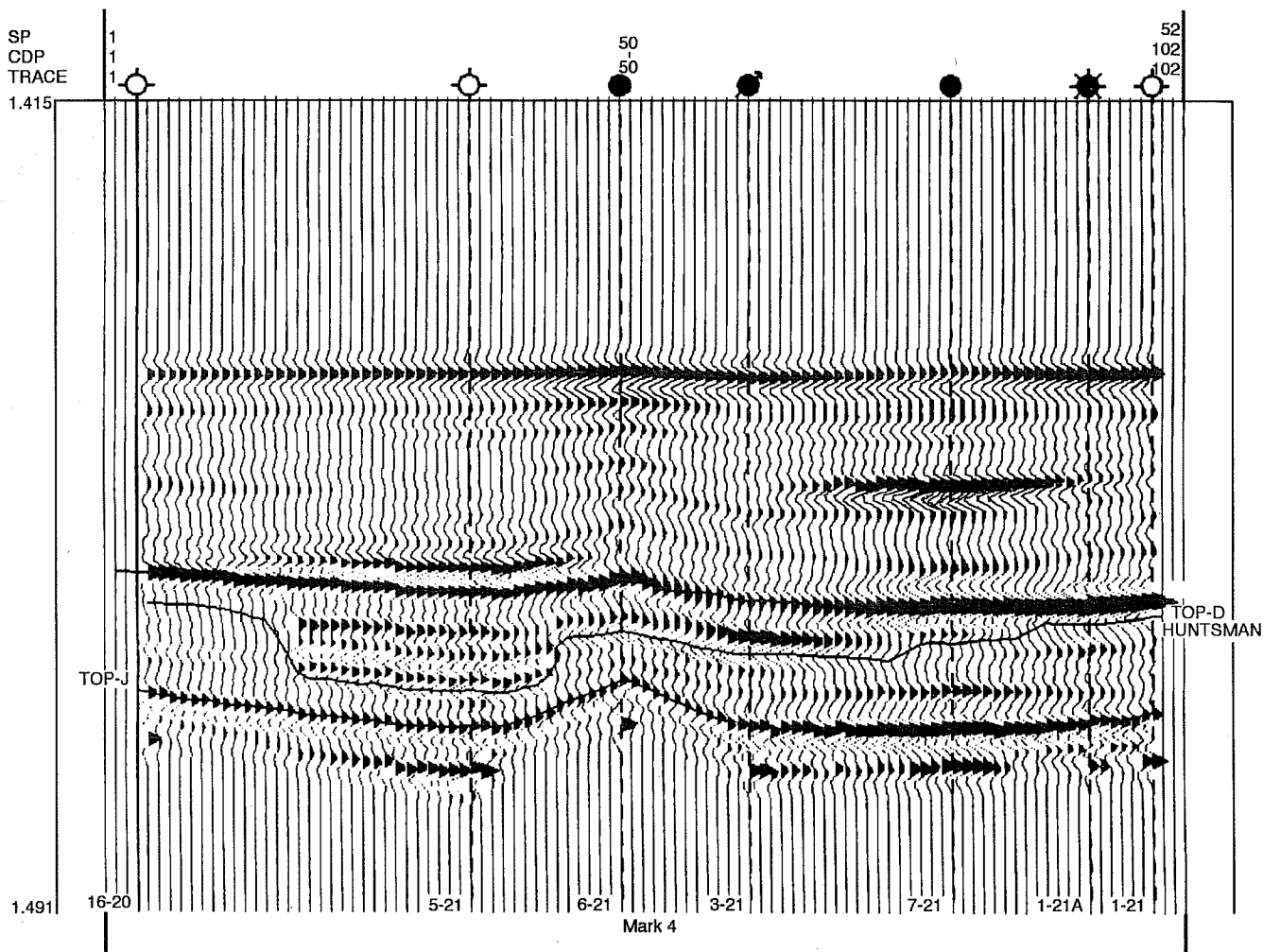


Fig. 8 Sooner synthetic seismic model—300 Hz.

resolved and gross sand thickness variations can be estimated from analysis of seismic amplitude and isochron data. Models with frequencies between 250 and 300 Hz exhibit the greatest resolution of D Sand internal stratigraphy; however, there is added background noise resulting from slight lithologic impedance variations. At present, it is not economically and technically feasible to acquire 300 Hz surface seismic data. These very high frequencies can only be acquired with cross-well-bore seismic tomography techniques.

Models at 125 Hz exhibit the clean development of a secondary peak associated with valley fill in the D Sand interval. Individual sandbodies and potential flow units are not observable at this frequency. The development of the secondary seismic peak indicates increased sand development and thickness. While surface seismic data with frequencies in the range of 125 to 150 Hz have been acquired in several producing fields, the increased cost related to this acquisition would be substantial because of the increased source effort and down-spacing of receiver and source points.

Resolution vs. detection of D Sand internal stratigraphy is controlled by the frequency content of the acquired seismic

data. To fully resolve the internal stratigraphic architecture into individual sandbodies and flow units, very high frequencies in the range of 200 to 300 Hz may be required. This range of frequency content can only be acquired with cross-well seismic tomography techniques. Detection of internal stratigraphy resulting from sandbody changes (thickness and geometry) appears to be observable at frequencies ranging from 50 to 150 Hz. This frequency range can be acquired through standard surface seismic techniques. Increased acquisition cost associated with increased data frequency content is the limiting factor in determining the confidence level of detection. Higher frequencies would result in higher levels of detection confidence but would cost significantly more. Interpretation methodologies would vary slightly according to the frequency content of the data.

Revisions to the Statement of Work and Budget

The lack of success in lateral drilling and recompletion has not changed the objective to target wells on the basis of

integrated geophysical, geological, and engineering study. There will be a slight reallocation of budget to allow completion of at least one vertical infill water injection well and the conversion of the SU No. 2-28 from gas injection to production. The remaining tasks will be accomplished as set forth in the statement of work.

References

1. T. M. Warren, W. J. Winters, H. B. Mount, and K. L. Mason, Short-Radius Lateral Drilling System, *J. Pet. Technol.*, 108-115 (February 1993).
2. D. S. Singdahlsen and M. T. Kramer, *3D Seismic Reservoir Characterization for the Independent Producer*, oral presentation to the Society of Exploration Geophysicists at the Development and Production Forum: Economic Impact of Geophysical and Geostatistical Reservoir Characterization, Big Sky, Montana, July 1994.

INCREASED OIL PRODUCTION AND RESERVES FROM IMPROVED COMPLETION TECHNIQUES IN THE BLUEBELL FIELD, UINTA BASIN, UTAH

Contract No. DE-FC22-92BC14953

**Utah Geological Survey
Salt Lake City, Utah**

**Contract Date: Sept. 30, 1993
Anticipated Completion: Sept. 29, 1998
Government Award: \$412,890**

**Principal Investigator:
M. Lee Allison**

**Project Manager:
Edith Allison
Bartlesville Project Office**

Reporting Period: July 1-Sept. 30, 1994

Objective

The objective of this project is to increase the oil production and reserves in the Uinta Basin by demonstration of improved completion techniques. Low productivity is attributed to gross production intervals of several thousand feet that contain perforated thief zones, water-bearing zones, and unperforated oil-bearing intervals. Geologic and engineering characterization and computer simulation of the Green River and Wasatch formations in the Bluebell Field will determine reservoir heterogeneities related to fractures and depositional trends. This will be followed by drilling and recompletion of several wells to demonstrate improved completion techniques based on the reservoir characterization. Transfer of the project results will be an ongoing component of the project.

Summary of Technical Progress

Outcrop Studies

Surface fracturing patterns may provide clues to subsurface fracturing patterns in the Bluebell Field. Data were collected from 29 stations in or near the Bluebell Field. All data are from sandstone or pebble conglomerate beds and were collected on or near horizontal surfaces. Azimuth orientations were measured on vertical or near-vertical fractures at each station. The azimuth orientations are shown in Fig. 1. All stations show two major joint sets. In general, one fracture set tends to follow the regional structural trend (bend) of the north margin of the Uinta Basin, and the other set is nearly orthogonal to the first. Apparently, the two fracture sets formed at the same time during the same fracturing event. No features of the fracture surfaces were preserved that could be used to determine direction of fracture propagation.

Porosity and permeability have been cross-plotted for the 32 core-plug analyses completed from outcrop samples. The data indicate that the feldspathic arenites tend to have the best porosity and permeability (samples containing visible fractures were not tested); however, six of the arenites have less than 10% porosity because of calcite cementation within pores. Relationships that may explain these low-porosity samples are being investigated (grain size, lithology above and below the sandstone, clay types, feldspar variation, and others). X-ray diffraction (XRD) identification of clay types is also under way.

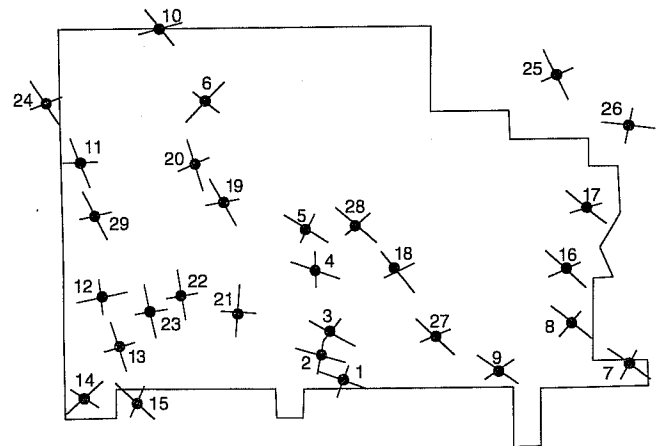


Fig. 1 Primary and secondary surface fracture orientations of the Bluebell Oil Field, Uinta Basin, Utah. All stations show two major joint sets. The longer lines represent the sets with the most abundant measurements and the shorter lines represent the secondary set. The associated numbers are station numbers that refer to the data table in an unpublished field report.

Subsurface Studies

Seven cores, totaling 1500 ft (457 m), have been described. Descriptions include lithology, sedimentary structures, fossil content, fracture description, and relative porosity. Thin

sections of core samples are being made to complete lithofacies identification. Core samples from various lithofacies will be used in fluid-sensitivity studies.

Digitizing of geophysical well logs in and around the Bluebell Field is complete. The database consists of 240 logs from 80 wells. The digital data will be used for field-wide correlation; for detailed porosity, clay content, and fluid-saturation calculations; and to generate structure and thickness maps.

The first draft of the well completion history database is finished. The database contains detailed completion of over 90 wells in the Bluebell Field. The database will be used to determine which methods and chemical additives are the most and least effective completion treatment. Additional data will be gathered from the operators as needed, and more wells will be added to the database.

Engineering Studies

West Study Site

Detailed characterization of the west study site (sections 9, 10, 15, and 16, T. 1 S., R. 2 W.) has begun. Productive beds in the lower Green River formation were correlated among all the wells in the study site. Thickness, porosity, and water saturations were determined at a 2-ft (0.6-m) scale for the reservoir simulation model. Drillstem test, perforation, completion, and production data for each of the wells were compiled and entered into the Utah Geological Survey (UGS) INTEGRAL *gim database.

Seven wells penetrated the lower Green River formation in the west study site. Three of these wells, Lamicq 2, Springfield 2-10C, and State 3-10C, were perforated in the lower Green River. The attributes of the model of the lower Green River reservoir at the west study site are

Reservoir extent	10,208 to 10,704 ft (3,111.4 to 3,262.6 m)
Grid	20 × 20 × 17
Grid size (x and y)	528 ft (160.9 m)
Porosity	Varied
Initial oil saturation	Varied, based on log calculations
Initial gas/oil ratio (GOR)	400 standard cubic ft/stock tank barrel (scf/STB) (70.4 m ³ gas/m ³ oil)
Oil gravity	35 °API
Gas gravity	0.75
Bubble-point pressure	2,010 psi (13,858 KPa)
Pressure gradient	0.47 psi/ft (3.2 KPa)
Bottomhole pressure	2,500 psi (17,238 KPa)

The simulated cumulative oil production from the area was 1.6 million (MM)STB (254,400 m³), and the simulated cumulative gas production was 636 MMscf (17,808,000 m³) compared with the actual production of 0.7 MMSTB (111,300 m³) and 478 MMscf (13,407,492 m³).

East Study Site

The Michelle Ute (sec. 7, T. 1 S., R. 1 E.) single-well model was modified to include all the beds that have been perforated in the well over the years (69 beds). The attributes of the model are

Reservoir extent	10,400 to 14,400 ft (3,169.9 to 4,389.1 m)
Grid	8 × 8 × 69
Grid size (x to y)	165 ft (50.3 m)
Porosity	0.0 to 0.16
Initial oil saturation	0.7
Initial GOR	900 scf/STB (158.5 m ³ gas/m ³ oil)
Oil gravity	35 °API
Gas gravity	0.75
Bubble-point pressure	3,200 psi (22,064 KPa)
Pressure gradient	0.5 psi/ft (3.4 KPa)
Bottomhole pressure	2,000 to 3,000 psi (13,790 to 20,685 KPa)

The field perforation schedule, which consists of continuously added new perforations over the years, was duplicated in the model. The simulated vs. actual oil and gas productions were matched by adjusting individual block permeabilities. The permeabilities varied from 0.03 millidarcy (mD) to 1.25 mD in this model. The cumulative oil and gas productions from the simulation matches well with the actual production history (Figs. 2 and 3). The closeness of the actual production history to

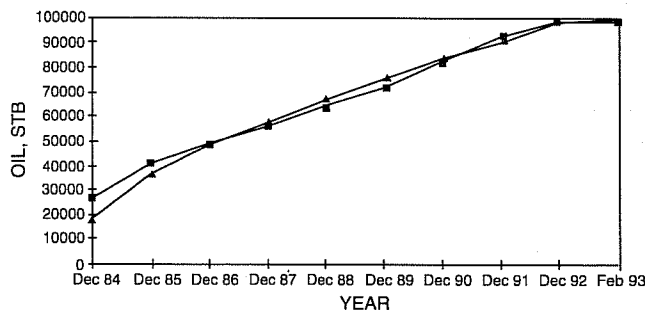


Fig. 2 Cumulative oil production from actual field data and simulation model data, Michelle Ute 1-7 (sec. 7, T. 1 S., R. 1 E., Uinta Basin meridian). —■—, field data. —▲—, simulation data.

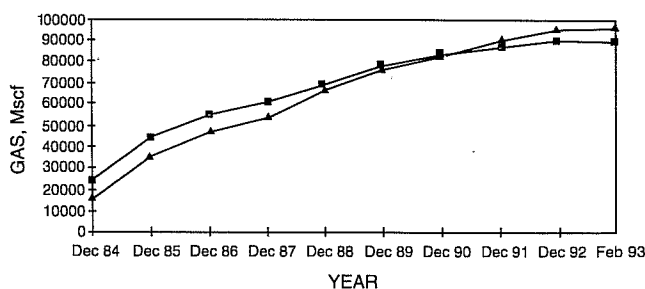


Fig. 3 Cumulative gas production from actual field data and simulation model data, Michelle Ute 1-7 (sec. 7, T. 1 S., R. 1 E., UBM). —■—, field data. —▲—, simulation data.

the simulated production suggests that the reservoir description and underlying production mechanisms are well represented by the model. A similar single-well model is being constructed for the Malnar Pike well (sec. 17, T. 1 S., R. 1 E.).

Technology Transfer

Maps and photographs of the Bluebell Field and outcrops of the Green River formation were displayed at the Utah Geological Survey booth at the Society of Petroleum

Engineers Annual Technical Conference and Exhibition in New Orleans, La., in September 1994.

A paper titled "Reservoir Characterization Through Facies Analysis of the Lower Green River Formation for Hydrocarbon Production Enhancement in the Altamont-Bluebell Field, Uinta Basin, Utah" will be presented at the Geological Society of America Annual Meeting in Seattle, Wash., in October 1994, and an abstract has been submitted to the American Association of Petroleum Geologists for presentation at the Annual Convention in Houston, Tex., in March 1995.

DYNAMIC ENHANCED RECOVERY TECHNOLOGIES

Contract No. DE-FC22-93BC14961

**Columbia University
New York, N.Y.**

**Contract Date: July 5, 1993
Anticipated Completion: Oct. 30, 1995
Government Award: \$7,742,000**

**Principal Investigator:
Roger N. Anderson**

**Project Manager:
Edith Allison
Bartlesville Project Office**

Reporting Period: July 1-Sept. 30, 1994

Objective

The objective of this project is to test the concept that the growth faults in a Gulf of Mexico field are conduits through which the producing reservoirs are charged and that enhanced production can be developed by producing from the fault zone. The field demonstration will be accomplished by drilling and production testing of growth fault systems associated with the Eugene Island Block 330 (EI 330) operated by Pennzoil in federal waters off Louisiana.

Summary of Technical Progress

Management Start-Up/Technology Transfer

This task is complete. Database Management is in process. During this quarter the simulation of fluid migration through the piping was done by a biased random walk in the upward direction. The bias simulates buoyancy, and the random walk

simulates diffusion. In addition, a Global Basins Research Network/U.S. Department of Energy (GBRN/DOE) exhibit was presented at the National Information Infrastructure Advisory Meeting, Columbia University, New York, N.Y., on Sept. 12, 1994.

Field Demonstration Experiment

The actual cost of the experiment is currently in negotiation with Pennzoil.

Reservoir Characterization

This task is in process. Work on the facies architecture of a shelf margin lowstand complex continued. Pressure mapping results for the Pathfinder well are reported in a paper submitted for publication.¹

Modeling

This task encompasses several subtasks. A Ph.D. thesis at Lamont-Doherty Earth Observatory (L-DEO) was defended that included a major study of the effects of overpressuring (inhibiting compaction) and salt diapirism on temperatures in the Gulf of Mexico. Geologic input is approximately 75% complete with three-dimensional (3-D) South Eugene Island description, present porosity distribution, and representative volume element (100 × 100 × 10 km³ of Gulf of Mexico water) two-dimensional (2-D) seismic lines. Near-fault details are nearly 90% complete, salt movement history is 60% complete, and geologic and geochemical observations are 30% complete. Modeling of fluid and salinity effects is complete and is in the preliminary stages of testing at Louisiana State University. Modeling of the effects of salt and sediment types on subsurface temperatures and the effects of gas venting on oil migration is in progress.

Geochemistry

Work progresses in analyzing the Pathfinder cores with development of an expanded geochemical program for the EI 330 field.

Technology Transfer

During this quarter an annual technical report was submitted to DOE (Aug. 15, 1994). The GBRN/DOE project was presented as a poster session at the Pennzoil Technology Conference, Houston, Tex. (Aug. 29, 1994). A well data volume for the Pathfinder well is being prepared for publication; it will include all raw data, processed data, and some preliminary interpreted data and will be made available in

the form of a CD-ROM (modeled after the initial reports of the Deep Sea and Ocean Drilling Programs).

Reference

1. B. Hart et al., Porosity and Pressure: Testing the Role and Under-compaction in the Development of Geopressures in a Gulf Coast Basin, submitted for publication (1994).

CO₂ HUFF 'N' PUFF PROCESS IN A LIGHT OIL SHALLOW SHELF CARBONATE RESERVOIR

Contract No. DE-FC22-94BC14986

**Texaco Exploration and Production, Inc.
Midland, Tex.**

Contract Date: Feb. 10, 1994
Anticipated Completion: Dec. 31, 1997
Government Award: \$474,870
(Current year)

Principal Investigator:
Scott C. Wehner

Project Manager:
Jerry Casteel
Bartlesville Project Office

Reporting Period: July 1–Sept. 30, 1994

Objective

The principal objective of the Central Vacuum Unit (CVU) carbon dioxide (CO₂) Huff 'n' Puff (HnP) project is to determine the feasibility and practicality of the technology in a waterflooded shallow shelf carbonate (SSC) environment. The results of parametric simulation of the CO₂ HnP process, coupled with the CVU reservoir characterization components, will determine if this process is technically and economically feasible for field implementation. The technology transfer objective of the project is to disseminate through an innovative plan the knowledge gained, in support of the U.S. Department of Energy's (DOE) objective of increasing domestic oil production and deferring the abandonment of SSC reservoirs.

Texaco Exploration and Production Inc.'s (TEPI) long-term plans are to implement a full-scale miscible CO₂ project in the CVU. However, a common finding throughout the

Permian Basin SSC reservoirs is that the current market precludes acceleration of such a capital-intensive project. The immiscible CO₂ HnP process might bridge this longer term miscible project with near-term results. A successful implementation would result in near-term production, or revenue, to help offset cash outlays. The DOE partnership provides some relief from the associated research and development risks, allowing TEPI to evaluate a proven Gulf Coast sandstone technology in a waterflooded carbonate environment.

Summary of Technical Progress

Porosity and Permeability Relationships: Characterization with Neural Networks

A more descriptive characterization of a reservoir would include a variance in permeability rather than the application of an average value. Permeability relationships fill an integral need for reservoir simulation by providing a method of distributing saturations and evaluating flow capacity. Past work involved the use of linear regressions to represent a scattering of core-measured porosity vs. permeability data.

This portion of the reservoir characterization applies artificial intelligence (AI) to determine porosity–permeability relationships and to derive values of permeability for all well traces in the study. The use of a neural network to derive permeability from wellbore measurements is a patented Texaco process.

AI is a name applied to several types of computer programs that attempt to simulate the learning processes of the human brain. The particular type of AI applied to develop the porosity–permeability relationship for this project is called a neural network. Commercial software is available for designing and applying neural networks. For this study, NeuroShell, a product of Ward Systems Group, Inc., and NeuralWorks, a product of NeuralWare, Inc., were used.

The data set supplied to the network during the learning phase included porosity and permeability values derived from core measurements obtained from 18 wells (aerially distributed) within the project area. These core data were reviewed for evidence of fracturing and suspect data were culled from the data set. This left slightly over 4000 data points to be used in training the network.

Back propagation networks consist of input nodes, where data are supplied to the network, and output nodes, where resulting values are generated. Between these two sets of nodes are one or more hidden layers of nodes. Operation of the network occurs in two phases. During the learning phase, the data supplied at the input nodes are acted upon by the network to generate a value at the output nodes. A comparison is made to the desired value, and the amount of error determines the value of a weighting function, which yields a better result the next time the data are presented. Learning continues by repeated presentation of data at the input nodes until the operator decides that the network has learned the relationship to the limit of its ability. The second phase of operation is to present the input nodes with data with unknown output values and let the network solve for the unknown values, on the basis of the results of the learning phase.

The general methodology used for this study consists of four steps: (1) decide which data to use to train the network, and assemble them in the proper format; (2) present the data to the network and allow learning to occur; (3) apply the network to a test data set held in reserve for this purpose; and (4) evaluate the effectiveness of the network.

After the above steps are complete, decisions are made as to what changes to the network or the training data set would most likely improve the performance of the network, and the methodology is repeated until the resultant network gives satisfactory performance. More than 50 repetitions of this process were completed before a network was finalized to apply to the wellbore data. A final report of the network study will be issued with the annual technical report. This study has several findings of note:

- Any input data used to train the network must also be available for all data points to be analyzed (for instance, if sonic travel time is used to train the network, then sonic data will be required to apply the network).
- A major hurdle to the application of neural networks in mature fields such as vacuum is the lack of consistent usable data

from well to well. The lowest common denominator of data for this project was normalized wireline porosity, location of the well in latitude and longitude, and macro-zonation of the reservoir. Better results could certainly have been achieved if, for example, sonic logs and resistivity logs had been available for all wells or pore-type descriptions.

- In spite of the limitations in data, the final network achieved a mean absolute deviation (error) of 7.28 mD vs. 10.96 mD for the standard linear regression analyses. In this case, the application of standard linear regression analysis would have resulted in data 50% less accurate than those obtained from the neural network.

Figure 1 is a scatter-plot of porosity vs. permeability on a semilog plot for a representative test set of the core data and the neural network solution.

Initial Water Saturation Distribution and Oil-Water Contact

One of the more important milestones associated with the reservoir characterization component of the project is determination of original oil in place (OOIP). Therefore, an evaluation of fluid saturations was warranted. Capillary pressure data, corrected for reservoir conditions, were used to define the initial saturations above an oil-water contact (OWC), or zero capillary pressure level [water saturation (S_w) = 100%]. Study of electric logs defined the OWC to be at 1000 ft from sea level datum. The average initial water saturation (S_{wi}) of the main pay zone was then established at 20% using the capillary pressure data.

It was first necessary to establish the OWC in order to apply the capillary pressure data. All known documented tests within the transition zone were included in the evaluation of the OWC. Standard electric wireline log (E-log) evaluation techniques were used to define the OWC. Field closure exists at 800 ft from sea level. However, stratigraphic facies changes and a lack of water influx during primary depletion, coupled with obvious

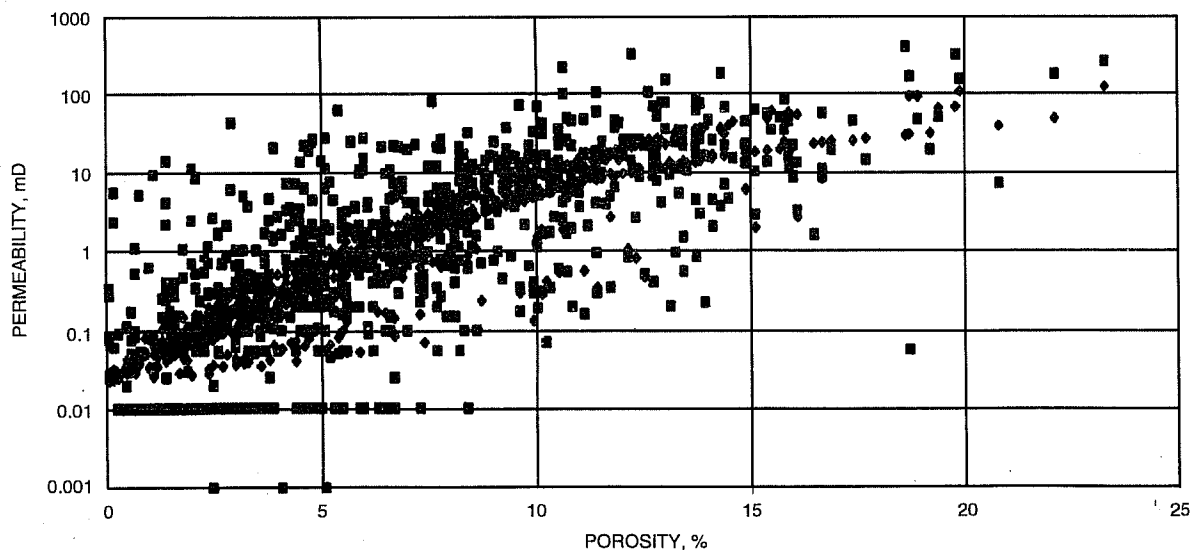


Fig. 1 Neural network solution. ■, core data. ◆, neural network.

hydrocarbon saturations well below this level on E-logs, suggest that the field is not in contact with any hydraulic pressure. Thus, a tilted zero capillary pressure level would not be expected. Until 1990, the lack of usable E-logs prohibited an accurate estimate of the OWC. Recent development of deeper reservoirs has provided a significant density of wireline data within the San Andres transition zone (TZ). Waterflooding influence was evident on these new E-logs. Because of compartmentalization and discontinuities within the reservoir, a ghost or shadow of the original saturation profile can be identified, especially in the non-waterflooded TZ. The OWC was found to be approximately 1000 ft from sea level.

The laboratory-derived capillary pressure data were related to the height above the zero capillary pressure, and corrected to reservoir conditions. The capillary pressure data resulted in an estimated 19.5% S_{wi} for the main pay zones of a test well (data set). This value was considered to be within the limits of accuracy and is historically supported by log-derived values of 20% as the average S_{wi} within the main pay. The capillary pressure data were thus reduced to a Leverett J function $J(S_w)$ and applied to the project database to distribute an S_{wi} profile for each well. The average S_{wi} for the pay zones in the same test data set as above, using the $J(S_w)$, resulted in a value of 20.9%, supporting the previous findings. Application of the $J(S_w)$ also honors the fractional flow curve end points. The culmination of this exercise will result in the selection of a pseudo-OWC surface, or an economically attractive OWC within the TZ, which will be used in the calculation of OOIP.

Geostatistical Realizations

Geostatistics is being used to distribute wellbore data to interwell locations (cells). A more realistic distribution of the data than the typical algorithm used in mapping software is expected as a result. Normalized porosity and permeability data from 455 wells in the project area were available for use. Markers within the pay were taken from the project database.

The first step involved screening the data. All sonic logs were removed from the population. It was believed that they were introducing statistical variations because of differences in their ability to recognize secondary porosity. The neutron-derived logs would show the secondary porosity. The normalization techniques used on these different logging suites resulted in a possibly poor sonic-core porosity relationship, which will be addressed at a later time. The well count used for variogram and gridding was reduced to 322.

Initial porosity variograms appear to be reasonable. The Grayburg Dolomite has its greatest correlation trend in a north-northeast to south-southwest direction. The Grayburg Sandstone and the San Andres have their greatest correlation trend in an east to west direction. Because of a relative lack of core permeability, bedding plane variograms were not attempted. Instead, a decision was made to use variograms from the porosity data and then use these porosity variograms for both porosity and permeability grids.

Preliminary three-dimensional (3-D) porosity grids have been created using Texaco's kriging gridding algorithm. Texaco

is in the process of optimizing the grids. Two sets of each are anticipated: fine meshes for near wellbore simulation and coarser meshes for interwell flow simulation. The coarser meshes will be made directly from the well data variograms rather than from averaged versions of the fine mesh grids. Grid size optimization is proceeding with input from the compositional simulation experts, so the end product will better support the simulation process.

As an alternate approach for distribution of permeability, consideration will be given to using the neural network capability to assign permeability values to each grid cell that directly corresponds to the geostatistically determined porosity.

Parametric Simulation

A study of the various parameters affecting the technology will be undertaken with a compositional simulator. An equation of state (EOS) has been developed and an investigation into the use of local grid refinement is under way.

Constant composition expansion experiments were run on samples of CVU crude oil with increasing concentrations of CO_2 . No single phase was formed below 6000 psia (equipment limitation) for any of the mixtures. Phases included a CO_2 -rich vapor (V), a hydrocarbon-rich dark liquid (L1), and CO_2 -rich clear liquid (L2). Below 1158 psia, V and L1 are present, and above 1316 psia L1 and L2 are observed. Between these two pressures all three phases are present. Parameters are adjusted in the three-parameter Peng–Robinson EOS to match this data and provide proper CO_2 -oil phase behavior descriptions for use in a compositional simulation model. Western Atlas' DESKTOP-PVT and VIP compositional simulators are being used in this exercise. Since compositional simulators are limited to two-phase equations of state, approximations were required to deal with the three-phase behavior observed in the laboratory experimentation.

Before the experimental data were matched, the C_{7+} fraction of the crude analysis was split into three pseudocomponents. In order to reduce the number of components and thus the run-time of the compositional simulation, the small amount of nitrogen was combined with the methane, and the C_5 and C_6 components were combined. Thus the system was represented with nine pseudocomponents including CO_2 .

The Omega A and Omega B EOS parameters for the three heaviest pseudocomponents and the binary interaction parameters between these pseudocomponents and CO_2 were adjusted to fit the experimental phase behavior data. Viscosities were matched by adjusting the critical z-factor of these three components in the Lohrenz–Bray–Clark viscosity correlation. To ensure proper CO_2 densities over the range of pressures anticipated in the CVU project, the CO_2 volume shift parameter was adjusted.

A reasonable match of the bubble points resulted. An excellent match was obtained for the relative volume as a function of pressure, the easiest property to match. A match of the liquid volume fraction at pressures below the bubble point was found, as was viscosity. A good match of CO_2 densities over the range

of pressures likely for the project was found. The hardest match was the L1 volume fraction for the high mol % CO₂ mixtures. More effort will be directed toward an improvement of the current match. Slim-tube experiments will be simulated to assist in development of a reasonable fit of the live oil-CO₂ phase behavior data, with special consideration for complexity of dealing with the three-phase system.

A local grid refinement option in Western Atlas' VIP simulator is available. This option allows for finer gridding in local regions within a coarser reservoir model. This will allow for smaller grids near a CO₂ HnP well while controlling computer run-time with larger grids in the surrounding reservoir. This option is a prerequisite to proper evaluation of the proposed technology.

An exercise was taken to evaluate the significance of grid size and various finite difference approximations on predicted oil recovery. A clear significance of nine-point vs. five-point finite difference approximations was found when dealing with a coarser grid. Local grid refinement in this case did not appear to have a significant effect on oil recovery. A finer grid was made that resulted in similar recoveries for both the five-point and nine-point approximations. The conclusion of these initial exercises

was that local grid refinement may not be necessary for a nine-point formulation. However, the benefits of local grid refinement to the analysis of near wellbore effects such as pressure, which will dominate much of the field demonstrations, have not yet been addressed.

Technology Transfer

A presentation was made to a consortium of 40 North American oil industry producers, service companies, laboratories, and educational institutions on October 4, 1994, at the Colorado School of Mines, Golden, Colo. The consortium was interested in the process as it relates to the potential of dynamic reservoir characterization. The presentation briefly covered the scope of the project and identified the general approach and technology, benefits, and anticipated results. The group is looking for a field location to perform a high resolution 3-D seismic group shoot. The goal is to monitor/track CO₂ in the reservoir. Numerous reporters have contacted the Program Manager for interviews concerning the project. Various articles have been published regionally and are being retained in Texaco's files.

Objective

The objective of this project is to provide the operators of the small- to medium-size oil field with the tools necessary for an enhanced oil recovery (EOR) evaluation of the same quality and sophistication that only large international oil companies have been able to afford to date.

Summary of Technical Progress

Project activity this quarter focused on data acquisition and organization. Well data, including drillers' logs, wireline logs, and seismic data, from the Crystal and other Dundee hydrocarbon fields in the Michigan Basin were purchased from Maness Petroleum Co. These data, when combined with the data compiled at Western Michigan University (WMU), should comprise a complete set of well information for the Dundee formation.

Twenty to thirty cores of the Dundee formation from throughout the state of Michigan are available. Cuttings samples are also available from 60 to 100 Michigan wells.

RECOVERY OF BYPASSED OIL IN THE DUNDEE FORMATION USING HORIZONTAL DRILLING

Contract No. DE-FC22-94BC14983

**Michigan Technological University
Houghton, Mich.**

Contract Date: Apr. 28, 1994

Anticipated Completion: Apr. 27, 1997

Government Award: \$800,000

**Principal Investigator:
James R. Wood**

**Project Manager:
Chandra Nautiyal
Bartlesville Project Office**

Reporting Period: July 1-Sept. 30, 1994

The storage locations of many of these cores and cuttings samples have been identified.

A well that will include both a horizontal and a vertical leg has been designed and permitted and will soon be drilled.

Project Management

Project management is being implemented through visits to all project sites, including visits to Houghton every six weeks for 4 to 5 d. These visits have served to keep project personnel aware of progress at each site and as a focal point to organize and present progress in a semiformal format. They also offer opportunity for the discussion of problems and the proposal of changes.

Reservoir Characterization

The goal of this task is to quantify reservoir heterogeneities and controls on producibility with the use of geologic, hydrologic, and engineering techniques. The Crystal field will be the focus of the characterization effort, but up to 30 other Dundee fields will also be studied. Data from 18 Dundee fields were entered into the TerraSciences TerraSystem database at WMU this quarter; this brings the total number of fields in the database to 30. Digital well data are available for 21 of these 30 fields. With the use of the TerraSciences TerraStation computer program, structure contour maps and isopach maps are being generated for horizons in these 21 fields. Table 1 lists all the oil and gas fields that produce or have produced from the Dundee formation in Michigan, and Table 2 lists the Dundee fields that are included in this study.

TABLE 1
Michigan Basin Dundee Oil and Gas Fields

Field name	County	Location	Date	Depth, ft	Area	Pay	Oil, bbl	Gas, Mcf
Adams	Arenac	26-19N-03E	1937	2958	350	15	1,685,976	0
Akron	Tuscola	26-14N-07E	1936	2678	1200	17	2,473,671	0
Arbela	Tuscola	33-10N-07E	1946	2557	450	7	382,290	0
Ashton	Osceola	05-18N-10W	1945	3645	200	5	526,505	0
Bard	Gladwin	06-17N-02W	1949	3933	170	6	598,674	0
Beaverton	Gladwin	11-17N-02W	1934	3929	330	12	904,832	0
Beaverton-West	Gladwin	19-17N-02W	1943	3876	260	2	251,898	0
Beaverton-South	Gladwin	36-17N-02W	1936	3845	720	12	1,862,335	0
Belly Achers	Montcalm	14-12N-06W	1944	3470	220	1	361,510	0
Bentley	Gladwin	29-17N-02E	1937	3510	1920	13	3,287,155	0
Billings-South	Gladwin	12-17N-01E	1957	3540	80	5	248,401	0
Billings	Gladwin	02-17N-01E	1949	3549	400	6	946,334	0
Birch-Bela	Saginaw	25-10N-06E	1951	2504	350	7	431,248	0
Birch Run	Saginaw	20-10N-05E	1954	2536	480	10	643,657	0
Brinton	Isabella	05-16N-06W	1967	4082	40	3	27,496	0
Broomfield	Isabella	09-14N-06W	1979	3752	520	3	411,299	0
Buckeye North	Gladwin	11-18N-01W	1936	3615	3160	14	20,722,296	9,781
Buckeye South	Gladwin	25-18N-01W	1936	3570	2490	11	5,338,937	0
Burdell	Osceola	19-20N-10W	1959	3678	120	4	161,004	0
Cat Creek	Osceola	04-17N-09W	1968	3696	300	4	510,123	0
Cato	Montcalm	06-12N-12W	1944	3542	670	3	1,199,173	0
Cedar	Osceola	28-18N-09W	1943	3810	420	2	1,216,297	0
Clayton	Ogemaw	31-21N-04E	1935	2465	1290	12	6,854,751	0
Coldwater	Isabella	08-15N-06W	1944	3692	3200	25	22,274,752	6,277,030
Cranberry Lake	Clare	01-20N-06W	1943	3835	70	2	2,243,869	0
Cranberry Lake East	Clare	08-20N-05W	1963	3760	16	6	848,224	0
Crystal Valley	Oceana	19-16N-16W	1971	2222	180	11	4,002	0
Crystal	Montcalm	02-10N-05W	1935	3187	2000	4	7,916,742	0
Currie	Isabella	05-16N-04W	1936	3918	40	2	212,286	0
Day	Montcalm	36-11N-06W	1954	3337	20	20	16,239	0
Day sec. 13	Montcalm	13-11N-06W	1971	3414	20	15	29,722	0
Deep River	Arenac	08-19N-04E	1944	2795	1060	145	27,189,771	0
Douglass	Montcalm	01-11N-07W	1945	3400	120	2	260,276	0
Eden	Mason	26-17N-16W	1948	2240	380	8	3,129,640	***330,378
Edenville	Midland	27-16N-01W	1938	3790	370	8	1,392,721	0
Edwards	Ogemaw	15-21N-01E	1951	3362	90	10	43,690	0
Elmwood	Tuscola	21-14N-11E	1945	2740	90	80	113,084	0
Entrican	Montcalm	21-11N-07W	1967	3312	200	2	159,206	0
Essexville	Bay	07-14N-06E	1944	2835	1730	17	3,815,456	3,249

(Table continues on next page.)

TABLE 1 (Continued)

Field name	County	Location	Date	Depth, ft	Area	Pay	Oil, bbl	Gas, Mcf
Evart	Osceola	23-18N-08W	1970	3755	1100	6	3,812,127	0
Fork	Mecosta	05-16N-07W	1942	3845	2700	8	7,777,026	0
Freeman-Redding	Clare	04-18N-06W	1938	3885	2800	19	16,957,088	1,945,432
Freeman-Lincoln	Clare	18-18N-05W	1980	3975	120	2	37,666	0
Geneva sec. 4	Midland	04-15N-02W	1975	3718	40	32	10,112	0
Geneva	Midland	19-15N-02W	1935	3671	70	2	63,143	0
Gibson sec. 20	Bay	20-18N-03E	1951	3097	30	11	40,464	0
Gilmore	Isabella	30-16N-05W	1955	3803	160	3	420,067	0
Goodwell east	Newaygo	26-14N-11W	1978	3294	440	20	81,418	****16,793
Goodwell	Newaygo	08-14N-11W	1982	3404	120	8	6,195	0
Hardy Dam	Mecosta	05-13N-10W	1966	3351	920	5	1,203,629	0
Harrison	Clare	07-18N-04W	1945	4190	80	13	179,767	0
Hatton	Clare	31-18N-04W	1941	3945	160	2	139,272	0
Home sec. 26	Montcalm	27-12N-06W	1970	3513	200	7	115,982	0
Hubbardston	Ionia	04-08N-05W	1947	3028	50	5	48,479	0
Isabella	Isabella	07-15N-04W	1948	3783	410	9	831,459	137,806
Jerome	Midland	07-15N-01W	1947	3743	260	10	262,440	0
Kawkawlin	Bay	01-14N-04E	1938	2830	6360	45	16,089,347	4,565
Lake George	Clare	06-18N-05W	1954	3968	100	2	392,270	0
Lakefield	Saginaw	01-11N-01E	1937	3185	10	12	36,656	0
Leaton	Isabella	25-15N-04W	1929	3657	510	8	1,863,346	0
Leroy	Osceola	27-19N-10W	1965	3796	80	4	50,331	0
Lincoln sec. 27	Isabella	27-13N-04W	1974	3577	80	10	16,688	0
Luther north	Lake	08-19N-11W	1970	3518	160	17	17,418	0
Marathon	Lapeer	18-09N-09E	1979	2629	80	5	33,985	0
McBain	Missaukee	19-21N-07W	1959	3969	920	15	3,458,435	0
Mills sec. 01	Midland	01-16N-02E	1957	3450	10	2	8,363	0
Mineral Springs	Osceola	20-20N-09W	1951	3854	240	7	315,700	0
Moffatt sec. 34	Arenac	34-20N-03E	1953	2984	10	4	9,426	0
Mt. Pleasant	Midland	18-14N-02W	1928	3545	5890	15	28,649,460	7,965,509
Mt. Forest	Bay	13-17N-03E	1947	3025	960	9	979,810	0
Mt. Haley	Midland	28-13N-01E	1934	3477	10	3	36,069	0
Nellsville	Roscommon	17-22N-04W	1957	3710	10	6	16,528	0
North Fork	Osceola	33-17N-07W	1951	3788	120	3	153,661	0
North Adams	Arenac	22-19N-03E	1940	2905	520	15	9,539,161	0
Otisville	Genessee	06-09N-08E	1944	2450	50	3	38,256	0
Pinconning	Bay	02-16S-04E	1944	2898	100	7	902,037	0
Pine River	Gratiot	31-12N-03W	1942	3280	90	2	13,285	0
Porter	Midland	22-13N-01W	1933	3415	6740	12	50,458,739	4,965,878
Prosper south	Missaukee	36-22N-06W	1967	3798	280	8	1,040,445	0
Prosper	Missaukee	26-22N-06W	1942	3837	520	4	1,892,033	0
Reed City	Osceola	31-18N-10W	1940	3490	5000	3	42,899,940	0
Reynolds	Montcalm	01-12N-10W	1954	3343	2100	2	4,799,625	0
Riverside	Missaukee	14-21N-07W	1942	3944	220	3	223,378	0
Robinson sec. 3	Ottawa	03-07N-15W	1956	2107	20	7	10,630	0
Rolland	Isabella	24-13N-06W	1979	3560	200	6	50,591	0
Sage	Gladwin	12-19N-02W	1971	3867	120	2	73,914	0
Sanford	Midland	13-15N-01W	1951	3755	260	3	225,808	0
Secord	Gladwin	11-19N-01E	1937	3437	20	5	12,024	0
Sherman	Isabella	04-14N-06W	1936	3650	1020	4	4,797,158	637,734
Skeels	Gladwin	30-20N-02W	1950	3840	50	7	1,008,455	0
Sterling	Arenac	18-19N-04E	1947	2872	200	17	488,261	0
Sterling sec. 30	Arenac							
Sylvan	Osceola	09-18N-07W	1948	3925	440	14	1,215,711	0
Vernon-Rosebush	Isabella	07-15N-04W	1933	3690	2060	6	7,970,701	435,378
Vogel Center	Missaukee	32-21N-06W	1966	3892	80	3	52,430	0
West Branch	Ogemaw	27-22N-02E	1933	2650	3630	20	11,974,587	0
Wheatland	Mecosta	07-14N-07W	1945	3690	100	2	141,631	0
White River	Muskegon	15-12N-18W	1950	2053	20	2	7,061	0
Winfield	Montcalm	20-12N-09W	1936	3340	120	1	119,312	0
Winterfield	Clare	35-20N-06W	1940	3794	2740	3	5,024,265	0
Wise	Isabella	28-16N-03W	1938	3700	1620	11	4,087,240	0

TABLE 2
Dundee Formation Fields Included in This Study

Field name	County	Location	Date	Depth, ft	Area	Pay	Oil, bbl	Gas, Mcf
Cranberry Lake	Clare	01-20N-06W	1943	3835	70	2	2,243,869	0
Cranberry Lake East	Clare	08-20N-05W	1963	3760	16	6	848,224	0
Freeman-Redding	Clare	04-18N-06W	1938	3885	2800	19	16,957,088	1,945,432
Lake George	Clare	06-18N-05W	1954	3968	100	2	392,270	0
Winterfield	Clare	35-20N-06W	1940	3794	2740	3	5,024,265	0
Skeels	Gladwin	30-20N-02W	1950	3840	50	7	1,008,455	0
Broomfield	Isabella	09-14N-06W	1979	3752	520	3	411,299	0
Coldwater	Isabella	08-15N-06W	1944	3692	3200	25	22,274,752	3,277,030
Currie	Isabella	05-16N-04W	1936	3918	40	2	212,286	0
Gilmore	Isabella	30-16N-05W	1955	3803	160	3	420,067	0
Isabella	Isabella	07-15N-04W	1948	3783	410	9	831,459	137,806
Leaton	Isabella	25-15N-04W	1929	3657	510	8	1,863,346	0
Sherman	Isabella	04-14N-06W	1936	3650	1020	4	4,797,158	637,734
Vernon-Rosebush	Isabella	07-15N-04W	1933	3690	2060	6	7,970,701	435,378
Wise	Isabella	28-16N-03W	1938	3700	1620	11	4,087,240	0
Fork	Mecosta	05-16N-07W	1942	3845	2700	8	7,777,026	0
Hardy Dam	Mecosta	05-13N-10W	1966	3351	920	5	1,203,629	0
McBain	Missaukee	19-21N-07W	1959	3969	920	15	3,458,435	0
Prosper	Missaukee	26-22N-06W	1942	3838	520	4	1,892,033	0
Prosper South	Missaukee	36-22N-06W	1967	3798	280	8	1,040,445	0
Riverside	Missaukee	14-21N-07W	1942	3944	220	3	223,378	0
Belly Achers	Missaukee	14-21N-06W	1944	3470	220	1	361,510	0
Cato	Missaukee	06-12N-12W	1944	3542	670	3	1,199,173	0
Crystal	Montcalm	02-10N-05W	1935	3187	2000	4	7,916,742	0
Douglass	Montcalm	01-11N-07W	1945	3400	120	2	260,276	0
Reynolds	Montcalm	01-12N-10W	1954	3343	2100	2	4,799,625	0
Cat Creek	Osceola	04-17N-09W	1968	3696	300	4	510,123	0
Cedar	Osceola	28-18N-09W	1943	3810	420	2	1,216,297	0
Evart	Osceola	23-18N-08W	1970	3755	1100	6	3,812,127	0
Sylvan	Osceola	09-18N-07W	1948	3925	440	14	1,215,711	0

Well-Log Acquisition, Digitization, and Analysis

Well data, including drillers' logs, wireline logs, and seismic data from the Crystal and other Dundee hydrocarbon fields in the Michigan basin were acquired from Maness Petroleum Co. Digitized logs of 342 wells that currently produce or have produced from the Dundee Formation in the seven-county study area were purchased from Maness Petroleum Co. Multiple logs exist for each well and include gamma-ray, caliper, lithodensity, neutron porosity, various types of resistivity, and some sonic logs. The logs total about 3 million linear feet of digitized data. All deep wells in the area are included in the log suite. The data compiled at WMU combined with the Maness data set complete a set of well information for the Dundee in this study area.

These data will be entered into files on the TerraSciences TerraStation computer program along with the data compiled at WMU. The use of a more flexible commercial database, such as Microsoft Access, to integrate and store the log and core data is being considered.

A number of operations will be performed to clean up and index the suite of well logs in each field before any calibration is attempted. Among these operations are depth-shifting, true vertical depth (TVD) and true stratigraphic thickness (TST)

corrections, normalization, and environmental corrections. These corrections will be performed on a commercially available log analysis computer program (e.g., T-Log from TerraSciences, Petrolog from Crocker Data Processing, or a similar program from another vendor). Core data will be used to aid in this calibration with the use of standard procedures.

Once the logs have been corrected, maps and log cross sections will be constructed. These will include well location maps, which show well type and well identifier; structure contour maps; isopach maps of selected intervals; initial production and cumulative production maps where data are available; and log cross sections. Preliminary versions have been prepared of a structure contour map on the top of the Dundee formation (Fig. 1), an isopach map of the top of the Dundee formation to the top of Dundee pay (Fig. 2), and a contour map of initial production values (Fig. 3), all for Crystal Field.

Core Acquisition and Analysis

Twenty to thirty cores of the Dundee formation from throughout the state of Michigan are available. Cuttings samples are also available from 60 to 100 Michigan wells. The storage locations of many of these core and cuttings samples have been identified. Table 3 contains a list of cores at WMU,

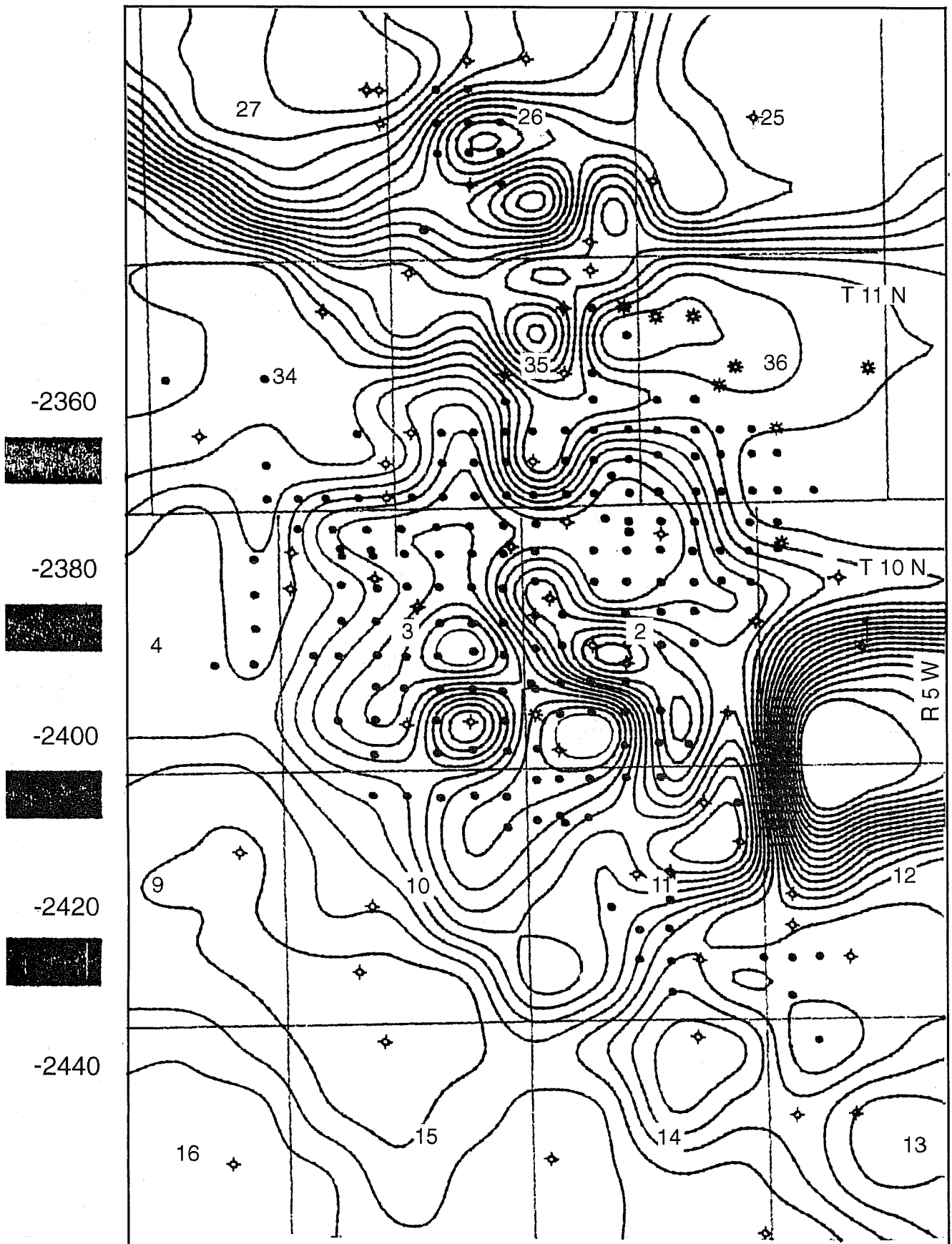


Fig. 1 Structure contour map on top of Dundee formation, Crystal field. Contour interval, 2.5 ft. (Art reproduced from best available copy.)

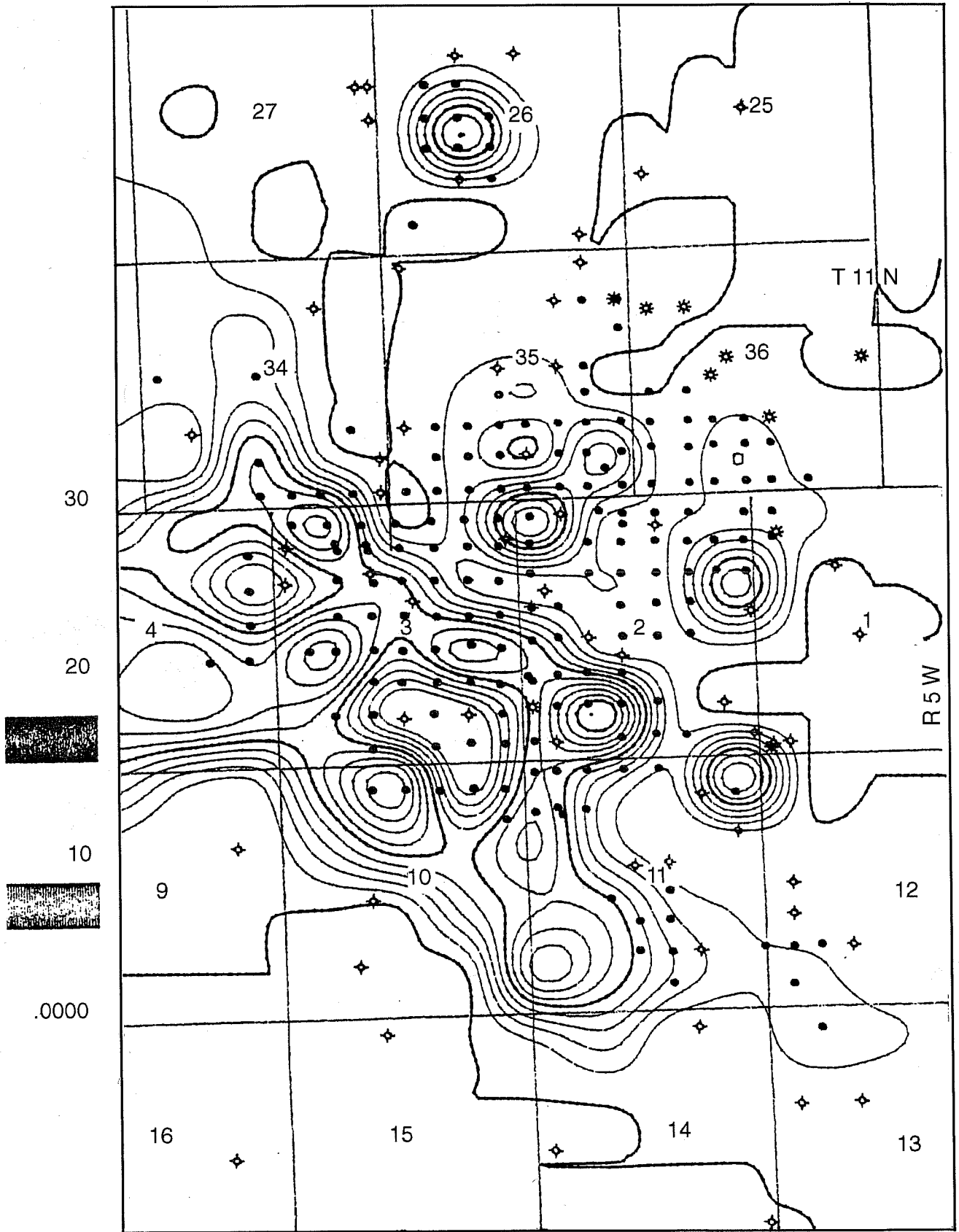


Fig. 2 Isopach map of top of Dundee formation to top of Dundee pay, Crystal field. Contour interval, 2 ft. TS, 5.1. (Art reproduced from best available copy.)

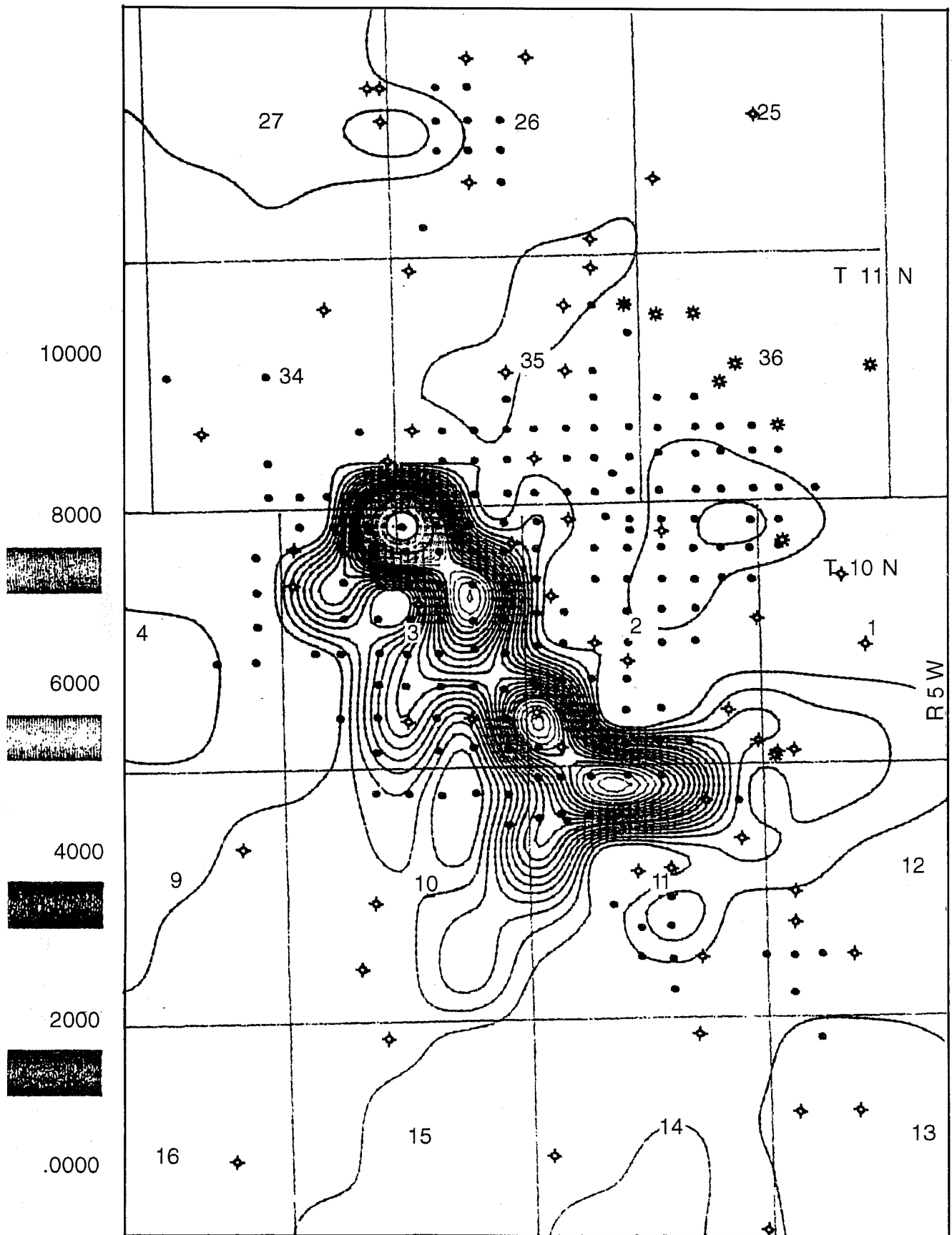


Fig. 3 Contour map of initial production, Crystal field. Contour interval, 250 bbl. TS, 5.1. (Art reproduced from best available copy.)

TABLE 3
Dundee Formation Core Collection*

County	Well name	Location						Formation	Core footage	Permit
Western Michigan University (36 Wells)										
Bay	Wood-Zimm/Krueger 2-8	995	FNL	885	FWL	NE	8 14N 3E	DUND-DUND	3558-3648	40122
Clare	Dart-Benchley 1-29	990	FNL	990	FWL	NW	29 20N 6W	BELL-RICH	3770-3807, 4950-5120	31186
Clare	Bwab-Cappaert 31-32A	330	FSL	330	FWL	NE	31 18N 4W	DUND-DUND	3903-3934	39618
Gladwin	Wiser-ST.B-6	729	FNL	673	FWL	NE	14 18N 1W	DUND-DUND	3595-3672	32780
Gladwin	Wiser-Arkwright 1-35	663	FNL	619	FWL	NE	35 18N 1W	DUND-DUND	3568-3628	35657
Gladwin	Wiser-Nash/Loar 2-35	560	FNL	660	FWL	SE	35 18N 1W	DUND-DUND	3620-3664	34621
Gladwin	Wiser-Bloomfield 1-1	655	FNL	660	FWL	NW	1 17N 1W	DUND-DUND		36765
Gladwin	Wiser-Woodring #5	350	FSL	660	FWL	SE	23 18N 1W	DUND-DUND	3585-3665	33009
Gladwin	Wiser-McMahon #1						36 18N 1W	DUND-DUND		
Gladwin	Wiser-Nash-Loar #1					SE	33 18N 1W	DUND-DUND		
Gladwin	Wiser-Woorward #1					NW		DUND-DUND		
Gladwin	Wiser-Rock #2							DUND-DUND		
Gladwin	Wiser-Wineman #2					NW	9 17N 1E	DUND-DUND		
Gladwin	Wiser-Havens #9						25 18N 1W	DUND-DUND		
Gladwin	Wiser-Oard #1						25 18N 1W	DUND-DUND		35697
Gladwin	Wiser-Fitzwater 1-26						26 18N 1W	DUND-DUND		
Gladwin	Wiser-Fitzwater 5-26					SE	26 18N 1W	DUND-DUND		34990
Gladwin	Wiser-Fitzwater 6-26						26 18N 1W	DUND-DUND		
Gladwin	Wiser-Oard 2-0	556	FSL	811	FWL	NW	25 18N 1W	DUND-DUND	3590-3648	41126
Gladwin	Wiser-Armstrong 1-0	1166	FNL	330	FEL	SW	23 18N 1W	DUND-DUND	3593-3651	41015
Gladwin	Wiser-Armstrong 2-0	330	FSL	1013	FEL	SW	23 18N 1W	DUND-DUND	3601-3656	41016
Gladwin	Wiser-Woodring Est2-0	1250	FNL	1280	FWL	SE	23 18N 1W	DUND-DUND	3590-3650	41014
Gladwin	Wiser-Irvin 3-0	639	FSL	628	FEL	NW	26 18N 1W	DUND-DUND	3570-3628	41017
Gladwin	Wiser-Sturm #3	660	FSL	738	FWL	NE	26 18N 1Q	DUND-DUND	3576-3634	41019
Gladwin	Wiser-Sturm 4-0	611	FNL	670	FWL	NE	26 18N 1W	DUND-DUND	3567-3613	41212
Gladwin	Wiser-Brushaber 2-0	560	FSL	660	FWL	SW	24 18N 1W	DUND-DUND	3592-3638	41013
Gladwin	Wiser-St. Buck D1-36	66	FNL	57	FWL	SE	36 18N 1W	DUND-DUND	3560-3619	
Gladwin	Wiser-Nusb/Kern 3W								3535-3596	
Gladwin	Wiser-Schrem/Shear 3-0								3565-3624	
Gladwin	Wiser-HAV/Denhams 1-0								3534-3595	
Lapeer	A&M Aq.-Kowalski 2-15	660	FSL	330	FWL	SE	15 9N 9E	REDC-RICH	2686-3158	36602
Missaukee	A&M Aq.-Gernaat 2-31	330	FNL	994	FWL	NE	31 21N 8W	DUND-RICH	3909-3939, 5025-5085	3625
Missaukee	Dart-Hamming 1-22	895	FSL	990	FEL	NE	22 21N 7W	TRAV-DUND	3215-3255, 3885-3925	31448
Newaygo	Che-Harris 2-8	660	FNL	990	FWL	SE	8 14N 11W	REDC-DUND	3398-3475	10322
Newaygo	Penin-McDonald 1-12	330	FSL	1019	FEL	SE	12 11N 11W	TRAV-REDC	2657-2705, 3202-3262	38437
Oscoda	Traver-St. Clint 1-10	419	FSL	824	FWL	SE	10 28N 3E	DUND-RICH	2330-2350, 3271-3331	35792
University of Michigan Subsurface Laboratory (35 Wells)										
Antrim	Sun-St. Mancelona A-1						36 29N 5W	DUND-BSIL	2553-4512	11572
Arenac	Bolder-St. Adam 1						14 19N 3E	TRAV-DUND	2878-3063	10572
Arenac	Basin-Sterling 1						8 19N 4E	DVNN-DUND	-2783	10691
Bay	Gulf-Schweirtz 1						1 14N 4E	DUND-DUND	2772-2862	9272
Clare	Pure-Hulder 1						18 17N 6W	TRAV-DUND	3885-3948	12376
Clare	Benedum-Woods Cor 1						3 19N 5W	TRAV-DUND	4000-4047	27390
Clare	Sun-Amstutz 1						8 20N 5W	DUND-DETR	3777-5139	25198
Gladwin	Hill-White 1						1 19N 2W	DUND-DUND	3904-3933	28835
Gratiot	MCGC-Shuttlew 1						5 10N 4W	TRAV-DUND	3241-3287	26779
Huron	Shell-Ashmore						20 15N 11E	DUND-CTRC	2696-7931	28772
Isabella	Rayburn-Clark 1						24 14N 5W	TRAV-DUND	3640-3738	15342
Isabella	Cities-Methner C-1						33 16N 3W	DUND-DUND	3687-3701	10898
Mecosta	MCGC-Depung 2						5 13N 10W	DUND-DETR	3361-3415	26652
Mecosta	MCGC-Shannon 1						5 13N 10W	DUND-DETR	3366-3426	26708
Mecosta	MCGC-Deporter 1						5 13N 10W	DUND-DETR	3360-3420	26734
Mecosta	MCGC-Deporter 2						5 13N 10W	DUND-DETR	3354-3414	26751
Mecosta	MCGC-St. Atena 1						6 13N 10W	DUND-DETR	3331-3359	26503
Mecosta	MCGC-Pruetz 1						6 13N 10W	DUND-DETR	3326-3386	26683

(Table continues on next page.)

TABLE 3 (Continued)

County	Well name	Location	Formation	Core footage	Permit
Mecosta	MCGC-Armstrong 1	8 13N 10W	DUND-DETR	3300-3382	26517
Mecosta	Leonard-Stout 1	26 13N 10W	DUND-DETR	3477-3525	22580
Missaukee	Ashby-Deruyer 1	92 1N 6W	DUND-DUND	3934-3950	9729
Missaukee	Pure-Nix 1	11 23N 5W	ANRM-DUND	2459-3199	9582
Montcalm	Leonard-Stiner 1	16 12N 8W	DUND-DETR	3520-3627	21970
Newaygo	Sun-Bradley 4	11 12N 13W	TRAV-PRDC	2305-6687	13816
Newaygo	Cities-Billings 3	8 14N 11W	TRAV-DUND	2747-3245	10468
Newaygo	Cities-Fetter 2	9 14N 11W	DUND-DETR	3278-3473	10374
Oceana	Noheco-Fedo 1-27	27 15N 16W	DUND-REDC	2617-2754	35393
Oceana	Carter-Golden A2	35 15N 18W	DUND-DUND	2222-2262	14897
Oceana	Carter-Lauber 12	6 16N 17W	TRAV-PRDC	1823-5382	17549
Osceola	MOCG-Rieman 1	4 17N 9W	TRAV-DUND	3708-3767	27191
Osceola	CPC-Dahmer 1	9 20N 7W	TRAV-RICH	3909-5181	25984
Wayne	Int. Salt-PCLM 49	2S 11E	DUND-SLIN	94-1170	80023
Wayne	Int. Salt-Airpo 5	3S 9E	DUND-SLIN	88- 856	80019
Wayne	Int. Salt-Airpo 4	3S 9E	DUND-SLIN	95- 801	80018
Wayne	Wyndot Chem-H-1A	3S 10E	DUND-SLIN	81-1547	80025
Central Michigan University (2 Wells)					
Montcalm	Leonard-Lee No. 1	08 11N 05W	DUND-DUND	3461-3496	24011
Osceola	Mich Con-Reiman 1	04 17N 09W	BELL-DUND	3708-3767	27191
State of Michigan at Marquette (8 Wells)					
Isabella	Sohio-Hoffman #2	29 16N 06W	DUND-DETR	3755-5090	11394
Isabella	Smith-Norfleet #1	33 16N 06W	DUND-DUND	3755-3789	11804
Kalkas	Sun-Brunn #1	06 26N 05E	TRAV-DETR	2021-4623	14638
Missaukee	Gordon-Miss. Lakes #1	29 23N 08W	TRAV-DUND	2990-3026, 3644-3655	11830
Osceola	Sohio-Buxton #1	13 17N 07W	DUND-DUND	3860-3878	12385
Osceola	McGuire-State A-1	34 18N 09W	DUND-DUND	3886-3908	10015
Sanila	Dow-Dow-ERDA #100	08 09N 15E	SUNB-DETR	820-2057 (Misc. Footages)	
Tuscola	Gulf-Lassiter #1	05 13N 09E	DUND-SYLV	2794-2974, 3498-3594, 4117-4120	10511

*Well information is stored according to the following format: (A6, 1X, I20,2(1X,I4,1X,A3), 1x,A2,1X,I2,2(1X,I2,A1), 1X,A9,1X,A31,1X,I5).

University of Michigan, Central Michigan University, and the State of Michigan core repository at Marquette. A database called COREDAT, provided by Maness Petroleum Co., is being used to search the drillers' reports and core analysis files for cores that may have been missed.

There are no cores in Crystal field, the site of the field trial in this study. The closest Dundee core is in an outpost well 8 to 10 miles from Crystal field. Thus acquisition of a good vertical core through the Dundee in Crystal field is an essential element of the reservoir characterization study. Porosity (p), permeability (k), and oil saturation (s) data for all the Dundee cores from wells in a seven-county area surrounding Crystal field are complete (Table 3). This includes data from some cores that are no longer available. These data as well as formation factor (f) will be entered into the database.

When all available core material has been identified, samples will be collected from each core to provide good coverage of all the lithofacies and porosity types present in the Dundee formation. Where possible, samples from both producing and nonproducing intervals will be gathered. In

areas where no cores are available, drill cuttings will be sampled. Drill cuttings collections are housed at WMU, the University of Michigan, Central Michigan University, and the Michigan Geological Survey in Lansing, Mich.

Optical methods will be used to perform point counts for mineralogy, grains, matrix, cement, and porosity on approximately 60 to 100 polished thin sections of core and cuttings samples. Each thin section will require about 300 point counts. If needed, image analysis will be used to supplement identification of phases and to determine shape factor and rock texture. The selection of samples for x-ray diffraction (XRD) and scanning electron microscope (SEM) analysis has begun, and a few preliminary SEM analyses have been made.

FTIR Spectroscopy

Fourier transform infrared (FTIR) spectroscopy analysis has begun. Standards and initial samples have been prepared. These FTIR data will be correlated with other data and will be used to help make log correlations.

Fluid Samples

Hydrocarbon and produced-water samples from the Crystal field have yet to be collected and analyzed. If possible, arrangements will be made to sample fluids from other Dundee fields as well. Inorganic geochemical analyses of produced brines will be used in conjunction with isotope and fluid inclusion analyses of core and cuttings to determine the origin and history of the porosity-producing dolomitizing fluid.

Database Management

This task includes all activities required to establish and maintain a database of all the data collected under this project. A commercially available computer database management program will be used. At WMU, the TerraSciences TerraStation program is being used to archive and manipulate project data. At MTU, the use of a multi-vendor applications package to handle database, mapping, log evaluation, two-dimensional (2-D) cross-sectioning, and three-dimensional (3-D) visualization needs is being evaluated. An attempt will be made to standardize software for the two projects. During this quarter a test database

was constructed in Microsoft Access, and its potential is favorable.

Drilling

A vertical well at an appropriate location in the project area has been designed and permitted and will be drilled. Drilling is expected to commence in late 1994 or early 1995 after completion of an environmental survey.

Technology Transfer

This task focuses on technology transfer of information derived in this study through academic, technical, and commercial channels.

Technical papers describing aspects of this project are being prepared and will be presented at professional meetings and symposia and published in appropriate journals.

A three-day workshop/conference at the University of South Florida in Tampa, Fla., is scheduled for January 19–21, 1995. This conference will focus on preliminary results from this project as well as on results from another DOE project that involves reservoir characterization of a field in California.

IMPROVED RECOVERY DEMONSTRATION FOR WILLISTON BASIN CARBONATES

Contract No. DE-FC22-94BC14984

**Luff Exploration Company
Denver, Colo.**

**Contract Date: June 10, 1994
Anticipated Completion: June 9, 1997
Government Award: \$483,284**

**Principal Investigator:
Larry A. Carrell**

**Project Manager:
Chandra Nautiyal
Bartlesville Project Office**

Reporting Period: July 1–Sept. 30, 1994

shallow-shelf carbonate reservoirs in the Williston Basin in Montana, North Dakota, and South Dakota.

Summary of Technical Progress

The majority of technical efforts during this quarter have been concentrated on the Ordovician Red River formation in Bowman and Harding counties of North Dakota and South Dakota.

The Cold Turkey Creek (Ordovician Red River) field area (T. 130 N., R. 10 W.) in Bowman County, North Dakota, has been identified as the most suitable candidate for a three-dimensional (3-D) seismic survey. Acquisition of the data should begin in November 1994 after the location and orientation are refined from integrated interpretations of reprocessed two-dimensional (2-D) seismic data and well-log formation tops.

Data obtained during the 1970s and 1980s from approximately 145 km (90 miles) in the Bowman County, North Dakota, area have been cataloged for possible reprocessing. Reprocessing of these older data for 14 lines over 56 km (35 mil) has been successful. Frequency has increased from 40 to 80 Hz at Red River time with much clearer resolution of faulting.

A 2-D seismic line has been shot over the Southwest (SW) Amor (Ordovician Red River) field (T. 130 N., R. 104 W.) area. This high-fold line is a prelude to 3-D survey design

Objectives

The objectives of this project are to demonstrate targeted infill and extension drilling opportunities, better determinations of oil in place, methods for improved completion efficiency, and the suitability of waterflooding in certain

parameters and a better understanding of a candidate Red River reservoir for testing water injectivity and possible unitization for secondary recovery by waterflooding.

Seismic modeling of seismic shear response has begun for the Ratcliffe study area in Richland County, Montana. A probable location has been identified for a multicomponent 2-D line that would cross Cattails (Madison Ratcliffe) field in T. 26 N., R. 59 E., Richland County, Montana. This acquisition will be scheduled after the modeling is complete.

Secondary recovery operations by water injection and reservoir parameters have been studied by history matching with the use of computer simulation at the West Buffalo Red River "B" Unit (T. 21 N., R. 3 E.), Harding County, South Dakota. Results obtained from the West Buffalo history match were applied to a waterflood prediction by computer simulation for the SW Amor (Red River) field in T. 130 N., R. 103 W., Bowman County, North Dakota.

A meeting was held with working interest owners (WIO) of the SW Amor (Red River) field (T. 129–130 N., R. 103 W.), Bowman County, North Dakota, to discuss possible interest in forming a waterflood secondary recovery unit testing new completion and seismic technology. A majority interest was obtained to proceed with the formation of a technical committee and to acquire additional seismic data for a better definition of portions of the reservoir.

Reservoir performance parameters for volumetric drainage, transmissibility, and water-drive index have been evaluated with the use of Fetkovich production type curves for a sampling of Red River wells in North Dakota.

Reservoir Analysis and Characterization

Geophysical Evaluations

Older vintage, low-fold, 2-D data from a total of 14 seismic lines covering 56 km (35 miles) in the Bowman–Harding Red River study area have been reprocessed. Reprocessing of similar vintage data for an additional 9 lines covering 58 km (36 miles) is nearing completion. The reprocessing procedure involves a state-of-the-art sequence, including refraction statics and radon stack, to provide higher frequency and therefore better resolution interpretation of the field area, to allow identification of optimal processing parameters for reprocessing other lines, and to determine the application of workstation technology to the interpretation of these data. Post-stack frequency–distance deconvolution was applied in order to increase the signal-to-noise ratio. Spectral whitening greatly increases the high-frequency data content, and refraction statics provide considerable improvement in static corrections and the structural reliability of the data. The radon stack provides markedly improved sections through noise and multiple rejection. This reprocessing sequence is particularly cost-effective and dramatic on lower-fold (6–12) data like those generally found for this area. The frequency reflector time at Red River is increased from 40 to 50 Hz to 75 to 85 Hz. The improved resolution obtained from the reprocessed lines provides an opportunity for some stratigraphic interpretation and subdivision of the Red River interval.

A coarse 2-D seismic grid covers the SW Amor (Red River) field, T. 129–130 N., R. 103 W., Bowman County, North Dakota (Fig. 1). Seven seismic lines covering 35 km (22 miles) shot in the 1970s were reshot to help develop optimal processing sequences and parameters and to determine if seismic data can help define fracture and porosity trends in the area. These data were acquired with conventional parameters for that vintage [i.e., six-fold, deep-hole dynamite (11 kg at 35 m, 25 lb at 115 ft) with short spread offsets (1557–68–0–68–1557 m or 5060–220–0–220–5060 ft) and 134 m (440 ft) group/268 m (880 ft) shot intervals]. At the Red River zone of interest, the highest frequencies observed on the stacked sections are 40 to 50 Hz, which does not provide sufficient resolution for detailed analysis of individual zones or differentiation of response from benches 21 m (70 ft) apart. The lines have numerous large skips where surface conditions precluded shooting. Data quality and acquisition parameters are representative of conventional/traditional Williston Basin seismic exploration tools. The frequency content and utility for conventional structural and isochron interpretation are within the norm.

Paleo-growth and fault timing appear to be complex, but preliminary results suggest that key growth for economic Red River reservoir development is Devonian and older. The interlake to Red River isochron and the interlake to Winnipeg isochron demonstrate early growth of the feature. Primary structural growth of the feature occurred by the end of interlake time and was accompanied by down-to-the-east faulting along its eastern flank. A major down-to-the-east fault bounds the field area to the east and has several associated smaller normal faults in the northern part of the area. Throw on these faults diminishes upward and is not detectable above the interlake horizon, which indicates that faulting is probably late Silurian to Devonian in age. The large fault bounding the field on the east side exhibits approximately 12 m (40 ft) of throw to the north near the 44-30 Nygaard well and an average of 6 to 9 m (20 to 30 ft) of throw to the south near the 1-32 Nygaard well. This amount of throw is significant enough to provide an effective communication barrier to Red River producing zones with thicknesses from 2 to 6 m (6 to 20 ft).

A new 2-mile line acquired at SW Amor extending southwest to northeast crossing the major field fault is providing data in secs. 30 and 31, T. 130 N., R. 103 W. (Fig. 1). New parameters include 20-fold, 34/100-m (110/330-ft) group/shot intervals and 2134-m (7000-ft)-long offsets. This line was designed and shot to provide extension of field area, understanding of fault trend, determination if higher resolution data can help in the definition of reservoir (i.e., porosity, thickness, and continuity), the partial assessment of amplitude vs. offset (AVO) and to aid in the selection of 3-D design and parameters in the Bowman area.

Additional older seismic data from the Grand River School area, T. 129 N., R. 101 W., Bowman County, North Dakota (Fig. 2). These data were of an older vintage and had been recorded analog but with similar parameters. The data for seven lines covering 21 km (13 miles) were converted from

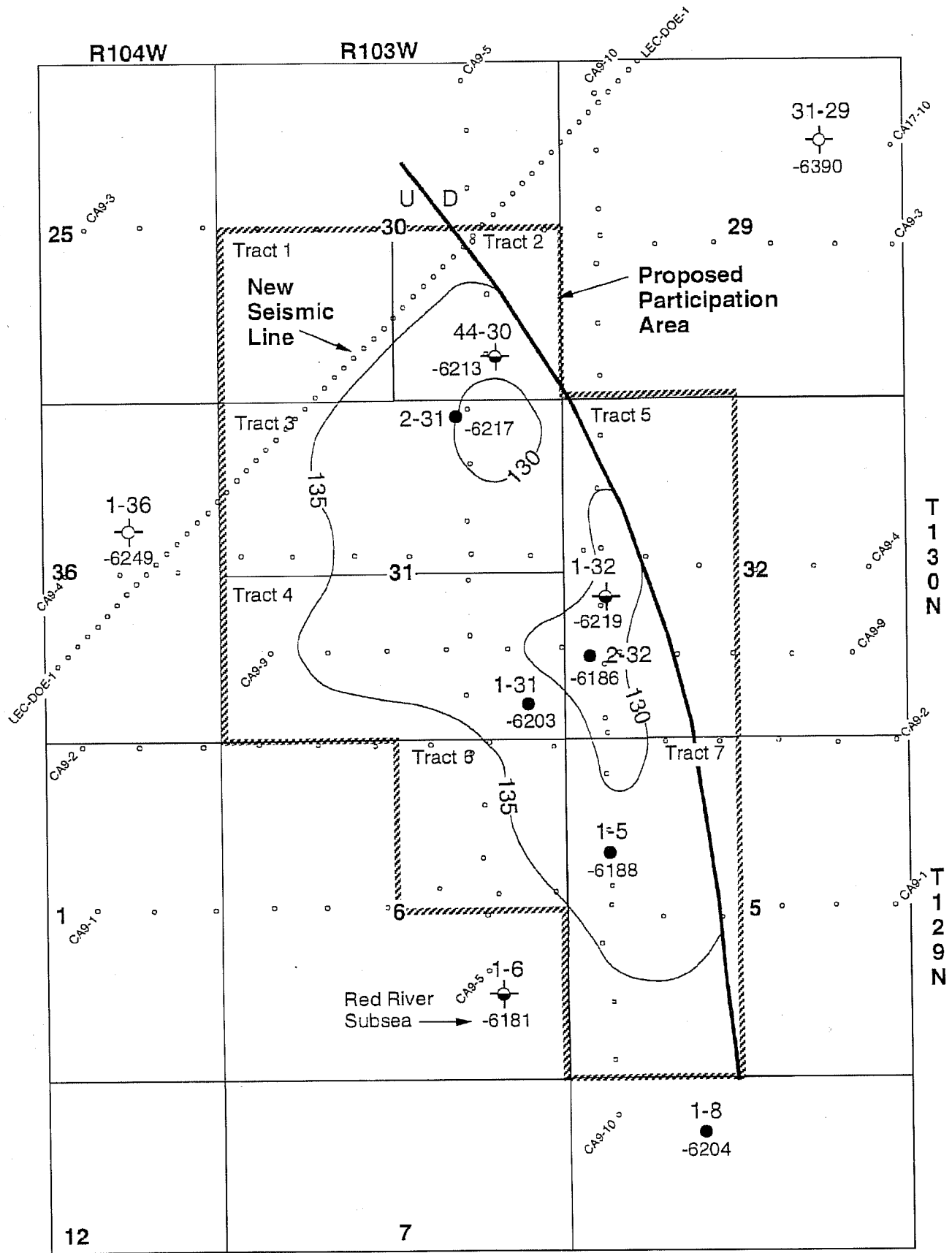


Fig. 1 Interlake-Winnipeg isochron productive limits, Southwest Amor area, Bowman County, North Dakota. Contour interval, 5 ms. (Art reproduced from best available copy.)

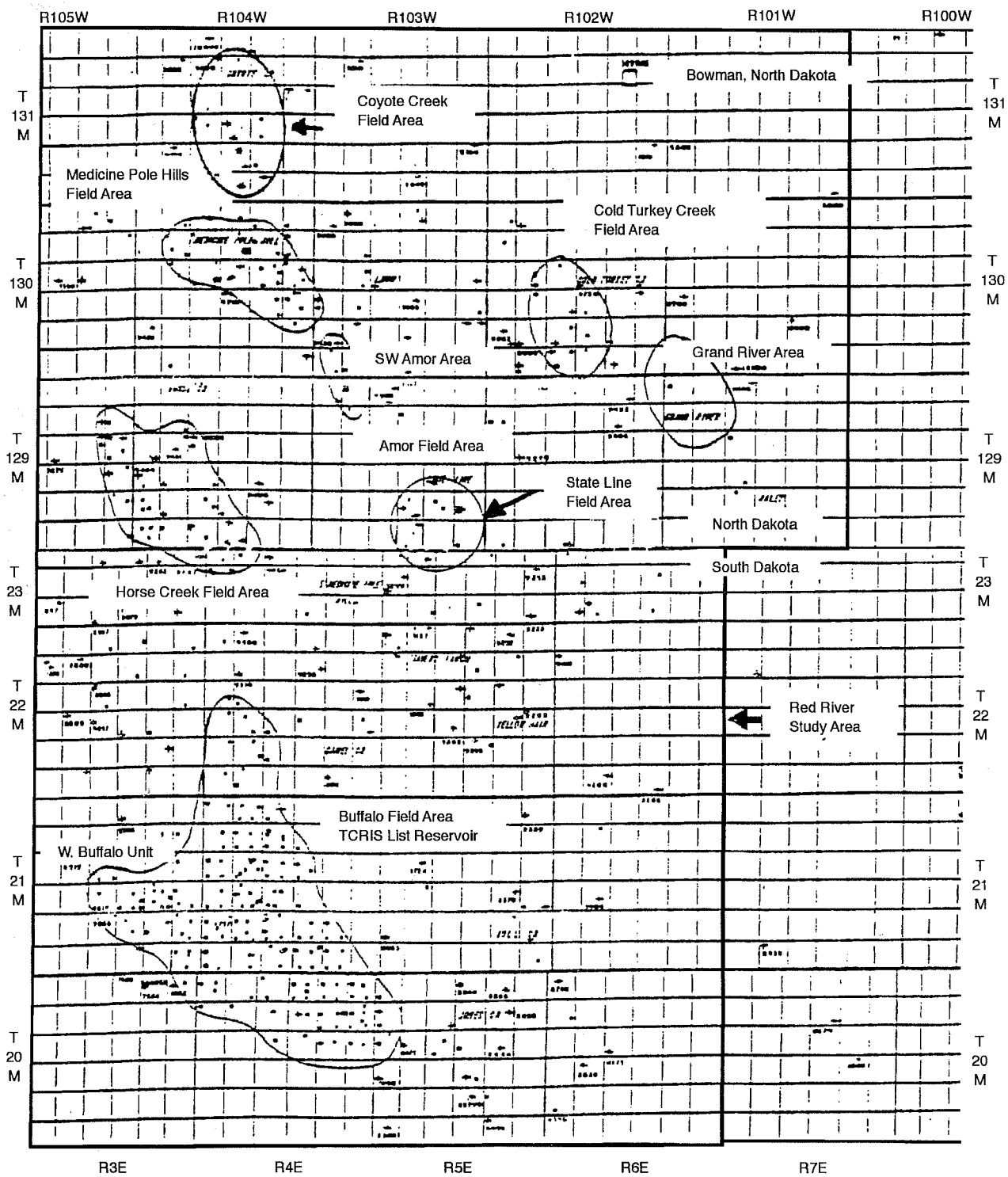


Fig. 2 Index map, Red River reservoir areas, Southern Williston Basin. (Art reproduced from best available copy.)

analog to digital and reprocessed with the same sequence determined from the Amor reprocessing. Again, the resulting sections showed lower noise, significantly higher frequency/resolution, and faulting.

Data for four lines at Cold Turkey Creek, T. 130 N., R. 102 W., Bowman County, North Dakota, were converted from analog to digital (Fig. 2). Data for five lines covering 37 km (23 miles) have been selected for reprocessing and are near completion. Data for two lines in the Stateline area, T. 129 N., R. 103 W., are being converted from analog to digital, and reprocessing of data for a total of four lines covering 21 km (13 miles) in that area is pending results from Cold Turkey Creek.

Work has been done to screen areas for the first 3-D survey in the Bowman–Harding area. A list of 19 Red River field areas in the Bowman–Harding study area was developed for screening potential 3-D seismic candidates and focusing the team for potential engineering and geological studies. Criteria were developed for ranking areas on the basis of project and economic objectives, ownership and operational ease, and potential for extrapolation to other fields in the area. The Cold Turkey Creek (Red River) area (T. 130 N., R. 102 W., Bowman County, North Dakota) was selected as the best candidate (Figs. 2 and 3) on the basis of the preceding criteria. Optimal field parameters are being developed and should be finalized in September or October 1994 after completion of modeling and reprocessing.

Seismic modeling in the North Sioux Pass (Ratcliffe), T. 26 N., R. 67–58 E., Richland County, Montana, area will include detailed compressional and shear modeling to determine optimal parameters for optimal design of a three-component seismic program for the area. A log suite, including sonic, density, neutron, spontaneous potential (SP), respectively, and gamma-ray porosity, was selected from the Superior Vanderhoof 2A, SE $\frac{1}{4}$, sec. 13, T. 25 N., R. 58 E., in the Cattails Field area near North Sioux Pass (Fig. 4). These data have been digitized and shear velocities are being estimated. Western Geophysical has agreed to provide shear analysis and full-wave field modeling to help determine feasibility and parameters for 3-D test line in the area.

Petrophysical Evaluations

Formation analysis of the Ordovician Red River at SW Amor was performed with digitized log data. The evaluated data consist of gamma-ray, neutron, and density porosity and dual laterologs. Water produced from each well was used for water resistivity (R_w). Water salinity varied considerably from well to well and possibly from each of the three main porosity benches (upper, middle, and lower) in the Red River (Fig. 5). R_w varied from 0.016 to 0.040 Ω -m at a reservoir temperature of 113 °C (235 °F). Water saturations were calculated and were found to be not particularly effective in discriminating between pay intervals with little water production and high water-cut intervals evaluated by drill-stem tests or by perforation.

Traditional log calculations can identify the intervals at low or irreducible water saturations but are ambiguous for discriminating between the moderate and high water-cut intervals because water salinity and R_w appear to vary horizontally between wells and vertically between porosity benches. Another complicating factor to R_w variation may be vertical communication by fractures or channeling behind the cement, induced by stimulation treatments by acidizing at high pressure. The variability of water salinity and R_w has been documented¹ at the South Horse Creek field (T. 129, R. 104 W.), Bowman County, North Dakota (Fig. 2).

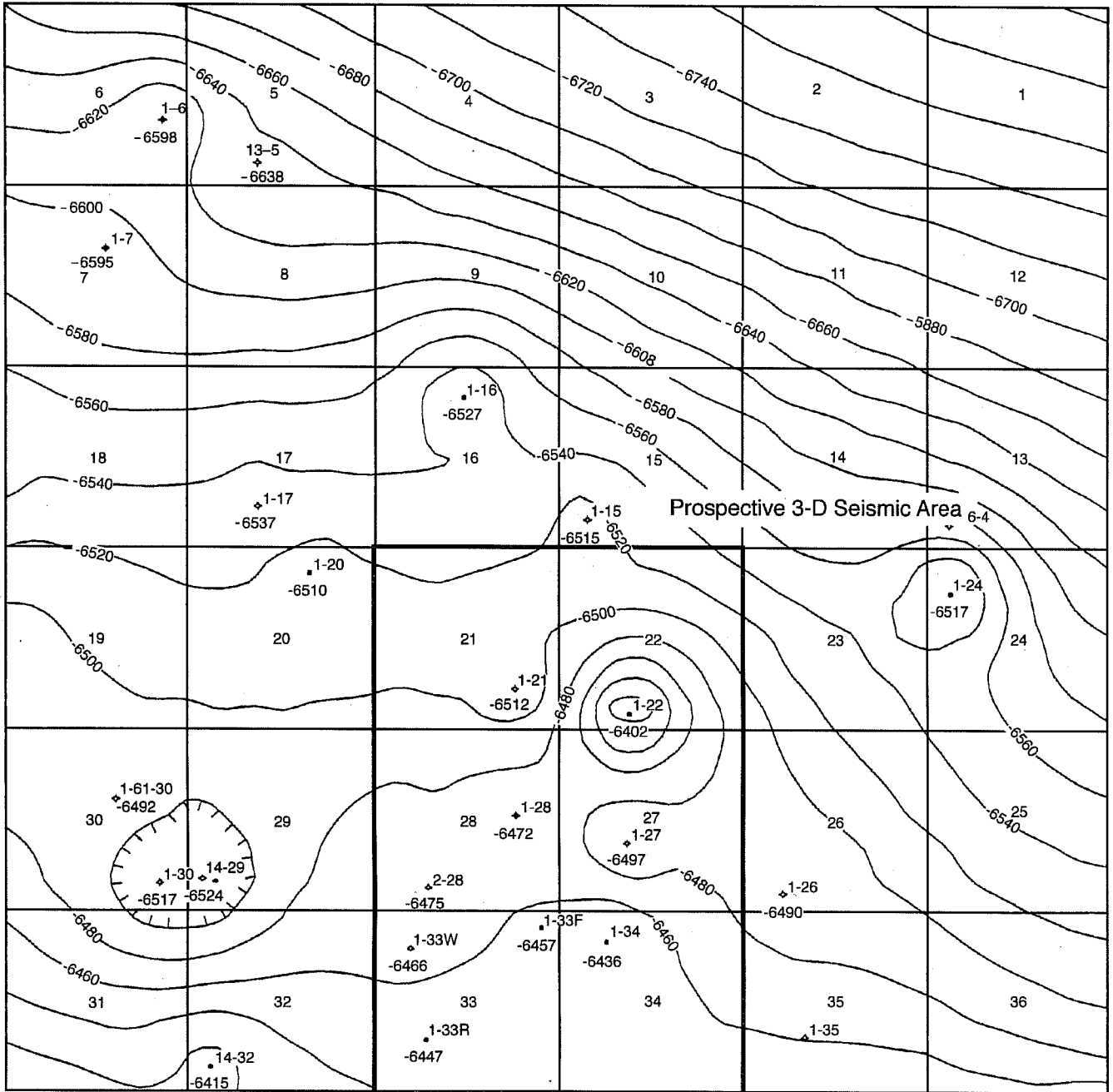
Geological Evaluations

Formation tops from the Greenhorn through the base of the Red River porosity benches have been picked for wells in portions of Bowman County, North Dakota (T. 129–132 N., R. 101–105 W.) and in Harding County, South Dakota (T. 23 N., R. 3–6 E.) (Fig. 2). These formation tops have been tied to seismic synthetics. Structure and isopach maps (and associated trend residual maps) are under evaluation for growth history and correlation with production, reservoir characteristics, and oil migration.

A wrench-style growth and structural model is being developed at a field and interwell scale for the Bowman–Harding Red River study area. A basement block framework is hypothesized as controlling the direction and extent of structural features in the Williston Basin. A wrench system is characterized by a series of geometrically arranged grabens, horsts, and half-grabens that may undergo continuous adjustment to compressional stress. Horizontal movement is generally greatest in the direction of displacement. One distinguishing feature of wrench faults is that they often take the form of scissor-type faults.

Work performed in a photogeologic–photogeomorphic mapping project from 1964 to 1970 by Gilbert Thomas² preceded a 1974 publication in which he describes a series of basement-weakness zones that trend northeasterly and northwesterly in the Williston Basin (Fig. 5). He defines a framework of possible basement blocks that probably strongly affect localization of oil and gas by influencing the stratigraphic and structural conditions. Differential simple shear on opposite boundaries of a block produced coupling across a block, which produced dragfold uplifts and downwarps, faulting, and fracturing.

In 1987, Donald Brown³ described the timing of these wrench-style deformation patterns. His work describes three potential stress orientations that probably influenced the structural architecture of Williston Basin. The oldest lineament orientation is northeasterly until late Devonian or early Mississippian time. In Devonian time, an abrupt and dramatic shift in orientation of the active shear zones occurred and reoriented to the northwest. During middle Mississippian time, the northeasterly shear orientations were reactivated. The realignment of regional forces would cause periodic movement of basement blocks in different directions through time. A block may have been elevated in Ordovician time, depressed in Silurian time, dormant in Devonian time, and elevated again in Mississippian time.



SCALE 1 inch = 4000 Feet

Fig. 3 Cold Turkey Creek area. Red River structure. Contour interval, 20 ft T. 130 N., R. 102 W. (Art reproduced from best available copy.)

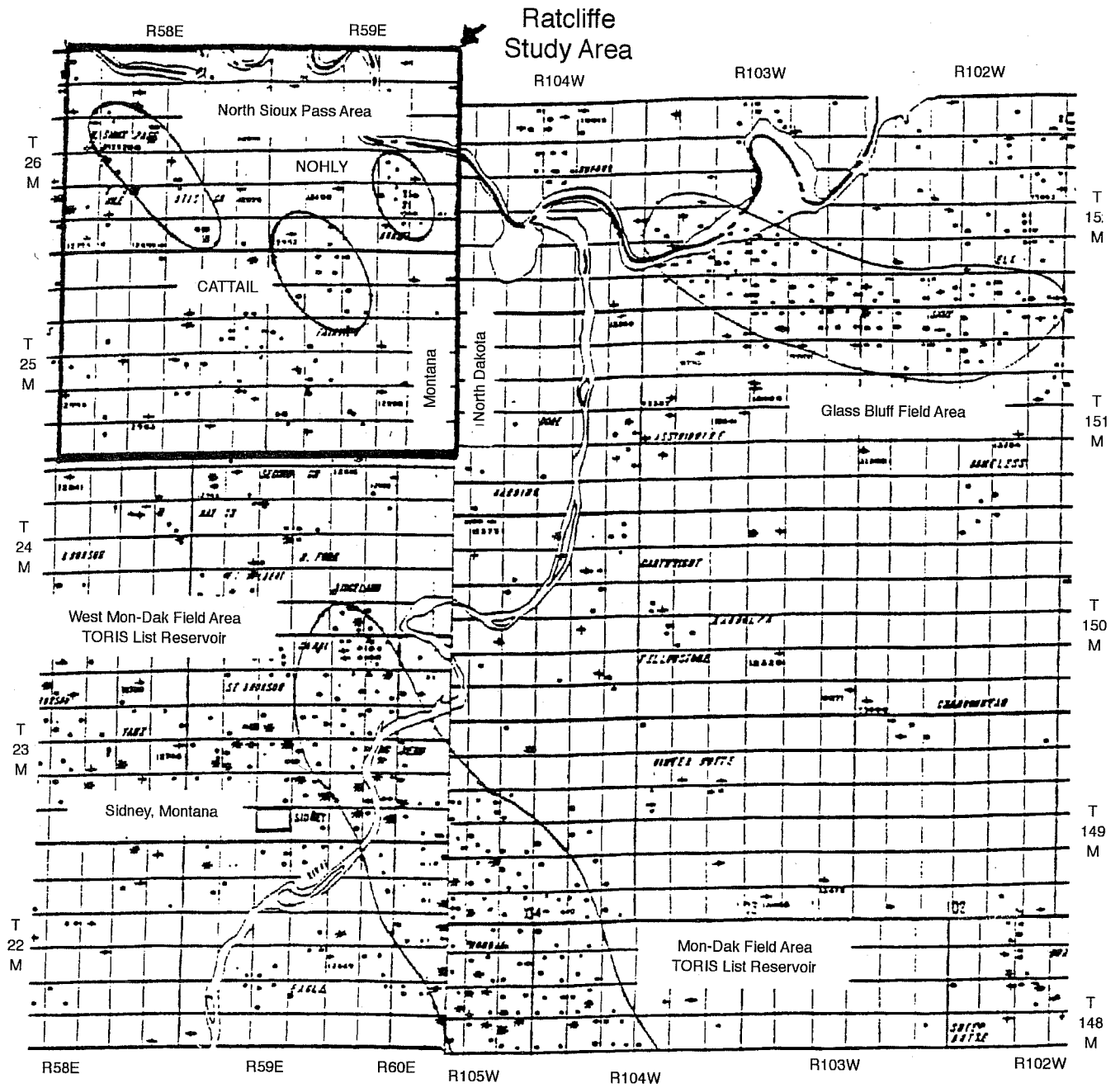


Fig. 4 Index map, Madison Ratcliffe reservoir areas, Southern Williston Basin. (Art reproduced from best available copy.)

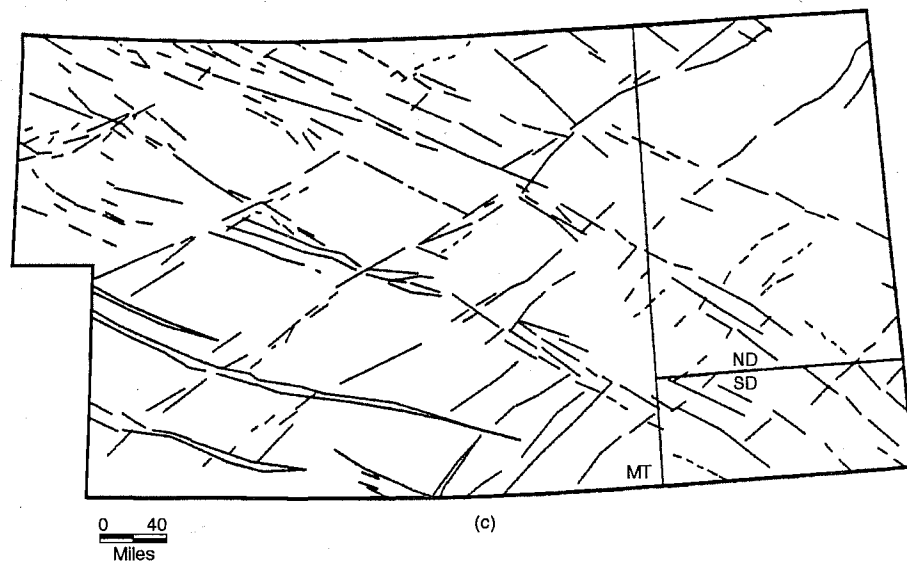
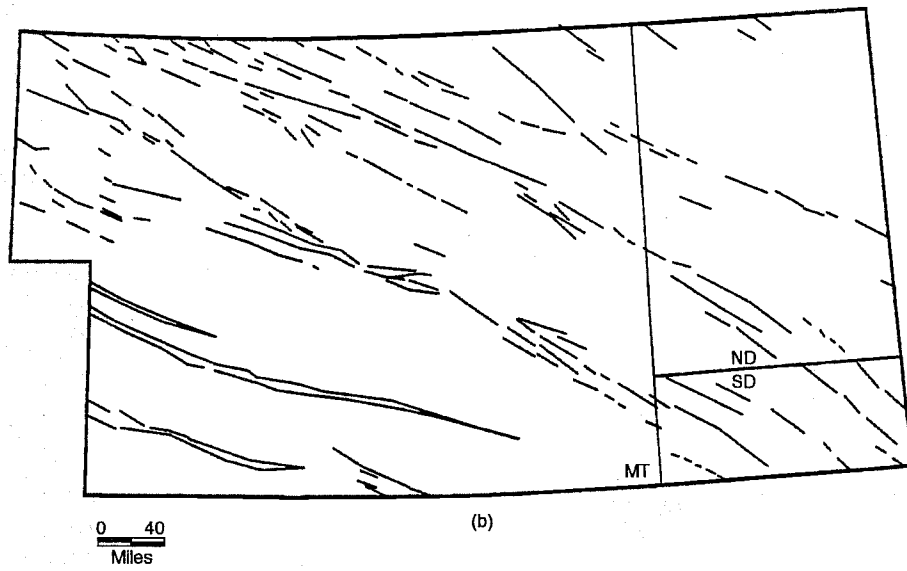
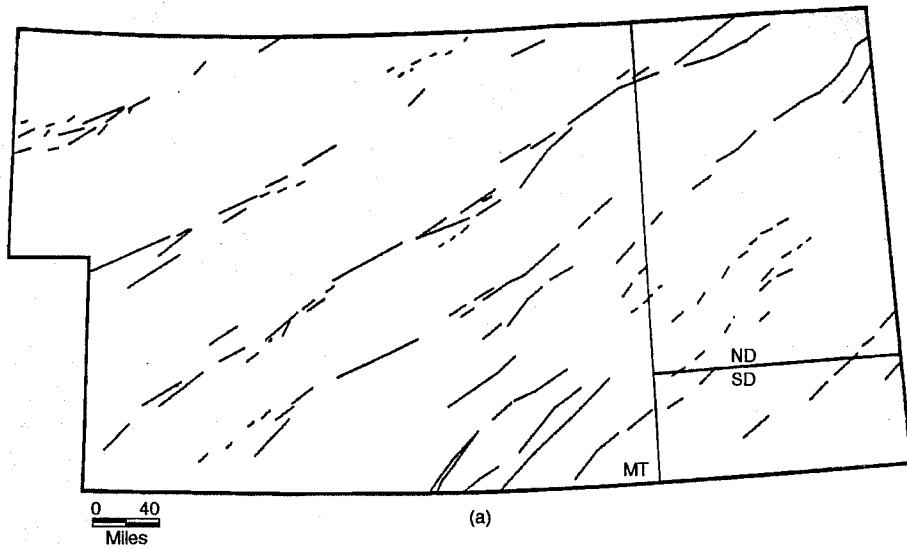


Fig. 5 Lineament pattern of Williston Basin. (a) Northeasterly lineaments. (b) Northwesterly lineaments. (c) Composite lineament patterns. (Adapted from Ref. 2).

Engineering Evaluations

Copies of Red River oil pressure–volume–temperature (PVT) studies have been obtained for the Medicine Pole Hills (Red River) field, Bowman County, North Dakota, and Buffalo (Red River) field, Harding County, South Dakota. These data were found to compare very well with oil PVT from empirical black-oil correlations. It is concluded that empirically determined oil PVT data can be used satisfactorily for engineering calculations and simulations where sufficient gas production data, oil gravity, and formation temperature are known. There are no plans for obtaining additional laboratory PVT analyses of Red River oil.

Production type-curve analysis has indicated several wells that have early time or transient behavior, which suggests nonradial drainage. These wells are believed to be near fault boundaries. The approach for identifying wells with nonradial drainage shapes is modeled after that of Fetkovich.^{4,5} As seismic data are reprocessed and interpreted, comparisons will be made for nonradial performance and identification of faults.

Producibility Problem Characterization and Analysis

Reservoir performance parameters for volumetric drainage, transmissibility, and water-drive index have been evaluated with the use of Fetkovich production type curves for a sampling of Red River wells in North Dakota. These reservoir parameters will be sorted by zone and applied statistically to paleo-growth data from logs and seismic surveys. Drill-stem test data and calculated reservoir parameters of transmissibility are being integrated with these results. The production evaluation by type curves will continue in the Harding County, South Dakota, portion of the Red River study area.

Typical values of transmissibility for the upper bench of the Red River have been found to be $10.5 \times 10^{-12} \text{ m}^3 \text{ Pa-s}$ (35 mD-ft/cP). With a typical thickness of 2.4 m (8 ft), oil viscosity of $0.5 \times 10^{-3} \text{ Pa-s}$ (0.5 cP), and oil volume factor of 1.3 reservoir barrels (RB)/stock tank barrels (STB), the resulting permeability to oil is $2.8 \times 10^{-3} \mu\text{m}^2$ (2.8 mD).

Recovery Technology Identification and Analysis

Waterflooding

The waterflooding history at West Buffalo Red River "B" Unit, T. 21 N., R. 3 E., Harding County, South Dakota (Fig. 2), has been evaluated by computer simulation history matching. This unit is determined to have an original oil in place (OOIP) of $3,275,000 \text{ m}^3$ (20,600,000 STB) under a net productive area of 1153 ha (2850 acres). There are 10 wells spaced on approximately 65-ha (160-acre) patterns. Water injection is through down-dip, peripheral wells. Recovery by primary production is predicted to be $365,700 \text{ m}^3$ (2,300,000 STB), or 11% of OOIP. The secondary recovery by waterflooding and current well configuration is predicted to be $795,000 \text{ m}^3$

(5,000,000 STB), or 24% of OOIP. The time to achieve this recovery is nearly 90 yr. The low primary recovery is attributed, in part, to a low bubble point pressure of less than 3448 kPa (500 psi).

Computer simulation for history matching and predicting remaining primary recovery at SW Amor (Red River), T. 130 N., R. 104 W., Bowman County, North Dakota, was performed (Figs. 1 and 2). The reservoir is produced by four wells spaced on approximately 65-ha (160-acre) locations, although the production units are 130 ha (320 acre) per field rules. The SW Amor wells produce mostly from the upper Red River interval (Fig. 6). The OOIP is determined to be $1,363,000 \text{ m}^3$ (8,573,000 STB) with a predicted primary recovery of nearly $325,900 \text{ m}^3$ (2,050,000 STB), or a recovery factor of 25%. The combined drainage area of the wells is determined to be 476 ha (1176 acres) and is in good agreement with the reservoir limits inferred from geophysical interpretations. The higher primary recovery from SW Amor compared with the West Buffalo Red River "B" Unit is attributed to lower oil viscosity and higher solution–gas content.

The configuration of the successful history match model was used to screen three development possibilities for the field, which include four additional infill wells for acceleration of primary (eight producers), secondary recovery with existing wells (two producers and two injectors), and four additional infill wells for secondary recovery with existing wells (four producers and four injectors). Secondary recovery by water injection with the existing wells was predicted to add an incremental $111,300 \text{ m}^3$ (700,000 STB); however, investment and economic calculations indicate a decrease in present worth from the status quo primary operations. The addition of four new wells for waterflooding results in a prediction of $184,400 \text{ m}^3$ (1,160,000 STB) over the current primary operations. The present value of recovery by this prediction is slightly less than double that of status quo remaining primary; however, the recovery time is predicted to be in excess of 40 yr. Any development plan for the field requires consideration that the effective lives of these wells may be 25 yr. The simulation studies indicate that infill drilling and enhanced completion efficiency are prerequisites for secondary recovery by waterflooding from this typical Upper Red River reservoir.

Technology Transfer

Two papers have been accepted for oral presentation at the Seventh International Williston Basin Symposium to be held July 21–25, 1995 in Billings, Mont.

A WIO meeting was held for the initiation of technical discussions and planning for project-related injectivity testing, seismic acquisition, and possible creation of a waterflood secondary recovery unit at SW Amor (Ordovician Red River) field.

Floodplain insurance maps for the project areas were obtained and delivered at the request of Technology and Management Services of Gaithersburg, Md., in July 1994. No additional request or communication has been received

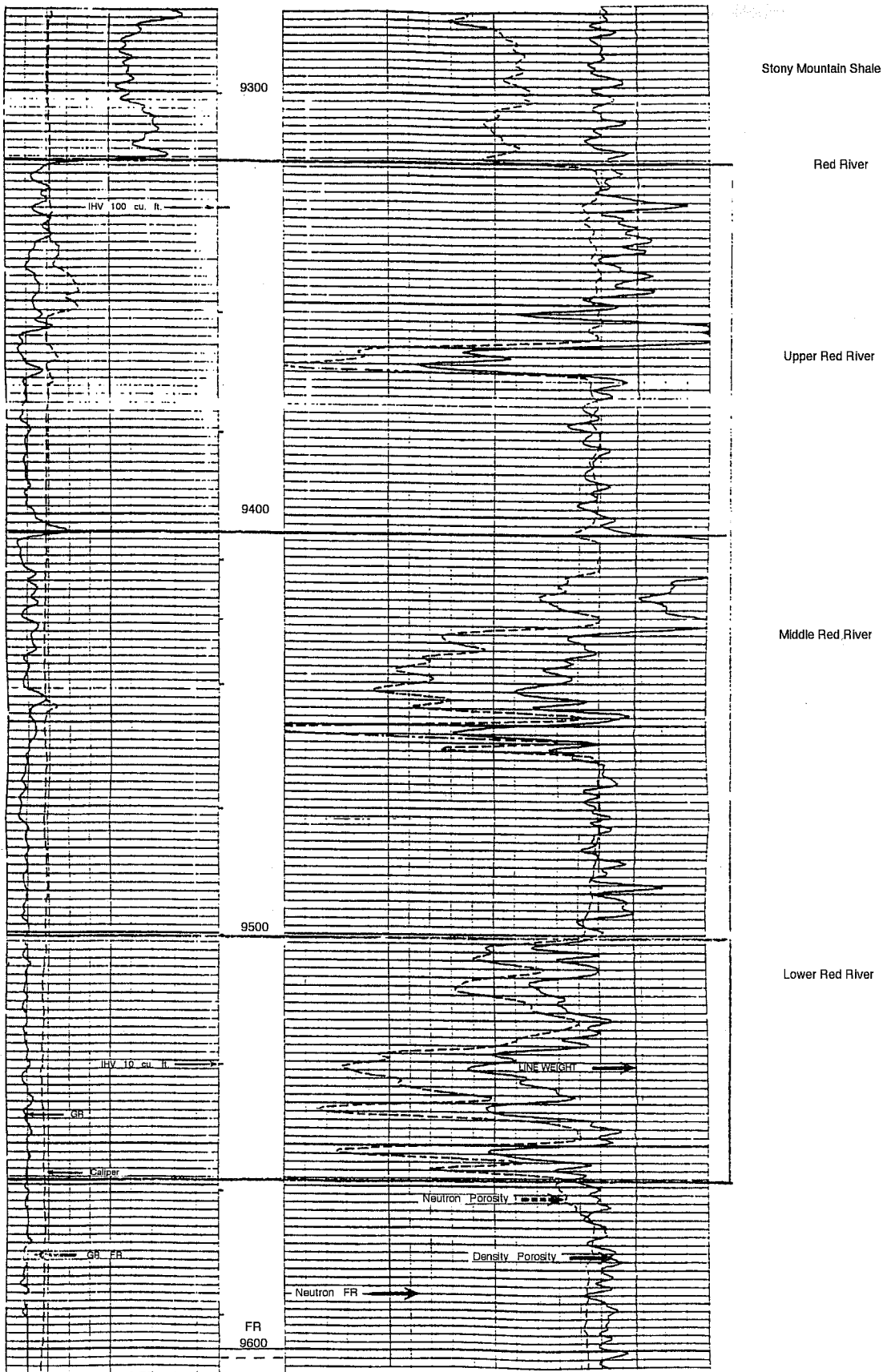


Fig. 6 Type log, Red River formation. Richards 1-33, Cold Turkey Creek field, sec. 33, T. 130 N., R. 102 W., Bowman County, North Dakota. (Art reproduced from best available copy.)

concerning National Environmental Protection Act requirements. All applicable state and county permits were obtained for seismic activities at SW Amor.

There have been no field demonstration activities involving well workovers, drilling, or injectivity tests during this quarter.

References

1. M. W. Longman, G. Fertal, and J. R. Stell, Reservoir Performance in Ordovician Red River Formation, Horse Creek and South Horse Creek Fields, Bowman County, North Dakota, *Am. Assoc. Pet. Geol. Bull.*, 76(4): 449-467 (April 1992).
2. G. E. Thomas, Lineament-Block Tectonics: Williston-Blood Creek Basin, *Am. Assoc. Pet. Geol. Bull.* 58(7): 1305-1322 (July 1974).
3. D. L. Brown and D. L. Brown, Wrench Style Deformation and Paleostuctural Influence on Sedimentation In and Around a Cratonic Basin, in *Williston Basin: Anatomy of a Cratonic Oil Province*, M. W. Longman (Ed.), Rocky Association of Geologists, Denver, Colo., pp. 57-66.
4. M. J. Fetkovich, Decline Curve Analysis Using Type Curves, *J. Pet. Technol.*, 32(6): 1065-1077 (June 1980).
5. M. J. Fetkovich and M. E. Vienot, Shape Factor, Ca, Expressed as Skin, *Sca, J. Pet. Technol.*, 37(2): 321-322 (February 1985).

APPLICATION OF RESERVOIR CHARACTERIZATION AND ADVANCED TECHNOLOGY TO IMPROVE RECOVERY AND ECONOMICS IN A LOWER QUALITY SHALLOW SHELF CARBONATE RESERVOIR

Contract No. DE-FC22-94BC14990

**Oxy USA, Inc.
Midland, Tex.**

**Contract Date: Aug. 3, 1994
Anticipated Completion: June 14, 1996
Government Award: \$1,922,000**

**Principal Investigator:
Archie Taylor**

**Project Manager:
Chandra Nautiyal
Bartlesville Project Office**

Reporting Period: July 1-Sept. 30, 1994

Objectives

The main objective of the project is to show that the use of advanced technology can improve the economics of carbon

dioxide (CO₂) projects in low-permeability reservoirs. The approach involves the use of tomography and pore throat measurements to enhance reservoir characterization. Cyclic CO₂ stimulations and fracture treatment will be used to increase and facilitate oil recovery to improve project economics. Reservoir description and simulation will be used along with cyclic CO₂ stimulations and fracture treatments to arrive at an optimum operating plan to be instituted during the second budget period. Official start-up of the project was Aug. 3, 1994, so Sept. 30, 1994, represents the end of the first quarter; however, work in the area of cyclic CO₂ stimulation and reservoir characterization had taken place before this quarter under pre-award approval. Objectives to be accomplished during the first quarter included (1) obtaining petrophysical data, (2) preparing for drilling of two observation wells, (3) designing and preparing for tomographic surveys, (4) adding injection surveys to petrophysical database, (5) initiating work on interpreting existing seismic surveys and using results to develop a relationship with petrophysical characterization, and (6) beginning cyclic CO₂ stimulation treatments.

Summary of Technical Progress

Reservoir Characterization

Updating Existing Characterization

Starting in the pre-award period, petrophysical data for all wells in the U.S. Department of Energy (DOE) area have been updated. Correlation of all wells with either core data or new log data has begun. Eight additional cores in the DOE area have been located. The first core has been described, and work is continuing on the remaining seven cores in the last quarter of 1994. An initial correlation and layering scheme, similar to the one used in the West Welch Phase I CO₂ feasibility study, is being attempted. This petrophysical model will be modified and improved as more data are obtained from observation wells and core descriptions.

Core analysis results have been received on the first observation well (WWU No. 4852). Core from the second observation well (WWU No. 7916) is still being analyzed. As this information is received, it will be integrated into the geophysical model.

Observation Wells

Drilling of the two observation wells was accelerated by the Technical Committee, which met Sept. 15, 1994, in an effort to facilitate the reservoir characterization study. Observation well WWU 4892 was drilled into the San Andres to a total depth of 5050 ft, and fiberglass casing was run across the San Andres formation to allow future monitor logging with induction-type tools. The well was cored and logged as shown in Table 1. The attempt to use a memory recording multi-shot tool for orientation coring was abandoned because of lost circulation problems.

TABLE 1

Drilling Results and Observation Wells, DOE Class II Project, West Welch Unit

Well	Location	Completion date	Total depth (TD), ft	Pay zone, ft	Casing	Cored, ft	Logs
WWU 4892*	1989 ft FNL and 1723 ft FWL, sec. 70, Blk M EL and RR survey	10/1/94	5050	4850 to 4926	Fiberglass liner, 4690 ft to TD	4830 to 4946	GR, DLL-MSFL-Caliper, FW Sonic, DS neutron, spectral density, CAST HF dielective
WWU 3916	661 ft FSL and 2327 ft FWL, sec. 69, Blk M EL and RR survey	10/10/94	5050	4798 to 4880	Fiberglass liner, 4750 ft to TD	4784 to 4900	GR, DLL-MSFL-Caliper, FW Sonic, DS neutron, spectral density, dipmeter, HF dielectrical

*Problem with oriented core device.

Tomography Survey

Data acquisition design for the tomography work was completed by Advance Reservoir Technologies (ART) during September 1994. Field testing of all instruments and test shooting will be completed in the first half of October 1994. Production shooting is scheduled to begin on Oct. 17, 1994; WWU 7916 will be used as the source well and WWU 3206 and 4824 as receiver wells. The tomography acquisition is expected to take about 6 weeks. Six wells were deepened and directionally surveyed during this quarter as shown in Table 2.

Injection Well Survey Data

All injection well surveys in the DOE area were obtained and digitized for addition to the stacked curves for personal computers (SCPC) database for the Welch area.

Vertical Seismic Profile

Vertical seismic profile (VSP) data will be acquired by ART upon completion of the tomography acquisition program with the use of tomography field equipment. Four horizons have been correlated throughout the three-dimensional (3-D) seismic volume. These horizons tied to synthetic seismograms generated from four seismic logs within

the DOE area correlating to the top San Andres, base San Andres (Top Glorieta), and two intermediate San Andres levels. The seismic response at the reservoir level does not match the synthetic seismogram developed from sonic log data. The VSP data to be obtained should result in a better tie at the reservoir level.

Laboratory Testing Requirements

The data analysis requirements for the observation well cores were determined at the Technical Committee meeting on Sept. 15, 1994. Plug samples will be analyzed at the Halliburton Laboratory to obtain data for fracture treatment design. One-third or one-fourth slabbing will be used on cores for reservoir characterization purposes; sufficient core volume will be left for plugs. Mercury injection and additional analysis of the ends of the plugs will be performed to aid characterization work. The conclusion was made that CO₂ velocity measurements needed for tomography interpretation could be delayed until Budget Period 2. The decision was made that core measured log properties were not needed unless the log correlations cannot be adequately developed. On the basis of experience at the South Welch Unit, the decision was made that the effects of hysteresis on core measurements should be obtained for different rock types.

TABLE 2

Well Work for Tomographic Data Acquisition, DOE Class II Project, West Welch Unit

Well	Completion date	Original total depth, ft	New total depth, ft	Amount deepen, ft	Comments
WWU 4843	9/12/94	4935	5135	200	Installed liner, perforated and acidized
WWU 4811	9/16/94	4914	5150	236	
WWU 4809	9/27/94	4935	5161	226	
WWU 4827	9/24/94	4903	5130	227	
WWU 7902	9/30/94	4894	5125	231	
WWU 7901	9/30/94	4913	5150	237	

Reservoir Management Plan Development

CO₂ Flood Design

In line with the Technical Committee's decision, bids were obtained and are currently being reviewed for evaluating hysteresis effects for the water-alternating-gas (WAG) process at West Welch. Fluid samples were obtained and recombined in the lab for CO₂ diffusion rate tests designed to determine the rate of molecular diffusion of CO₂ through the Welch crude oil. Four separate tests were run at 2000 psi with preliminary results indicating that the rate of diffusion was higher than for previous tests of Welch crude at 1000 psi. Final results of this testing will be available in the next quarter.

Cyclic CO₂ Stimulation Evaluation

Before any injection, pressure buildup data were obtained on five cyclic CO₂ stimulation wells with the use of acoustic well sounders and 5-d shut-in periods. Automate version 2.3 pressure transient software was used to analyze the data. The afterflow rates measured during the shut-in period were used in a multi-rate superposition analysis to account for the effect of rising fluid levels on the bottomhole pressure (BHP) data. This methodology gave good results on three of the wells, but the other two wells apparently had leaking standing valves, which invalidated the approach. Table 3 summarizes the data obtained from the buildup surveys.

inject 10 MMCF of CO₂ at a BHP less than the estimated formation parting pressure of 3200 psia. During injection, the BHP increased from 1741 psia to a maximum of 3385 psia, which occurred during a 40-min spike. If this spike were ignored, the maximum BHP was 3180 psia. Flowback of this well will begin in October 1994 after a 15-d soak period.

Technology Transfer

A poster session entitled "Application of Reservoir Characterization and Advanced Technology Improves Recovery and Economics in Lower Quality San Andres" was presented at the 1994 SPE Permian Basin Oil and Gas Recovery Conference.¹

Appropriate technical forums sponsored by professional and technical societies have been identified for a several-year period and are being targeted for specific aspects of this project as results become available. In addition, technology transfer is being carried out informally on a company-to-company basis. Oxy personnel have already met with Texaco engineers to share results of CO₂ cyclic injection at South Welch Unit and Texaco's Mabee CO₂ flood. This dialogue will continue as both sides gain additional experience. Oxy and ART personnel have also held discussions with Amoco tomography experts to discuss the possibility of data sharing on the West Welch project. Stanford University has shown an interest in becoming involved in the tomography project from the standpoint of having a team of

TABLE 3

Pressure Buildup Analysis, Cyclic CO₂ Wells, DOE Class II Project, West Welch Unit

Well	Gross interval, ft	Mobility, mD/cP	Absolute permeability, mD	Skin factor	P*, psig	Assumed drainage area	
						Area, acre	P, psig
WWU 4835	70	0.73	2.34	-3.3	2735	10	566
WWU 4843	75	1.67	5.1	-0.8	1986	10	923
WWU 4847	75	0.8	3.0	3.2	1689	10	1228
WWU 4851	Invalid data						
WWU 3205	Invalid data						

During September 1994, 5.1 million cubic feet (MMCF) of CO₂ was injected into well WWU 4835 in 213 h [574 thousand cubic feet per day (MCFPD)]. The objective was to inject a minimum of 5 MMCF of CO₂ at a BHP of less than 2500 psia with an average injection rate greater than 500 MCFPD. During injection, BHP increased from 1413 psia to a maximum of 2779 psia. It was necessary to increase the maximum BHP after 43 h of injection to achieve the volume and rate objectives. Flowback on this well will start in October 1994.

Approximately 10.3 MMCF of CO₂ was injected into WWU 4851 over a 330-h period (1.3 MCFPD). There was some question as to the actual amount injected because of malfunction of the injection meters. The objective was to

graduate students working with the data over a several-year period. Such an arrangement would undoubtedly generate a number of publications. The reservoir characterization aspects of the Welch field have been discussed with the Bureau of Economic Geology, and this relationship will continue.

Reference

1. A. R. Taylor, R. L. Doty, E. J. Behm, Rene Ulmschneider, and George Watts (OXY USA Inc.); T. S. Hickman (T. Scott Hickman & Associates, Inc.); George Underwood, (GeoStrat Services); and J. H. Justice (Advanced Reservoir Technologies), *DOE Class II Oil Program: Application of Reservoir Characterization and Advanced Technology Improves Recovery and Economics in Lower Quality San Andres*, paper SPE 27659 presented at the SPE Permian Basin Oil and Gas Recovery Conference, Midland, Tex., March 16-18, 1994.

**IDENTIFICATION AND EVALUATION
OF FLUVIAL-DOMINATED DELTAIC
(CLASS I OIL) RESERVOIRS IN
OKLAHOMA**

Contract No. DE-FC22-93BC14956

**Oklahoma Geological Survey
University of Oklahoma
Norman, Okla.**

**Contract Date: Jan. 15, 1993
Anticipated Completion: Dec. 31, 1997
Government Award: \$1,390,752
(Current year)**

**Principal Investigators:
Charles J. Mankin
Mary K. Grasmick**

**Project Manager:
Rhonda Lindsey
Bartlesville Project Office**

Reporting Period: July 1–Sept. 30, 1994

Objectives

The Oklahoma Geological Survey (OGS), the Geological Information Systems (GIS) Department, and the School of Petroleum and Geological Engineering at the University of Oklahoma are engaging in a program to identify and address Oklahoma's oil recovery opportunities in fluvial-dominated deltaic (FDD) reservoirs. This program includes the systematic and comprehensive collection and evaluation of information on all of Oklahoma's FDD reservoirs and the recovery technologies that have been (or could be) applied to those reservoirs with commercial success. This data collection and evaluation effort will be the foundation for an aggressive, multifaceted technology transfer program that is designed to support all of Oklahoma's oil industry, with particular emphasis on smaller companies and independent operators in their attempts to maximize the economic producibility of FDD reservoirs.

Specifically, this project will identify all FDD oil reservoirs in the State; group those reservoirs into plays that have similar depositional and subsequent geologic histories; collect, organize, and analyze all available data; conduct characterization and simulation studies on selected reservoirs in each play; and implement a technology transfer program targeted to the operators of FDD reservoirs to sustain the life expectancy of existing wells with the ultimate objective of increasing oil recovery.

The elements of the technology transfer program include developing and publishing play portfolios, holding workshops to release play analyses and identify opportunities in

each of the plays, and establishing a user lab called the OGS Geosystems Extension Laboratory. The laboratory will contain all the play data files, as well as other oil and gas data files, together with the necessary hardware and software to analyze the information. Technical support staff will be available to assist interested operators in the evaluation of their producing properties, and professional geological and engineering outreach staff will be available to assist operators in determining appropriate recovery technologies for those properties.

Summary of Technical Progress

The execution of this project is being approached in three phases. Phase 1, Planning and Analysis, includes system design, play definition, and database development activities. Data from the Natural Resources Information System (NRIS), an Oklahoma data system that has been developed through the support of the U.S. Department of Energy's Bartlesville Project Office, have provided the foundation for this data collection effort. Phases 2 and 3 include project implementation and technology transfer activities in which the collected information is organized and made available to the industry through various methods.

During this quarter, phase 1 activities are being completed, and plans are being developed for phases 2 and 3 that include modifications to the original schedule and a milestone log for those phases. A revised Management Plan will be submitted that reflects these changes.

Phase 1: Planning and Analysis

Design/Develop Database Systems

As reported last quarter, discussions had been initiated regarding the long-term utility of the current database management system for user-lab applications. Several different options have been reviewed, and most of them have been deemed inadequate for supporting the very large, multi-user databases that will be available through the user-lab computer network. Reviews were completed this quarter, and Oracle was selected as the most appropriate software for the application with user interfaces to be developed in the Visual Basic language. This approach should provide the required flexibility, efficiency, and security for entering and storing data and will allow links to the Windows-based applications programs that are planned for the lab.

The FDD database systems that were developed for this task will continue to be used for the foreseeable future because the new Oracle development will concentrate on reformatting the NRIS well, lease, and field mainframe databases for personal computer-level access. Eventually, the three FDD databases also will be converted, and thus the documentation for those databases will not be completed until after that conversion.

Data Research

Primary efforts for this quarter were devoted to data research activities. Project staff provided three new data packages to the Oklahoma Nomenclature Committee (ONC). These packages contained maps and print listings of fields, leases, and wells for areas with large volumes of oil production from unassigned leases (i.e., leases outside field boundaries). The packages assist the committee delineate the official oil-field boundaries in which FDD reservoirs occur. Packages this quarter included an 18-township area in Blaine and Dewey counties with high unassigned Morrow production; an 18-township area in the north-central panel, primarily Oklahoma county, with large volumes of unassigned Prue and Skinner; and a 9-township Morrow production area near the Postle field in Texas county. As the ONC defines new field boundaries, the NRIS field files are updated to reflect the changes. Updates were processed this quarter from 54 townships that previously had been provided to the ONC.

Public domain data research continued as a primary emphasis during this quarter as project staff continued to collect data on FDD reservoirs from literature and theses. Research during this quarter addressed the Virgilian (Hoover, Elgin, and Endicott), Missourian (Layton, Osage-Layton, and Cottage Grove), Peru, Red Fork, Booch, and Bartlesville plays. The data captured in these searches are being entered into the databases and are being used to develop trend maps that show the geographic extent of the FDD plays.

The reservoir characterization and simulation efforts for the Red Fork sand in the Glencoe Southeast field are nearing completion, and those for the Booch sand in the Greasy Creek field were initiated. Complexity will be increased with the Greasy Creek Booch study because three separate Booch intervals have been identified in the study area. Within the Morrow play, the Rice Northeast field has been identified as the target candidate, but the characterization study has not been initiated. Research is under way to identify an appropriate field for the Missourian play.

Data capture continued for the reservoir and bibliography/recovery technology data elements.

Play ID/Folio Plans

Routine meetings of play leaders continued, where various aspects of the play definitions are discussed and plans

have been developed for the ongoing work. During this quarter the decision was made to drop the Virgilian play from the list of plays for the publication and workshop presentations. This decision was based on the fact that, even though Virgilian sandstones (Hoover, Elgin, and Endicott) reflect FDD depositional environments, the oil production from those sandstones has ranged from minimal to nonexistent.

Efforts this quarter also included the further development of plans for producing the play folio publications and conducting the workshops. Discussions have included the development of estimated drafting and cartographic requirements for each presentation and the development of a tentative schedule for the plays. The current list of plays, in order of planned presentations, is as follows: (1) Morrow play, (2) Booch play, (3) Upper Missourian play (Layton, Osage-Layton, and Cottage Grove), (4) Prue/Skinner play, (5) Cleveland play and Peru play (combined workshops for two plays), (6) Red Fork play, (7) Bartlesville play, and (8) Tonkawa play.

Computer Applications

User-lab development activities include both the acquisition of hardware and software and the development of user interfaces for the data and applications that will be available through the user lab. Oracle has been selected as the most appropriate database management system for user-lab applications. The selection of Oracle, as well as the overall needs for system security and multi-user accessibility, requires that a new system network be selected and installed. The current peer-to-peer network will be replaced with a Novell system.

Additional discussions also took place regarding the business management and operation of the lab facility. A plan is being developed to address such items as operating hours, staffing plans, training, security, and user fees. Research also is being conducted into the options for off-site access to the user facility.

Management/Reporting

The completion of management reporting requirements continues to present some problems, even though the overall project is showing satisfactory progress.

**AN INTEGRATED STUDY OF THE
GRAYBURG/SAN ANDRES RESERVOIR,
FOSTER AND SOUTH COWDEN
FIELDS, ECTOR COUNTY, TEXAS**

Contract No. DE-FC22-94BC14982

**Laguna Petroleum Corporation
Midland, Tex.**

**Contract Date: Aug. 2, 1994
Anticipated Completion: Feb. 2, 1998
Government Award: \$71,200
(Current year)**

**Principal Investigators:
James J. Reeves
David A. Rowland
Robert C. Trentham**

**Project Manager:
Chandra Nautiyal
Bartlesville Project Office**

Reporting Period: July 1–Sept. 30, 1994

Objectives

The principal objective of this study is to demonstrate a methodology for reservoir characterization of shallow-shelf carbonate reservoirs that is feasible for the independent operator. Furthermore, this study will provide one of the first public demonstrations of the enhancement of reservoir characterization with high-resolution three-dimensional (3-D) seismic data. This project will evaluate the Grayburg and San Andres reservoirs in the Foster and South Cowden Fields of Ector County, Tex. A multidisciplinary approach to waterflood design and implementation, along with the addition of reserves by selective infill drilling, will be applied. This approach in reservoir development is believed to be applicable to a wide range of shallow-shelf carbonate reservoirs throughout the United States. Technology transfer will occur through all phases of the project.

Summary of Technical Progress

Seismic Data Acquisition

During August 1994 the 3-D seismic survey over the project area was shot by Dawson Geophysical. Initially, a sweep test was designed to determine the proper sweep parameters for the survey. An 8- to 110-Hz nonlinear 6-dB per octave sweep was determined to be optimum from the test. A 10-s sweep with a 13-s listen time was used. Four vibrators were used with each vibration point, sweeping a total of eight

times at a fixed location. Digital recording was done with an input/output (I/O) System II at a 2-ms sample rate. A three-quarters Nyquist frequency low-cut antialias filter was applied during data acquisition. Approximately 3.5 square miles of data were shot with a fixed spread consisting of 679 geophone groups and 438 vibrator locations. Typically, the receiver line spacing was 660 ft and the source line spacing was 1320 ft. Sources and geophone groups were spaced 220 ft along the lines. The survey was shot so that two different bin sizes (110 ft × 110 ft or 55 ft × 55 ft) could be used to stack the data.

Because of the many cultural obstructions in the area, Vibro Tech, Inc., was used to measure peak ground velocities to monitor drive levels of the vibrators to ensure that there would be no structural damage to houses, buildings, and wells on the Laguna leases. Company guidelines for seismic data acquisition were followed on the Phillips lease.

Nearly every well position and every source-geophone station position in the project area were accurately surveyed. Any station location moved greater than 10 ft by the seismic crew was resurveyed.

Seismic Data Processing

The data are still being processed at Dawson Geophysical. The following applications have been made: geometry installation, trace editing, spherical divergence correction, refraction statics, residual statics, velocity analysis, and brute stack. A preprocessing sequence is being designed to choose the optimum deconvolution algorithm. This will attempt to collapse the recorded wavelet in the data to a zero-phase, band-limited wavelet that will ensure a close tie of the seismic data with the synthetic seismograms generated from wireline logs in the project area.

Subsurface Mapping

A total of 18 tops (Santa Rosa through San Andres) have been correlated for 80 wells in the immediate area of the project, including a detailed correlation of parasequence sets within the Grayburg. A computerized spreadsheet containing all tops and sub-sea depths has been created. All the wireline logs in the Phillips and Laguna leases have been digitized in the Grayburg-San Andres intervals, including depth shifting, normalization, and generation of pseudo-sonics (when feasible) to support the 3-D seismic interpretation and modeling.

Data from three cored wells were also placed in a computerized spreadsheet format for later evaluation. Permission was obtained to use core taken from the study area in the Arco No. 10 L. E. Brock well.

Engineering Data

Various engineering data and reports have been obtained from Phillips, Laguna, and other operators with production near the study area. These reports include Amoco Foster Field Waterflood Study; Unocal Moss Unit Waterflood Study; Fina Emmons Unit Waterflood Study; Laguna well files on the

Witcher, Brock, Foster, and Foster-Pegues leases; and Phillips well files on the Maurice lease.

These data will be critical for the waterflood design. Statistical analyses were run on routine core data to determine reservoir porosity and permeability. Representative values for rock compressibility, capillary pressure, gas-oil relative permeability, and water-oil relative permeability were evaluated. Fluid property data were analyzed to determine representative physical properties of gas, oil, and formation water.

Reservoir Rock Properties

For purposes of obtaining representative average values of porosity and permeability for both the Grayburg and San Andres formations, a 3% porosity cutoff and only those samples measuring a permeability of 0.1 mD or greater were counted as pay. The 0.1-mD permeability cutoff is the industry standard adopted for Permian Basin dolomites. Conversely, various porosity cutoff values are reported in the literature, which give rise to some controversy as to which porosity cutoff value is better. George and Stiles¹ conducted a study on the effect of porosity cutoff values on three Permian Basin dolomite reservoirs. They reported that in one case 56% of the samples with 3% porosity would be pay. Thus, if a porosity cutoff value greater than 3% were selected, significant reserves would be excluded in the determination of original oil in place.

The fact that wells in the study area exhibit low producing rates for extended periods of time indicates that low-permeability flow compartments are contributing to primary recovery.

Porosity

Routine core analyses are available from three wells cored in the study area. The first, the Witcher No. 6, was drilled and completed in July 1970. Coring commenced at a depth of 3850 ft with the use of a 4-in. diamond core bit. A total of five cores were taken from the Grayburg with coring continuing to a depth of 4205 ft. Recovery was 100%, which gives a total of 175 ft of core. A sixth core was cut in the San Andres formation from a depth of 4260 to 4314 ft. Water-base mud was used in the coring operation.

A total of 92 whole-core samples, all from the Grayburg formation, were used to conduct measurements in the laboratory. Measured values include absolute permeability (both maximum and 90-degree), porosity, and residual oil and water saturations. Most of the samples tested indicated that permeabilities were less than 0.1 mD. Only 15 samples tested survived the dual cutoff requirement.

No samples obtained from the San Andres interval in the Witcher No. 6 were tested in the laboratory for porosity or permeability.

The Brock No. 10 well was drilled and cored in May 1979. Again, the drilling fluid was saltwater based, and full-diameter cores were cut. The cored interval was from 4290 ft (San Andres formation) with 100% recovery. A total of 55 samples were

tested for porosity and permeability, with 49 samples surviving the dual cutoff tests. Thus a total of 64 samples from the San Andres Formation were available for obtaining average values.

The Foster-Pegues No. 3x well was cored in mid-1981 beginning at a depth of 3850 ft and continuing to a depth of 4086 ft (Grayburg formation). A total of 111 samples were used to measure porosity and permeability, of which only 37 qualified as pay. An additional 15 samples were used in measuring water-oil relative permeability and flood-pot tests, however, which gives a total of 52 values of porosity and permeability for the Grayburg formation.

Statistical analyses were conducted on these data for both the Grayburg (52 values) and San Andres (64 values) formations. These results are summarized in Table 1 and show good agreement with results reported from adjacent leases currently undergoing waterflood operations. These include Amoco's South Foster Unit and Unocal's Moss Unit being flooded in the Grayburg formation, and Fina's Emma Unit undergoing a waterflood in the San Andres.

Figures 1 and 2 show, respectively, the porosity and permeability histograms for the Grayburg formation. Figure 3 is a semilog plot of permeability vs. porosity. A good correlation is seen from this plot. Likewise, Figs. 4 to 6 are plots for the same parameters for the San Andres formation.

TABLE 1

Tabulation of Results of Statistical Analyses of Core Data—Foster Field

	Laguna	Amoco	Unocal
Grayburg			
Number of samples	52	163	508
Porosity, %			
Arithmetic average	6.53		
Weighted average	6.39	5.48	
Permeability, mD			
Arithmetic average	4.99		2.1
Weighted average	4.99	3.23	
Geometric average	1.06		0.95
Log k vs. porosity average	1.18		
50% > value on D-P plot*	1.25		
Permeability variation†	0.874		0.745
San Andres			
Number of samples	64		
Porosity, %			
Arithmetic average	8.41	8.9	
Weighted average	8.41		
Permeability, mD			
Arithmetic average	1.30		
Weighted average	1.30		
Geometric average	0.72		
Log k vs. porosity average	0.80		
50% > value on D-P plot*	0.82		
Permeability variation†	0.688		

*A plot of permeability data on log-normal paper.

†Dykstra-Parsons permeability variation—an empirical measure of reservoir heterogeneity.

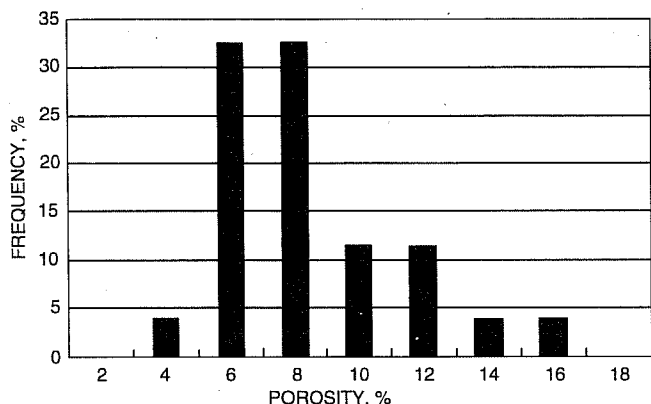


Fig. 1 Porosity histogram for Foster Field study, Grayburg formation.

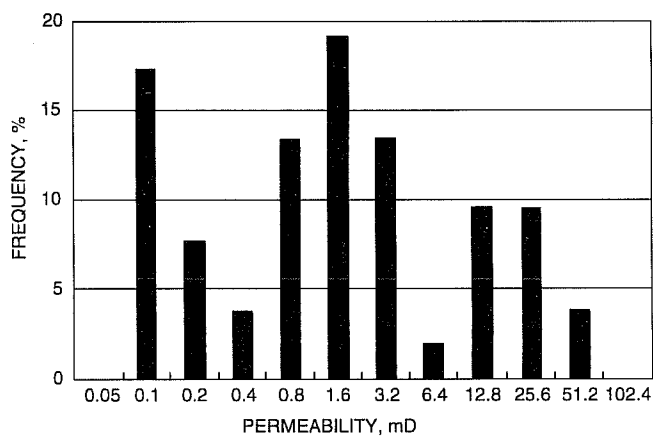


Fig. 2 Permeability histogram for Foster Field study, Grayburg formation.

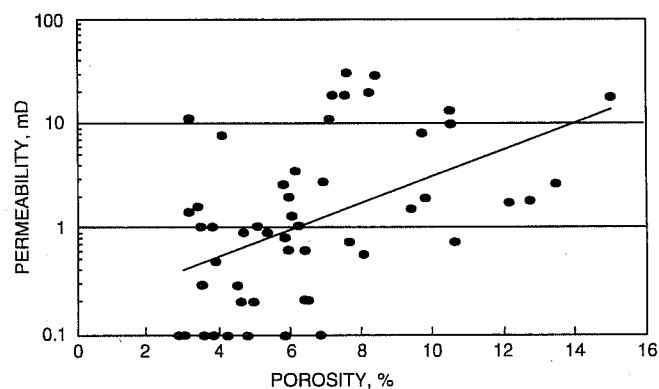


Fig. 3 Log permeability vs. porosity correlation for Foster Field study, Grayburg formation. $\text{Log } k = -0.7691 + 0.1290 \cdot \Phi$.

Technology Transfer

The Texas Tech University Center for Applied Petro-physical Studies has been selected as the technology transfer agent. The close relationship developed between the technical

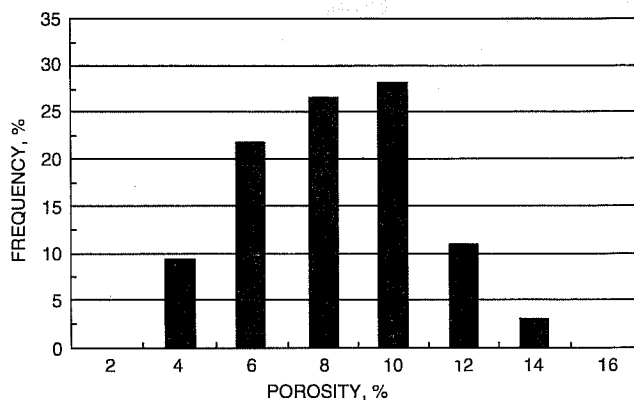


Fig. 4 Porosity histogram for Foster Field study, San Andres formation.

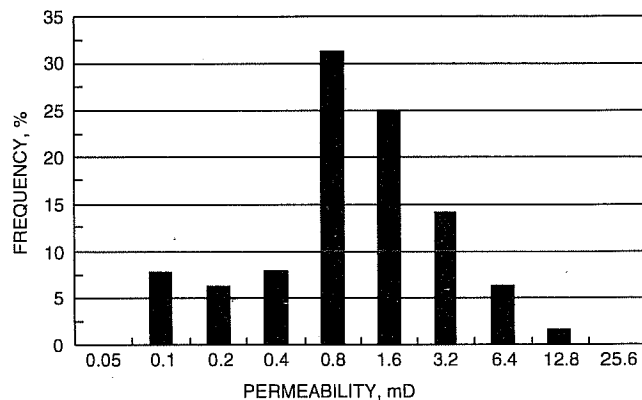


Fig. 5 Permeability histogram for Foster Field study, San Andres formation.

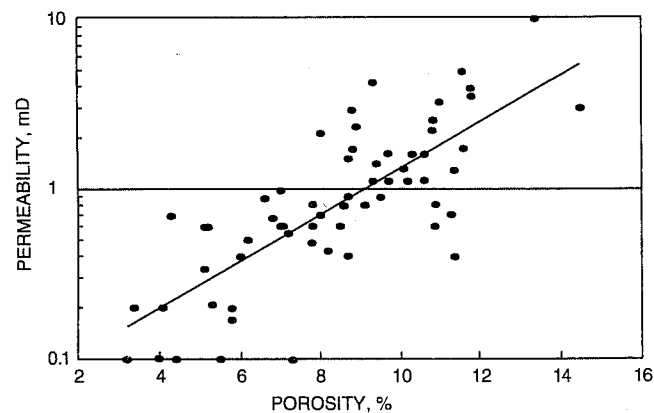


Fig. 6 Log permeability vs. porosity correlation for Foster Field study, San Andres formation. $\text{Log } k = -1.241 + 0.136 \cdot \Phi$.

team and Texas Tech University has already resulted in a useful exchange of ideas for the study.

A number of operators having Grayburg-San Andres production near the study area have been contacted to obtain reservoir data and to exchange ideas on reservoir

characterization methodologies. Several operators have allowed a review of their well logs, cores, production statistics, two-dimensional (2-D) and 3-D seismic data, Vibroseis* sweep test, and waterflood studies. The companies with whom discussions have been held include Unocal, Fina, Amoco, M. D. Mark, Phillips, Great Western Drilling, Chevron, and others. The project geologist has visited Grayburg-San Andres outcrops with Chevron personnel to assist in characterizing these reservoirs.

The process of finalizing agreements with a number of development companies to use their software in this study continues. Verbal approval to use most of the software has been obtained. Signed agreements are in place with Schlumberger GeoQuest to use their Interactive Exploration System and with Scientific Software Intercomp to use their WorkBench software. The software will be loaded on a Sun SPARCstation 5 at Spectrum Services, Inc., in Midland, Tex., and is available to the project team. Signed agreements are expected to be in place to use Landmark ZMAP, Advanced

*A trademark of Conoco, Inc.

VISUAL DISPLAY OF RESERVOIR PARAMETERS AFFECTING ENHANCED OIL RECOVERY

Contract No. DE-AC22-93BC14892

**Michigan Technological University
Houghton, Mich.**

**Contract Date: Sept. 29, 1993
Anticipated Completion: Sept. 30, 1996
Government Award: \$272,827**

**Principal Investigator:
James R. Wood**

**Project Manager:
Robert Lemmon
Bartlesville Project Office**

Reporting Period: July 1-Sept. 30, 1994

Objective

The objective of this project is to provide the operators of small- to medium-size oil fields with the tools necessary for an enhanced oil recovery (EOR) evaluation of the same quality and sophistication that only large international oil companies have been able to afford to date.

Geophysical Prospector, TerraSciences TerraStation, and GX Technology seismic modeling software.

Industry demonstration examples with the use of the data for this study will be developed for most of the software used in the project. Contractors providing cross-well tomography services are interested in shooting a demonstration cross-well seismic program for the study. An industry demonstration example would be developed that would integrate 3-D seismic data with the cross-well seismic program. Results would be published through Texas Tech University Center for Applied Petrophysical Studies and the Gas and Oil Technology Exchange and Communication Highway available through the New Mexico Tech Petroleum Recovery Research Center. Additional companies who want to conduct similar projects may be identified.

Reference

1. C. J. George and L. H. Stiles, Improved Techniques for Evaluating Carbonate Waterfloods in West Texas, *J. Pet. Technol.*, 30(11): 1547-1554 (1978).

Summary of Technical Progress

Spatial Database Manager

A test database was constructed in Microsoft Access with favorable potential. A database was assembled, input templates (dialog boxes) with drop-down menus were constructed, and standardized reports that draw from the database were designed. Access is an extremely flexible database program that can easily be tailored to most purposes, and because it is a Microsoft product, it has the same logical structure and intuitive feel as Windows and Visual Basic. It is widely available, well-supported, and inexpensive and therefore represents an excellent choice for the small independent producer. Therefore, access has been chosen for the database management platform. Building and filling the project database is a major undertaking that will involve a large effort.

Extensive research still being done on commercial products that are available or will soon become available on the personal computer (PC). With the availability of the new 486-100 and 586 processors, many of the major software companies that primarily supplied software for workstations are moving into the PC environment. Zycor, Intergraph, TerraSciences, Geographix, and several others have made major advances in porting their software down to the PC. Each system has its strengths and weaknesses. Most systems are modular.

The Crocker Data Processing (Crocker) Petrolog program provides comprehensive log evaluation capabilities and is being used in-house by Digital Petrophysics Inc. (DPI) for

correcting and archiving all of the log data for the project. DPI staff are familiar with the package, and it will be the primary vehicle for analysis of log data for the project. Because Petrolog is modular, only a core package of modules need be purchased by most small independents. Software packages by TerraSciences and Geographix are also being evaluated.

Petrospec Computer Co.'s PCMS mapping package (a derivative of Landmark's Zycor mapping system) appears to be the best mapping package available for petroleum geology applications. It can handle faults and the detailed mapping necessary for reservoir volumetric calculations, whereas many other programs cannot.

Several two-dimensional (2-D) and three-dimensional (3-D) visualization packages are being evaluated. Intergraph is in the process of porting its software down to the PC. Its 2-D and more basic 3-D applications are currently operational on the PC. Intergraph expects to have its 3-D volume visualization program functioning on the PC soon. A 3-D visualization software system from Spyglass, Inc., was obtained for evaluation but proved inadequate in its present form because of its inability to handle faults and other geological discontinuities. Spyglass software will continue to be monitored.

Database Initialization

Individual databases were set up in Lotus and Quattro Pro spreadsheets to archive and display X-ray diffraction (XRD), Fourier transform infrared spectroscopy (FTIR), and mineralogical data. Macros and templates were developed to display data in Lotus graphs and charts. Data from analysis of samples from the Gary Drilling Co., KLC 44, well No. 375x in Pioneer field and the UNOCAL McKittrick Front 415 and 418 wells in Cymric field were used to develop and test the programs. Development and use of these databases and macros are continuous.

Database Management

Every manager and site now has a high-end PC (486-based computer or better) with which to access the database and run the visualization applications programs. These computers have been networked and linked to a common server at Michigan Technological University (MTU). Data and files are being regularly transferred between MTU, Bakersfield, Calif., and La Habra, Calif. During June 1994 this capability was used by all three sites simultaneously to help prepare a Class III proposal to the U.S. Department of Energy (DOE) and continues to be an extremely effective way of transferring reports, data, and figures between sites with a minimum amount of time and effort.

Organization and Management

Although project members are located at four sites (Tampa, Fla.; Houghton, Mich.; Bakersfield, Calif.; and Los Angeles, Calif.), project coordination has been successful.

Budget Management and Quarterly Reports

The project budgets have been reprogrammed and a system has been set up for logging, recording, and archiving all invoices related to this project. All expenses are tracked as they occur and are allocated to the proper tasks. A convenient way to visualize the project budgets by monthly expenditures, cumulative expenditures, and projected expenditures using Lotus graphics has been developed. This has been a considerable aid to managers trying to track and control their budgets.

Data Collection

Well Logs and Well Data

Munger maps that cover the Pioneer Anticline and the entire area northward to the McKittrick Front area of Cymric field were scanned into the Canvas (Deneba) drafting program and digitized into several layers. Fifty-three wells that penetrate the Miocene Monterey formation, the principal interval designated for visualization, were identified on the Pioneer Anticline. Forty-five of these wells have wireline logs.

Log Database Management. DPI staff constructed a Quattro Pro spreadsheet to collect well location and depth, well log, and sample data during the interim period until the Microsoft Access database management system is completed. Data can be exported easily from this Quattro Pro inventory file to any database. Tops of the Miocene were picked in each of the 45 wells on the Pioneer Anticline, their X-Y locations at the appropriate depths were calculated for each well, and both were placed in another spreadsheet. From there they can be exported to any mapping or visualization program. Digital log databases are being stored in standard interchange formats (ASCII or LIS) within the log evaluation applications program—in this case the Crocker Petrolog program—for exchange with other programs.

Log Digitization. Major progress was made on this large and critical subtask during FY 1994. Log correlation, log analysis, and reservoir visualization cannot proceed until all of the logs from all the Monterey wells on the Pioneer Anticline are digitized and corrected. All of the wireline logs from the 45 logged wells that penetrate the Miocene Monterey formation on the Pioneer Anticline have been digitized.

Core and Sample Acquisition

Core and Cuttings. Sidewall core and cuttings samples recovered from one of the 13 Pioneer field wells (Gary Drilling, KLC 44, well No. 375x) were shipped to MTU in December 1993 for petrographic, petrophysical, and geochemical analyses. XRD, FTIR, and scanning electron microscope (SEM) analyses were performed on selected samples. Spreadsheets and macros were constructed to store, reduce, and plot the data.

In April 1994, researchers met at the UNOCAL Research Center in Brea, Calif., to view and sample the cores from the UNOCAL McKittrick Front Nos. 415 and 418 wells in

Cymric field. These wells have modern log suites and long conventional cores with extensive petrophysical data sets that will be used to calibrate the logs from the Pioneer Anticline. More than 700 ft of conventional core is available from the No. 418 well alone. It has been photographed under white and ultraviolet (UV) light; analyzed at 1-ft intervals for porosity, permeability, grain density, and oil and water saturation; and subjected to spectral gamma ray analysis. This unique and extensive data set will be instrumental in the analysis of the Pioneer Anticline.

Fifty-nine additional samples were collected and described for petrographic and geochemical analyses. The samples represent 13 different lithotypes that affect reservoir quality and log character. The samples were forwarded to MTU where they are being analyzed by SEM, XRD, and FTIR. They are being used as calibration samples to develop and refine SEM, XRD, and FTIR analytical techniques in diatomite reservoirs. After the techniques have been sufficiently developed, all of the samples will be analyzed, and the results of these analyses will be integrated with the petrophysical data collected on these cores by UNOCAL.

ARCO/UNOCAL Core. Project members will approach ARCO and attempt to acquire additional core and cuttings samples from several ARCO wells in the vicinity of Pioneer field. As wells elsewhere on the Pioneer Anticline are inventoried, other operators may also be contacted. DPI will approach ARCO and/or Western Geophysical to request access to several seismic lines shot over the Pioneer Anticline. If access can be arranged, picks on the top of the Miocene and on other stratigraphic markers will be used to further improve control on the structure of the anticline for the visualization package.

Fluids. Several oil samples from Pioneer field wells were forwarded to MTU for analysis in August 1994. FTIR analyses will be performed at MTU, and conventional organic geochemistry analyses will be subcontracted.

Data Analysis and Measurement

Petrophysics

Extensive petrophysical data sets were acquired from UNOCAL for the cores from the UNOCAL McKittrick Front Nos. 415 and 418 wells in Cymric field. Petrophysical data from these two wells will be essential for calibrating the logs from uncored wells that penetrate the same stratigraphic intervals on the Pioneer Anticline.

FTIR Spectra. Techniques are being developed for performing quantitative analyses of rock samples using FTIR. Sample preparation, accumulation of a suite of mineral standards, and development of reliable analytical techniques are critical to this endeavor. Much of the work to date has concentrated in these areas. Preliminary FTIR analyses on selected sidewall core and cuttings samples from Gary Drilling, KLC 44, well No. 375x and from the two UNOCAL McKittrick Front wells have been performed.

Petrology

XRD and SEM analyses of samples from both Pioneer and Cymric fields are under way. Techniques are being developed for quantifying mineralogy in the fine-grained diatomaceous rocks that compose the Monterey reservoir using XRD and SEM techniques. Mineralogy cannot be quantified through conventional thin-section point-count analysis because the rocks are too fine-grained. Less deeply buried parts of the reservoir contain significant quantities of Opal-A, which is amorphous and therefore transparent to X-rays, making mineralogical quantification by XRD particularly difficult. The present approach is to combine XRD analyses with energy dispersive spectral (EDS) analyses performed on the SEM to improve analytical accuracy. Each sample will be placed on an X-Y stage in the SEM; EDS analyses will be performed at points on a grid; and the results will be evaluated by comparison to XRD and conventional thin section examination.

Polished thin sections were prepared on 16 samples from UNOCAL McKittrick Front well No. 418. Plane-light petrography, SEM image analysis, and EDS-SEM point-counts will be performed on each of these samples. XRD analyses will be performed on splits of the same samples.

XRD. XRD analyses have been performed on selected samples of sidewall core and cuttings from the Gary Drilling, KLC 44, well No. 375x and on continuous core samples from the two UNOCAL McKittrick Front wells. Spreadsheets and macros to store, reduce, and plot the XRD data have been constructed.

SEM Image Analysis. Image analysis work has begun on samples from the Gary Drilling, KLC 44, well No. 375x in Pioneer field and from the two UNOCAL McKittrick Front wells in Cymric field. SEM photomicrographs were made of selected samples. Sixteen polished thin sections were prepared for experimental EDS point-count analysis.

Polished thin sections were prepared on 16 samples from UNOCAL McKittrick Front Well No. 415. Plane-light petrography, SEM image analysis, and EDS-SEM point-counts will be performed on each of these samples. XRD analyses will be performed on splits of the same samples.

Petrographic Examination. Thin-section petrographic examination of the polished sections that will be used in the experimental EDS point-count analysis was completed. These data will be used as an independent comparison to the XRD and EDS analyses.

Log Calibration

All the cored wells and several uncored wells with good log suites were included in a preliminary log calibration study. Core data were plotted on a large-scale output log along with raw log data and were compared with core photographs and with the core itself. Core data were also compared with log data using a variety of statistical techniques in order to obtain correct parameters for entry into standard algorithms for calculating matrix density, porosity, and water saturation.

No published analytical models exist for diatomaceous rocks, so DPI is using a model it has developed. Calibration of such a model in rocks of this type is time-consuming. DPI expects to further refine the input parameters with rock data from analytical work in progress at MTU.

Data Preparation. Wireline logs for all of the wells for which good logs had been obtained were digitized. This includes most of the wells on the structure. If other logs are located, they will also be digitized. It is time-consuming to construct a log database for cross sections and analytical work. This work is being carried out at DPI.

Model Selection. The measurement and prediction of lithology and fracturing are important parts of a reservoir evaluation in diatomites. The models that have been selected for this project can be applied to all wells with resistivity and density-neutron logs, and they are capable of predicting matrix density, clay volume, diatomite facies, and accessory minerals, such as carbonates, porosity, permeability, and water saturation, as well as providing a qualitative measure of fracturing and fracture potential. The rock analysis data that will be available from MTU will provide for better calibration of standard models and will also allow application of several enhanced options that require good rock measurements.

The output of these models is the primary input to the reservoir visualization program. Comparative plots were constructed of core and log data for the two McKittrick Front wells in Cymric field. These plots were used in conjunction with core descriptions and core photos to guide sampling of the core.

One well in Pioneer field, Tenneco 62x-30, was cored. Model selection and log analysis for this well have been completed. Plots showing variation with depth in measured and calculated log parameters, along with core-property data, were prepared for each cored interval in the well and were later presented in a poster display at the annual meeting of the American Association of Petroleum Geologists held in Denver, Colo., June 11–15, 1994.

Modeling

Geochemical Modeling

The geochemical modeling program CHILLER will be used to model fluid–rock interaction. This has practical significance because of active steamflooding of the Monterey and Etchegoin formations elsewhere in the southern San Joaquin Valley. Work has begun to simplify data input and to work on a graphical output interface for rapid visual display of output.

Workshops

The plan is to present two different workshops for industry. The first will be on design, construction, and operation of a database that will handle most of a small independent oil company's needs; focus will be on understanding database design and operation. The second workshop will concentrate on design and implementation of a reservoir characterization and visualization study.

